CHAPTER 1: Introduction and Literature Review

1.1 Introduction

The primary building block of coral reef ecosystems, whether an isolated mid-ocean atoll or a complex system of thousands of reefs, are the individual coral colonies that combine to form the reef structures which host coral communities. The state of a coral reef community (i.e. percentage coral coverage, dominant growth forms and size classes), or any other ecosystem, at any given time is the result of interactions between a range of disturbances and routine ecological processes that operate across a continuum of spatial and temporal scales (Gunderson et al 2002). The biological (living coral colonies) and structural (dead coral framework and rubble) legacies left behind in coral communities after a disturbance influence both the vulnerability of those communities to further disturbance and their ability to maintain current community structure: ecological resilience (Nystrom and Folke 2001). While some disturbances, particularly damage from tropical cyclone waves, can affect large areas with a single event, damage is invariably patchy in distribution because vulnerability varies at many scales, from individual coral colonies upwards. Thus, disturbance regimes need to be understood at regional scales (100s of km) to capture their full extent, and at very local scales (10s of m) to assess their potential impacts. Doing so has proved difficult because direct observations of damage are typically only possible at very local scales, at which high variability obscures regional patterns (Schneider 2001). A few studies have attempted to characterise the dynamics of large, infrequent disturbances across broad regions – for example, periodic forest fires and volcanic eruptions – but only for land-based ecosystems (Turner and Dale 1998). This thesis provides the first such characterisation for a large marine ecosystem by modelling the

dynamics of tropical cyclone disturbance across the Great Barrier Reef (GBR) over 35 years (1969-2003).

This thesis describes a cross-disciplinary project that operates at the nexus between the meteorology of tropical cyclones, coral reef ecology and the regional geography of the Great Barrier Reef (Figure 1.1).

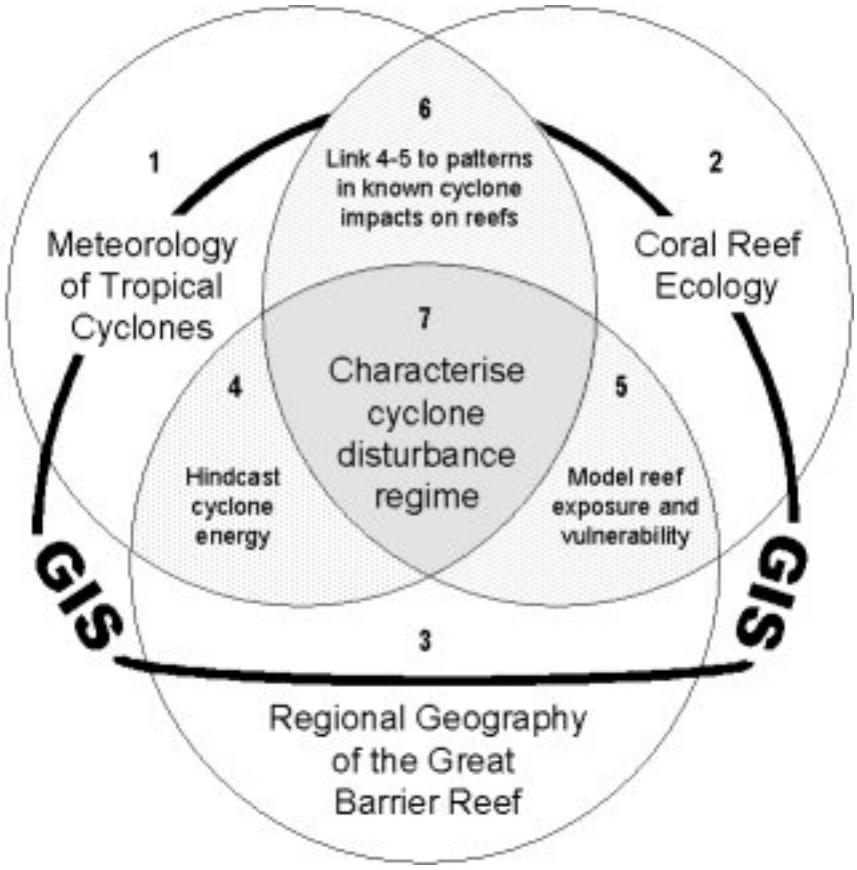

Figure 1.1 Overview of the theoretical basis for the research.

The fundamental aim of the research is to characterise the tropical cyclone disturbance regime in the GBR region at scales down to tens of metres on individual reefs, referred to here as 'sites'. To do so, I: 1) reconstructed the distribution of cyclone energy for the past 35 years (1969-2003) in the GBR, 2) modelled reef

exposure and vulnerability to that energy, 3) linked measures of cyclone energy and reef vulnerability to patterns in known cyclone damage to reefs, and 4) used the resultant model to predict cyclone damage for each cyclone over the time series. GIS was used as a modelling platform and unifying framework. The tasks outlined above draw upon various combinations of the three key areas. For example, hindcasting cyclone energy (4) required applying meteorological models (1) within the GBR (3). Modelling the exposure and vulnerability of reef sites to physical damage from waves (5) required consideration of the basic structure of coral reef communities (2) as well as the spatial arrangement of the reefs that they occupy within the GBR region (3). Finally, modelling damage (6) required understanding how the physical processes driven by cyclones (1) operate as an ecological disturbance at the scale of individual reef habitats (2). The remainder of this chapter will review the scientific literature in each of the first three key areas, as well as that for GIS.

The theoretical basis for specific approaches taken to achieve items 4-7 will be explored in subsequent chapters (chapter 4: hindcasting cyclone energy, chapter 5: modelling reef exposure and vulnerability, chapter 6 and 7: characterising the cyclone disturbance regime). Chapter 2 explores the cyclone disturbance regime in the GBR from 1910 to 1999 using distance to the cyclone path as a proxy for disturbance potential. Chapter 3 assesses the adequacy of this approach through a case study of five cyclones for which patterns of disturbance have been documented in the GBR.

1.2 Meteorology of tropical cyclones

The Australian Bureau of Meteorology (BOM) defines a tropical cyclone as a "non-frontal synoptic scale cyclonic rotational low pressure system of tropical origin, in which 10 minute mean winds of at least 17.5 $m.s^{-1}$ (gale force) occur [with] the belt of maximum winds being in the vicinity of the system's centre" (McBride and Keenan 1982). Thus, cyclones (Figure 1.2) are characterised by inward spiralling winds that create wide rain bands around the storm.

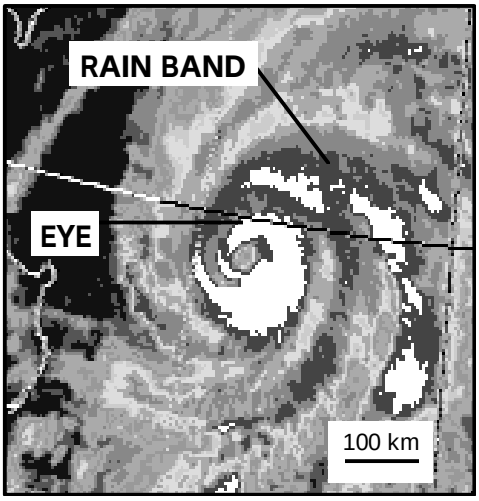

Figure 1.2: Simplified profile of a typical tropical cyclone. Adapted from Willoughby 1988.

The highest winds typically (but not always) enclose a roughly circular region of relative calm known as the "eye." Wind intensity gradually increases from near zero within the cyclone eye to a maximum velocity just outside the eye wall (termed the radius of maximum winds). For most cyclones, wind speeds decrease very rapidly with distance outward from the radius of maximum winds (Holland 1980). Occasionally, exceptionally small (Cyclone Ada 1970) or large (Cyclone Justin 1997) cyclones develop, where wind speeds decrease unusually rapidly or slowly with distance outward from the radius of maximum winds. The size of the cyclone is only weakly related to its intensity (Merrill 1984). However, the highest winds generated

by a large cyclone of a given intensity will cover a broader area than normal (Callaghan and Smith 1998). Eye width often varies considerably over short time periods (minutes to hours). Although changes in eye width can be important for modelling cyclone movement and intensity, frequent detailed estimates are rarely made. Given this, meteorologists estimate that typical eye widths fall between 10-40 km (Willoughby 1988) - for the GBR, and the mean eye width is about 30 km (J. Callaghan, BOM, pers comm). The area of maximum winds is typically found about 30 km from the centre of the cyclone eye in the front left quadrant with respect to the direction of the storm's forward motion (Young and Hardy 1993) in the southern hemisphere. This asymmetry decreases when a cyclone moves very slowly or not at all, which is rare. In that case, large swells generated in the area of maximum winds may propagate ahead and outrun the storm (Young 1988). Typically, however, the largest waves are found within the area of maximum winds. Adding to this effect is the elevated sea level (storm surge) caused by unusually low air pressure within the storm system as well as wind effects and wind-generated currents, the magnitude of which is typically greatest within the front left quadrant of the cyclone in the southern hemisphere (Hopley 1974b). The level of storm surge experienced depends on several factors, most notably the intensity of the cyclone (more intense = lower central pressure = higher surge potential) and its angle of approach, and the local bathymetric configuration. For example, the maximum surge recorded in Queensland was 12.2 metres at Bathurst Bay in 1899 (Hopley 1974b). Actual wave heights will depend also on the tidal cycle at the time of the cyclone's passage – when this coincides with high tide, the rise in sea levels can be quite dramatic. Superimposed on this elevated sea level are the wind-generated waves (Hopley 1974b). For cyclones embedded within a larger monsoon trough (as is common in the GBR), high winds (and

subsequent waves) may also occur outside the cyclone circulation due to large-scale pressure gradients (McConochie et al 1999).

1.2.1 Cyclone Formation and Movement

Cyclones form over areas of warm open ocean, and develop from pre-existing cloud clusters in these regions. In the Australian region, this confines the formation of the majority of cyclones (~95%) to an area roughly between 9^0 S and 19^0 S (McBride and Keenan 1982). Since cyclones rarely form when sea surface temperatures drop below 26.5^0C, the cyclone season in southwest Pacific / Australian region generally extends from November to May, with a peak in January and/or February (Holland 1984a, b & c, McBride and Keenan 1982). The number and location of tropical cyclones in the GBR varies considerably between and within years due to variations in sea surface temperatures and local air circulation caused by the El Nino - Southern Oscillation (Lough 1994, Dong 1988, Emanuel 1987).

Cyclones are sustained in part by proximity to warm water and they quickly weaken once they move over land or cold water. Relatively small exposed land areas, such as reef tops and continental islands, have little effect on the overall strength of a cyclone, though they may reduce wind speeds and wave heights locally. In the southwest Pacific, the majority of cyclones move in a southeasterly direction (Holland 1984a & b), but in north Queensland, the most intense storms often move westward towards the coast before recurving to the southeast (Holland 1984c). More than half of these cyclones decay at sea, and most of those that cross land are weakening (Holland 1984b & c).

Predicting the path of any given cyclone more than a few hours in advance is very difficult as cyclone paths can be erratic at time scales of hours to days and space scales of tens to hundreds of kilometres (Holland and Lander 1993). Particularly difficult is determining, in real time, when a change in cyclone direction represents a transient detour versus a substantial track change (Holland and Lander 1993). Cyclone paths can be affected by interactions between the storm and the surrounding environment, such as the presence of other tropical cyclones, large and meso-scale atmospheric features (trade winds, subtropical ridge), or by moving over land (Holland and Lander 1993). Paths are also sensitive to factors within the storm itself, such as changes in the structure of the eye (Willoughby 1990, Samsury and Zipser 1995).

1.2.2 Cyclone Tracking in Australia

Cyclones are rarely measured directly due to the danger posed by high winds and large waves, the tendency of instruments to fail when maximum conditions are reached, and the difficulty of predicting where a cyclone will move. Although it is possible to obtain direct measurements by flying through storms with specially designed aircraft, in Australia this has only been done for two cyclones - Kerry and Rosa in 1978-79 (Lourensz 1981). Meteorologists instead rely on land-based radar, satellite imagery (Dvorak 1975), and observations from ships and remote automatic weather stations at reefs to detect and estimate the basic characteristics of cyclones, such as their location, central pressure, and radius of maximum winds (Lourensz 1981). In addition, a series of automatic stations record tidal height along the Queensland coast, thus capturing major storm surge events, such as that generated by cyclone Pam in 1974 (Hopley and Harvey 1974).

BOM maintains an extensive digital database of cyclones dating back as early as the turn of the century (Davidson and Dargie 1996). The estimated location of each cyclone at 6 hourly, 3 hourly or 1 hourly intervals is provided, along with central pressure, speed and direction measurements and category ranking. This data is provided free of charge for research purposes. Other data, such as estimates of the radius of maximum winds, records of how the eye positions were estimated, and maximum predicted wind and wave speeds are intermittently provided. Estimates of storm surge are not included.

There is considerable positional and attribute error in the cyclone database due to the lack of direct observations (Davidson and Dargie 1996, Holland 1981). Tracking cyclone eye positions is typically easier when they are more intense because the cyclone eye often becomes more clearly defined as the storm strengthens (Figure 1.3), though high-level cloud may obscure even a well-defined eye (Holland 1981).

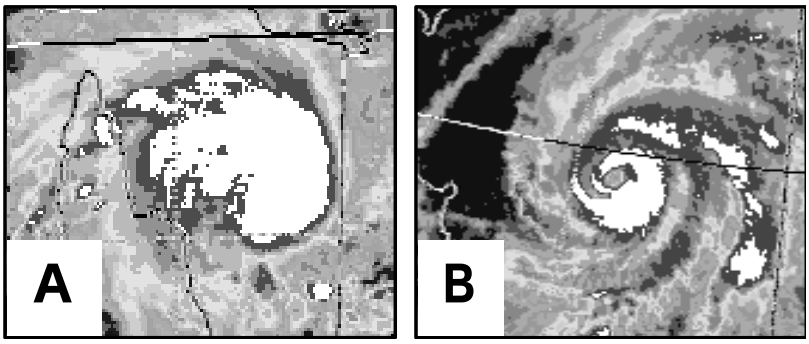

Figure 1.3: Satellite images of tropical cyclone eyes. Note that though the cyclones are of similar intensity, in [B] the eye is clearly visible, and in [A] it is obscured by upper atmosphere clouds. Satellite images provided by the School of Electrical Engineering, JCU.

Cyclones that track closer to land (within range of coastal radar) can be analysed with greater accuracy. Before 1969, when satellite imagery became widely available, meteorologists had great difficulty in detecting and tracking cyclones beyond radar

range (Holland 1981). For cyclones tracked post 1968, Holland (1981) estimates errors in the position of the cyclone eye from ± 20-50 km for storms within 500 km of the coast, and from ± 50-100 km for storms beyond. F. Woodcock, BOM (unpublished data) assessed the difference in cyclone eye position and intensity estimates between initial forecasts and subsequent refinement of the data, which provides a measure of the uncertainty in the data, from 1910 to 1995. He found that the majority of cyclone eye positions were subsequently altered by less than 100 km, although the maximum change was more than 400 km (Figure 1.4). This is not a true measure of error, however, because the altered positions are still only estimates themselves.

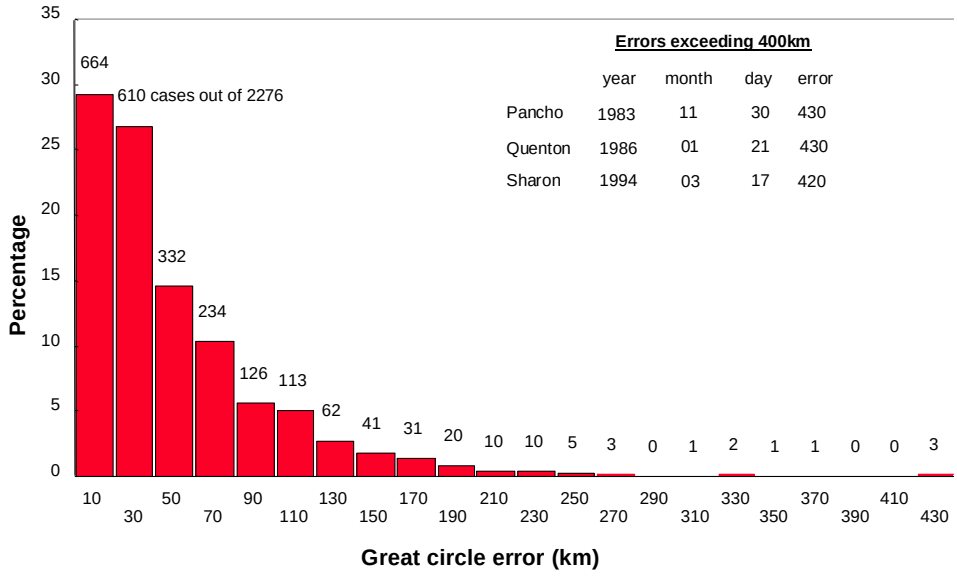

Figure 1.4: Estimated errors in initial cyclone positions based on subsequent data (adapted from F. Woodcock, BOM, unpublished data).

1.2.3 Cyclone Intensity

Cyclones are powered by the difference in pressure between the centre of the storm (central pressure) and the ambient environment. Since variations in the ambient

pressure are typically small, the central pressure alone provides a reasonable indication of cyclone intensity. Cyclones intensify as central pressures fall. The lowest central pressure on record (Typhoon Tip) was 888 hPa, recorded in the North Pacific in 1979. In the GBR, initial central pressure estimates are often subsequently altered by up to 15 hPa in either direction (Figure 1.5), though a reduction is more common (showing an initial underestimate of cyclone intensity).

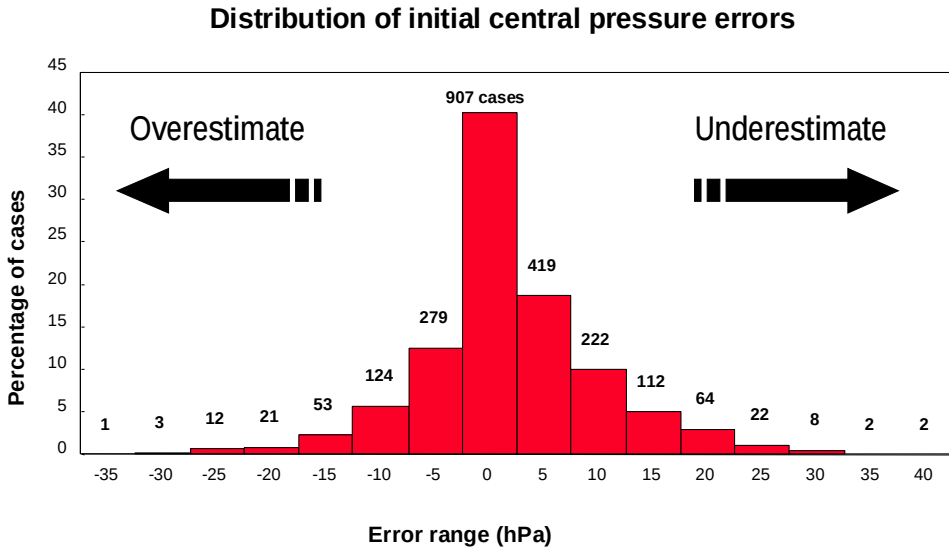

Figure 1.5: Estimated errors in initial cyclone intensity measures based on subsequent data (adapted from F. Woodcock, BOM, unpublished data).

Holland (1981) also estimated that central pressures can be in error by up to 15 hPa, though he stressed that the error estimates are themselves uncertain. BOM continues to investigate ways of reducing errors in the database (Davidson and Dargie 1996).

In Australia, tropical cyclone intensity is ranked based on central pressure and maximum wind speeds (Table 1.1). In other parts of the world, where stronger cyclones are variously termed hurricanes (North America) or typhoons (northwest

Pacific), another system called the Saffir-Simpson scale (Simpson and Riehl 1981) is used. Category 1 on the Saffir-Simpson scale is roughly equivalent to category 3 on the Australian scale – less severe storms are recognised in other parts of the world as tropical depressions or tropical storms. Cyclones that remain in, or have weakened to, a formative stage are recorded as category 0 on the Australian scale, and tropical depressions elsewhere.

Table 1.1: The Australian scale for ranking cyclone intensity by central pressure and maximum wind speeds.

Category	Average Wind Speed (m/s)	Strongest Gust (m/s)	Central Pressure (hPa)
0	17+	-	~1000
1	17 - 25	35+	1000 - 985
2	25 - 33	35 - 47	985 - 970
3	33 - 44	47 - 62	970 - 945
4	44 - 56	62 - 78	945 - 920
5	56+	78+	< 920

While category 0 and 1 cyclones exhibit similar minimum wind speeds, the former are less organised and do not normally show central pressures lower than about 1000 hPa.

1.2.4 Cyclone-Generated Winds and Waves

A network of wave buoys (maintained by the Queensland government's Beach Protection Authority) and a series of automatic weather stations on islands and reefs (maintained by BOM and the Australian Institute of Marine Science) record wind speeds and wave heights in the GBR. Despite this, very few direct observations of cyclone winds and waves exist across the region, especially for storms before the

early 1990s. For suitable data to be recorded, a cyclone had to pass near an operational buoy or station that did not fail under the conditions - this was rare for the GBR over the study period (Table 1.2).

Table 1.2. Direct observations of cyclone energy in the GBR available and relevant for use in this thesis.

Station	Location		Owner	Cyclones (19xx)	Wind	Waves
	Lat (^{0}S)	*Long (^{0}E)*				
Cairns	16.73	145.71	BPA	Justin (97)		x
Creal Reef	20.53	150.38	BOM	Ivor (90); Celeste (96); Justin (97)	x	
Emu Park	23.31	151.07	BPA	Justin (97)		x
Fitzroy Island	16.93	146.00	BOM	Ivor, Joy (90)	x	
Frederick Reef	20.94	154.40	BOM	Justin (97)	x	
Gannet Cay	21.98	152.47	BOM	Celeste (96); Justin (97)	x	
Green Island	16.76	145.97	BOM	Celeste (96); Justin (97)	x	
Hamilton Island	20.35	148.95	BOM	Celeste (96); Justin (97)	x	
Hayman Island	20.06	148.95	BOM	Althea (71)	x	
Hay Point	21.27	149.31	BPA	Justin (97)		x
Holmes Reef	16.47	148.87	BOM	Justin (97)	x	
Hook Reef	19.74	149.17	BOM	Justin (97)	x	
Mackay	21.04	149.55	BPA	Justin (97)		x
Townsville	19.16	147.06	BPA	Justin (97)		x

Due to this general lack of direct observations, meteorologists have developed a range of mathematical models to estimate cyclone wind and wave conditions (see chapter 4). In the southern hemisphere, cyclone winds spiral inward towards the eye in a clockwise direction, with the highest wind speeds found in a crescent shaped region in the front left quadrant at the radius of maximum winds (Figure 1.6 - A).

Predicted wind speeds are used to hindcast significant wave heights, directions and periods. These hindcasting models are simplest when the cyclone of interest is located over deep water, moving relatively slowly and is stable in speed and intensity

(Young 1988). As for the wind field, a typical deep water wave field contains a crescent of highest energy (wave heights) located at the radius of maximum winds in the front left quadrant with respect to the direction of forward motion of the cyclone (Figure 1.6 - B). Complete wave models require complex numerical solutions of non-linear wave equations. However, simpler parametric versions of these numerical models are often used, particularly for operational forecasting. Young (1988b) developed such a model for hindcasting cyclone waves.

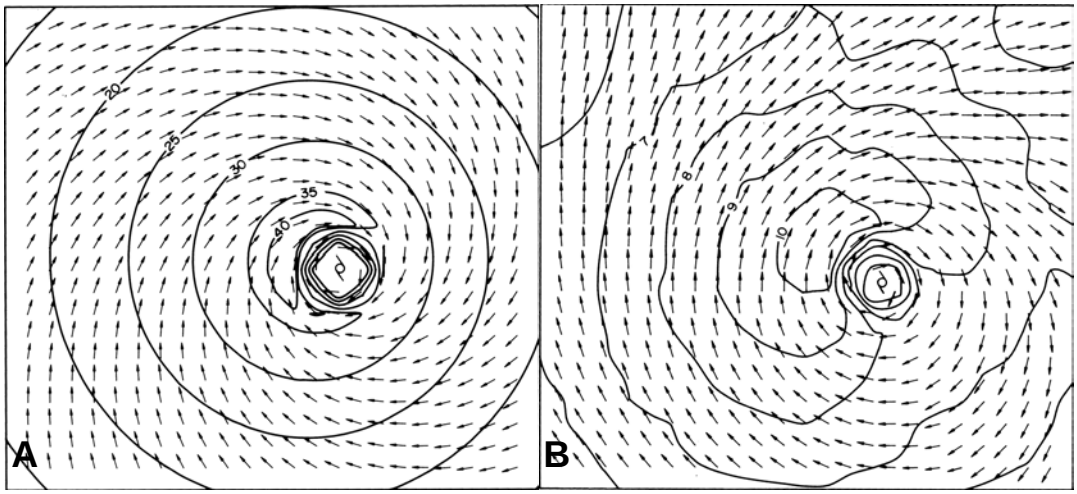

Figure 1.6: A typical hindcast cyclone wind field (A) and the associated wave field (B). The arrows indicate the direction to which the wind is blowing. The cyclone is moving towards the top of the page. (Adapted from Young and Hardy 1993).

Unfortunately, the model only applies to cyclones in deep (>50 m) water. Though easily implemented in GIS, its use would only be appropriate for part of the tracks of a few relevant cyclones, and thus was not suitable for use in this thesis.

Concurrently with the present study, Hardy et al (2001) developed a numerical wave model specifically for the GBR, which they used to model cyclones in the shallow waters of the GBR. This approach was invaluable for the development of a statistical characterisation of the long-term wave climate of the GBR over a range of spatial

scales, and in the extreme conditions associated with cyclones. However, the level of uncertainty in the wind predictions, which will be demonstrated in Chapter 4 (section 4.6), suggest their use to generate wave maps for specific cyclones would not be justified without substantial effort customising the wind model for each cyclone with field data, as was done by McConochie et al 1999. However, even with a highly fitted wind model, uncertainties inherent in the position and intensity of cyclones (see Chapter 4, section 4.4.7) - particularly for those early in the time series - would remain. Further, actual wave height at any given location during a cyclone will also depend on the water depth (the complex bathymetry of the GBR is poorly known), the tide (predicting the tide in detail for each site of interest [n=24,224] every hour during each cyclone [n=85] would be very time intensive), and storm surge (implementing these models requires detailed bathymetry). Although all three are important, modelling them was beyond the scope of this thesis. It would be ideal to predict the potential for cyclone wave damage to reefs by using measures of wave power or significant wave height. However, most of the GBR is protected from long period swells by the reefs themselves (Young and Hardy 1993), and ten metre surface wind speeds (hindcast by this thesis) provide a reasonably good estimate of local wind-sea (B. Harper, Systems Engineering Australia Pty Ltd, pers comm.). Finally, local scale factors influencing reef exposure and vulnerability to cyclone waves are important for predicting much of the pattern of damage (Massel 1996). My approach was to hindcast the magnitude and duration of local wind-sea (see chapter 4), develop models that characterise each reef site's exposure and vulnerability to damage from that energy (see chapter 5), and test how well these simple measures were able to predict the distribution of wave damage observed for five test cyclones (see Chapter 6).

1.3 Coral reef ecology

Coral reefs occur in the world's tropical and subtropical regions (Figure 1.7). Their growth is constrained by a range of physical-chemical, biological and geological factors, most notably temperature, saturation state, light and nutrient availability, and salinity (Table 1.3). For example, coral reefs are found where annual water temperatures reach at least 20^0C for most of the year and day lengths are relatively uniform (Wilkinson 1999). The limits imposed by maximum temperature are less clear. Though damage to corals from intermittent high sea temperatures (bleaching) has been well documented, other data suggest that reefs are able to grow in areas with consistently high temperatures (Kleypas et al 2001).

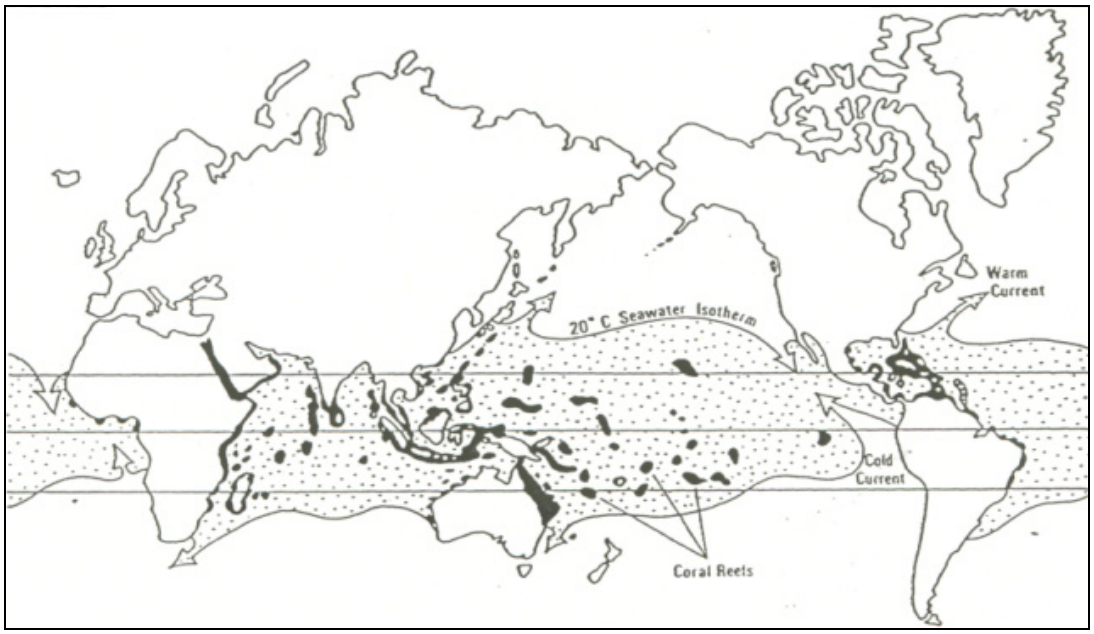

Figure 1.7. Distribution of coral reefs world-wide (Adapted from Veron 1986).

Table 1.3: Factors influencing the distribution of coral reefs worldwide (Adapted from Hubbard 1997, Kleypas et al 2001 and Wilkinson 1999).

	Factors	Limits of growth	Optimal range	Other considerations
Physical - chemical	Temperature	18-36^{0}C	22-28^{0}C	Can tolerate short-lived extremes.
	Saturation state	Require super-saturated state		
	Light	0-100 m	0-60 m depth (mid to outer shelf), 0-30 m (inner shelf)	Require relatively even day length and low turbidity
	Salinity	20-55 ppm	32-40 ppm	Require slow rates of change
	Nutrients	Require sufficient water flow and light to secure nutrients, at risk from excessive sedimentation.		
	Exposure to air	Can tolerate limited exposure.		
	Wave energy / storms	Very strong wave climate may favour algae over hard corals. Require sufficient time between successive events for recovery to maintain coral-dominated state.		
	Sea level	Require slow rates of change.		
Biological	Coral/algal diversity	Lack of sufficient grazers, chronic pollution and recurrent disturbance may favour algal growth over hard corals.		
	Competition with algae			
Geological	Substrate	Require sufficient space on a stable surface for larval settlement.		
	Sea-level history	Require suitable platforms for growth in the past, which kept pace with sea-level change.		

The structure of the coral colonies that make up reefs is built, in large part, by the secretion of calcium carbonate by individual coral polyps (calcification – Hallock 1997). Recent research has shown that the degree of carbonate saturation within the water column affects the rate of calcification (Kleypas et al 2001). Corals also require adequate light to enable photosynthesis by their symbiotic zoozanthellae partners, which limits the depth to which they can survive. While some have been found at depths as great as 100 m (Veron 1986), corals most frequently occur at or above 50-60 m depth in the clear waters of the mid continental shelf and above 20-30 m depth in the more turbid waters of the inner shelf (Wilkinson 1999). In general, corals thrive where salinity ranges between 32 and 40 ppm. Though they have been observed in areas where salinity approaches 55 ppm, this is only tolerable if the rate of change of salinity is slow enough for them to adapt. For this reason, coral reefs are typically absent from areas adjacent to the mouths of large river systems, where plumes of fresh water periodically cause rapid drops in salinity (Wilkinson 1999).

Coral reefs exhibit a wide range of forms, from linear strips situated along coasts or islands, to large platforms found in the mid to outer continental shelf, to atolls built on the subsiding remains of former mid-oceanic islands. These basic forms - shaped by environmental gradients (particularly exposure to wave energy), past and present sea-level, and other factors - can be further classified by their development along an evolutionary trajectory. This level of development is characterised by the reef's position relative to sea level and its basic geomorphological features, such as the degree of development of an algal pavement, rubble zone and reef flat (Hopley 1983). The form of a reef, in turn, controls to some degree the amount of material (sediments and unconsolidated reef debris) available for future incorporation into the reef

framework. For example, reefs in a very late stage of development (planar forms) by far retain more sand than other types (Hopley et al 1989), which can lead to infilling of the reef lagoon (typical of late stage reefs). The form of a reef also influences the spatial distribution of key gradients (such as wave energy and depth) around that reef. For example, reefs classified as patches (early stage of development) are located at depths shallow enough to be exposed to waves, but have yet to develop wave resistant structures such as algal ridges. In contrast, for crescentic reefs (later stage of development), these features are well defined, resulting in distinct areas of high wave exposure at the edge of the reef facing the typical angle of wave approach versus areas of low exposure around the back of the reef. So, within a given reef of a particular form, distinct regions (zones) that vary in the structure and dominant growth forms present are shaped by gradients in the extent of wave exposure as well as light and depth (Done 1983). For example, the leading edge of a reef that is highly exposed to waves will be dominated by coral forms that are small in size, streamlined, and orientated in the most frequent flow direction (Koehl 1984, Tunnicliffe 1982). In contrast, areas of the reef that are normally sheltered from wave action are more likely to be dominated by larger and more fragile forms, such as branches and plates. In general, the state of a reef at any give time is the result of the complex interplay between the ecology and geomorphology of the reef and the natural processes that shape its form and composition (Woodroffe 2003).

Coral reefs are one of the most productive ecosystems in the world, and the most persistent over the geological history of the Earth (Veron 1995). Scientists have yet to agree on a standard definition of a coral reef (Kleypas et al 2001) - variations are a mix of references to biological features (interlocking coral and algal colonies, mostly

sessile), geologic features (carbonate, cemented / consolidated, wave resistant) and environmental requirements (marine, warm, well-lit). Coral communities have been defined as "local assemblages of stony coral and other conspicuous benthic populations which can co-habit with them (i.e. algae, soft corals, zooanthids) on reefal or non-reefal substrates" (Done 1999). They may or may not build a reef, depending on environmental conditions (Kleypas et al 2001). This thesis considers only the coral communities present on actual reefs.

Coral reefs are valued for their role in supporting fisheries, protecting shorelines, providing habitat for a diverse range of species, and attracting tourists. Recognition of these values in the face of increasing human use has led to efforts for their protection, such as the establishment of marine protected areas in which destructive human activities (mineral extraction) are banned and other human uses (fishing, tourism) are restricted temporally and spatially. To evaluate the effectiveness of regulation of the human use of reefs, it is also important to understand the spatial and temporal characteristics of unmanageable impacts like cyclones.

1.3.1 Disturbance of reefs

Human disturbance of reefs ranges from discrete, localised events such as ship groundings (Hatcher 1984, Littler and Littler 1989), tourist pontoons scraping the reef during heavy seas (Ayling and Ayling 1997), damage from recreational SCUBA divers (Tratalos and Austin 2001), point source pollution (Al-Moghrabi 2001) and destructive fishing methods (McManus et al 1997), to more diffuse and pervasive broad-scale events such as chronic pollution combined with other disturbances (Grigg 1995), long-term overfishing combined with other disturbances (Hughes 1994,

Jackson et al 2001, Hughes et al 2003), and perhaps even loss of global habitat potential from rising sea temperatures and decreasing aragonite saturation due to global climate change (Guinotte et al 2003).

Understanding human impacts on reefs is complicated because these disturbances do not occur in isolation (Brown 1997). Reefs are also affected by a range of natural disturbances, such as predation by crown-of-thorns starfish and physical damage from tropical cyclone waves (Grigg and Dollar 1990, Done 1992a, Sebens 1994). These natural disturbances can make the detection and delineation of human impacts difficult by producing high spatial and temporal variability in broad measures of coral community structure over decadal time scales (Done 1997). Changes in coral reef communities also result from day to day processes that cause the 'routine mortality' that contributes greatly to the apparent health of the reef (Hughes and Connell 1999). Part of the reason for the high variability is that the frequency and spatial extent of natural disturbances overlap in time and space (Figure 1.8), which influences the vulnerability of reefs to damage. For example, a reef structure made up of standing dead corals that were killed by crown-of-thorns starfish may be more easily broken and battered by cyclone waves than the same corals would be if in a living state (Rogers et al 1982). In this way, the history of disturbance at a particular site strongly influences how future disturbances will shape community structure and function (Hughes 1989).

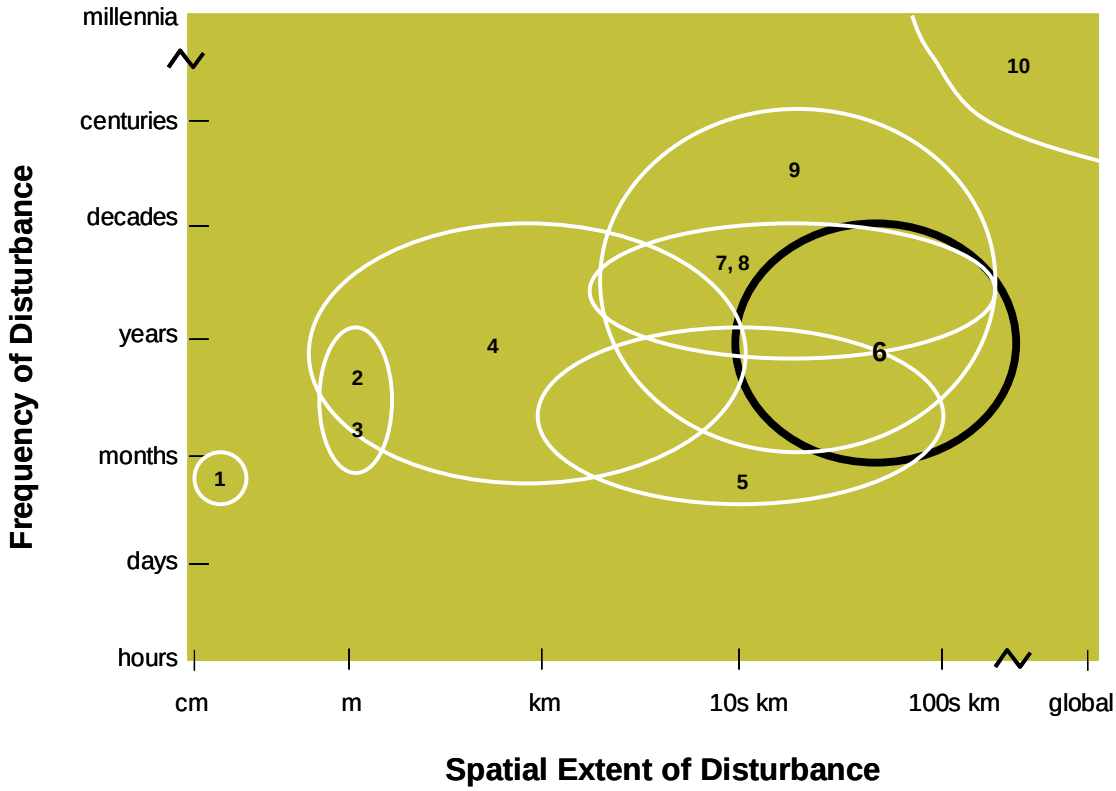

Figure 1.8. Overlap in space and time between natural disturbance regimes that affect coral reef communities. 1 = Predation and grazing, 2 = Bioerosion, 3 = Disease (individual corals), 4 = Freshwater river plumes, 5 = Storms, 6 = Tropical cyclone waves, 7 = Mass bleaching, 8 = Crown-of-thorns starfish predation, 9 = Epidemic disease, and 10 = Changes in sea-level / water temperature. Adapted from Jackson (1991).

For example, the extent of coral coverage and dominant colony size class on a reef depends on the time since the last disturbance of a given magnitude (Figure 1.9). If left undisturbed indefinitely (A), a reef community gradually develops larger colonies and higher coral coverage until crowding causes corals to compete for space. These interactions can result in mono-specific stands of fast growing species (Connell 1978). In contrast, reef communities that endure frequent severe disturbance (B) do not have time to fully recover from one disturbance before the next one hits. Such communities are unable to progress beyond the early stages of any successional trajectory and, so long as new colonies can establish, can be dominated by younger and / or smaller, wave-adapted coral colonies (Done 1997) often with relatively low overall coral coverage.

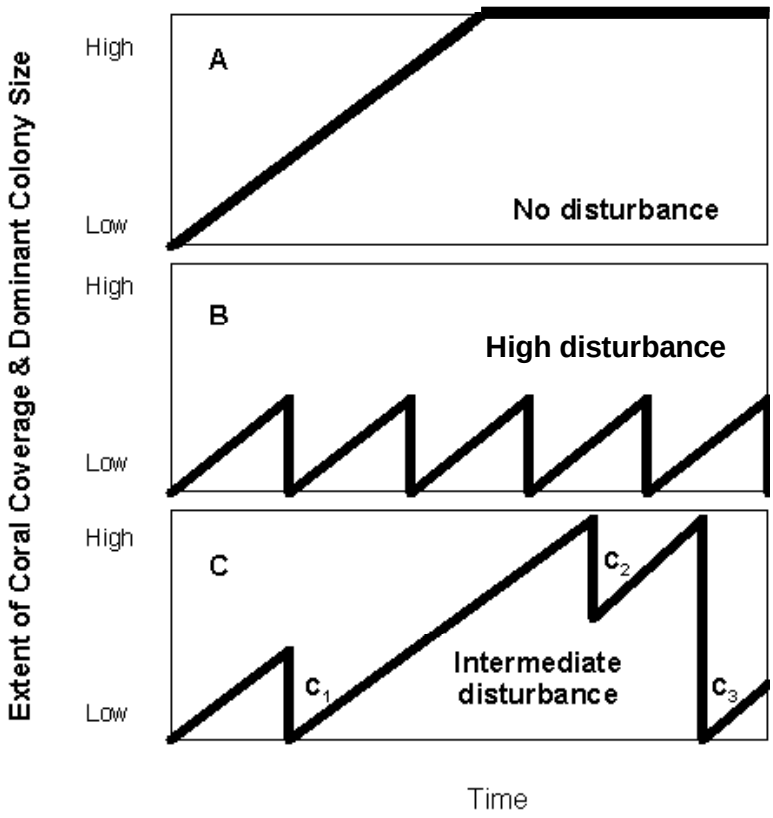

Figure 1.9: Effects of cyclone disturbance regimes on the extent of coral coverage and dominant colony size (thick black line) over decades (adapted from Done 1992a and Dollar and Tribble 1993). As the time since the last disturbance increases, coral coverage and the dominant colony size increase until crowding results in biological interactions that reduce species diversity. In A, the maximum coverage that can be supported in the available space is reached. In B, periodic major disturbance reduces coral coverage and colony size before the maximum can be reached. In C, the timing of intermittent minor (C_2) and severe (C_1 and C_3) disturbances determine whether and for how long the maximum is reached. Note that the colony size – disturbance relationship is more complex for massive corals and in general has a more gradual slope than shown here.

Reef communities more often sustain disturbances of a range of intensities at irregular intervals (C) - intermediate disturbance. Their extent of coral coverage and dominant colony size at any given time depends on the intensity and the length of time between disturbances. Moreover, the extent of variability in reef structure depends directly on the temporal and spatial scale of observation - structure is highly variable when examined over relatively short time periods and across small distances yet remarkably stable over broad areas and geological time frames (Pandolfi 2002). From a management viewpoint, a short time frame (years to decades) and small distances

(metres to kilometres) are important - at these scales, reef structure is highly variable. Understanding what we see on a reef at any given time requires that we recognise these complex interactions between normal conditions and the history of human and natural disturbances.

1.3.2 Resilience of reefs

A useful concept for examining reef disturbance is 'ecological resilience' (Figure 1.10), which defines the magnitude of disturbance(s) that an ecosystem can absorb before shifting into an alternate state (Gunderson et al 2002). This assumes that more than one possible equilibrium state exists for the ecosystem (multiple stable states).

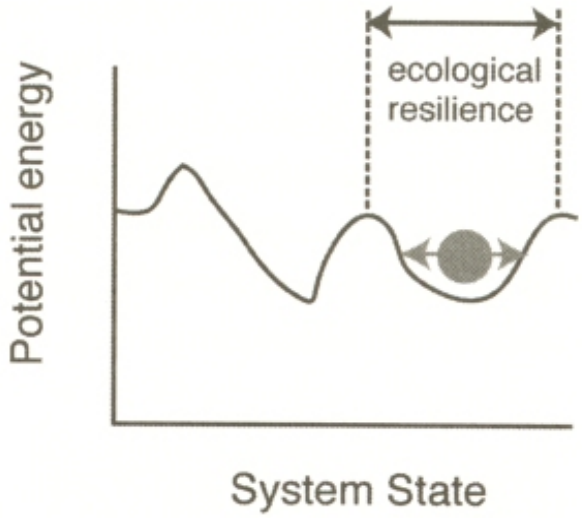

Figure 1.10: Stability landscape representing the dynamics of a system and its ecological resilience. The ball represents the system 'state'. The state can be changed by disturbances, which move the system along a stability landscape. The shape of the landscape is determined by controlling variables of the system. The ecological resilience of a system corresponds to the width of the stability basin. Adapted from Gunderson et al 2002 (Figure 1.1.1, p 5).

For a coral reef community, this can mean a ‘phase shift’ from the typical hard coral dominated state to dominance by various combinations of turf and algae (McClanahan et al 2002), which may occur gradually or abruptly depending on the circumstances

(Done 1992a). For example, Hughes (1994) documented a rapid shift in Jamaican coral reefs from hard coral to algal domination due to the cumulative effects of a mixture of overfishing and hurricane damage over time. A phase shift may result at a site when the disturbance regime of that site changes (for example, multiple storms damaging the site more frequently than normal), or when the resilience of the ecosystem declines (for example, due to reef degradation from chronic pollution or loss of a keystone species from overfishing), or both (Nystrom et al 2000). Accordingly, an increased likelihood of phase shifts is possible as coral reef communities respond to the rising levels of stress (eg, more frequent cyclones) that may occur with global climate change (Pittock 1999). There is some suggestion that human disturbances in general may even act to drive phase shifts (Nystrom et al 2000). Connell (1997), for example, has suggested that reef communities are less likely to recover within a measurable time period from human, rather than natural, disturbances. This may be due to shorter return times between human disturbances (Hughes and Connell 1999). Or it may be that human disturbance is more likely to affect the environment directly (for example, changing the reef structure and thus the local water depth) than indirectly (killing individual corals but not limiting their future ability to grow there) (Connell et al 1997). The resilience of coral reefs to these disturbances depends on broad scale patterns in the reef 'seascape' that support the ability of individual coral communities to recover and/or adapt to disturbance (Nystrom and Folke 2001). For example, the ability of coral communities to re-establish themselves after a disturbance can highly depend on recruitment of new corals. The extent of connectivity between a particular reef and others within the larger seascape (as determined by its relative position and ocean currents) largely

determines the availability of coral larvae at a particular location (Nystrom and Folke 2001).

1.3.3 Understanding disturbances

Disturbances have always been a part of the environment of coral reefs. However, their impacts on coral reef ecosystems are poorly characterised (Hammer and Wolanski 1988, Done 1992a, Sebens 1994). The degree to which reef community structure and function will be altered by disturbances depends not only on the type, intensity, extent, timing, and frequency of the disturbances (Lirman and Fong 1997, Nystrom et al 2000), but also on the nature of the coral communities themselves (Done 1992b), which can vary significantly across small distances due to zonation and patchiness (Done 1983) and over short time periods due to 'routine mortality' (Hughes and Connell 1999). Thus, at the local scale, quantitatively assessing the impact of a given disturbance requires very detailed information about the patchy mosaic of the target community and the reef conditions present at the site (including the recent history of disturbances) before and after the disturbance. This type of data (Connell et al 1997) is very time consuming and costly to gather, is still very limited and is never likely to be obtainable except by serendipity, and then at very local scales. A more tenable goal is the characterisation of the natural disturbance regimes that affect reef areas. The major natural disturbances that affect the GBR region include: broad-scale bleaching (Berkelmans 2002), crown-of-thorns starfish predation (Moran 1986), exposure to fresh water plumes during flood events (King et al 2001), and physical damage from tropical cyclones (Massel and Done 1993).

1.3.4 Tropical cyclone disturbance

While many studies have examined damage from particular cyclones on specific reefs, very few studies have considered more than a single cyclone and more than a single reef at a time (see section 1.3.6). To date, very few attempts have been made to model a cyclone disturbance regime. Woodley (1992) did so for a single site in Jamaica and Treml et al (1997) for several sites in the Lesser Antilles. Both used only the distance to a cyclone's path as a proxy for disturbance potential. However, deeper understanding of the potential implications for reef recovery from cyclones requires modelling the regime across entire regions of interconnected reefs. Massel and Done (1993) estimated the frequency of reef exposure to significant wave heights based on cyclone central pressures (1910-1980) across the GBR using models of deep water and shoaling waves. However, they did not consider the effects of within and between reef shelter, or the differences in vulnerability of different reef communities to that energy. It is vital to consider the distribution of actual cyclone energy (known to be spatially variable) and reef exposure to that energy (also variable). This thesis aims to characterize the tropical cyclone disturbance regime across the entire GBR using meteorological and ecological models within a GIS framework, reconstructing a probable cyclone disturbance history of the region over the past 35 years (1969-2003).

1.3.5 Cyclone damage types

Tropical cyclones generate unusually high winds, changes in sea level, and heavy rainfall, all of which can affect reefs. Given sufficient fetch, sustained high winds build large waves, which break in shallow reef areas and can move sediments and physically damage individual coral colonies as well as the reef framework itself. The

associated storm surge and tidal height at the time of the cyclone can add to wave heights (Scoffin 1993, Hopley 1974b), though surge is likely most important for reefs located on the inner continental shelf (D. Hopley, JCU, pers comm.). The combined effect of waves, surge and high tide can result in waves breaking on areas of the reef normally sheltered from wave action, which are more vulnerable to damage (Harmelin-Vivien 1994). Because normally sheltered reef sites are more vulnerable, cyclone damage can be particularly severe when waves approach from an unusual direction, as was the case for cyclone Althea in 1971 (Hopley 1974a).

This thesis only examines the direct mechanical effects of cyclone waves on reef communities, even though cyclones do produce a range of other impacts and interactions that can also be important to reef ecology and structure. For example, heavy wave action may stir up sediments, reducing light availability and potentially burying individual corals upon resettlement (Harmelin-Vivien 1994). After a cyclone, sea levels can fall, and if this persists, can kill corals by exposure to air during low tide (Harmelin-Vivien 1994). The heavy rains often associated with cyclones may result in local flooding (which can be exacerbated by elevated sea levels). Floodwaters subsequently entering the sea during major events form plumes of fresh water that can persist for days to weeks and extend for 10s to 100s of km from the river mouth (Wolanksi and Van Seddon 1983, King et al 2001). As corals require saline water to survive, even relatively short-term persistence of a fresh-water plume over a reef community can harm or kill individual corals, often by causing them to 'bleach' (expel their symbiotic micro-algal partner, thus turning white in colour). For example, DeVantier et al (1997) found intense, localised bleaching along near shore reefs of the GBR from a flood plume generated by decaying ex Tropical Cyclone

Sadie. Finally, heavy rain may fall directly on reefs after the cyclone has weakened and crossed land, which could result in fresh water stress to corals occurring after they have already been physically damaged by large waves (Harmelin-Vivien 1994).

Coral reefs sustain both direct and indirect structural damage from breaking waves and wave-borne debris. For example, following Cyclone Ivor, Done et al. (1991) found both direct physical damage: changes to the reef matrix (Figure 1.11), dislodgment of massive coral heads (Figure 1.12), stripping of soft corals (Figure 1.13), and breakage of hard coral (Figure 1.14); and indirect damage from burial by sediments stirred up during the cyclone (Figure 1.15). Similarly, following cyclone Justin, this author and a team of researchers found widespread breakage of coral across entire reef slopes (Figure 1.16).

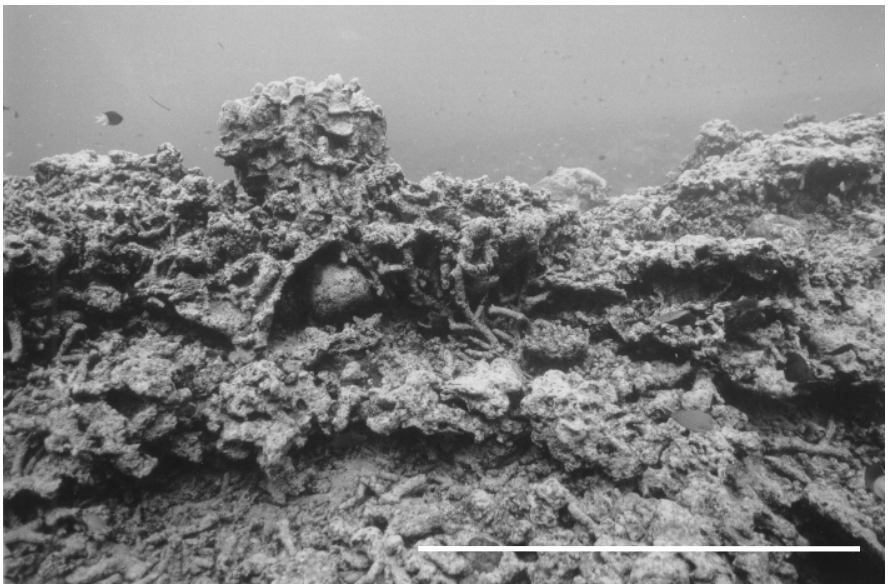

Figure 1.11: Wave induced changes to the reef matrix during Cyclone Ivor, 1990. The white bar equals ~50 cm. Photograph by Dr. Terry Done.

Figure 1.12: Dislodgement , breakage, and burial of massive coral heads during Cyclone Ivor, 1990. The white bar equals ~1 metre. Photograph by Dr. Terry Done.

Figure 1.13: Stripping of soft corals from the reef framework during Cyclone Ivor, 1990. The white bar equals ~ 1 metre. Photograph by Dr. Terry Done.

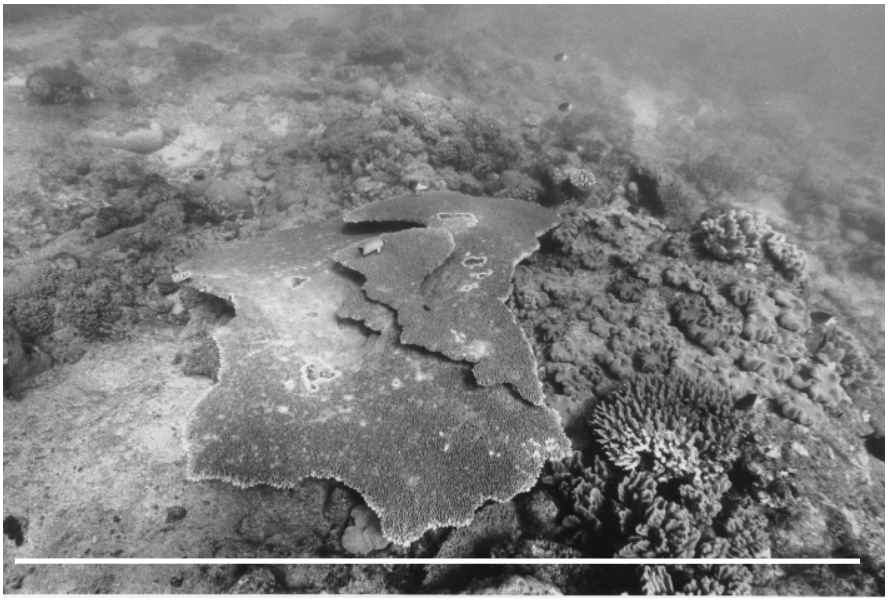

Figure 1.14: Breakage of a large plate coral during Cyclone Ivor, 1990. The white bar equals ~ 2.5 metres. Photograph by Dr. Terry Done.

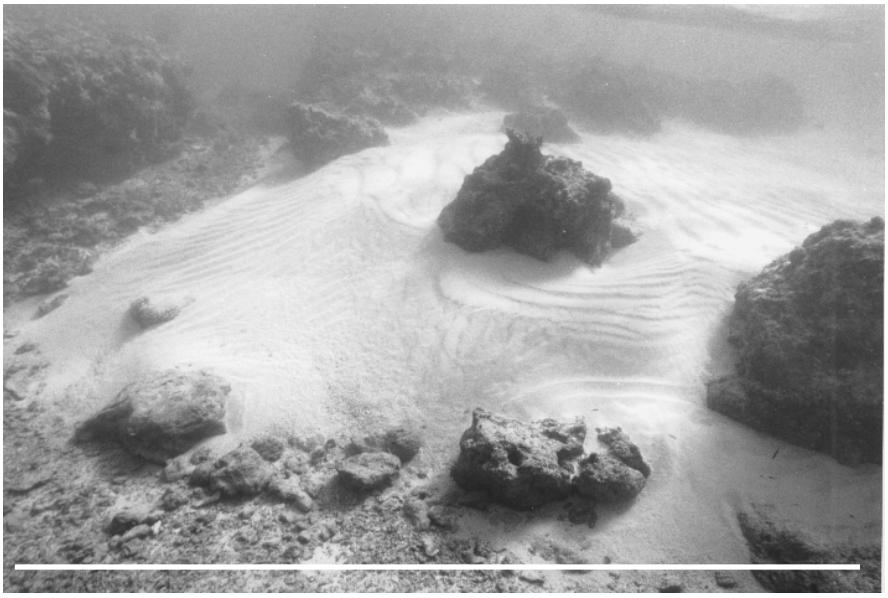

Figure 1.15: Burial of coral by deposition of sediment resuspended during Cyclone Ivor, 1990. The white bar equals ~4 metres. Photograph by Dr. Terry Done.

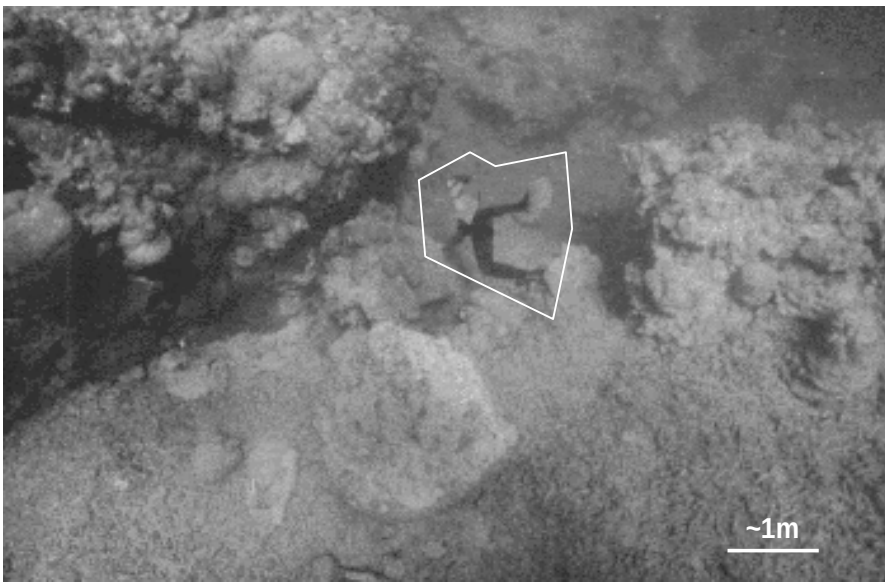

Figure 1.16: Widespread breakage of coral during Cyclone Justin, 1997. Inside the white polygon is a man duck-diving down the reef slope. Photograph by Dr. Terry Done.

The types of damage sustained by coral communities at a reef site during a given cyclone depend on the level of wave energy released (Figure 1.17) and the vulnerability and degree of exposure of the site to that energy (Done 1992b, Massel and Done 1993).

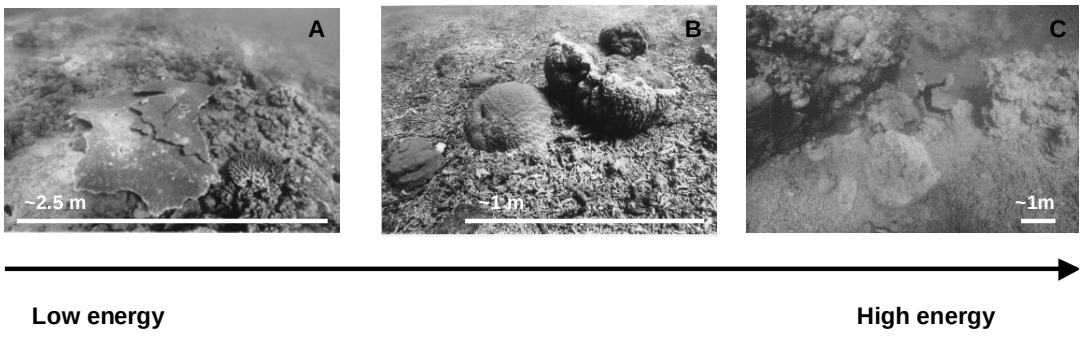

Figure 1.17: Examples of damage to coral reef communities during Cyclone Ivor (A & B) and Justin (C) that required varying levels of wave energy. A - breakage of large plates (low energy), B - dislodgment of massive corals (high energy), and C - stripping entire reef sections bare (high energy). Photographs provided by Dr. Terry Done, AIMS.

For example, relatively low wave energy can snap coral branch tips and plates, while higher and more sustained wave energy is required to strip entire sections of the reef bare. In general, high-energy damage is more dramatic and easier to identify in the field. The magnitude of wave energy needed to damage corals also depends on the wave climate normally experienced by the part of the reef on which they reside. Sections of reefs have been shown to vary greatly in morphology due to local-scale differences in typical wave heights and directions (Roberts et al 1977). These differences result in zonation (i.e. crest, lagoon, and slope), producing characteristic growth forms and species assemblages (Done 1983) that vary in their vulnerability to damage from waves. The greatest potential for damage occurs when cyclone waves approach a part of a reef that is normally sheltered from heavy wave action (Harmelin-Vivien 1994). In this case, corals are often more fragile and / or weakly attached - much less wave energy is required for damage to occur than in wave exposed zones that are routinely exposed to the same forces.

Wave damage at a site may occur immediately when the site is impacted by a breaking wave, a short time later when it is battered by wave-borne debris or buried by reworked sediment, or much later when surviving coral fragments die from predation or other effects (Harmelin-Vivien 1994). Periodic disturbance of coral communities by cyclone waves disrupts normal changes to community structure (succession) by damaging or killing individual corals, and by changing the mix of species types, growth forms and age classes within a given site. These changes may be positive or negative, depending on the time scale of observation and the perspective from which they are considered. For example, if several large massive coral colonies are dislodged from the reef during a cyclone, this represents a loss of

coral coverage in the short to medium term. However, over decades to centuries, the change may eventually enhance species diversity by opening up space for colonisation at the site (Connell and Keough 1985).

Sustained high-energy waves can alter the reef substratum and change the physical nature of the reef. The evidence of this damage, such as storm ridges (Scoffin 1993) or coral micro-atolls (Hopley and Isdale 1977), can be used to identify cyclone events long (up to millions of years) after they occurred (Pandolfi 2002). These geomorphologic changes can lead to long-term ecological changes. For this reason, Connell (1997), in his study of reef recovery from disturbance, distinguishes between damage that affects the reef environment directly (i.e. changes to reef morphology that affect hydrodynamics, changes to average water quality) and damage that affects the reef community (death of individual corals). He suggests that coral recovery from direct disturbance to the reef environment is difficult (if not impossible). For example, a cyclone that damaged the reef flat at Heron Island (far southern GBR) changed patterns in water circulation. Corals were subsequently exposed to air at low tide (Connell et al. 1997), which continued to limit recovery. In contrast, cyclone waves can deposit piles of sediment or dead coral fragments on the reef flat, which subsequently act as a dam that retains water in areas that would normally be exposed to air at low tide (Hopley and Isdale 1977). This same process can have a negative effect if cyclone waves remove an existing moat. However, the evidence left behind by some types of cyclone damage is less persistent. For example, damage that does little to change the overall reef structure (soft coral stripping, trenching and breakage) can be quickly obscured by normal processes of recovery on a reef. Thus, using Connell et al's (1997) criteria for classifying cyclone wave damage, coral

communities would recover most readily from low-energy damage such as breakage, soft coral stripping and debris scars (Figure 1.18). This thesis models both high and low energy types of cyclone damage over an ecological (decades) rather than geological (up to millennia) time scale.

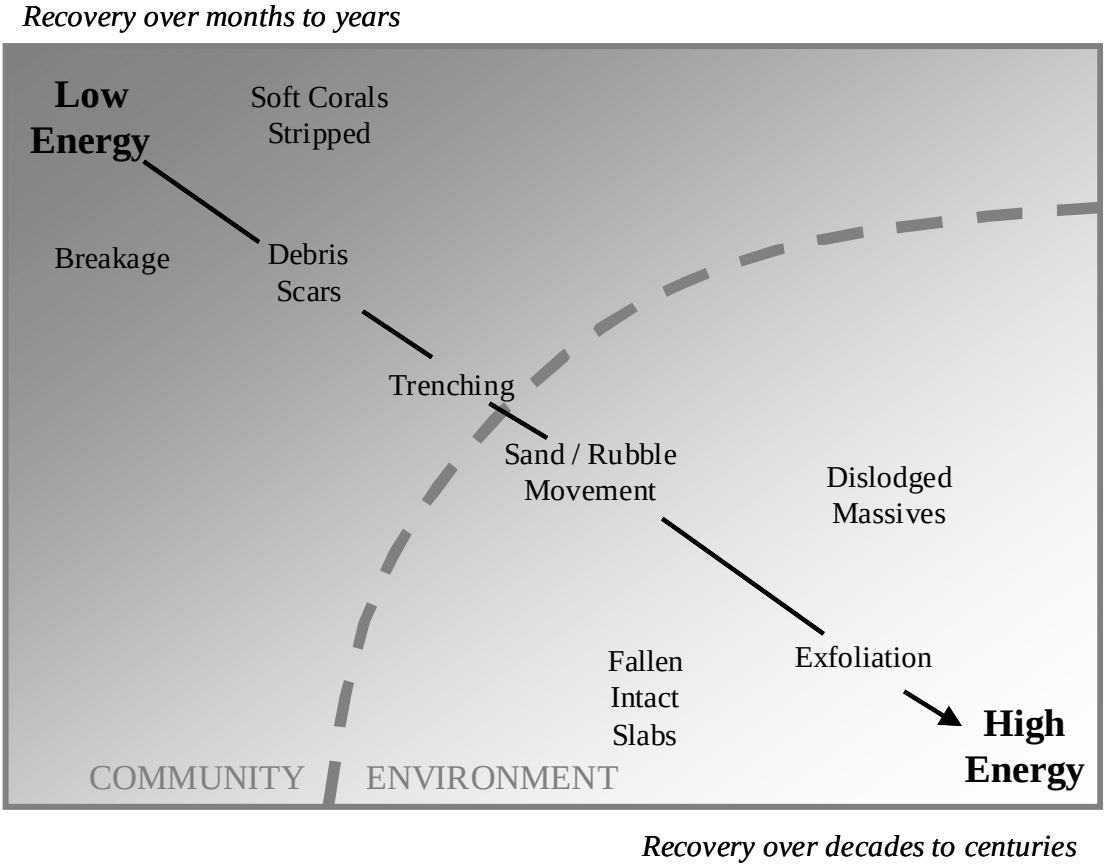

Figure 1.18: Types of cyclone wave damage on reefs and their implications for recovery.

1.3.6 Cyclone damage studies

Many studies worldwide have documented cyclone wave damage to reefs (Table 1.4). While the earliest studies examined severe cyclone damage to the GBR, overall the research effort has concentrated most heavily in the Caribbean (particularly in Jamaica and the US Virgin Islands). Less than half of the number of studies

published for the Caribbean were produced for either the Pacific or the GBR, both of which span much larger geographic areas and include more reefs. In addition, most of the studies were very local-scale in nature, examining a single cyclone event and one or two reefs at a time. The last reviews of this literature were undertaken nearly a decade ago, from both an ecological (Harmelin-Vivien 1994) and a geomorphologic (Scoffin 1993) perspective.

Table 1.4: Major published ecological studies documenting physical damage from tropical cyclone waves to coral reef communities via field observations, 1925-2002.

Region	Studies	#
Caribbean	Antonius 1972; Ball et al 1967; Blair et al 1994; Bythell et al 1993; Bythell et al 2000; Edmunds and Whitman 1991; Fenner 1991; Glynn et al. 1964; Glynn et al 1998; Goreau 1959; Graus et al 1984; Highsmith et al 1980; Hillis and Bythell 1998; Hubbard et al 1991; Kjerfve et al 1986; Kjerfve and Dinnel 1983; Knowlton et al 1981; Kobluk and Lysenko 1987; Kobluk and Lysenko 1992; Lirman and Fong 1995; Lugo-Fernandez et al 1994; Mah and Stearn 1986; Perkins and Enos 1968; Porter et al 1981; Rogers et al 1991; Rogers et al 1982; Rogers et al 1983; Stoddart 1962, 1963, 1965, 1971, 1985; Tilmant et al 1994; Treml et al 1997; Williams 1984;Witman 1992; Woodley 1980; Woodley et al 1981; Woodley 1992; Yoshioka and Yoshioka 1989.	41
Pacific	Baines et al 1974; Blumenstock 1958, 1961; Blumenstock et al 1961; Cooper 1966; Dollar and Tribble 1993; Emery 1962; Harmelin-Vivien and Laboute 1986; Hobson et al 1995; Littler and Littler 1989; Loubersac et al 1988; Maragos et al 1973; Mergner 1985; Ogg and Koslow 1978; Randall and Eldredge 1977; Wells 1951.	15
Great Barrier Reef	Ayling and Ayling 1997; Cheal et al 2002; Connell et al 1997; Done 1992b; Done et al 1986; Done et al 1991; Flood and Jell 1977; Harriott and Fisk 1986; Hedley 1925; Hopley 1974a; Moorhouse 1936; Rainford 1925; Riddle 1988; Stephenson et al 1958, Van Woesik et al 1991.	14

NUMBER OF CYCLONES

Since the vulnerability of a reef to physical damage depends very much on its current state (for example, dominant colony size class and growth forms), it would be preferable to examine reefs both before and after a cyclone. Because it is difficult to predict when and where a cyclone will track in sufficient detail to plan a survey, and because coral communities continually change over time, most studies have examined impacts only after the event, with the notable exceptions of Guam and Discovery Bay, Jamaica for which detailed before and after studies have been conducted. Similarly, most of the studies (75%) examined the impact of a single cyclone event (Table 1.5), and ~96% examined less than ten events.

Table 1.5: Number of cyclone events considered by major published studies examining the physical damage to coral reef communities from tropical cyclones (1925-2002).

# Cyclone Events Studied	# Papers
1	53
2	11
3	1
4	1
6	1
17	1
39	1
147	1

A notable exception is the Connell et al (1997) study, which tracked changes in coral communities at Heron Island reef from 1962-1992, fortuitously documenting physical damage most likely caused by some of the 17 cyclones that passed near the study area. The two largest studies took a different approach, estimating the potential for cyclone damage based on proximity to a cyclone's path rather than measuring damage directly in the field. Woodley (1992) assessed the potential for reef disturbance from

39 hurricanes that passed near Discovery Bay, Jamaica from 1870-1989. His analysis suggested that hurricanes have passed near the area less than normal in the latter years, which may mean that these reef communities were less disturbed then than what had been normal for the time series. Treml et al (1997) assessed the disturbance potential of several reef communities in the Lesser Antilles from 147 hurricanes that passed nearby from 1494-1995. Chapter 2 of this thesis uses a similar approach for the GBR, examining the disturbance potential at 218 reefs (that have been periodically monitored by AIMS since 1992) from 172 cyclones that passed nearby between 1910 and 1999. This provides a worst-case scenario of cyclone disturbance of the GBR (not all reefs located near the cyclones would have actually been disturbed) over the past 90 years. Chapter 7 of this thesis uses a more involved modeling approach to predict cyclone damage of four types (breakage, dislodgement, exfoliation, severe damage of any type) across 24,224 reef sites in the GBR for 85 cyclones over the past 35 years (1969-2003).

NUMBER OF REEFS

Nearly 60% of published studies examining cyclone damage to reefs assessed only one reef, and only four studies (~6%) surveyed more than ten reefs (Table 1.6). This may partly be due to the large concentration of studies in Jamaica and the Virgin Islands (~18%) - areas that contain small clusters of reefs. The largest study published to date surveyed 35 reefs (Done 1992b) located near the path of cyclone Ivor (north central GBR, 1990). Chapter 3 of this thesis describes a field study that examined cyclone damage to 14 reefs in GBR from Cyclone Justin (1997), plus a related questionnaire which yielded damage observations for an additional 35 reefs (in total, 46 reefs were examined).

Table 1.6: Number of reefs considered by published studies examining the physical damage to coral reef communities from tropical cyclones (1925-2002).

# Reefs Studied	# Papers
1	40
2 to 10	23
10+	4

LACK OF BROAD-SCALE / LONG-TERM STUDIES

Very few studies have examined the impacts of multiple cyclones on more than one reef. In fact, half of the published studies examined the impact of a single cyclone on a single reef. Only one study (Treml et al 1997) examined more than five events on more than five reefs. However this study did not include any direct field observations. Harmelin-Vivien and Laboute (1986) examined the impacts of six hurricanes on four reefs. Glynn et al (1998) examined the impacts of three cyclones on 15 reefs. Chapters 4 - 7 of this thesis model the potential for impacts of 85 cyclones on 24,224 reef sites across the GBR, using the limited existing reef damage data for five well-characterized cyclones to hindcast likely patterns of damage for the remaining 80 events for which damage was not surveyed.

Some past cyclone damage in the GBR may be inferred from the AIMS Long Term Monitoring database (1992 to present) and other past GBR studies. For example, cyclone damage was occasionally noted in surveys of crown-of-thorns starfish (Pearson 1974). In addition, surveys of surface damage from cyclones (Hopley 1972, Hopley 1974a) indicate that underwater coral communities located in the same area were very likely damaged as well. Finally, evidence of extensive storm surge along

the Queensland coast from a distant but unusually strong cyclone - Pam 1974 (Hopley and Harvey 1974) suggests that long period swell generated seaward of the GBR likely affected at least the reef sites exposed on the outer continental shelf.

Not all studies involved new field surveys (these are not listed in Table 1.4). Some researchers have explored the implications of cycles of disturbance and recovery without reporting experimental results or by re-analysing already published data. For example, Hughes and Connell (1999) used long term data sets from Heron Island and Jamaica to illustrate that processes of recovery from disturbances are equally as important to coral reef community dynamics as the initial damage - coral communities at Heron Island were able to recover from repeated cyclone impacts relatively quickly while those in Jamaica were unable to recover due to overfishing combined with repeated hurricane damage. Further, Connell (1997), using long term data sets from around the world, proposed that recovery from disturbances is likely to be slower when the impacts sustained affect the reef environment directly rather than indirectly (via the reef communities). Other studies have used innovative approaches that enabled investigation at broader temporal and spatial scales. For example, using models to examine threshold wave heights capable of dislodging massive corals, Massel and Done (1993) estimated that these corals could only be dislodged if not firmly attached to the immovable substratum. They also found that cyclones that are intense enough to potentially generate damaging waves return most frequently to the central GBR. At a scale of thousands of years, Nott and Hayne (2001) used wave models to predict the magnitude of wave energy needed to create coral boulder ridges observed in the GBR. From this, they estimated that very intense ‘super cyclones’ crossed the region every 200-300 years over the past 5,000 years. At even broader scales, Pandolfi (2002) used fossil records of reefs to examine patterns of reef

persistence and variability over the past 125,000 years across the Caribbean Sea. He found that the nature of ecological dynamics in reefs depends directly on the scale of observation. Broad-scale studies such as these provide a valuable context within which to consider the field-based studies, which are still predominantly conducted at very local scales. Both types of studies continue to be necessary, as much remains to be learned, particularly in terms of reef community processes of succession and recovery (Hughes and Connell 1999).

1.4 Regional Geography of the Great Barrier Reef

The GBR extends over 2,000 km off the southeast coast of Queensland, Australia (Figure 1.19) and forms the largest system of corals and associated life forms in the world (Craik 1992). Nearly 3,000 reefs, ranging in size from 1 ha to over 100 sq km, are scattered throughout the vast GBR region ($340{,}000^{+}$ km^2), along with 618 continental islands and 300 cays. Reefs in the region vary widely in form, ranging from fringing reefs adjacent to inshore islands, to widely separated platform reefs found on the mid to outer continental shelf, to clusters of ribbon reefs found along the outer continental shelf (Wells 1988).

Recently, Lewis (2001) described the geographic context of the GBR using a digital elevation model (DEM), from which he derived the basic physical properties of the region. The continental shelf from which the reefs rise varies in form, from relatively shallow, narrow and steep in the far north, to deep, wide and flat in the far south.

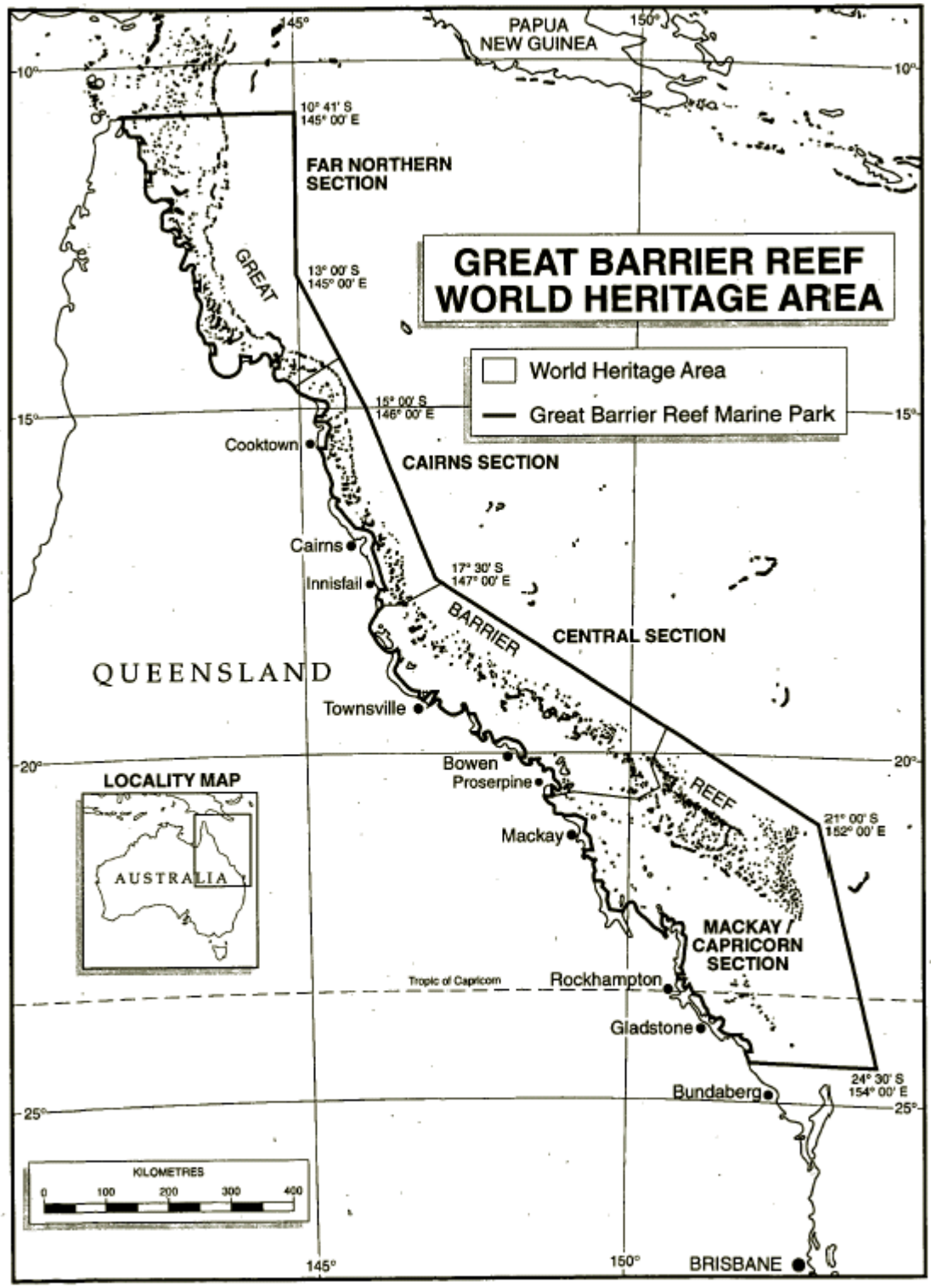

Figure 1.19. The Great Barrier Reef Region (Source: Great Barrier Reef Marine Park Authority).

Accordingly, there is generally a greater water volume south of 18^0S. The density of reefs (as measured by percentage area of the shelf covered by reef) declines from north to south. Submerged patch reefs, planar reefs, ribbon reefs, and fringing and

incipient reefs are more common in the northern half of the GBR while crescentic and lagoonal reefs are more common in the south (this generally agrees with an earlier analysis by Hopley et al 1989). The degree of closure (estimated by Lewis 2001 as the degree to which the outer reefs form a continuous barrier) of the GBR varies along its length from more than 80% to less than 10%. More than half of the GBR is more than 60% enclosed, with the least closure evident south of 22^0S. As a result of this, the degree of exposure of reefs to the dominant incoming wave direction (southeasterly trades) increases southward, with highest values south of 21^0S. Also important in the GBR region is its tidal regime, which has an unusually high range - from a minimum of 2.35 m in the far south to a maximum of 10.36 m between 21^0S and 22^0S (Maxwell 1968). Both tidal range and the water currents generated by the tides may play a large role in shaping reef development, especially for sites sheltered from oceanic swell (Maxwell 1968).

Recently, the Great Barrier Reef Marine Park Authority (GBRMPA) initiated a process to rezone the entire GBR, through the Representative Areas Program (GBRMPA 2003). This program aims to "maintain biological diversity, allow species to evolve and function undisturbed, provide an ecological safety margin against human induced disasters, provide a solid ecological base from which threatened species can recover or repair themselves, and maintain ecological processes and systems" (GBRMPA 2003). This aim recognises that the timing, location and intensity of natural disturbances such as tropical cyclones are beyond human control, and that attempting to preserve a given state of an ecosystem is less appropriate than maintaining the ecosystem elements and processes of self perpetuation (Baker 1992). An understanding of where and how often both natural and anthropogenic

disturbances occur, the spatial and temporal distribution of their impacts, and the ability of coral reef communities to recover is therefore needed. In this context, the work described in this thesis contributes to defining the meaning of 'state' for the GBR. Particularly, it aims to characterise the spatial distribution of damage risk by cyclone waves over time. This can be used to assess the relative contribution of the cyclone disturbance history to determining the nature of coral communities found across the GBR at a given time.

1.5 Geographic Information Systems (GIS)

Termed by Longley et al (1999) as "the art, science, engineering and technology associated with answering geographical questions", GIS is variously defined as both a technology (computer hardware and software designed to capture, store, analyse, and visualize geographically referenced data) and a cross-disciplinary science (drawing upon geography, computer science and related disciplines). Wright et al (1997) argue that activities broadly characterized as "doing GIS" fall along a continuum between these two positions (Table 1.7). The research described by this thesis primarily uses GIS as a tool to aid in characterizing the tropical cyclone disturbance regime in the GBR. However, several aspects of the project required adapting existing GIS analysis tools to create customized, advanced tools using macro programming. These analyses (for example, implementing cyclone wind models in GIS, measuring reef exposure, calculating reef aspect, visualization of cyclone energy distribution and uncertainty) are advanced uses of GIS tools and toolmaking. The project relies upon the science associated with GIS, but its primary focus is to apply that science towards a separate and unrelated goal (a greater understanding of cyclone disturbance of GBR reefs).

Table 1.7: Continuum of definitions of GIS used in research ranging from 'as a tool' to 'as a science' (Adapted from Wright et al 1997).

	GIS as a Tool	GIS as Toolmaking	GIS as Science
Aims…	…are not defined by the fact that GIS is used.	…are concerned with improving the utility of GIS as a tool.	…are concerned with the fundamental issues raised by using GIS.
"Doing GIS"…	...does not automatically mean "doing science".	...only means "doing science" if significant, original advances are made.	...means "doing science" because it contributes to the body of human knowledge.
Example	Applying fuzzy logic to a particular research question.	Developing tools making it easier to use fuzzy logic in GIS.	Developing a fundamental new theoretical model for representing imprecise data (fuzzy logic).

Goodchild and Longley (1999) note how research meeting certain conditions particularly benefits from using a GIS framework (Table 1.8). Modelling the cyclone disturbance regime of the GBR would not be feasible without the use of GIS due to the vast area which must be covered at a high resolution, the complexity of the requisite data, the importance of location to cyclone disturbance risk, and the importance of the spatial modelling of reefs in determining their exposure to cyclone waves. GIS has been a valuable framework for the study, despite some continued limitations (see Kemp 1993, Fotheringham and Rogerson 1993, Goodchild 1992, Michener et al 1994). These include the difficulty of implementing continuous mathematical functions within discrete GIS data structures, a lack of built-in tools to deal effectively with error and uncertainty, and a limited ability to model beyond two dimensions.

Table 1.8: Conditions that indicate that research would benefit from a GIS approach (adapted from Goodchild and Longley 1999) and the degree to which they are met by this thesis.

Condition	Relevance to this project
Data are geographically referenced and this is essential to the analysis.	The relative location of reefs and cyclone energy is integral to the risk of disturbance.
Data includes a range of vector data types.	Several key databases (cyclone eye positions, reef outlines, etc) are in vector form.
Topology (spatial relationships between features) is important to the analysis.	The spatial patterning of reefs directly influences their exposure to cyclone waves.
Curvature of the earth is important to the analysis, requiring methods of projection and analysis on curved surfaces.	The GBR extends nearly 2,000 km along the Queensland coast, so the earth's curvature applies.
Large volume of data.	Study area = 340,000+ sq km, includes 24,224 sites on 2,728 reefs, and examines 170 cyclones.
Data needed from a range of sources.	Data obtained from the Bureau of Meteorology, GBRMPA, AIMS, and others.
Features of interest have many attributes to manage.	Vector databases all contain multiple attributes of interest.
The project is cross-disciplinary.	Covers three major disciplines (meteorology, coral reef ecology, geography) and touches on several others (fluid dynamics, landscape ecology, management).
Visual display of the data and results to varied audiences is important.	Visualisations of cyclone energy, uncertainty and reef vulnerability are essential to convey the results to scientists and managers of varied backgrounds.
Output or data will be used as input to further research.	Cyclone disturbance of the GBR is of interest to GBRMPA and AIMS.

These limitations reflect the disparity between GIS as a science (spatial questions posed from a theoretical point of view) and GIS as a tool (most GIS users employ only basic tools leaving GIS toolmakers with little motivation to implement advanced functionality). Until recently, the use of GIS to understand and manage coastal and marine environments was limited to a few scattered applications. The complex and highly variable nature of coastal and marine data pose considerable challenges to GIS (Wright and Goodchild 1997, Goodchild 2000): features and processes at sea often lack abrupt boundaries that can be easily defined in a discrete GIS data model; the oceans have no geodetic framework in place to which features can be referenced.

Further, coastal and marine features typically change position more frequently, and do so in four dimensions (x, y, z and time) rather than two. The resolution needed to represent features is not always equal in all dimensions, and the expense and logistical difficulty of gathering data in the marine environment has resulted in a sparsity of spatial data (Wright and Goodchild 1997).

In summary, interpreting the changing state of the complex mosaic that is the GBR ecosystem is a major challenge for reef science. A successful characterisation of the cyclone disturbance regime could greatly add to our ability to understand the workings of this system.

1.6 Aims and Objectives

The primary aim of this project is to characterise the tropical cyclone disturbance regime for the GBR region over the past 35 years (1969-2003). The objectives that must be met to achieve this aim include (Figure 1.20):

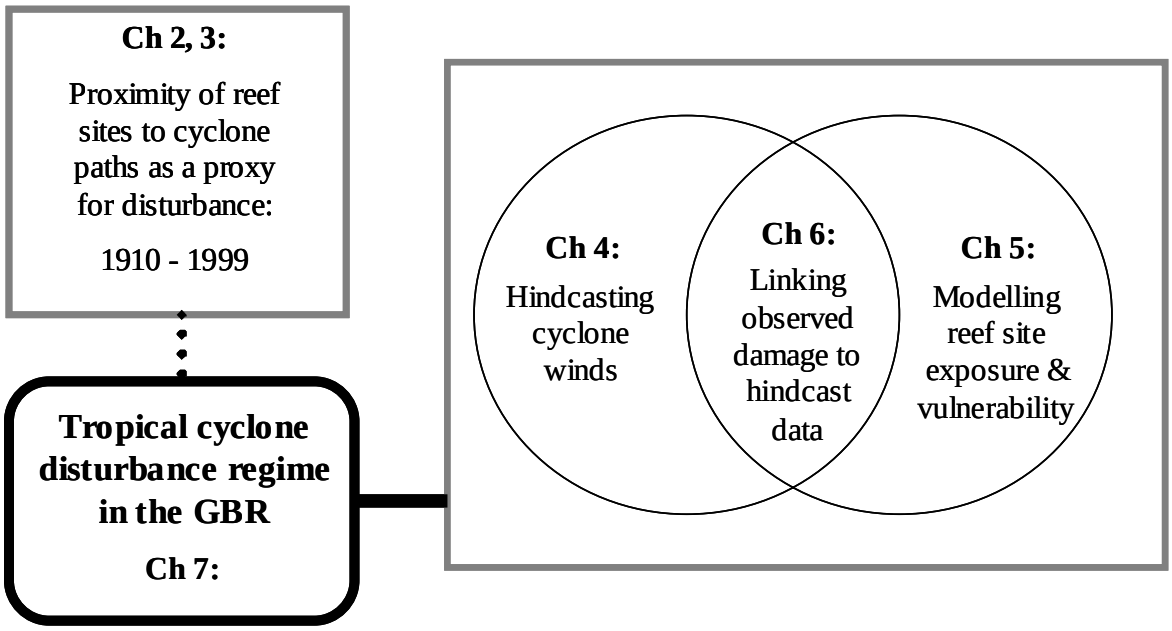

Figure 1.20. Overview diagram of this thesis.

- Assess the limitations of using proximity to the cyclone path alone as a proxy for the potential for reef community disturbance (Chapters 2 and 3).

- Implement and test models to reconstruct the distribution of cyclone energy across the GBR using five test cyclones (Chapter 4).

- Explore techniques developed from ecological and spatial models to estimate reef community exposure and vulnerability to that energy using five test cyclones (Chapter 5).

- Link the cyclone energy and reef exposure and vulnerability factors predicted above to field observations of actual cyclone damage using classification and regression tree (CART) analysis (Chapter 6).

- Use the resultant model to predict the cyclone disturbance history for the 85 cyclones that have passed near the GBR from 1969 to 2003 (Chapter 7).

- Examine the basic characteristics (intensity, frequency, duration) of cyclone disturbance across the reef communities of the GBR (Chapter 7).

CHAPTER 2: Potential for cyclone disturbance, 1910-1999

2.1 Overview

The proximity of a reef to a cyclone path is the simplest proxy possible for damage potential at that reef. Calculated for the entire time series of cyclones (1910-1999), it provides a broad characterization of the GBR cyclone disturbance regime (Figure 2.1).

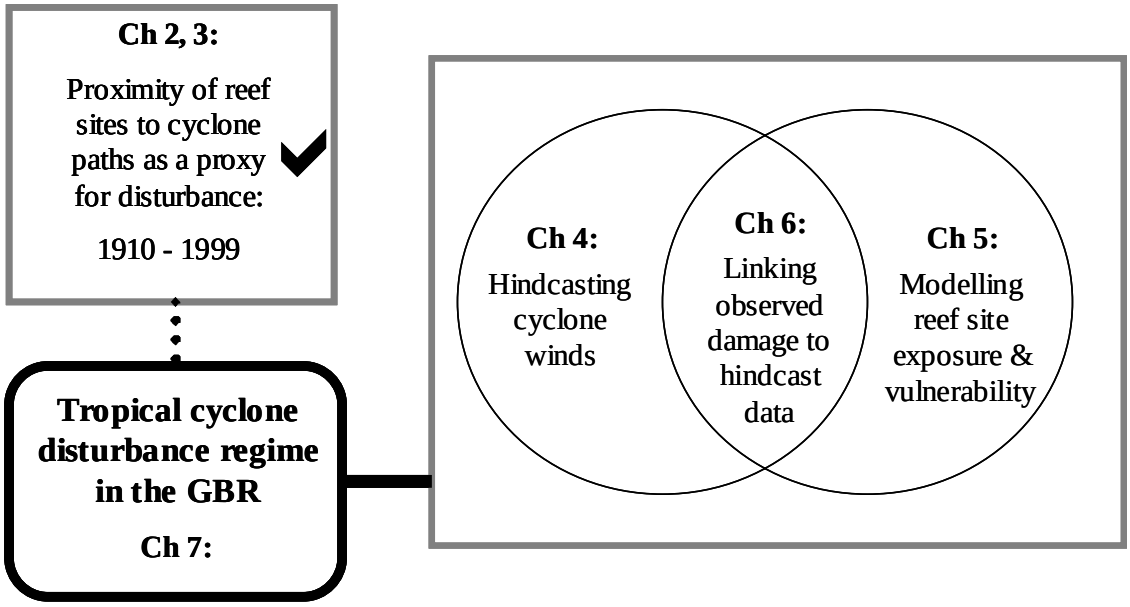

Figure 2.1. Overview diagram of this thesis. The check mark indicates the current chapter.

The remainder of the thesis presents a much more in-depth effort to characterize the cyclone disturbance regime over the latter portion of the time series - 1969-2003.

2.2 Introduction

In the period 1910-1999, nearly half (170) of the 342 tropical cyclones identified in Queensland waters tracked near (within 100 km, as explained in section 2.2.2) the GBR (Figure 2.2).

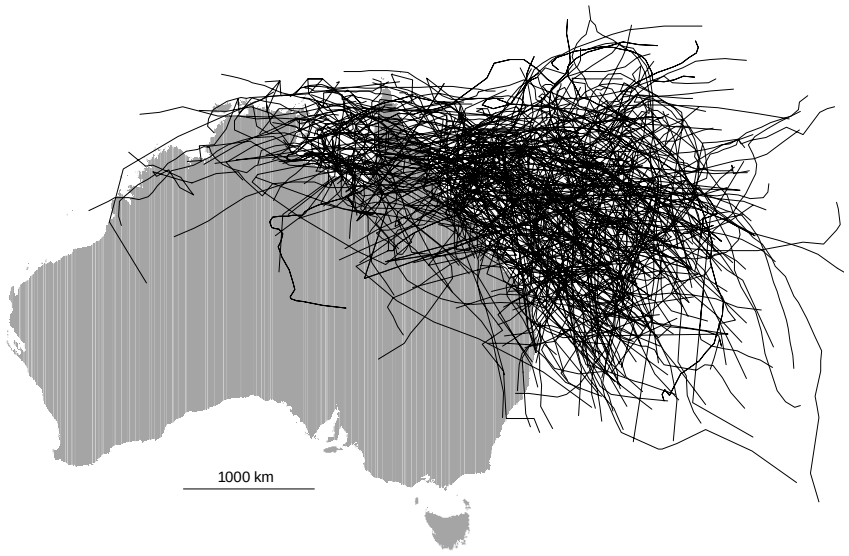

Figure 2.2: Tropical cyclone paths near Queensland, Australia from 1910 to 1999. Tracks were generated from the tropical cyclone database (Australian Bureau of Meteorology 2002).

It is likely that many of these had the potential to generate waves of sufficient energy to damage coral reef communities. Whether or not this potential was realised depended on many factors, such as the intensity and speed of the cyclone, its nearest proximity and angle of approach with respect to particular reefs, and the vulnerability of those reefs to wave damage (Harmelin-Vivien 1994). With basic meteorological

data, it is possible to model these factors, as will be shown in Chapters 4 and 5 of this thesis.

The path taken by each of the cyclones that passed near the GBR was constructed from data provided by the Australian Bureau of Meteorology (Australian Bureau of Meteorology 2002) using methods that are described in Chapter 4. For much of the time series (1910-1968), the positional accuracy of these paths is highly uncertain, with potential errors of up to 250 km in any direction (Holland 1981). Despite this, and because cyclone paths within the GBR are known to be highly variable over time (Holland 1984a), the full time series was examined using the proximity of each cyclone to reefs across the GBR as a proxy for the potential for disturbance.

2.2.1 Selecting study reefs

The damage potential based on distance alone was investigated for 218 reefs on the GBR (Figure 2.3). These were reefs at which ecological surveys by the AIMS Long Term Monitoring (LTM) program are documented in status reports for 1996, 1997, 1998, and 2000. These sites were chosen with the ultimate aim of being able to compare actual measures of reef community structure (ie current coral coverage) with those predicted by the frequency and timing of cyclone disturbance events, once a sufficient time series of coral coverage measurements is assembled. Each reef's position was recorded in GIS as the latitude and longitude of its centroid. Of these

reefs, 96 (44%) had been surveyed three times or more over the time period. Reefs in the central GBR (south of 14^0S and north of 22^0S) are best represented in the monitoring program to date.

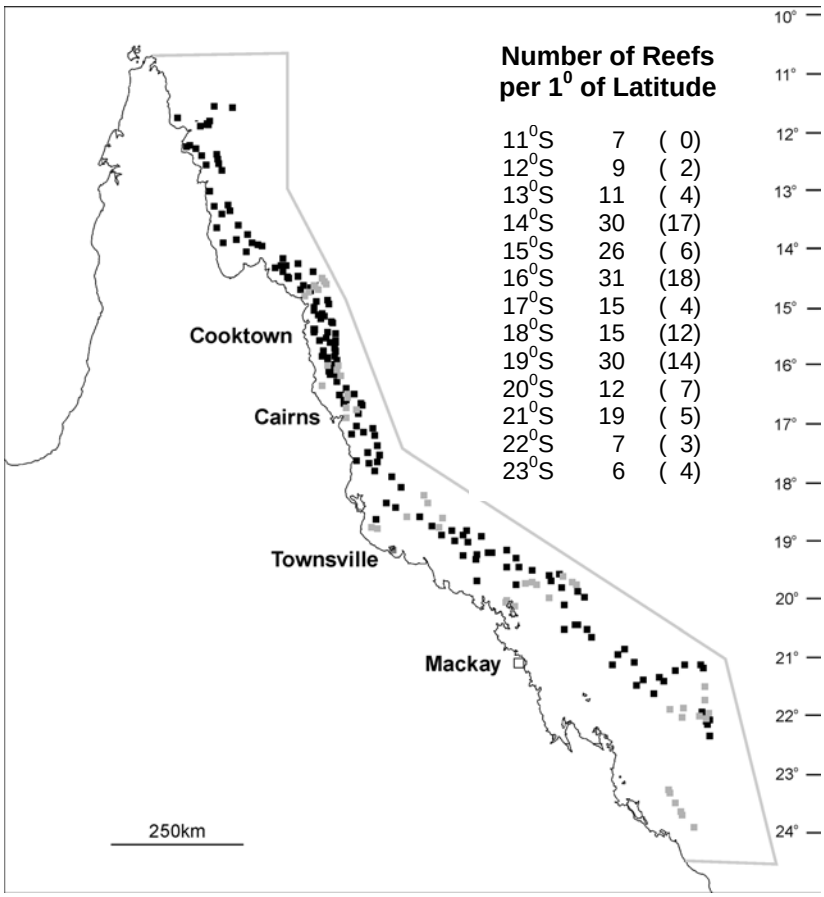

Figure 2.3: Location of reefs where at least one (black squares) or at least three (gray squares) surveys were conducted from 1992 to 1999 by AIMS. The gray polygon outlines the GBR Marine Park. The number of reefs that were monitored for each 1^0 of latitude is listed (number of reefs surveyed at least three times are in brackets).

2.2.2 Setting disturbance thresholds

Of the two studies that have investigated cyclone damage to more than a handful of reefs for more than one or two events (Woodley 1992, Treml et al 1997), both used distance to the cyclone path as a proxy for the potential for disturbance. For example, Woodley (1992) assumed that coral communities (specifically, *Acropora spp*) at Discovery Bay, Jamaica could have been damaged if located within 65 km of a hurricane path. Similarly, Treml et al (1997) assumed islands in the Lesser Antilles could have been damaged by high winds if located within 35 km (severe) and 60 km (minor) of a hurricane.

In the GBR, most cyclones pass through relatively quickly, usually within a day (notable exceptions include cyclones Kerry - 1979, Rewa - 1992, and Justin – 1997, which persisted for weeks). In addition, the GBR acts as almost a complete barrier to waves generated seaward of the region (Young and Hardy 1993). For these reasons, cyclone waves that damage GBR reefs (except for those located on the outermost shelf – ie ribbon reefs) typically build from local, wind-driven seas. As a result, this damage predominantly occurs in close proximity to the cyclone's path, and its severity generally decreases with distance from the path. For example, Done (1992b) found scattered patches of damage extending from the cyclone's path to a distance of about 100 km. Moderate to severe damage was limited to within about 30 to 50 km. Connell et al (1997) attributed a decline in coral coverage observed on Heron Island Reef to cyclones located as far as 100-200 km away. Based on these observations, the

potential for *any* disturbance was assumed to exist for all reefs located within 100 km of any particular cyclone's path, and *major* disturbance for all reefs located within 25 km of a cyclone's path.

2.2.3 Estimating cyclone disturbance potential

The minimum distance from each LTM reef to the closest segment of each cyclone's path was calculated using GIS and the results exported to a spreadsheet in Excel. For each cyclone, reefs located within 25 km were assigned a value of 2, those within 100 km were assigned a value of 1, and those beyond 100 km were assigned a value of 0. From this dataset, four interrelated measures of disturbance potential were compiled (any disturbance = 1 or 2, major disturbance = 2). The timing of cyclone disturbance was measured in yearly increments (measuring timing in days was not justified given a general inability to model coral recovery from cyclone damage on short time scales). Because the cyclone season typically spans from November to May, cyclones that occurred in November or December were considered as part of the following year. For example, a value of 1990 would be recorded for cyclones that tracked near the GBR during November or December 1989.

The cyclone-free interval represents that uninterrupted time period during which no cyclone paths were located within 100 km (any disturbance) or within 25 km (major disturbance) of the reef in question. The number of cyclone-free intervals provides a

measure of the frequency of predicted disturbances over the time series at each reef. The median length of the cyclone-free intervals provides a measure of how long reefs were typically cyclone-free (the median is used because cyclone-free intervals tend to form a negative exponential distribution, see Baker 1992, Xue and Neumann 1984). The maximum length of cyclone-free intervals was also recorded (i.e. the longest time corals have been able to grow undisturbed), as was the number of years since the last predicted disturbance (i.e. the most recent cyclone-free interval in the time series, measured from 1999). Comparing this to the length of the median cyclone-free interval (by subtracting the median length from the most recent length) indicates the degree to which current conditions at a reef reflect what was typical for that reef over the entire study period (Woodley 1992).

It is important to note that, for sites to which a cyclone did not pass nearby (within 100 or 25 km) in the first or last years of the study period (1910 and 1999), the least and most recent cyclone-free intervals (first and last) are 'open' and thus may be underestimates (known in statistics as 'censoring' – see D'Addio and Rosholm 2002, Singer and Willett 1991). In the former case ('left-censoring'), the year in which the last cyclone passed near a site prior to 1910 is unknown. In the latter case ('right-censoring'), the number of years it will take before the next cyclone passes near a site after 1999 is unknown. The presence of censoring in the time series primarily affects the calculation of the return interval (median length of cyclone-free intervals), by potentially underestimating its value. However, removing all sites affected by

censoring from the analysis is unacceptable due to the low number of sites, particularly in the far north where cyclones are least frequent. Removing the censored intervals from the time series of individual sites is also unacceptable. For example, the left-censored periods are typically quite long – their removal would bias the calculation of the median interval more than does the fact that they represent an underestimate of the true length of the initial interval. In general, the uncertainty introduced into the results by censoring is considerably less than that created by other unavoidable sources (most notably errors in the positioning of the cyclone paths and the lack of consideration of intensity). For the more sophisticated cyclone disturbance history described in the remainder of this thesis, however, steps were taken to address the issue of censoring (see chapter 7).

Each of the four measures described above was calculated for each LTM reef using Excel. This was done separately for predictions of any versus major disturbance potential. To identify broad trends in these measures, the GBR was divided into one-degree latitude by one-degree longitude blocks (Figure 2.4), within which values for the reefs were averaged.

	Longitude												
Latitude	142	143	144	145	146	147	148	149	150	151	152	153	*Total*
10	0	0	0										0
11	0	6	1										7
12		9											9
13		7	4										11
14		0	10	20									30
15				26									26
16				24	7								31
17					15								15
18					6	8	1						15
19					1	2	12	12	3				30
20							2	4	5	1	0		12
21								0	2	7	9		18
22								0	0	0	8		8
23									0	2	4		6
24										0	0	0	0
Total	0	22	15	70	29	10	15	16	10	10	21	0	218

Figure 2.4. The Great Barrier Reef divided into one-degree latitude by one-degree longitude blocks. The number within each block indicates the number of reefs periodically monitored by AIMS located therein: white = 0, light grey = 1-9, dark grey = 10-19 and black = >20.

2.3 Disturbance potential in the GBR

2.3.1 Distribution of cyclone paths

Over the past 90 years (1910-1999), fewer cyclones (3-7) tracked through the far north (north of 12^0S) than the rest of the GBR (mean = 19, Figure 2.5). In contrast, up to 10 times more cyclones (30-31) tracked through the central GBR near Townsville (18-19^0S at 147^0E). In general, the number of cyclones declined with movement

north and south from this central GBR 'hotspot'. The lack of reported cyclones in the far north, however, could be partly due to under-reporting in the early part of the time series when cyclone detection was difficult in remote areas (Holland 1981), although fewer cyclones generally form close to the equator due to lessening of the Coriolis Effect.

	Longitude												
Latitude	142	143	144	145	146	147	148	149	150	151	152	153	*Mean*
10	6	4	3										4
11	6	7	5										18
12		12											12
13		14	11										13
14		22	19	18									20
15				21									21
16				20	29								25
17					25								25
18					24	31	30						28
19					21	31	23	18	23				23
20							21	23	26	29	27		25
21								17	21	20	22		20
22								13	18	16	22		17
23									5	13	21		13
24										10	15	17	14
Mean	6	12	10	20	25	31	25	18	19	18	21	17	19

Figure 2.5: Number of cyclones that tracked within each one degree latitude by one degree longitude block from 1910 to 1999: white = less than 10, light gray = 10-10, dark gray = 20-29, black = 30 or more. Note: many cyclones passed through more than one block.

More cyclones tracked near LTM reefs after the start of the 1970s (Figure 2.6), possibly because cyclones were generally under-reported before 1969 (Holland 1981).

The exception to this was around the time of World War II when military activity in the Coral Sea was high.

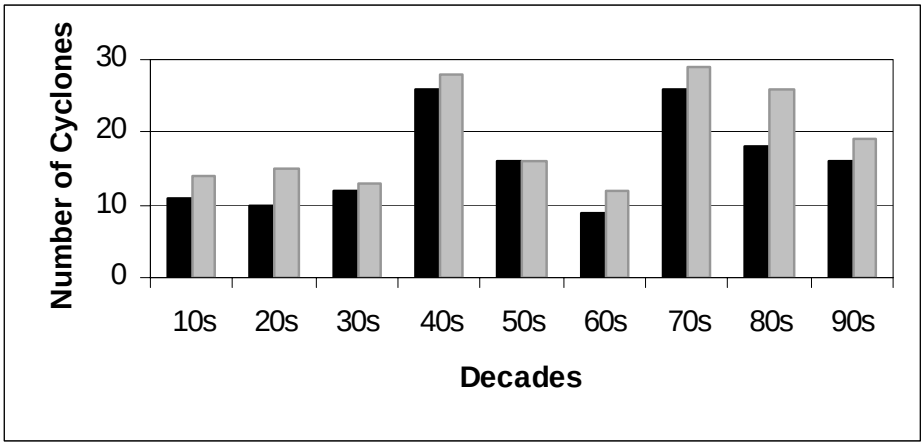

Figure 2.6: Number of cyclones that tracked within 25 km (black bars) or 100 km (gray bars) of at least one AIMS LTM reef in each decade from 1910 to 1999. Note: the gray bars include the black bars.

The density of cyclone paths in the GBR was greatest in the 1940s and 1970s (Figure 2.7). Further, fewer cyclones tracked through the far north than the rest of the GBR over the early part of the time series, especially in the 1910s, 1930s, and 1950s. It seems unlikely that the unusually straight set of cyclone paths shown in the southern GBR from 1910-1919 would repeat exactly during the following decade. This is likely due to an error in the cyclone database.

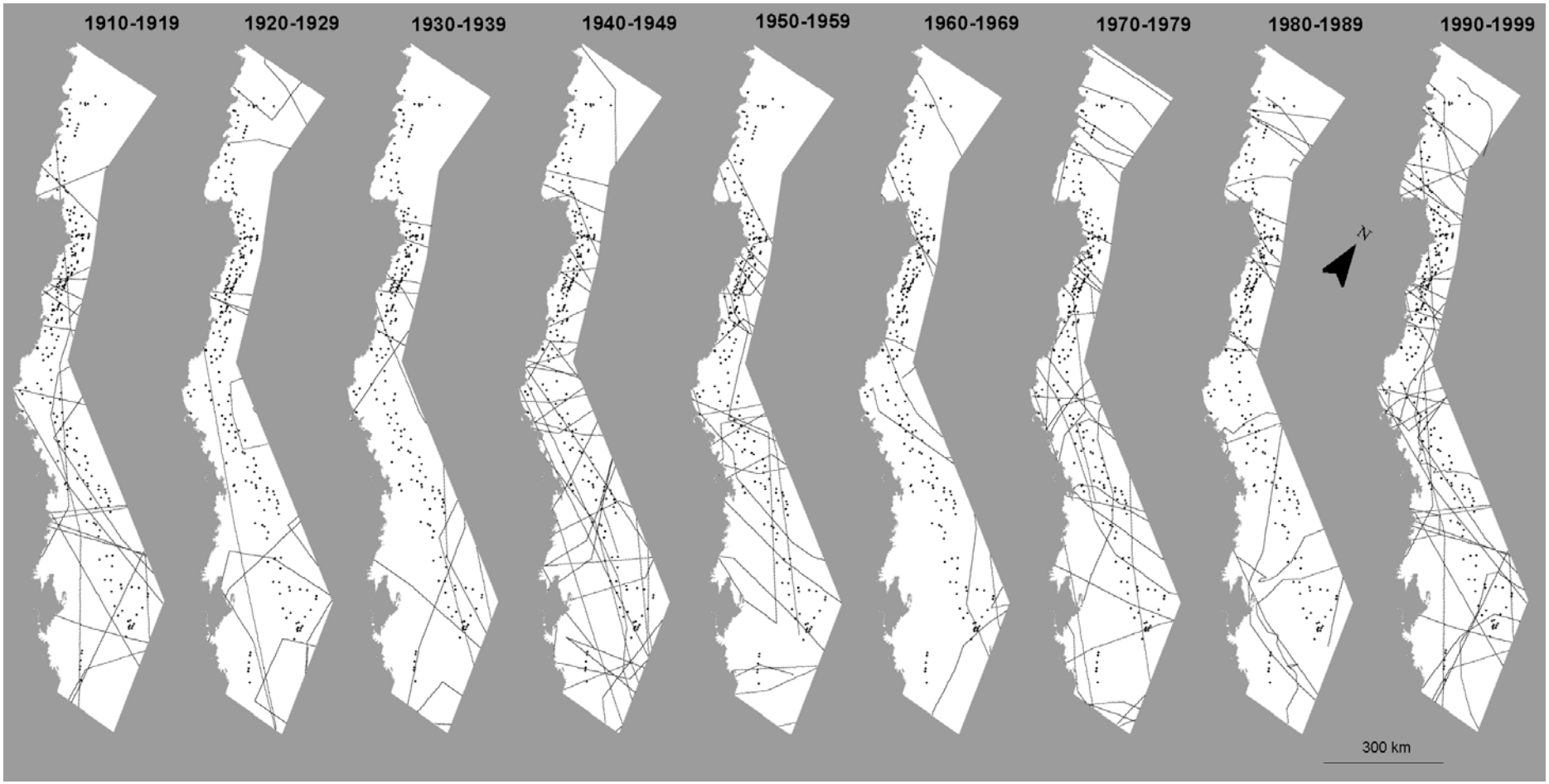

Figure 2.7: Tropical cyclone paths through the Great Barrier Reef by decade from 1910 to 1999. Black squares indicate the location of AIMS LTM reefs. The white shading shows the extent of the GBR Marine Park. Grey lines show cyclone paths.

2.3.2 Variability across the GBR

The minimum distances between each LTM reef and each cyclone were averaged by decade, grouped by AIMS sector (see Sweatman et al. 1998), and tested for differences over time and space using a multivariate repeated measures test. To remove heteroscedasticity from the data (unequal variances over the time series), a cube root transformation was used (Zar 1996). This test revealed significant differences ($p=0.05$) between time sectors (decades) as well as between geographic regions (sectors). This suggests that the proximity of cyclone paths to LTM reefs varied considerably across and along the GBR region as well as over time, reflecting the erratic nature of the cyclone paths shown in Figure 2.2 and Figure 2.7.

2.3.3 Incidence of disturbance potential

The potential for any disturbance was relatively common across the GBR – all areas were located within 100 km of a cyclone path at least ten times over the past 90 years (Figure 2.8-A). This was particularly true for the southern GBR. Accordingly, the median cyclone-free interval was very short – less than five years across the entire region (Figure 2.8-B). The lengths of the cyclone-free intervals were highly variable, with the majority of the LTM reefs experiencing at least one cyclone-free period that was a decade or more long (this extended to three decades in the far north - Figure 2.8-C). Finally, most of the GBR (as represented by LTM reefs) was located within 100 km of a cyclone path very recently (Figure 2.8-D).

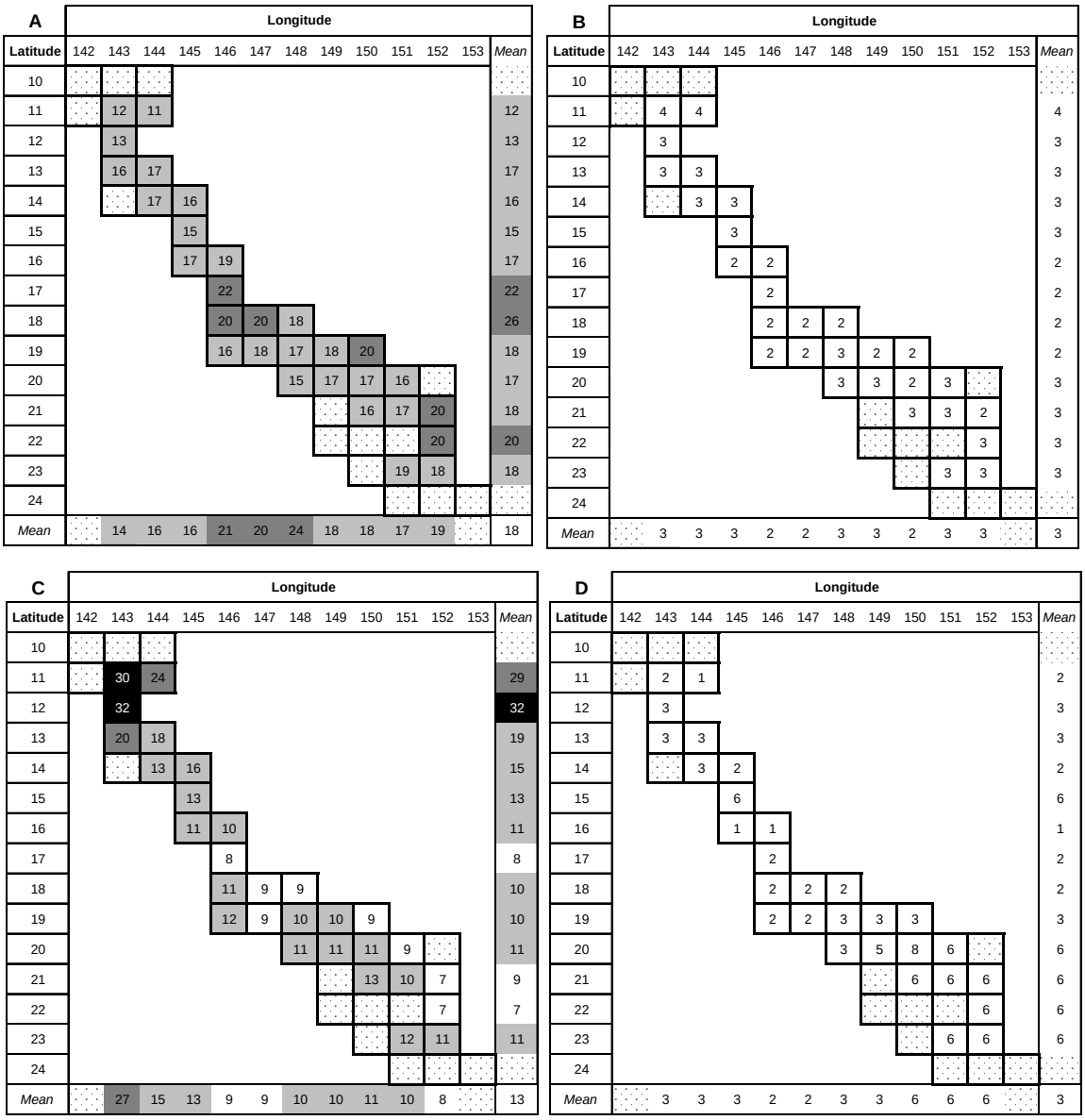

Figure 2.8. Potential for any disturbance. Distribution of AIMS LTM reefs located within 100 km of a cyclone path across the GBR from 1910 to 1999: A – number of cyclone-free periods, B – median length of cyclone-free periods, C – maximum length of cyclone-free periods and D - number of years since the last distant cyclone (as of 1999), averaged in each 1^0 latitude by 1^0 longitude box. The colour of each box indicates the relative number of years: white = <10, light grey = 10-20, dark grey = 20-30, black = >30. White boxes with black dots indicate that no reefs were surveyed.

In contrast, cyclones passed within 25 km of reefs much less frequently (Figure 2.9-A). This was particularly true for the northern GBR where only four cyclones passed within 25 km of any LTM reefs over the time series. Thus, the median cyclone-free interval was up to four times as long (Figure 2.9-B) than was the case for any disturbance.

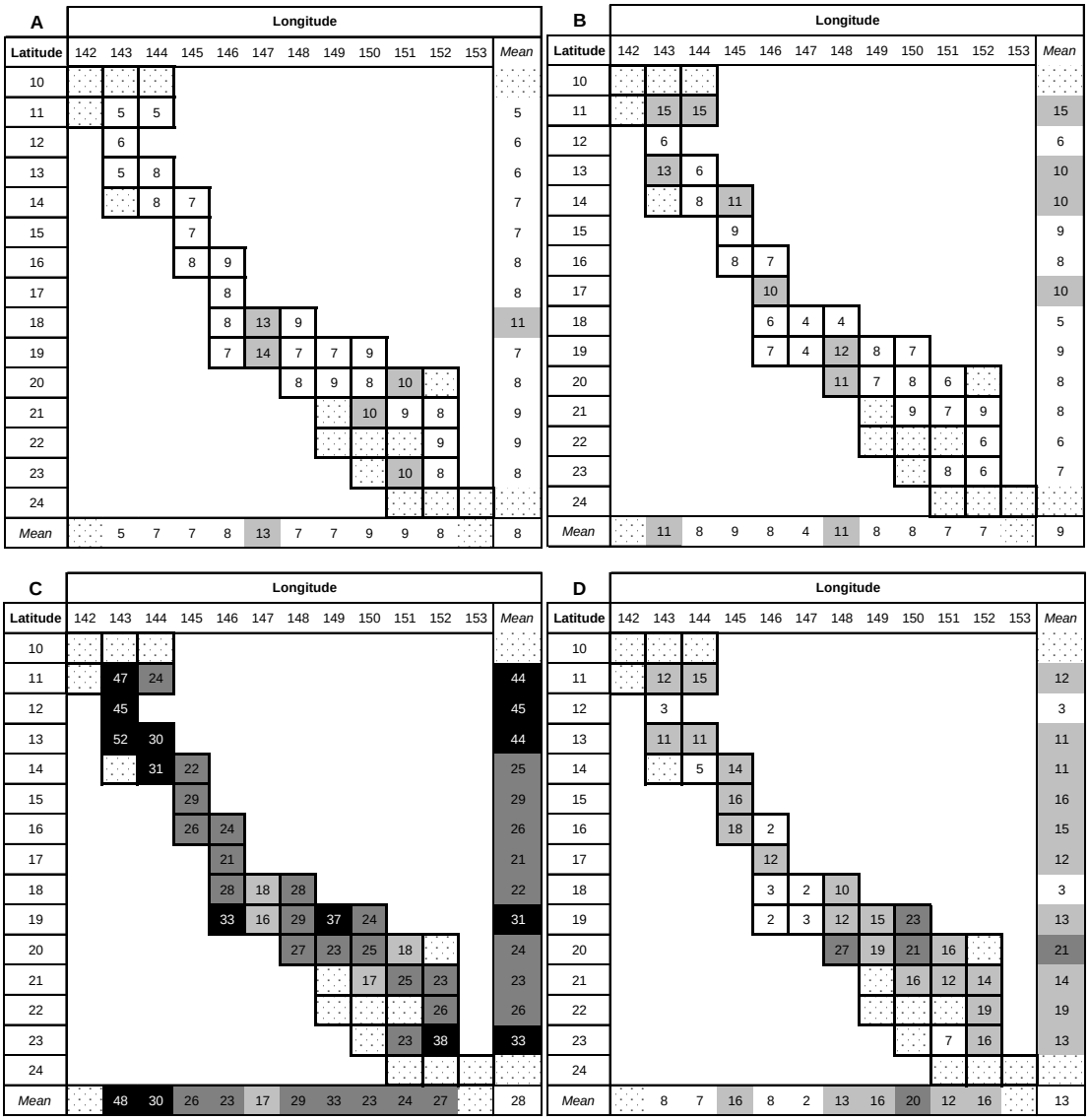

Figure 2.9. Potential for major disturbance. Distribution of AIMS LTM reefs located within 25 km of a cyclone path across the GBR from 1910 to 1999: A – number of cyclone-free periods, B – median length of cyclone-free periods, C – maximum length of cyclone-free periods and D - number of years since the last nearby cyclone (as of 1999), averaged in each 1^0 latitude by 1^0 longitude box, averaged in each 1^0 latitude by 1^0 longitude box. The colour of each box indicates the relative number of years: white = <10, light grey = 10-20, dark grey = 20-30, black = >30. White boxes with black dots indicate that no reefs were surveyed.

Coral communities have thus had more time to grow between major disturbances, albeit the cyclone-free intervals were still quite variable. For example, some reefs in the far north had cyclone-free intervals of four to five decades at least once during the

time series (Figure 2.9-C), which would likely be sufficient for recovery from even severe cyclone damage. In general, these maximum cyclone-free intervals were much longer for major disturbances (mean = 28 years) than otherwise (mean = 13 years). Finally, with the exception of the reefs located offshore between Townsville and Cairns, most of the GBR had not had a cyclone path pass within 25 km over the last ten to twenty years (Figure 2.9-D).

To estimate how the timing of the most recent disturbance event differed from what was typical for the time series (recent disturbance anomaly), the median number of years between disturbances was subtracted from the number of years since the latest disturbance (measured from 1999, Figure 2.10).

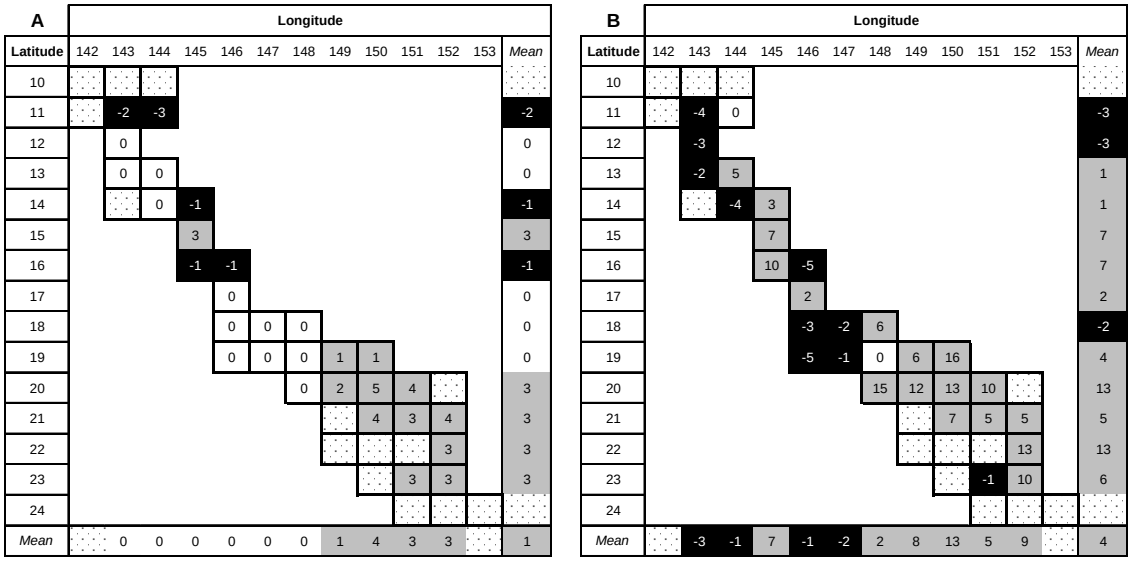

Figure 2.10. Recent disturbance anomaly. Distribution of AIMS LTM reefs across the GBR and the timing of the most recent disturbance relative to the median cyclone-free interval from 1910 to 1999: number of years since the latest disturbance (measured from 1999) minus the median number of years between disturbances for A – any disturbance, and B – major disturbance, averaged in each 1^0 latitude by 1^0 longitude box. Black boxes (negative anomaly values) indicate that the latest disturbance occurred more recently than normal (less time to recover). Gray boxes (positive anomaly values) indicate that the latest disturbance occurred less recently than normal (more time to recover). White boxes (zero anomaly values) indicate that the latest disturbance occurred at the median interval. White boxes with black dots indicate that no reefs were surveyed.

For any disturbance (Figure 2.10 – A), the mean anomaly value for all LTM sites was slightly positive (+1), although the sites were evenly split between negative (more disturbed recently than normal), zero, and positive (less disturbed recently than normal) values. However, a distinct spatial distribution of anomaly values was apparent when LTM sites were averaged by one degree latitude / longitude box. LTM sites with a negative anomaly (more disturbed recently than normal) were limited to the northern GBR (north of 17^0S), while sites with a positive anomaly (less disturbed recently than normal) were primarily concentrated in the southern GBR (south of 18^0S), and sites with neutral values (timing of recent disturbance was indicative of that of the entire time series) were found in the central and mid northern GBR. In contrast, for major disturbance (Figure 2.10 - B), the mean anomaly value for all LTM sites was more strongly positive (+4), with a positive anomaly value recorded for nearly 60% of the sites. Further, zero anomaly values were much more rare (~6% of sites) than for any disturbance. In general the magnitude of the anomaly was much stronger for major disturbance (as these events are more rare), particularly for positive anomalies. However, for some sites this effect may be overstated if censoring is considerable, particularly on the left side of the time series (ie, if the earliest cyclone-free interval is actually much longer than measured). Finally, the spatial distribution of anomaly values was much less distinct for major disturbance, although the highest positive anomaly values for major disturbance were still found in the southern GBR.

2.3.4 Summary

The paths taken by tropical cyclones through the GBR are erratic and quite variable over time. Therefore, the timing of predicted disturbances (when based on proximity

to the path alone) were also quite variable. For example, on average, reefs located within the box situated at 12^0S and 143^0E were located within 25 km of a cyclone path six times, with a median cyclone-free interval of six years (range – 1 to 45 years). As would be expected, most of the GBR was much more frequently located within 100 km, rather than 25 km, of a cyclone path, and thus had a probability of sustaining any, rather than major, disturbance. However, the intensity of the cyclone is also important - for the most part, a weak cyclone could not generate major disturbance regardless of how close it tracked to a reef. These issues of cyclone intensity and the potential for reef damage are investigated in Chapters 3, 4 and 6. Finally, roughly equal numbers of the LTM sites were disturbed more (northern GBR), less (southern GBR) and equally (central GBR) recently than normal for any disturbance, while for major disturbance most sites were disturbed less recently than normal.

2.4 Implications for coral reef communities

In 1992, AIMS established the LTM program to 'detect changes over time in reef communities at a regional scale' (Sweatman et al. 1998) by surveying reefs which span the entire width and breadth of the GBR. Reefs, spread across the vast GBR region, are subject to varying conditions in both the ambient environment and from episodic natural disturbances. While LTM reefs have been monitored since 1992, natural cycles of disturbance operate over decadal (or longer) time scales. So, a key question to ask is how the state of coral communities (i.e. % coral coverage) on reefs monitored during the 1990s fits within a long-term picture for the GBR. Woodley (1992) posed such a question for the north coast of Jamaica, finding some evidence

that dense thickets of branching corals observed in the 1950s, 60s and 70s were not typical over 120 years due to changing patterns in cyclone disturbance. This chapter poses a similar question for the GBR, asking whether the timing of cyclone disturbance in recent times (within the last decade) was typical of what happened over the past 90 years (1910-1999). The results suggest that, for all disturbances, this is only the case for about one third of the GBR, with reefs to the south less disturbed and reefs to the north more disturbed recently than what was typical for the entire time series. This suggests that reefs in the southern GBR (~one-third of sites) may have had more time to recover from the latest disturbance than normal – coral communities in these areas may contain larger colonies and greater coral coverage at present than would be expected on average over the time series. For major disturbance, the latter was true (more time to recover recently than normal) for nearly 60% of the GBR, although the spatial pattern was less distinct.

It is also useful to consider whether coral communities generally have had enough time to recover between subsequent cyclone disturbances – that is, whether cyclone disturbance is high (not enough time to recover) or intermediate (sometimes enough time to recover) in the GBR (see Figure 1.9, chapter 1). To do so requires an estimate of the time needed for coral communities to recover from a minor versus a major disturbance. If, for example, we assume that this recovery period is a decade for major disturbance, then all of the reefs (on average) would have had enough time at least once during the last 90 years to recover (intermediate disturbance). However, if we assume that coral communities require more than 50 years to recover from a major disturbance, then very few of the LTM reefs would ever have had time to recover (high disturbance). If we assume that coral communities need five years to recover

from a minor disturbance, then all of the LTM reefs have had plenty of time to recover at least once (average maximum cyclone-free period = 13 years), but not always (median cyclone-free period = 3 years). Research suggests that percentage coral cover can 'recover' from zero in 5-10 years, whereas coral age structure or repair of framework can take decades or even centuries (Done and Potts 1992). Thus, the nature of the cyclone disturbance regime (high versus intermediate) depends on how disturbance is defined and measured.

Ultimately, it would be valuable to test the degree to which broad measures of coral community structure (% coral coverage, dominant growth form and size class) can be predicted for a particular time period at a site based on the history of cyclone disturbance alone. This is not possible at present due to insufficient data. For example, it would be unreasonable to attempt to predict absolute percentages of coral coverage from the cyclone history alone because local scale processes and other disturbances are likely to obscure the disturbance signature. Instead, with a sufficient time series of data, one could estimate whether the extent of coral coverage in a particular year was unusually high (suggesting less cyclone disturbance recently than normal), typical (suggesting the timing of the last cyclone disturbance was normal) or low (suggesting more cyclone disturbance recently than normal), and test this against the cyclone history. The techniques presented in this chapter could be used to extend the cyclone disturbance history until such time that a sufficient set of coral coverage and associated data have been gathered to enable such a test.

2.5 Conclusions

This analysis used the distance of a reef to the nearest cyclone path as the sole indicator of the potential for any versus major disturbance from that cyclone. Key factors that influence the likelihood of disturbance, most notably the cyclone intensity, could not be considered due to a lack of data for much of the time series. Thus, the frequency of major disturbance was very likely overestimated because severe cyclones tend to be rare in the GBR. For example, Puotinen et al. (1997) found that, in the period 1969-1997, relatively weak (category 1 or 2) cyclones were much more common in the GBR region than severe cyclones (category 3, 4, or 5). Further, only 14 of the 84 cyclones (16.7%) that tracked near the GBR between 1969 and 2000 were severe while located inside the region. In addition, while cyclone damage to reefs has been observed to occur within 100-200 km of a cyclone path (Van Woesik et al 1991, Done 1992b, Connell et al 1997), it is also known to be highly patchy in distribution within that zone (Harmelin-Vivien 1994). So, many of the reefs located within the threshold distance for disturbance would not actually have been damaged. Thus, the results of this analysis represent a 'worst case scenario' for cyclone disturbance of the GBR. Another consideration is that the spatial distribution of the LTM reefs within each of the one-degree latitude by longitude boxes is not indicative of the actual frequency of reefs. A more extensive set of reefs, designed to reflect the relative distribution and size of reefs within each box, is therefore needed to effectively identify trends in cyclone disturbance across the GBR. This is presented in Chapter 7. These issues are addressed in the remainder of this thesis, which aims to characterize the cyclone disturbance history over the period from 1969-2003, for which adequate data is available to model the potential for cyclone disturbance of reefs in more depth. Chapter 3 examines the extent to which

considering the distance to the path alone could predict patterns of reef damage from five cyclones for which field observations of damage was available (Ivor, Joy, Justin, Althea and Celeste). Chapter 6 presents a statistical model with which cyclone damage can be predicted from measures of hindcast cyclone energy (Chapter 4) and reef exposure and vulnerability to that energy (Chapter 5). Chapter 7 presents the results of using that model to predict damage across the GBR from each cyclone that passed near the GBR from 1969-2003.

CHAPTER 3: Distance as a proxy for cyclone disturbance potential

3.1 Overview

Tropical cyclones generate high winds that, with adequate fetch, build heavy seas in the vicinity of the storm system. The resultant large waves breaking along shallow reefs can damage coral communities in a range of ways, depending on the magnitude and duration of the wave energy and the vulnerability of the communities. Examining the combination of the maximum intensity and size of a cyclone may indicate the types and severity of wave damage that was possible, but not the spatial distribution of that damage around the cyclone path. For normal sized cyclones in the GBR, wave damage appears to be restricted to a zone located within about 100-200 km from a cyclone path (Done 1992b, Connell et al 1997). Given this, and the general lack of direct measurements of cyclone energy, the distance of a reef site from the cyclone path has been used as a crude proxy for the potential for wave damage (for example, Treml et al 1997, Woodley 1992, chapter 2 of this thesis). Because many additional factors affect both the spread of cyclone energy around the path and the vulnerability of reef sites to that energy, a significant percentage of sites within the predicted damage zone will not actually be damaged. In addition, establishing the damage zone for unusually large and/or stationary cyclones is problematic. For example, large waves generated in the maximum wind region can ‘out run’ the cyclone (Young 1988), potentially damaging reef sites located hundreds of km away from the cyclone centre. This chapter uses field data of wave damage from three cyclones in the GBR to demonstrate that while cyclones of characteristic combinations of size and intensity do produce similar types and severities of damage (disturbance signatures), the spatial

distribution of this damage cannot be adequately predicted by proximity to the cyclone path alone.

Chapter 2 used distance to the cyclone path alone as a proxy for disturbance potential for a subset of the GBR (AIMS long term monitoring sites) from 1910-1999. The present chapter assesses the limitations of that approach, and establishes the need for the more detailed modelling that is presented in the remainder of the thesis (Figure 3.1).

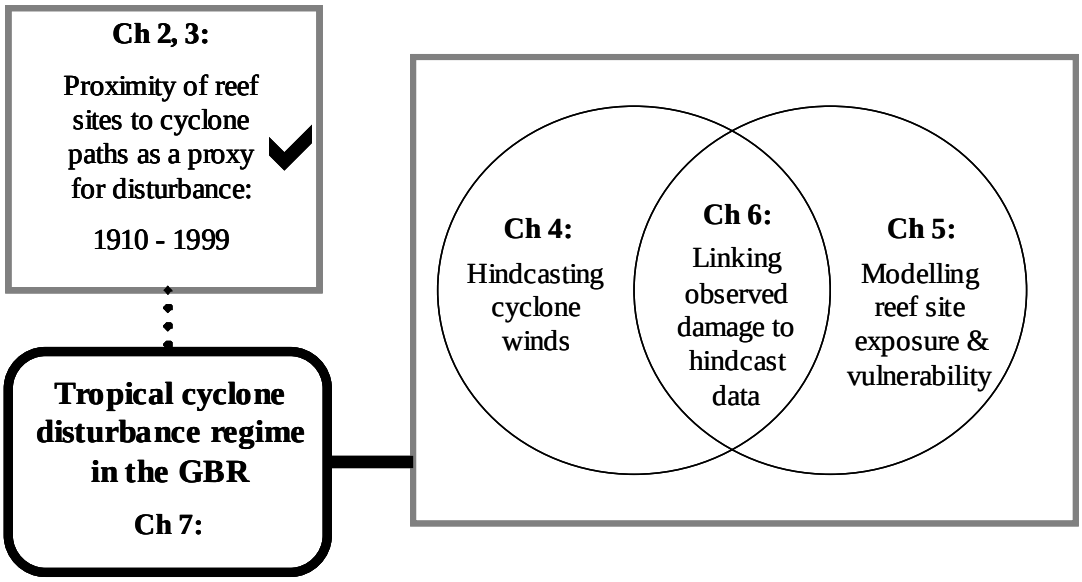

Figure 3.1. Overview diagram of this thesis. The check mark indicates the current chapter.

3.2 Introduction

Despite the devastation that cyclone waves can cause to coral reef communities, field observations of damage over the past 35 years are relatively rare. Because it is impossible to predict the path of a cyclone, most ecological studies of cyclone damage to reefs are opportunistic in nature. Often it is when physical damage or loss of coral

coverage is observed in the field that researchers question whether a cyclone could have been the cause. In the absence of observations at the site directly before and after the cyclone in question, the simplest and most intuitive way to assess whether this was likely is to consider the proximity of the cyclone to the site. For example, Connell et al (1997) observed sites at Heron Island Reef over a 30-year period and postulated that several incidences of coral cover loss could have been caused by cyclones tracking nearby. However, several other factors besides distance to the path greatly influence the potential for damage, most notably the cyclone intensity and size of its circulation.

3.2.1 Distance as a proxy for damage potential

The proximity of reef sites to a cyclone path is a convenient measure to use as a proxy for the potential for wave damage. Because cyclone wave damage is known to be highly patchy in spatial distribution (Harmelin-Vivien 1994), this method simply identifies areas within which damage may have occurred. In many cases, so little data about particular cyclones exists that this approach is the only reasonable method possible, particularly for studies with a long time series where field measurements of neither cyclone energy nor actual damage are available. For example, Woodley (1992) used a threshold distance of 65 km to assess the potential of each of 39 hurricanes that passed near Discovery Bay, Jamaica from 1874-1988 to destroy stands of *Acropora spp* corals. Similarly, Treml et al (1997) assumed islands in the Lesser Antilles could have been damaged by high winds if located within 35 km (severe) and 60 km (minor) of hurricanes that tracked near the region from 1886-1995. In chapter 2 of this thesis, threshold distances of 25 and 100 km were used to indicate risk of

major and any disturbance at 213 GBR reefs from cyclones passing nearby from 1910-1999.

The highest wind speeds and wave heights at any given position of a cyclone are generally found near the radius of maximum winds and gradually decrease with distance from the eye (Holland 1980). As a cyclone moves, so does this high-energy zone, generating a swath of maximum winds and waves around the cyclone path. Consequently, holding other factors constant, the frequency and severity of wave damage to reefs could be expected to generally decrease with distance from the cyclone path. Because the highest cyclone energy at any given eye position is concentrated in the front left quadrant (southern hemisphere), cyclone energy and reef damage potential are generally highest on the left side of the cyclone path. Although waves may propagate beyond their region of formation when cyclones move very slowly, this is relatively rare in the GBR. Thus, for the most part, wave damage to reefs could be expected to decrease with distance from the cyclone more quickly on the right side (southern hemisphere) of its path (Table 3.1). Based on Table 3.1, a cyclone moving southward through the GBR between Innisfail and Townsville would be expected to damage 253 reefs (Figure 3.2) to varying degrees: 21% - high, 36% - low, and 43% - very low.

However, using distance to the cyclone path alone to predict wave damage is simplistic for a variety of reasons. Most obviously, cyclones are known to vary in intensity, speed of forward motion, and size along their paths, which greatly affects the spatial distribution of the high winds and waves that they generate.

Table 3.1: Threshold distances from the cyclone path within which wave damage of varying severity (based on the extent to which damage is widespread across a range of types – see Figures 1.17, 1.18 and Appendix 3) could be expected to occur. Based on Done 1992b and discussion with T. Done (1994). Shaded boxes indicate distances within the range of positional uncertainty in the cyclone path (see section 4.4.7).

Severity of wave damage		**Distance to the cyclone path (km)**	
		Right	*Left*
High	Damage of at least 3 types is widespread.	0 - 25	0 - 50
Low	Damage of at least 1 type is widespread.	25 - 50	50 - 100
Very Low	No observed damage is widespread.	50 - 100	100 - 200

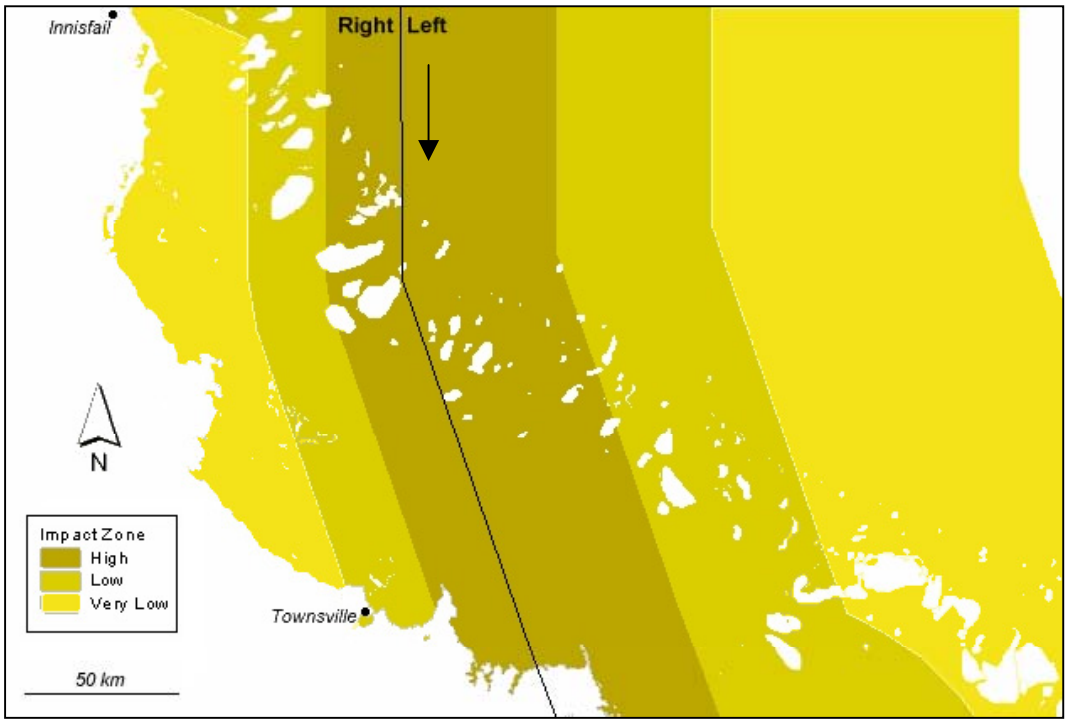

Figure 3.2: Expected distribution and severity of wave damage based only on the distance to the cyclone path (thin black line). The coast, islands and reefs are shaded white.

Further, for cyclones that are unusually large or very slow moving, cyclone energy may not decrease with distance from the path as expected (see Chapter 4). Equally important is the highly variable nature of reef vulnerability to damage from waves. Vulnerability at each site of interest depends on a range of factors, such as its relative exposure to incoming cyclone waves, its history of disturbance, and the normal wave climate (see Chapter 5).

3.2.2 Importance of cyclone intensity and size

The intensity of a cyclone (weak = categories 0-2, strong = categories 3-5) determines the maximum wind speeds and wave heights possible (see Table 1.1 in chapter 1). To predict the distribution of the damage they cause, however, also requires a measure of the area across which these high-energy conditions extend. For this, the areal extent of the cyclone circulation (size) is as important as its intensity. In a typical sized cyclone, maximum wind speeds decrease rapidly with distance from the radius of maximum winds (Holland 1981), and are concentrated in close proximity to the cyclone path. In an unusually large cyclone, the wind gradient is flatter (the high wind region extends much further from the cyclone centre), expanding the region of maximum wave formation. The opposite is true for an unusually small cyclone. Cyclone size is only weakly correlated to intensity (Merrill 1984). For example, Cyclone Tracy (Australia, 1974) and Typhoon Tip (north Pacific, 1979) were both very intense, but vastly different in size. Tracy's region of high winds, on average, extended only ~50 km from the eye (Australian Bureau of Meteorology 1977) while Tip's extended over 1,100 km (Dunnavan and Diercks 1980).

Meteorologists measure cyclone size either by 1) determining the average extent of a threshold wind speed (usually gale force winds, 17 $m.s^{-1}$) or 2) finding the average radius from the eye to the last closed isobar - ROCI (Merrill 1984). Synoptic charts showing pressure gradients are used for the latter measurement. Figure 3.3 illustrates the differences in ROCI for an unusually small (A), typical (B) and unusually large (C) cyclone. Cyclones with a ROCI greater than 4 degrees latitude (~ 444 km) are generally considered to be large (Merrill 1984), though a threshold value of 500 km is used for the GBR (Callaghan and Smith 1998) because cyclones in the Australian region tend to be larger in size than elsewhere (Holland 1984c). To examine the relative size of cyclones within the GBR, the mean size was calculated for all cyclones for which size was recorded in the Australian Bureau of Meteorology's tropical cyclone database (Australian Bureau of Meteorology 2002). This included 54 cyclones from 1984 to 2000 (n=1163). Cyclones with an average ROCI greater than 2 standard deviations from the mean for the GBR, or with an average radius of gales winds greater than 500 km, were classified as large. Cyclones with an average ROCI or average radius of gales less than 111 km (as per Callaghan and Smith 1998) were classified as small. The remaining cyclones were classified as typical in size.

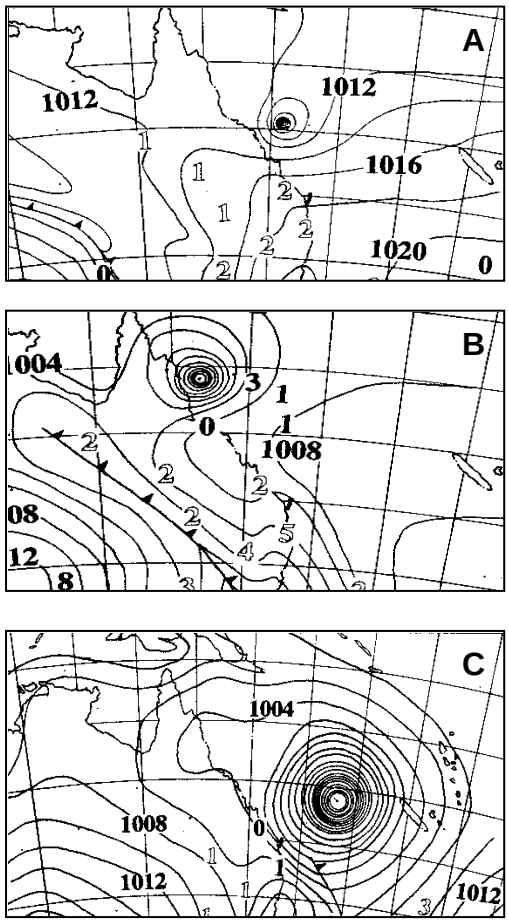

Figure 3.3: Synoptic charts showing typical surface air pressure profiles for cyclones with a geometric size that is: A - unusually small (Ada 1970), B - typical size (Joy 1990), and C - unusually large (Betsy 1992). Cyclone size is measured as the average radius (km) from the cyclone eye to the last closed isobar (ROCI). Charts were obtained from the Bureau of Meteorology, Brisbane Office, Severe Weather Section.

Most cyclones from 1984 to 2000 (73.2%) were typical in size (Figure 3.4). Of those, almost half were strong at some point during their life cycle. In contrast, large (18.5%) and small (11.2%) cyclones were less abundant. Large + weak cyclones (2) and small + strong cyclones (1) were particularly rare over the past two decades. Although size measurements are missing from the cyclone database before 1984, some notable large and small cyclones and their general impacts across the region before that time have been identified (Callaghan and Smith 1998).

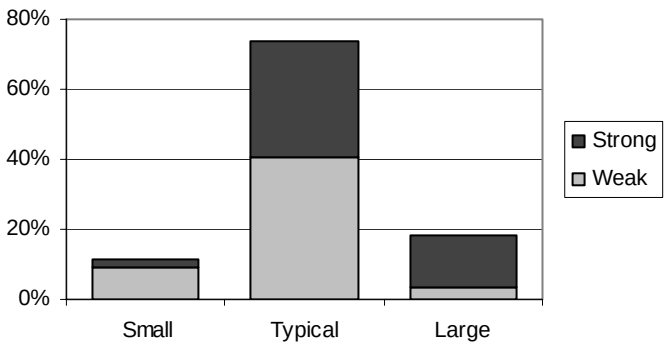

Cyclone size	Cyclone Intensity	
	Weak (0-2)	*Strong (3-5)*
Small	**9.3%** (Gillian '97)	**1.9%** (Ada '70)
Typical	**40.7%** (Justin '97)	**33.3%** (Ivor & Joy '90)
Large	**3.7%** (Justin '97)	**14.8%** (Pam '74)

Figure 3.4: Frequency of cyclone sizes and intensities in Queensland waters from 1984 to 2000 (54 cyclones, n=1163). Big cyclones had average ROCI values at or above 500 km. Small cyclones had average ROCI values at or below 111 km. Strong cyclones had minimum central pressures at or below 970 hPa. Data was obtained from the Bureau of Meteorology Tropical Cyclone Database as of March 2002.

For example, cyclone Ada was small and strong, and caused severe damage when it passed through the Whitsunday Islands region in 1970. In contrast, cyclone Agnes was large and strong when it crossed the Queensland coast at Townsville in 1956. While reef damage was not recorded, it was likely because extensive wind damage on land was reported from as far away as Cairns. Cyclone Pam was also large and strong, causing significant storm surge along the entire Queensland coast south of Cairns despite never tracking closer than 450 km to the coast (Hopley and Harvey 1974). The swells it generated likely affected a large number of reefs along the outer continental shelf. Given that large and strong cyclones can potentially affect such a large area, it is of concern that nearly 15% of the cyclones fall within this category.

We can define six characteristic cyclone events based on cyclone size and intensity (Table 3.2). The potential for large waves to form will vary for each characteristic

event (as the extent and intensity of the maximum wind region changes). Presumably, then, the types and severity of damage (see Figures 1.17, 1.18 in chapter 1) caused by each combination of size and intensity would differ as well.

Table 3.2: Predicted characteristics of wave damage from combinations of cyclone size and intensity.

Cyclone size	**Cyclone Intensity**	
	Weak (0-2)	*Strong (3-5)*
Small	Very localised and patchy low-energy damage **1**	Very localised high-energy damage, scattered low-energy damage **2**
Typical	Localised low-energy damage **3**	Localised high-energy damage, scattered low-energy damage **4**
Large	Widespread low-energy damage, localised high-energy damage **5**	Widespread high-energy damage **6**

3.3 Case studies

The severity (as measured by the extent to which damage was localised versus widespread within a site) and types of damage (low versus high-energy, see Figures 1.17 and 1.18 in chapter 1) expected to be possible from each characteristic event ranges from very localised low-energy damage (ie breakage of scattered small colonies) for a small and weak cyclone to widespread and catastrophic high-energy damage (ie exfoliation on entire sections of reef) for a large and strong cyclone. Cases 3 – 5 can be tested using field observations of wave damage in the GBR from cyclones Ivor (1990), Joy (1990) and Justin (1997).

3.3.1 The dataset

Eighty-five cyclones have tracked near (within 100 km) the GBR from 1969 to 2003. However, detailed field observations of the resultant wave damage on GBR reefs are rare (Table 3.3), documenting the effects of only five cyclones in four seasons at 397 sites on 133 reefs. The 397 sites surveyed are biased towards the presence rather than absence of damage.

Table 3.3. Field observations of cyclone wave damage on the GBR from 1969 to 2003.

Year	Cyclone	# Sites	# Reefs	% Sites Damaged	Region	Source
1971	Althea	32	13	100	Townsville, Whitsundays	Pearson 1974, reported in Hartcher 2001
1990	Ivor	63	33	75	Far north - Cooktown	Done et al 1991
1990	Joy	186	33	63	Cairns - Cooktown	Ayling 1991
1996	Celeste	7	6	63	Whitsundays	Malcolm et al 1996
1997	Justin	54	13	56	Townsville, Whitsundays	This thesis
1997	Justin	55	35	60	Cooktown - Swains	This thesis (questionnaire)
TOTAL		**397**	**133**			

This is not surprising given the known patchiness of cyclone damage and the need to target surveys (to ensure finding at least some examples of damage) for logistical reasons. Table 3.3 does not include a long-term study of Heron Island (Connell et al 1997). Because that study examined a single reef (though for seven cyclones), the

sample size is too small to use for this project. Also not included are two surveys undertaken following cyclone Winifred in 1986 (Done et al 1986, Harriott and Fisk 1986) and one following cyclone Rona in 1999 (Cheal et al 2002). These were not suitable due to very limited sample sizes and lack of detail in the damage reports. Additional surveys documenting surface damage to island and coastline features (i.e. beach erosion) from cyclones such as Althea and Emily (Hopley 1972) indicate that some reef damage was likely. This data was not used, however, due to the difficulty of integrating it with the more detailed surveys. Finally, for cyclones Althea and Celeste, only information about the presence or absence of damage is available. Thus, this thesis used the field surveys from cyclones Ivor, Joy and Justin as the primary dataset. Data from cyclones Althea and Celeste was incorporated where possible and appropriate.

The number of sites and reefs surveyed, and their distance from, and position with respect to, the cyclone path differed for cyclones Ivor, Joy and Justin (Table 3.4). Ayling 1991 surveyed the most sites and reefs. Done et al (1991) surveyed sites at reefs located on the strong and weak side of Cyclone Ivor's path, while Ayling 1991 surveyed sites located only on the weak side of Cyclone Joy's path. The author surveyed sites in the Townsville region located on the strong side of Cyclone Justin's path. Sites surveyed in the Whitsunday Islands region were damaged when the cyclone was stationary and thus symmetrical (the side of the path was irrelevant). Cyclones Ivor and Joy were intense (category 3 and 4) when located near the surveyed sites, while cyclone Justin was weak (category 2). Cyclone Ivor passed through the GBR within a day, while Joy persisted for about a week, and Justin for nearly a month.

Table 3.4: Location of field sites at reefs surveyed following cyclones Ivor, Joy, and Justin.

	Done et al 1991	**Ayling 1991**	**Puotinen et al 1997 - field survey**	**Puotinen 1997 - questionnaire**
Cyclone	Ivor	Joy	Justin	
Dates	19 Mar 1990	22-27 Dec 1990	6-23 Mar 1997	
Maximum category near sites	3	4	2	
Number of sites surveyed	46	212	55	55
Number of reefs surveyed	35	46	13	36
Distance of sites from the path	0.5 - 124 km	37-222 km	~250 km	5-508 km
Side of the path	Most on left (strong) side	All on right (weak) side	On both sides	On both sides

Each survey used random snorkel and/or SCUBA swims to assess the severity of a range of damage types (see Figure 1.18 in chapter 1) observed in the upper few metres (usually 0-12 m depth). Each site was assigned a damage score between 0 and 5 for each of the eight types of damage. Scores of 1 versus 5 indicated very localised versus very widespread incidence of damage across the site, respectively. The definition of damage types differed slightly between the field surveys and were thus standardised to facilitate comparisons (Table 3.5). Where damage types were consolidated to form a single category, the maximum value was retained. Methods of assigning the damage scores also varied slightly between surveys. For example, half scores (ie 0.5) were used during the cyclone Joy survey – these were rounded up to

the next highest whole number. In addition, damage during cyclone Justin was scored on a scale of 0 to 3 rather than 0 to 5. These scores were transformed to fit within the latter scale using linear interpolation.

Table 3.5: Types of damage surveyed following cyclones Ivor, Joy, and Justin.

Description of damage	Done et al 1991	Ayling 1991	Puotinen et al 1997 (field survey)	Puotinen 1997 (questionnaire)	**New damage category**
Coral breakage		**x**	**x**		1
Broken coral tips	**x**				
Snapped plate corals	**x**				
Staghorn colonies totally demolished				**x**	
Staghorn colonies with tips broken				**x**	
Large areas of freshly killed / broken coral				**x**	
Evidence of soft corals ripped off	**x**	**x**	**x**		2
Piles of rotting material (algae, soft corals)				**x**	
Debris scarring on intact coral heads	**x**	**x**	**x**		3
Craters in reef matrix	**x**				4
Scooping of reef matrix	**x**				
Trenching / stripping of reef matrix			**x**		
Reef top swept clear				**x**	
Sand scouring		**x**			5
Sand movement	**x**		**x**		
Evidence of sandblasting of corals and gross sand movement				**x**	
Rubble movement		**x**			
Extensive tracts of recent staghorn rubble				**x**	
Collapse of large intact reef slabs					6
Dislodgement of massive coral heads	**x**	**x**	**x**		7
Large coral heads overturned				**x**	
Exfoliation (disintegration of reef matrix)	**x**	**x**	**x**	**x**	8

Low-energy ↑ ↓ High-energy

Sites located at the higher energy reef front were generally surveyed more often (except for cyclone Joy) and were damaged more often than sites located at more sheltered reef backs (Table 3.6).

Table 3.6. Field observations of wave damage presented by cyclone and type of habitat.

Cyclone	**Habitat**	Damage?				*Summary*
		No		**Yes**		
		#	*%*	*#*	*%*	
Ivor	*Back*	4	57	3	43	Mostly fronts were damaged. Fronts surveyed the most.
	Front	12	24	38	76	
	Other	0	0	6	100	
Joy	*Back*	76	72	30	28	Mostly fronts were damaged. Fronts and backs surveyed equally.
	Front	44	42	62	58	
Justin	*Back*	14	58	10	42	Mostly fronts were damaged. Slightly more fronts surveyed.
	Front	10	33	20	67	

Although the sites surveyed following cyclone Joy were split evenly between fronts and backs, a greater percentage of damaged sites were still located at fronts. This suggests that the direction from which large waves approached most reef sites was typical of ambient conditions. The direction towards which each part of a reef faces (aspect) also affected the likelihood of damage at the sites surveyed (Table 3.7). For cyclone Ivor, sites located on reef sections facing to the north were damaged most, while the opposite was true for cyclone Joy. For cyclone Justin, the greatest concentration of damage was found at southerly aspects. The least damage was found at westerly aspects for both Ivor and Justin, and to the north for Joy. Clearly, the dominant incoming wave direction during a cyclone is important and it differed for cyclones Ivor, Joy and Justin.

Table 3.7. Field observations of cyclone wave damage by cyclone and aspect of site.

Cyclone	**Aspect**	Damage?				*Summary*
		No		**Yes**		
		#	*%*	*#*	*%*	
Ivor	*North*	5	16	27	84	North damaged most. West damaged least.
	South	2	18	9	82	
	East	5	36	9	64	
	West	4	67	2	33	
Joy	*North*	33	53	29	47	South damaged most. North damaged least.
	South	29	47	33	53	
	Central	32	52	30	48	
Justin	*North*	7	58	5	42	South damaged most. West damaged least.
	South	9	32	19	68	
	East	4	50	4	50	
	West	4	67	2	33	

In general, high-energy damage (ie dislodgement of massive corals, exfoliation – see Figures 1.17, 1.18 in chapter 1) was least prevalent for cyclone Justin and most prevalent for Ivor. For the latter, high-energy damage was found within about 50 km of the cyclone path, and low-energy damage out to 100 km. For cyclone Joy, high-energy damage was concentrated within ~100 km of the path, and low energy damage was observed as far as ~200 km. For cyclone Justin, high-energy damage was observed at only one site, which was located more than 250 km away from the cyclone at the time. Low energy damage was scattered across nearly two-thirds of the GBR region. See Appendix 3 for more information.

3.3.2 Nature of the cyclones

Cyclone size, as measured by ROCI, varied throughout the life cycle of cyclones Ivor, Joy and Justin (Figure 3.5).

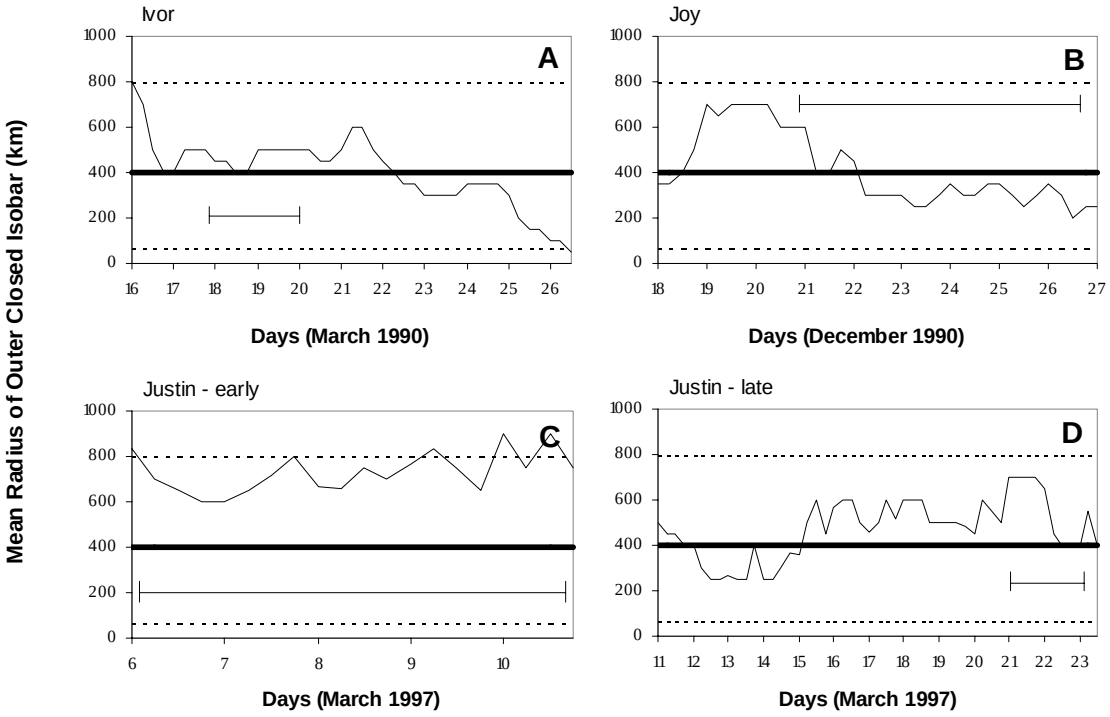

Figure 3.5: Variation in the geometric size of storm circulation as measured by the mean radius from the eye to the outer closed isobar (km) for cyclones: A - Ivor, B - Joy, C - Justin (early phase), and D - Justin (late phase). Cyclones are considered to be unusually large where radii are equal to or greater than 2 standard deviations (thin dotted lines) from the mean (thick black line). The mean and standard deviation was calculated from all cyclone observations for which geometric size was measured (54 cyclones from 1984-2000, n=1163). Data was obtained from the Bureau of Meteorology Tropical Cyclone Database as of March 2002. The thin bars indicate the time during which the cyclone was close enough to affect the study sites.

Although the size of both Ivor and Joy decreased over time, even at their largest both were' typical' in size for the GBR (within two standard deviations of the mean). Cyclone Justin, on the other hand, remained nearly stationary in the Coral Sea from 6-11 March (Hanstrom et al 1999). At this time, Justin's eye was very large, with a radius of 100 km (Callaghan 1997). In contrast, a typical eye in the north Pacific ranges between 16 and 30 km (Weatherford and Gray 1988) and in the GBR is 30 km (Callaghan 1997). Justin's size dropped dramatically as the cyclone weakened and tracked northeast, and remained within typical range until its eventual decay.

Figure 3.6 shows the maximum predicted geographic extent of gale force (17 $m.s^{-1}$) and hurricane force (33 $m.s^{-1}$) surface winds (another measure of cyclone size) for cyclones Ivor, Joy and Justin (note that actual wind speed will vary within this zone, see chapter 4 for more information). Although cyclone Justin was weak during its early phase, it generated gale force winds that consistently extended to a radius of about 600 km from the cyclone eye. This is about three times greater than was the case for cyclone Joy even though Joy was much more intense. Similarly, the spread of gale winds during cyclone Ivor remained confined to a radius of about 200 km, with a brief maximum of 400 km. Clearly then, early Justin was a large cyclone (spread of gales greater than 500 km) while Ivor, Joy and late Justin were not.

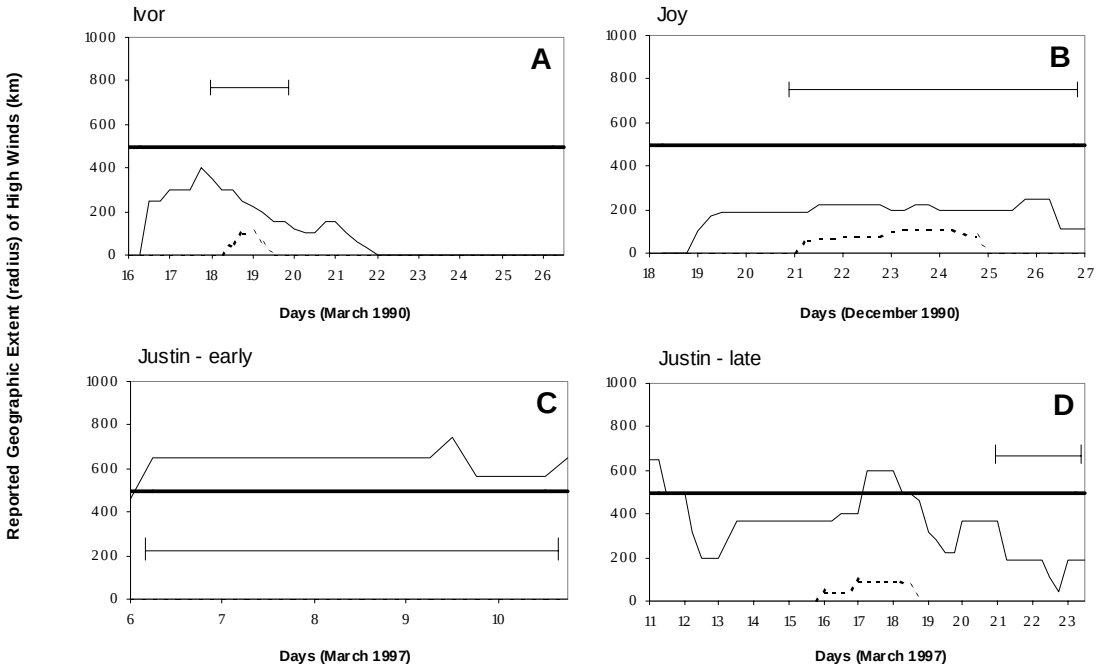

Figure 3.6: Geographic extent (average radius from eye) of gale force winds (solid line) and hurricane force winds (dotted line) reported during cyclones: A - Ivor, B - Joy, C - Justin (early phase), and D - Justin (late phase). The thick black line shows the threshold (500 km) for large cyclones. The thin bars indicate the time during which the cyclone was close enough to affect the study sites. Wind speed data was obtained from the Bureau of Meteorology Tropical Cyclone Database as of March 2002.

Maximum wind speeds, on average, increase as cyclone intensity increases (Shea and Gray 1973). Accordingly, predicted maximum winds were clearly highest during cyclone Joy, which was the most intense of the three cyclones (Figure 3.7). However, as was shown in Figure 3.6, Joy's hurricane force winds were restricted to a radius of about 100 km from the cyclone eye. In contrast, cyclone Justin's winds never reached hurricane force during its early phase, but extended over a huge area. During the second phase of the cyclone, winds strengthened to hurricane force for about two days while it tracked near Papua New Guinea, and then weakened to just above gale force as it crossed the Queensland coast. Hurricane force winds persisted for about a day during cyclone Ivor while it was strong, covering a similar radius as Joy.

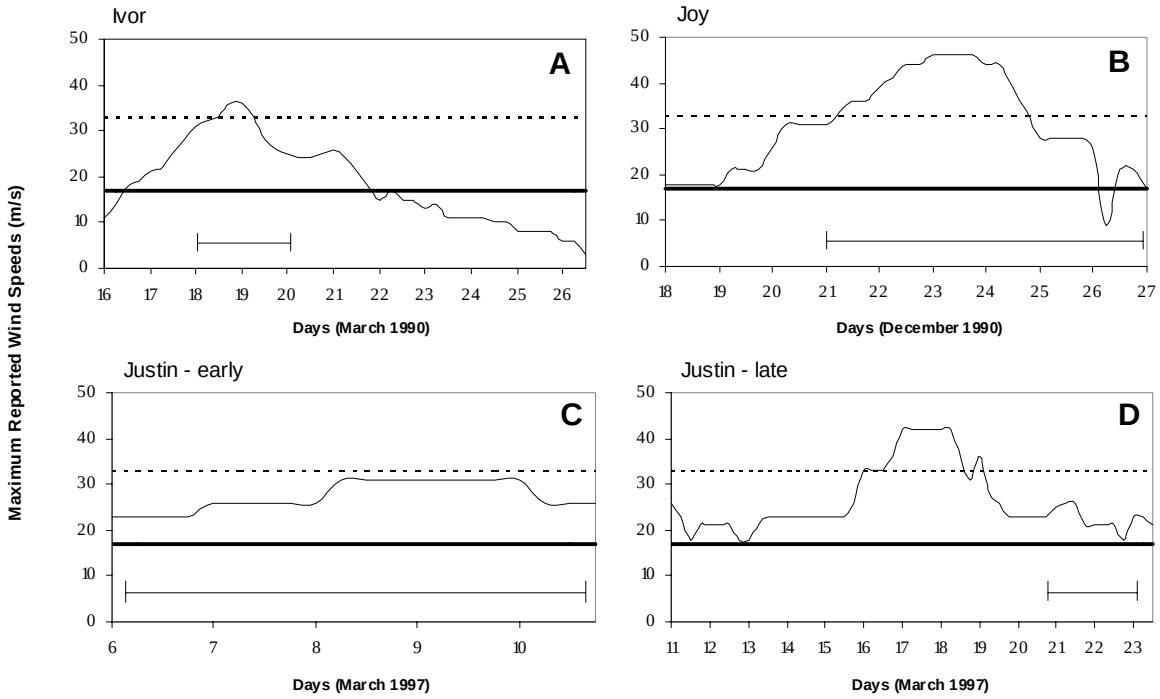

Figure 3.7: Maximum wind speed ($m.s^{-1}$) during cyclones: A - Ivor, B - Joy, C - Justin (early phase), and D - Justin (late phase). The thick black line and thin dotted line show gale force and hurricane force winds, respectively. The thin bars indicate the time during which the cyclone was close enough to affect the study sites. Wind speed data was obtained from the Bureau of Meteorology Tropical Cyclone Database as of March 2002.

With higher wind speeds, a greater amount of energy is available for wave formation. However, several factors influence the magnitude of the waves that a cyclone can generate from a given wind speed. The speed at which the cyclone is moving, the distance of open ocean over which the wind can blow unobstructed (fetch), and the duration of the prior two conditions are also important (Jelesnianski 1993). Thus, a very slow moving cyclone located over open ocean for a long period of time will be more effective at generating waves for a given wind speed. Accordingly, the maximum waves reported during the early phase of cyclone Justin (Figure 3.8) were consistently higher than those observed during cyclones Ivor and Joy (though the data set is incomplete), even when the latter generated wind speeds that were up to one-third higher.

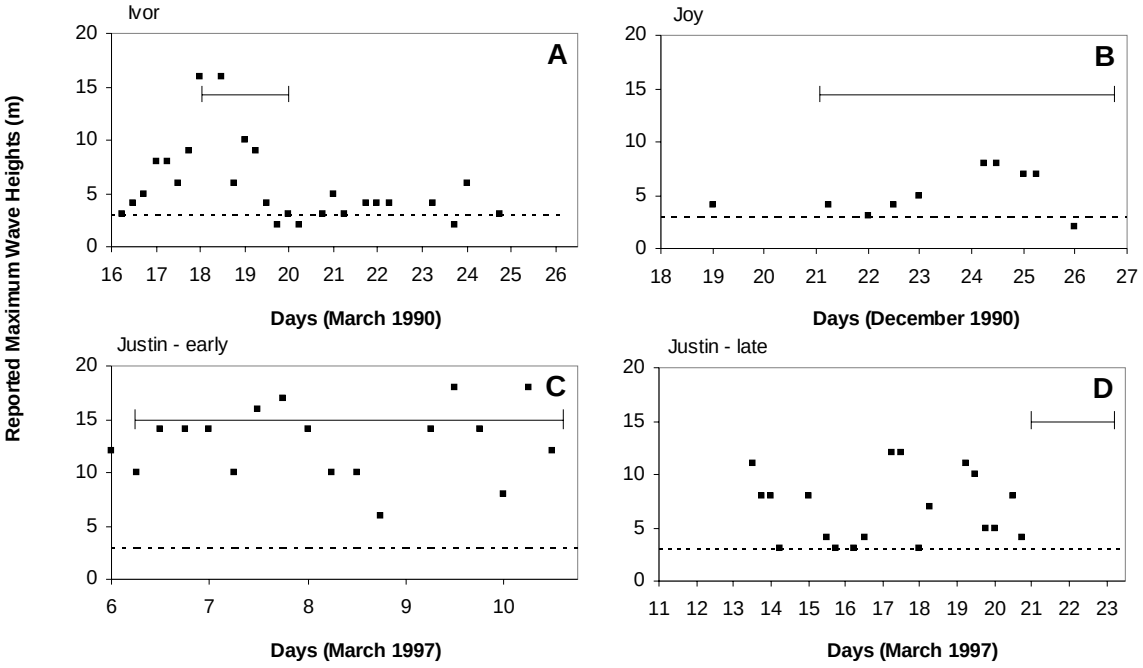

Figure 3.8: Reported maximum wave heights during cyclones: A - Ivor, B - Joy, C - Justin (early phase), and D - Justin (late phase). The dotted line shows the approximate broken wave height needed to produce a characteristic type of high-energy damage: dislodgment of unattached 1 metre wide massive corals at 6 metre depth (Massel and Done 1993). The thin bars indicate the time during which the cyclone was close enough to affect the study sites. Wave height data was obtained from the Australian Bureau of Meteorology's Tropical Cyclone Database (as of 2002).

Further, because gale force winds extended over such a large area during cyclone Justin, the wave generation region was larger than normal. Waves over 8 meters high were recorded near Mackay at a distance of nearly 470 km from the cyclone centre (Hanstrom et al 1999). Thus, maximum waves generated during the early phase of Justin, even though it was of weak intensity, were theoretically sufficient to produce a characteristic high-energy type of cyclone damage: dislodgment of unattached, 1 metre sized massive coral at 6 metres depth (Massel and Done 1993). Evidence of this type of damage was observed following Justin at Oublier Reef (see next section). In general, maximum waves decreased in height as Justin contracted to a more typical size even though it intensified. Unfortunately data is missing towards the end of the late phase of the cyclone when it passed close to the survey sites. Interestingly, cyclone Ivor generated a peak of much higher maximum waves than Joy (although the Joy observations are incomplete) from considerably lower wind speeds. Both cyclones were similar in size and moved at about the same speed. One possible explanation is that cyclone Joy tracked more erratically towards the coast than Ivor. The abrupt changes in Joy's direction could have produced more confused seas, reducing overall wave heights.

3.4 Implications for predicting reef damage

3.4.1 Cyclone size and intensity as a predictor of damage

The cyclones differed in the distribution, frequency, severity and types of damage (as defined in Table 3.5, Figures 1.16 and 1.17 in Chapter 1) they caused (Figure 3.9). Further, the extent to which a particular type of damage was observed at a study site

was classed as high (widespread, damage score $\geq$ 3) or low (localised, damage score 1-2).

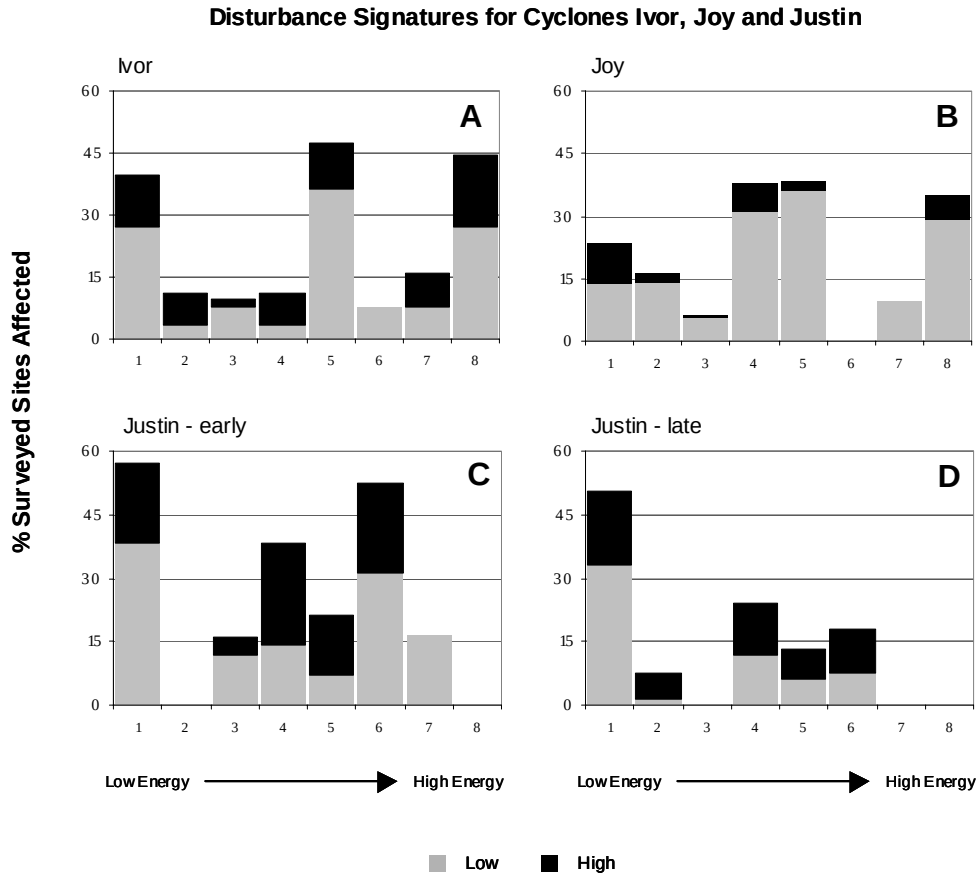

Figure 3.9: Disturbance signatures observed at coral reef communities surveyed following cyclones: A - Ivor, B - Joy, C - Justin (early phase), and D - Justin (late phase). Gray and black bars indicate the proportion of sites that sustained low versus high damage, respectively. The height of each bar shows the total % of surveyed sites damaged. Each bar (1-8) represents a type of damage, ranging from those that require relatively low energy (far left) to those that require relatively high energy (far right). Damage types are as follows: 1 = breakage, 2 = soft corals stripped, 3= debris scars, 4= trenching / stripping of reef matrix surface, 5 = rubble and/or sand movement, 6= entire slabs of reef dislodged, 7 = massive corals (eg, Porites sp.) dislodged, and 8 = exfoliation (entire sections of reef removed).

The proportion of high versus low damage and the frequency of damage was greater for Ivor than for Joy across all types except rubble / sand movement (5 on Figure 3.9) despite the fact that Joy was more intense than Ivor when closest to the study sites. For cyclones Ivor and Joy, the disturbance signatures were dominated by high-energy damage (types 5-8). Low-energy damage was less widespread, with the exception of

coral breakage (type 1). In contrast, the early phase of Justin generated very widespread low-energy damage (breakage at 60% of sites), some widespread intermediate damage (stripping at nearly 45% of sites) and scattered, patchy high-energy damage (dislodgment of massive corals at less than 15% of sites). No exfoliation (the highest energy type) was recorded following Justin, though it was widespread for sites affected by Ivor and Joy.

Further, the cyclone Justin questionnaire results indicate that damage extended across much of the GBR - from north of Cooktown to the far south. This is supported by reports of heavy swell and seas throughout coastal waters between Townsville and Cairns and massive beach erosion between Cairns and Innisfail (Hanstrum et al 1999) - conditions that are certainly sufficient to disturb reefs. Different again was the late phase of Justin (when the cyclone was very weak), which produced widespread low-energy damage (breakage at over 50% of sites) and no high-energy damage.

While the greatest potential energy for disturbance was generated by cyclones Joy and Ivor (high intensity – categories 3 and 4), this energy was distributed across a limited geographic area (typical size). In contrast, though the early phase of cyclone Justin produced lower potential energy (low intensity – category 2), it was spread over a very large area (large size). In addition, the cyclone was nearly stationary for almost a week while located over the open ocean. This virtually unlimited fetch allowed seas to reach full development (wind energy translation to waves at higher than normal efficiency for a cyclone). Because of this, even a relatively weak cyclone like Justin was able to cause widespread low-energy damage and patchy, limited high-

energy damage nearly equivalent in severity (but less widespread) than those generated by cyclones Ivor and Joy.

Presumably, a cyclone both large and strong could cause widespread catastrophic damage. Nearly 15% of Queensland cyclones since 1984 were both large and strong. Most of these cyclones tracked well seaward of the GBR while strong (Puotinen et al 1997), which may have limited their effect on reefs. However, the significant storm surge recorded during the large and strong cyclone Pam (Hopley and Harvey 1974) indicates that even a cyclone located quite distant from the GBR (~450 km from the coast) has the potential to damage at least the outer shelf reefs. Where possible, it would be useful to extend the time series of cyclone size further into the past to better estimate how frequently large and strong cyclones pass near the GBR and potentially damage coral communities. For example, by dating coral ridges and using models to predict the magnitude of wave energy needed to create them, Nott and Hayne (2001) were able to estimate that very intense 'super cyclones' crossed the GBR every 200-300 years over the past 5,000 years. At present, no field data is available for the GBR directly documenting reef damage from a large and strong cyclone. When the opportunity arises, priority should be given to documenting this type of disturbance signature.

3.4.2 Proximity as a predictor of damage

The relationship between the maximum severity of damage observed and the distance to the cyclone path (maximum severity of damage across all types, averaged by damage score) varied between cyclones Ivor, Joy and Justin (Figure 3.10).

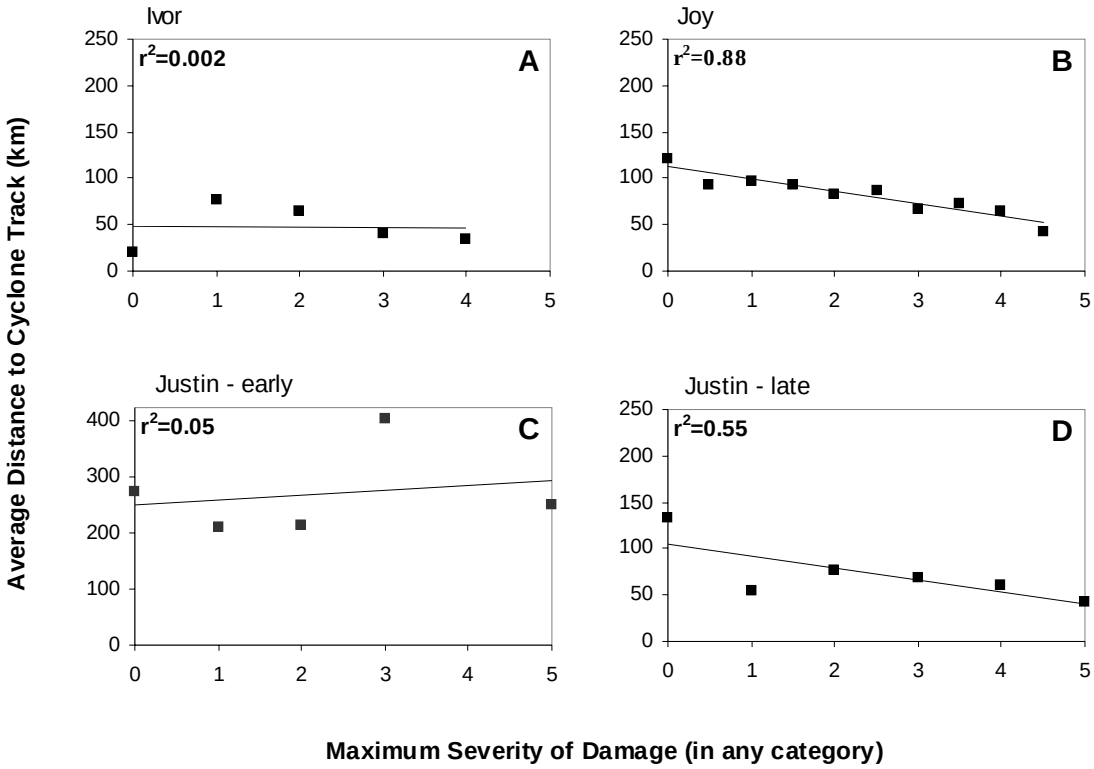

Figure 3.10: Relationship between the maximum severity of damage (across all types) and average distance (km) to the cyclone path for Cyclones: A - Ivor, B - Joy, C - Justin (early phase), and D - Justin (late phase). Distances were averaged by damage score (1 – very localised, 5 = very widespread). Cyclone paths were generated from the Australian Bureau of Meteorology's Tropical Cyclone Database (as of 2002).

Joy (B) exhibited the classic pattern one would expect, with damage severity declining with distance from the cyclone path. Ivor (A), on the other hand, showed no statistical relationship between the severity of damage and distance to the path. This could be due to differences in the survey designs. The Joy survey had a much larger sample size, extended further from the cyclone path (220 km, versus 124 km for Ivor), and included many more reefs likely to sustain no damage (Joy - 81, Ivor - 7). In contrast, the Ivor survey recorded a higher proportion of sites with no damage near the path. Because some sites surveyed near the path may not be damaged due to other confounding factors (shelter effects), inclusion of reefs far from the path (predicted to be undamaged) is necessary to offset this effect. When these false

negatives were removed from the Ivor data set, damage severity was highly negatively correlated with distance from the path (r^2=0.88). Another difference between the two surveys is that all the Joy sites were located on the right (weak side) of the path, while the Ivor sites were mostly located on the left (strong side) of the path. It may be that the linear relationship between distance and the severity of damage is stronger on the weak side of the path.

A trend similar, but weaker, than that for cyclones Ivor and Joy was observed during the later phase of Justin (D). However, there was no clear relationship between damage severity and distance during Justin's early phase (C) when it was unusually large, nearly stationary, and relatively weak.

When this was examined in more detail on a site-by-site basis (rather than an average by distance), the proximity of a site to the cyclone path was a poor predictor of damage. This was assessed for each surveyed site by predicting the severity of damage, summed across all eight types – total damage score, based on distance to the cyclone path alone (as in Table 3.1 and Figure 3.2), and then comparing these predictions to what was recorded during the field surveys. Each type of damage was assigned a score between 0 and 5 for each of the eight types of damage. Threshold total damage scores of 5 and 15 were used to define categories of very low (< 5), low (5-15) and high (>15) damage severity. These thresholds were chosen to approximate the extent of damage across all types of damage - a site that sustained high (widespread – individual damage score of 5) damage for only one type would earn a total damage score of 5, and a site that sustained high damage for three types would earn a total damage score of 15.

For the sake of simplicity, local shelter effects are not taken into account in this analysis. Nor are potential errors in the path of the cyclone (positional uncertainty is addressed in Chapter 4). The strength of the relationship between observed damage and that expected based on proximity to the cyclone path alone indicates the extent to which these variables need to be considered.

IVOR

Distance to the cyclone path did a poor job predicting the severity of damage during cyclone Ivor (Table 3.8).

Table 3.8: Comparison of the predicted versus observed severity of wave damage (total damage scores = high (≥ 15), low (5-15) or very low (<5) during cyclone Ivor, based on distance to the cyclone path alone as defined in Table 3.1.

Observed Damage	**Predicted Damage (Table 3.1)**					
	High		*Low*		*Very Low*	
	Left	Right	Left	Right	Left	Right
High	11.54%	9.09%	20.00%	n/a	0%	n/a
Low	7.69%	18.18%	40.00%	n/a	0%	n/a
Very Low	80.77%	72.73%	40.00%	n/a	100.00%	n/a

Although no severe damage was observed at distances predicted to sustain minimal damage, only a small proportion of the damage observed in the predicted high damage zone was actually severe. Instead, the majority of the damage in this zone was very minor (Figure 3.11). This assumes that there are no shelter effects and that the plotted position of the cyclone path is correct. However, cyclones that track near the

Queensland coast can be in error by ±50 km in any direction (Holland 1981). If the true path was actually located 30 km to the south of the reported path, all the very low damage sites would have been on the sheltered (right) side of the cyclone path.

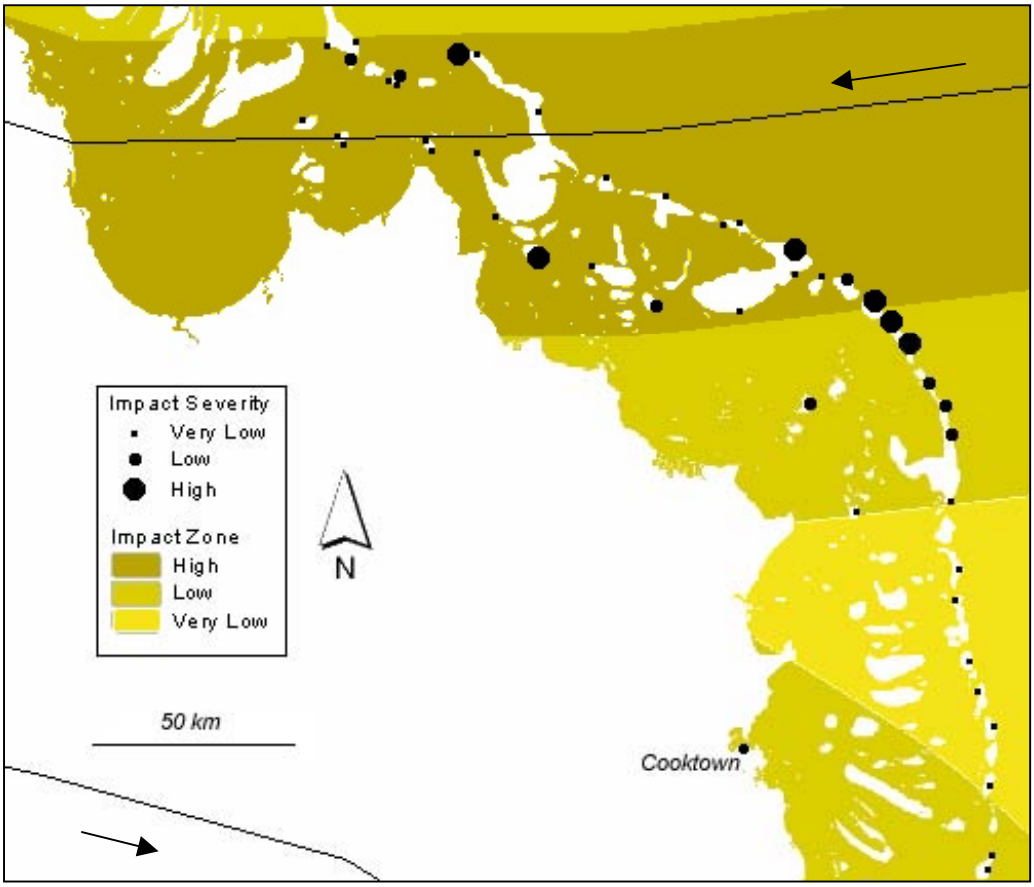

Figure 3.11: Zones of high, low and very low wave damage expected during cyclone Ivor based on distance to the cyclone path (thin black line) alone (defined in Table 3.1) versus the severity of actual damage observed after the cyclone by Done et al 1991. The coast, islands and reefs are shaded white.

JOY

The severity of wave damage from cyclone Joy was also poorly predicted by distance to the cyclone path alone (Table 3.9).

Table 3.9: Comparison of the predicted versus observed severity of wave damage (total damage scores = high (≥ 15), low (5-15) or very low (<5) during cyclone Joy, based on distance to the cyclone path alone as defined in Table 3.1.

	Predicted Damage (Table 3.1)							
Observed Damage	*High*		*Low*		*Very Low*		*None*	
	Left	Right	Left	Right	Left	Right	Left	Right
High	n/a	0.00%	n/a	50.00%	n/a	50.00%	n/a	0.00%
Low	n/a	0.00%	n/a	12.00%	n/a	80.00%	n/a	2.00%
Very Low	n/a	0.00%	n/a	6.41%	n/a	41.67%	n/a	51.92%

None of the sites at which severe damage was recorded fell within the predicted high damage zone (Figure 3.12). Instead, they were split between the low and very low damage zones. Similarly, only 12% of the sites at which minor damage was recorded were located within the low damage zone. Instead, 80% were found in the very low damage zone and 2% were found in the no damage zone. Finally, sites at which very minor damage was recorded were predicted best by distance, with nearly half found in the very low damage zone and only just over 6% found in the low damage zone.

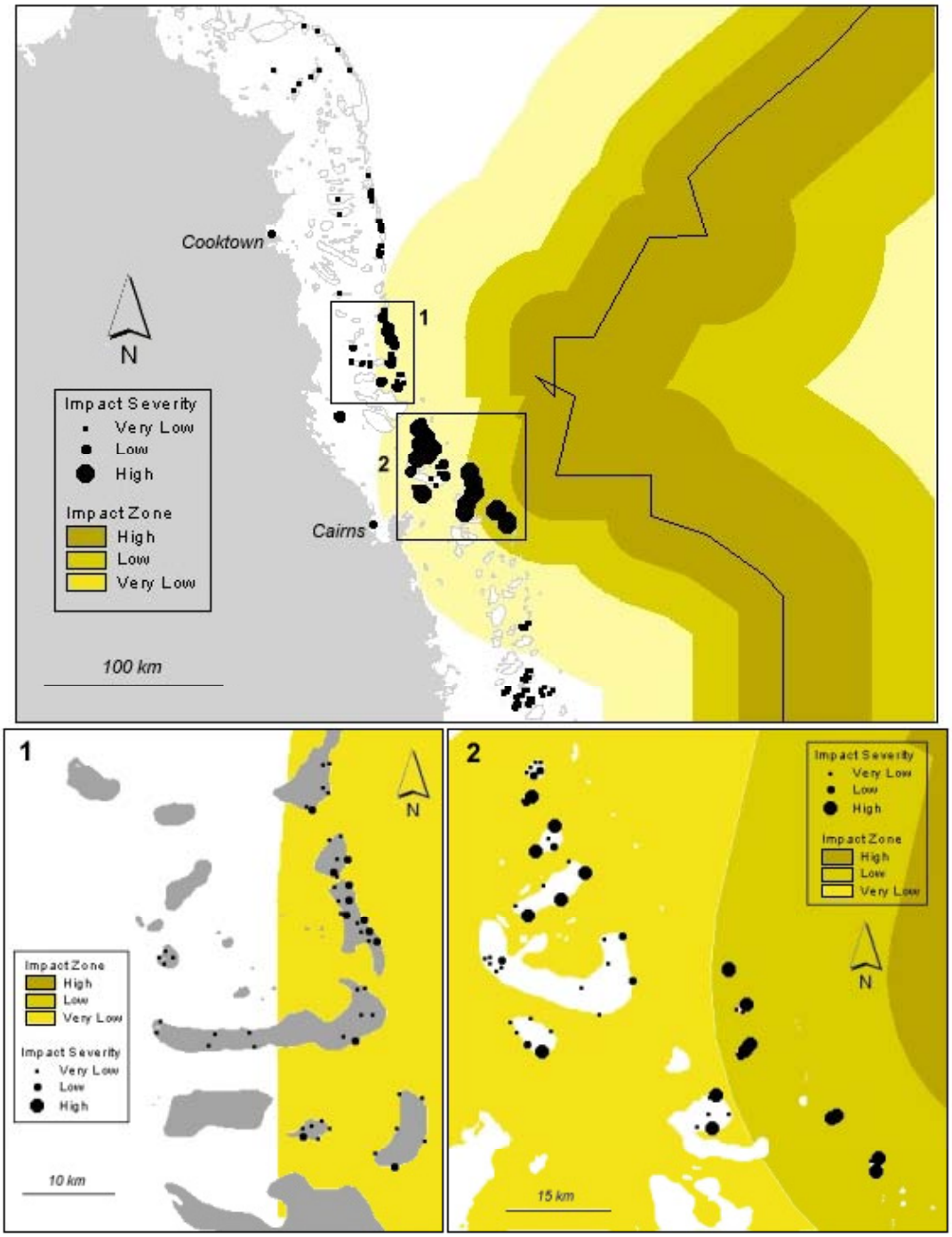

Figure 3.12: Zones of high, low and very low wave damage expected during cyclone Joy based on distance to the cyclone path (thin black line) alone (defined in Table 3.1) versus the severity of actual damage observed after the cyclone by Ayling et al 1991. The coast, islands and reefs are shaded white (gray in panel 1).

JUSTIN

The severity of wave damage during cyclone Justin was again very poorly predicted by distance to the cyclone path alone (Table 3.10).

Table 3.10: Comparison of the predicted versus observed severity of wave damage (total damage scores = high ($\geq$ 15), low (5-15) or very low (<5) during cyclone Justin, based on distance to the cyclone path alone as defined in Table 3.1.

Observed Damage	**Predicted Damage (Table 3.1)**			
	High	*Low*	*Very Low*	*None*
High	0.00%	0.00%	0.00%	100.00%
Low	0.00%	0.00%	0.00%	100.00%
Very Low	11.54%	44.23%	0.00%	44.23%

Only one reef site sustained severe damage, and it was predicted to sustain none. The same was true for minor damage. The 52 sites at which very minor damage was recorded were predicted to sustain low (~45%), no (~45%), or high (~12%) levels of damage – none were predicted to be very low (Figure 3.13). Damage to the surveyed sites took place when cyclone Justin was far away but unusually large and almost stationary, rather than when it was closer to the sites but weaker. Thus, sites located farther from the cyclone path experienced higher levels of wave damage than those located in closer proximity.

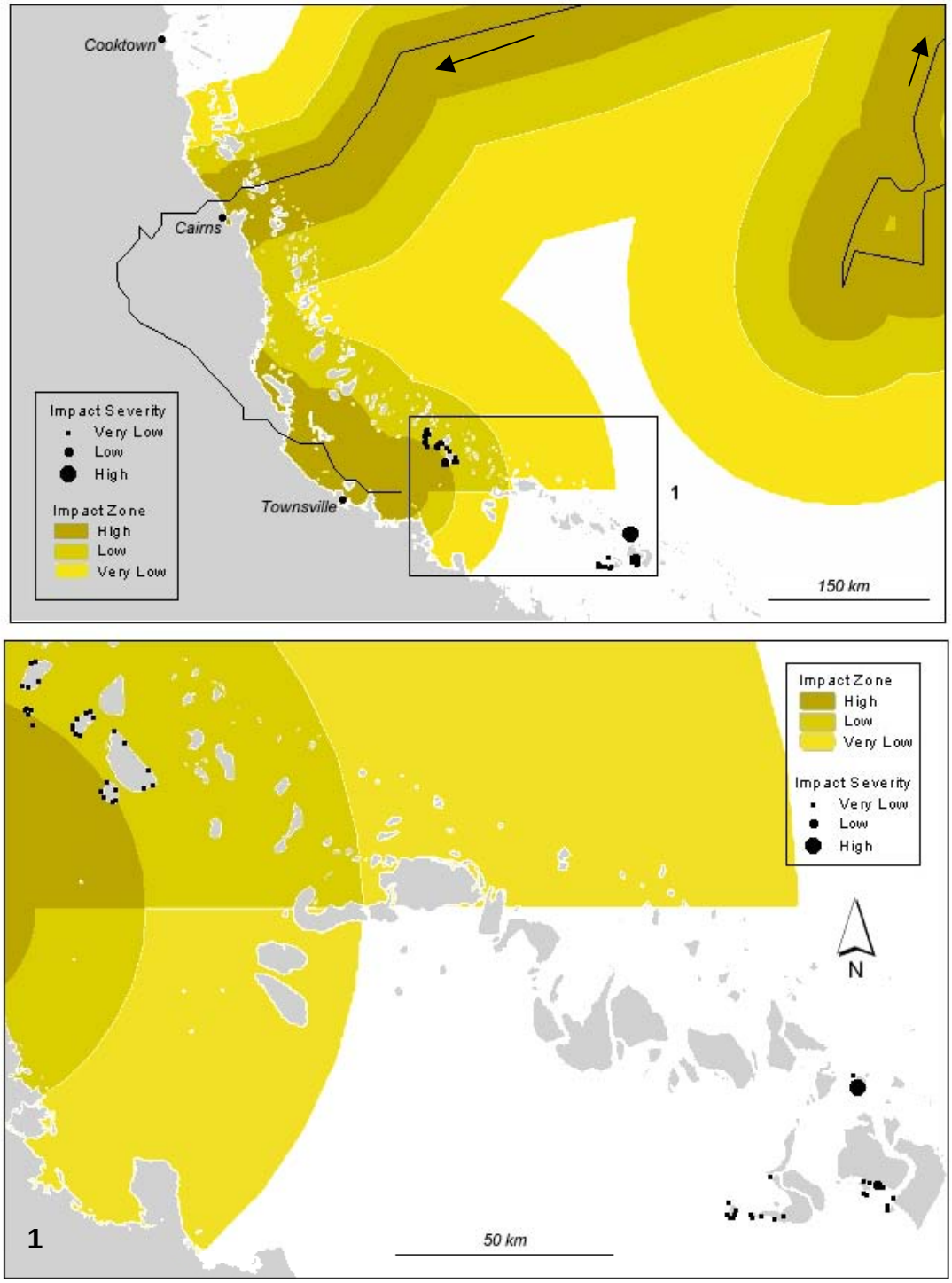

Figure 3.13: Zones of high, low and very low wave damage expected during cyclone Justin based on distance to the cyclone path (thin black line) alone (defined in Table 3.1) versus the severity of actual damage observed after the cyclone by the author. The coast, islands and reefs are shaded gray.

3.4.3 Summary

Cyclones Ivor, Joy and Justin each generated a 'disturbance signature' in the distributions, severity and types of damage that their wave energy produced on reefs. While each disturbance signature was unique, characteristic differences between them due to cyclone intensity and size were apparent. Cyclones Ivor and Joy, which were relatively intense but typical in size, generated high-energy damage (dislodgment of massive coral heads, exfoliation) near the cyclone path and scattered low-energy damage (coral breakage) further away. During its early phase (when the cyclone was weak but unusually large in size), Justin generated widespread, low-energy damage (breakage, trenching) and limited patchy high-energy damage (dislodgement of massive corals). The latter were equivalent in severity to those found after cyclones Ivor and Joy, and were located at sites more than 200 km away from the cyclone path. In contrast, sites surveyed offshore from Townsville, though located close to the cyclone path, experienced widespread low-energy damage (breakage) and no high-energy damage. While the severity of damage overall declined with distance from the path during cyclone Joy, this relationship was less apparent for cyclone Ivor, and totally absent for cyclone Justin. The distance to the cyclone path alone was insufficient to predict the spatial distribution of levels of damage for any of the cyclones.

3.5 Conclusions

Any cyclone will produce a unique disturbance signature in the patterns of damage it leaves behind in coral reef communities. These signatures are influenced generally by the combination of a cyclone's size and intensity, which represents variation in the

energy potentially available from the cyclones (least energy from a small and weak cyclone, most energy from a big and strong cyclone). Differences in cyclone size and intensity result in broad differences between disturbance signatures (predominance of high or low wave energy damage). More specific differences (spatial distribution of levels of damage) reflect the extent to which cyclone waves actually reach coral reef communities and the vulnerability of different types of communities to a particular set of wave forces.

Using distance as a proxy for disturbance potential is clearly inadequate to predict the spatial distribution of levels of damage across reefs. If distance is the only feasible approach to estimating damage potential (such as for GBR cyclones before 1969), the results should be interpreted as a worst-case scenario of the potential risk for damage. In other words, it defines the band in which damage might be expected to occur on sites exposed to cyclone-generated waves.

To build a more realistic cyclone history of the GBR requires detailed modelling of cyclone energy as well as reef exposure and vulnerability to that energy. Chapters 4 and 5 describe methods developed to carry out that modelling, using the five cyclones for which field data exists (Ivor, Joy, Justin, Althea and Celeste) as case studies. Methods for hindcasting cyclone winds are presented in chapter 4, while chapter 5 develops measures of reef exposure and vulnerability. Chapter 6 takes the measures developed in Chapters 4 and 5 and links them to the damage field survey data in a statistical model, which is used to predict the spatial distribution of damage types for the entire time series of cyclones. Chapter 7 presents the resultant cyclone history for the GBR.

CHAPTER 4: Hindcasting cyclone winds

4.1 Overview

A cyclone wind hindcasting model was implemented in GIS and used to reconstruct the spread and intensity of high winds associated with each of the 85 cyclones that passed near the GBR from 1969 to 2003. The model was tested using the five cyclones for which field observations of wave damage were available (cyclones Ivor, Joy, Justin, Althea and Celeste). Where possible, model results were compared to field measurements of wind speed and direction from weather stations to verify the model. The purpose of this chapter is to present the model and its implementation in GIS, assess its performance for the test cyclones, and illustrate how it was used to generate cyclone energy parameters of relevance in explaining spatial patterns of known wave damage to reefs (Figure 4.1). The utility of these parameters for predicting observed wave damage from the five test cyclones is tested statistically in Chapter 6. Subsequently, relevant cyclone energy parameters were hindcast for the entire set of cyclones, the results of which are presented in chapter 7.

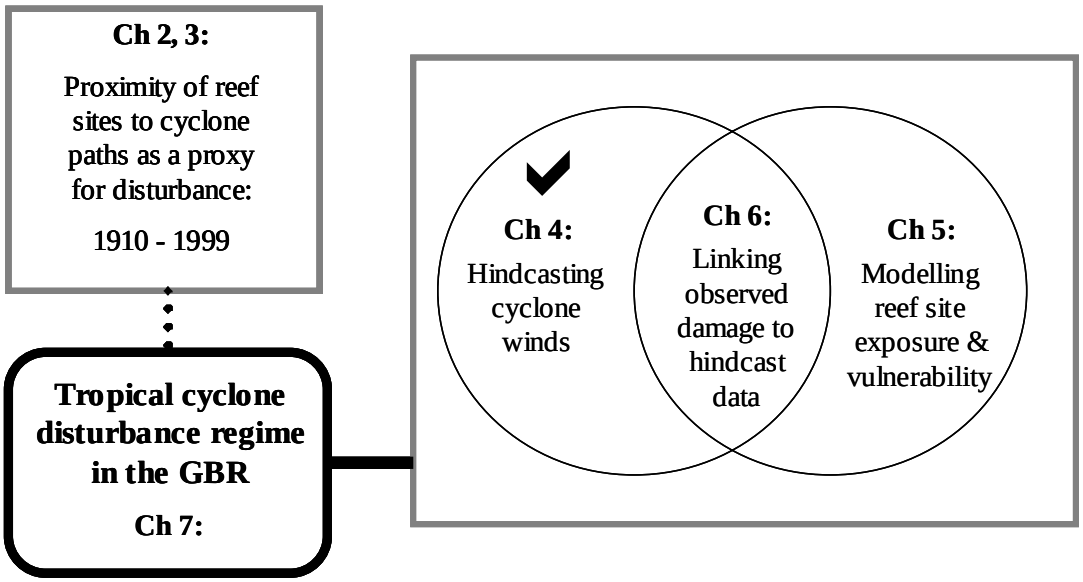

Figure 4.1. Overview diagram of this thesis. The check mark indicates the current chapter.

4.2 Introduction

Direct measurements of cyclone wind speeds and wave heights are rarely possible. However, there are a range of mathematical models that predict the distribution of cyclone energy from basic characteristics that are routinely estimated by meteorologists (eye position, central pressure, speed and direction of forward motion). These models are used in 'real time' to track and predict the movement and intensity of cyclones that threaten to cause harm to people and/or natural resources (forecasting). They can also be used to reconstruct cyclone conditions from past events (hindcasting).

I used a cyclone wind model (McConochie et al 1999) and the BOM's cyclone database to hindcast cyclone wind energy across the GBR from each cyclone that tracked near the region from 1969 to 2003. I implemented the model in GIS due to its ability to integrate, manage, analyse and visualise spatial data. Workstation Arc-Info within ArcGIS was chosen as the primary analysis platform due to its flexibility, speed, and wide range of sophisticated analysis tools in both raster and vector environments. ArcView 3.3 was used for visualisation and mapping of the results.

The model generally predicted wind speeds to within 10 $m.s^{-1}$ and wind directions to within 45 degrees (with the exception of wind directions during cyclones Ivor and Althea).

4.3 Preparation for hindcasting

Before hindcasting cyclone energy was possible, the cyclone database needed to be formatted and imported into GIS to create eye positions, standardise them to a one-hourly interval, and generate lines from the eye positions to represent cyclone paths.

4.3.1 Importing cyclone data into GIS

The cyclone database, as it is freely available on the BOM web site (http://www.bom.gov.au), is formatted as an ASCII text file that contains a multitude of attributes for each eye position of each of all cyclones recorded from 1910 to the present. This data was imported into an Excel spreadsheet. A separate worksheet was created for each cyclone for the geographic coordinates (longitude and latitude) and for the associated attributes (number, name, year, month, day, time, central pressure (hPa), category, speed of forward motion ($m.s^{-1}$) and direction of forward motion. A separate vector GIS data layer (coverage) was generated for each cyclone in the database by importing the spreadsheets in Arc-Info.

4.3.2 Standardising eye positions

Cyclone observations are recorded by the BOM at varying time intervals, depending on the proximity and potential danger of the system to coastal communities. This ranges from one-hourly intervals, when the cyclone tracks near populated areas, to up to twelve-hourly intervals when it tracks far from the coast (but potentially near GBR reefs). The eye positions and their attributes for each cyclone were standardised to a one-hourly interval (Figure 4.2) using linear interpolation. This was done using a

series of automated scripts written in Arc Macro Language (AML), which were edited slightly to run for each of the 85 cyclones (see Appendix 2).

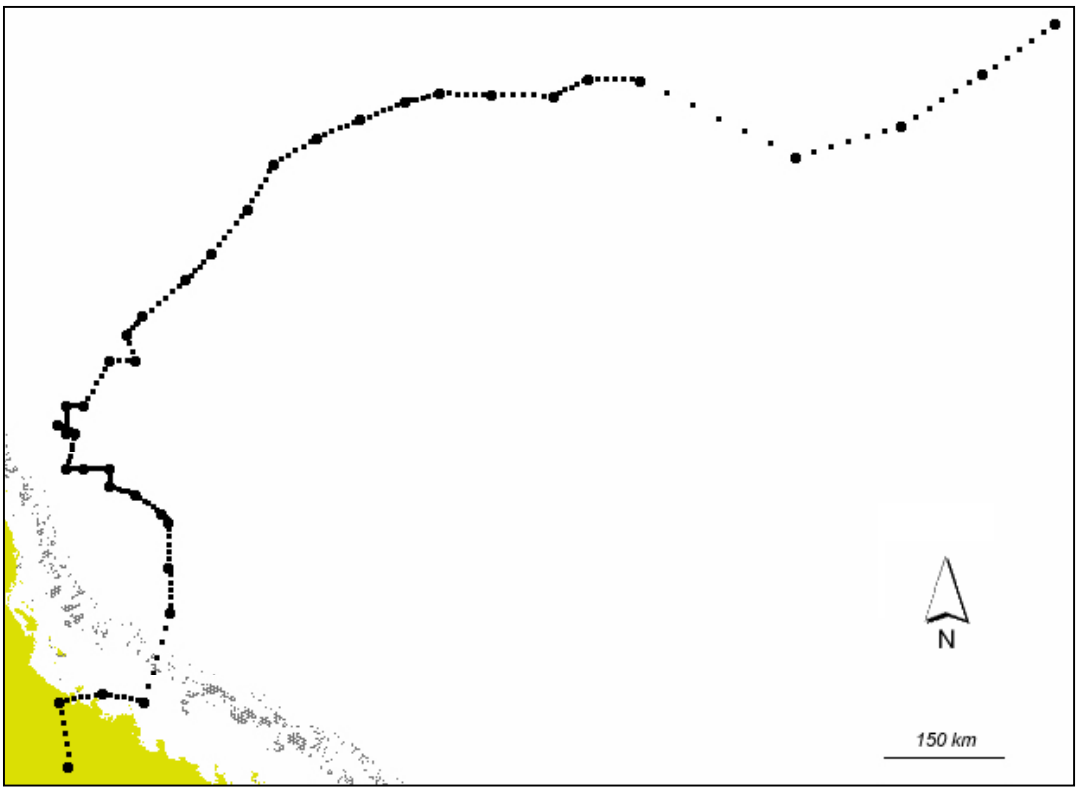

Figure 4.2: GIS vector point coverage showing the eye positions of cyclone Joy (1990). Large circles indicate the original positions recorded in the BOM cyclone database, and small squares show the interpolated positions needed to represent the cyclone position every hour.

Initially, each cyclone was also linearly interpolated to a ten-minute interval to minimise the problems associated with using discrete 'snapshots' to model a continuous phenomenon (see section 4.3.5). However, hindcasting at a ten-minute interval quickly became unmanageable due to the resultant excessive need for computer disc space and processing time. Subsequently, following Thompson and Cardone 1996, I chose to use a one hourly interval.

4.3.4 Generating cyclone paths

A separate GIS vector line coverage was generated from the original eye position point coverage for each cyclone using a series of automated scripts written in AML (see Appendix 2). While it is possible to connect the eye position points with a range of different curves, straight lines were used in the absence of evidence supporting a more complex approach. The resultant cyclone paths were used for the analysis described in chapter 2 and to create an atlas of cyclones in the GBR, published in 1997 (see Appendix 6).

4.4 Error and uncertainty

The ability to hindcast cyclone energy in the GBR is limited by a general lack of key data sets, as well as high levels of uncertainty in the data that is available and in the hindcasting models themselves (Table 4.1).

Table 4.1: Challenges associated with hindcasting cyclone energy.

Issues	Explanation
Cyclone Eye Positions	Estimated positional error ±20-200 km. Largely unreliable before 1969.
Cyclone Intensity	Estimated intensity error ±30 hPa. Largely unreliable before 1969.
Cyclone Paths	Cyclone movement between eye positions unknown and presumed linear.
Cyclone Eye Width	Often difficult to measure, often not recorded, very important to cyclone energy models.
Cyclone Models	Mesoscale in nature (1s-10s km) - don't incorporate local scale effects such as rain bands.
Model Validation	Very limited field observations available, with poor spatial coverage over the GBR.

4.4.1 Eye Positions

Cyclones are tracked using a combination of satellite and radar imagery and land and ship based observations. The timing of the observation varies depending on the proximity of the cyclone to land-based communities. The quality of the observation depends on the combination of methods used (radar produces the most accurate observations, though many cyclones track outside of radar range). For the most part, the method used to establish the cyclone eye position is recorded in the cyclone database. While cyclone eye positions have been recorded in Australia since the early 1900's (circa 1910), the quality of these positions is largely unacceptable before the advent of widely available satellite imagery in 1969 (Holland 1981). Researchers at the Australian Bureau of Meteorology Research Centre estimate that errors in initial cyclone positions can exceed 400 km in any direction (Figure 4.3 - A), though most are within 100 km (Woodcock 1995). While this does not reveal the level of error remaining in the revised cyclone tracks, it suggests a high level of positional uncertainty.

4.4.2 Intensity

The magnitude and extent of the winds and waves generated by a particular cyclone depends largely on its intensity. The central air pressure (in hPa) of a cyclone is commonly used as a measure of intensity. As central pressure falls, the difference in air pressure between the cyclone and the external environment increases, powering the storm. Central pressure is rarely measured directly and is typically estimated using satellite imagery (Dvorak 1975).

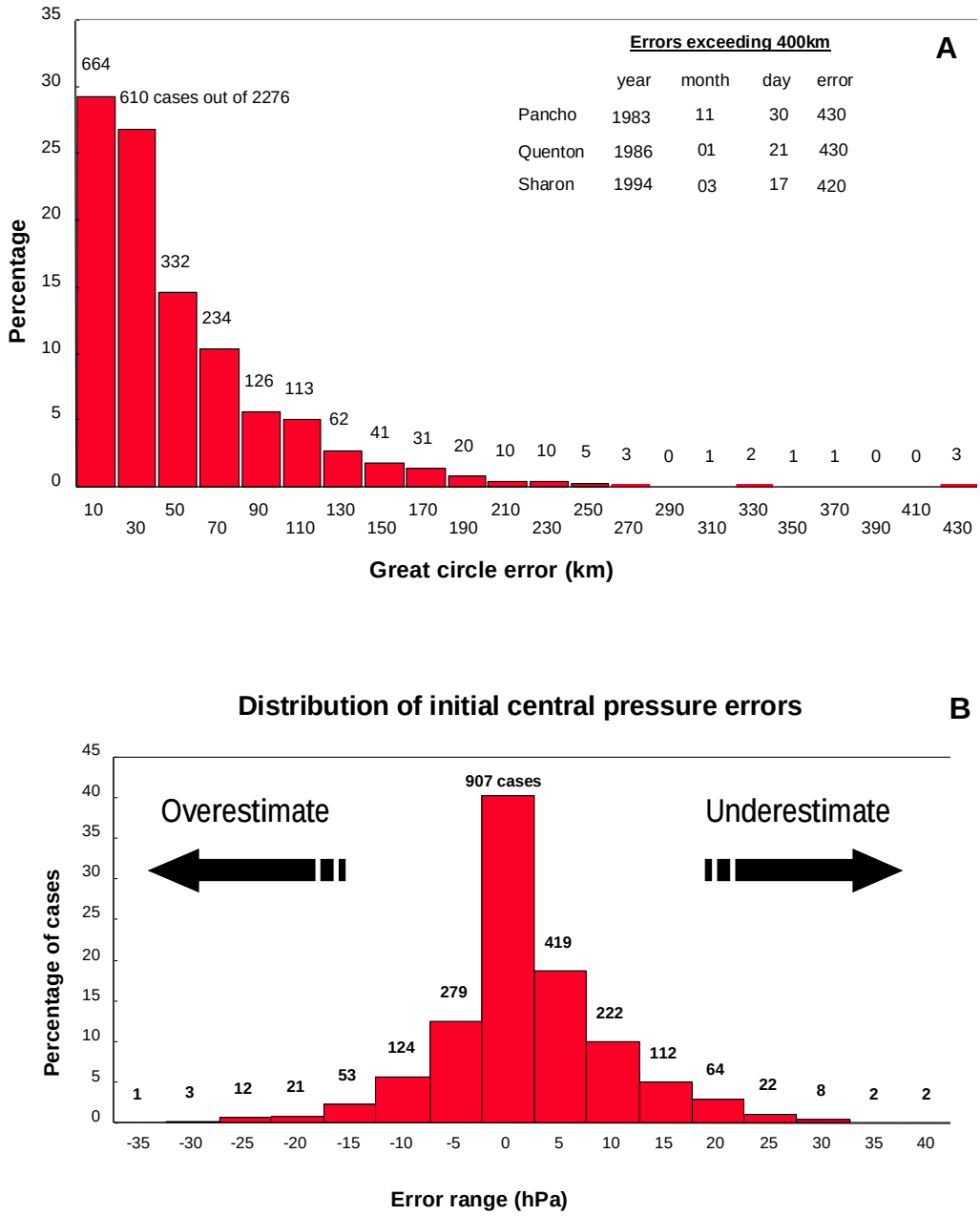

Figure 4.3: Estimated errors in initial measurements of tropical cyclone: A) eye positions and B) intensity (adapted from Woodcock 1995) based on subsequent data.

It can also be measured directly if the eye passes over an instrument, giving a more accurate estimate. In some cases, no satellite data is available, and the intensity is inferred from wind measurements using meteorological models that link wind speed to intensity (Holland 1980), giving a less accurate estimate. The technique used to estimate intensity is often recorded in the cyclone database. As with the location of

eye positions, central pressure measurements have also been found to be in error (Figure 4.3 - B), suggesting considerable uncertainty in cyclone intensity estimates. Over time, cyclone intensity is underestimated more frequently than overestimated (Woodcock 1995).

4.4.3 Cyclone Paths

Positional uncertainty in the individual eye positions introduces uncertainty into the path of the cyclone that they define. Beyond this, there is also uncertainty in determining the path between observed eye positions (how to 'join the dots'). When a cyclone moves slowly and its eye positions are observed frequently, the distance between observations, and thus the uncertainty in defining the path, is low. However, eye positions are often estimated infrequently (six to 12 hours apart) when cyclones track far from populated areas, and cyclones can move at nearly 40 km / hour. While the paths of cyclones generally tend to be curvilinear as they track from the tropics to the poles, local scale meanders in the paths follow no standard pattern.

It is possible to generate cyclone paths in GIS using other than a linear method to join the observed eye positions. For example, as a test I built several cyclone paths using first a linear and then a cubic spline interpolation to 'join the dots'. I then assessed the average distances between the two paths for each of the cyclones. In general, these differences were slight and fell well within the known positional uncertainties of the cyclone eye positions. Thus, I interpolated the cyclone eye positions to one hourly intervals using a linear distance approach.

4.4.4 Eye Width

As discussed in chapter 1, cyclones typically contain a relatively calm region at the centre of the storm circulation called the eye. Wind speeds are near zero within the eye, while they are at their maximum around the boundary (the eye wall). Over time, as the eye moves, areas previously located within it become subject to high winds as the radius of maximum winds shifts. This produces a swath of highest winds equal in width to the eye width. Defining the diameter of the eye is thus quite important to accurately hindcasting the cyclone energy field. Eyes are also very dynamic in their structure, sometimes developing a double eye structure (Willoughby 1990). In addition, the presence of upper atmospheric cloud can make it difficult to measure eye width from satellite imagery (Figure 4.4).

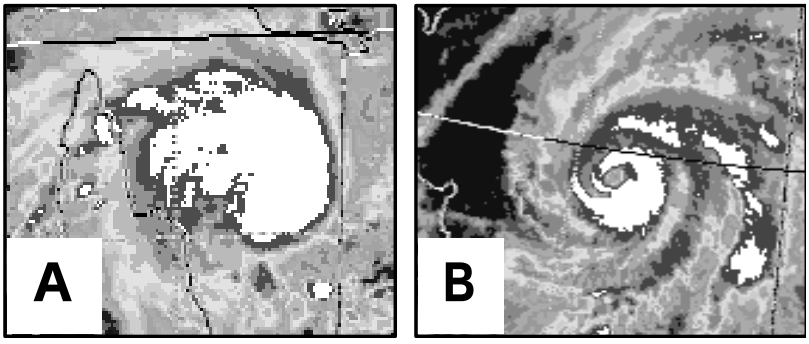

Figure 4.4: Satellite images of tropical cyclone eyes. Though the cyclones are of similar intensity, in B the eye is clearly visible, and in A it is obscured by upper atmospheric clouds.

Consequently, eye width is not always recorded in the tropical cyclone database, particularly when the cyclone is located beyond radar range. For example, less than 3% of recorded eye positions during cyclone Justin included estimates of eye width

(Table 4.2). For cyclones Joy and Celeste, this approached 20% and 15% respectively, while it was less than 5% for cyclone Ivor.

Table 4.2: Percentage of eye positions during cyclones Althea, Ivor, Joy, Celeste and Justin for which eye width was recorded in the cyclone database.

Cyclone	Year	# Observed Eye Positions	# Eye Width Estimates	%
Ivor	1990	43	2	4.444
Joy	1990	37	9	19.57
Celeste	1996	12	2	14.29
Justin	1997	71	2	2.74

4.4.5 Cyclone Models

Meteorological models used to estimate cyclone energy are designed to operate across broad spatial scales (with a resolution of 1-10 km). The processes that control the finer scale dynamics of cyclones (such as detailed processes within rainbands) have not yet been adequately modelled. Moreover, insufficient field data exists to do so, especially for the past. Also, cyclones are affected by factors that operate over extensive areas (1000s of km). This limits the spatial resolution at which they can be modelled (due to unreasonable requisite processing times and disc space needs), even with the commonly used nested grid approach (for example Hardy et al 2001). The degree to which finer scale differences are important to identifying patterns in reef damage depends on the extent to which they affect the formation, magnitude and propogation of large waves. Given that wave damage can vary over 10s to 100s of

metres of distance along a single reef, there is a definite mismatch of scales between cyclone hindcast energy and reef exposure / vulnerability and observed damage.

A related issue is the temporal resolution of the cyclone hindcasting models - time, space and data limits the number and spacing of time steps that are used to model a cyclone. Typically, one hourly steps are used though cyclone dynamics (such as eye width) can vary considerably on shorter time frames. Despite this, Thompson and Cardone (1996) suggest that the basic cyclone structure changes slowly and can be adequately modelled over time steps as far apart as 6 to 24 hours. Further, waves take time to build from sustained wind conditions. As long as the conditions observed at each initial time step represent average conditions, then a one hourly time step may be acceptable. Finally, in reality as a cyclone moves, the resultant winds and waves around the calm eye move with it. However, when a series of 'snapshots' are used to model cyclone energy as is required in a discrete digital model, there are artificial breaks in the wind and wave fields between the modelled eye positions. These can create artificial 'holes' (in GIS maps) of low energy in areas located near the calm eye, particularly when the cyclone is moving quickly and the one hourly eye positions are thus located far apart. While the overall energy experienced at an area located during the eye for a time would be expected to be lower than otherwise, some energy would have filled the gap left by the eye as the cyclone tracked up to, and then away from, that area. I was able to eliminate these ‘holes’ in initial tests of the model by using a 10-minute time step. However, using this time step for all 85 cyclones was unworkable due to excessive processing time and disc space needed. The holes are visible in the maps presented within this chapter, but I used analyses that were not distorted by their presence.

4.4.6 Validation

Given sufficient in situ measurements, cyclone wind and wave fields can be built directly from field data (Thompson and Cardone 1996). However, this is rarely possible in the GBR. Instead it is necessary to rely on generalised models built from observations of a range of cyclones measured mostly in other regions (transects have been flown through only one cyclone in the GBR and one in Western Australia). This requires some form of validation to assess how well the modelled winds and waves match what field observations exist. Ideally, field data would span the life of the cyclone and include full spatial coverage of the region being modelled. In the GBR, this is not the case - observations are spatially restricted, are not equally distributed around the cyclone's path, and often contain missing values. For these reasons, the validation that is possible is only suggestive of the true performance of the model used.

Variation between the model results and reality may be due to limitations of the model in general. For example, most hindcasting models are designed to operate at a resolution of 1-10 km. Measured wind speeds may vary within this distance, such as from interaction with local topography as winds encounter islands. Validation is complicated by the availability and quality (or lack thereof) of some of the key input data sets (particularly the eye width measurements). For this reason, researchers often experiment with various input values for data that is lacking or questionable until a best fit of the model to the observations is found (for example, McConochie et al

1999). This level of manipulation is time consuming and requires considerable expert knowledge, and was thus not undertaken for this thesis.

4.4.7 Visualising Uncertainty

Major uncertainties inherent in this project are unavoidable, making it vital to estimate the confidence of the results (and thus how they should be appropriately used). Visualisation can be used to assess the implications of large uncertainties in the position of the cyclone eye to the modelling based on those positions. The cyclone database records the method(s) used to estimate each cyclone eye position - by direct observation, radar, satellite, or a combination of these. As previously mentioned, Holland (1981) and Woodcock (1995) have estimated the level of potential uncertainty associated with using each of these methods, and some of them are relevant here.

POSITIONAL UNCERTAINTY

To visualise this potential error, I used GIS to construct uncertainty circles (based on Holland 1981) around each eye position for cyclones Ivor, Joy, Celeste and Justin (see Appendix 2). Cyclone Althea was not modelled as the cyclone database lacked the necessary data. The radius of each circle was set to equal the likely maximum positional error for the eye position on which it was centred. Thus, each cyclone eye position could be located anywhere within its uncertainty circle. To get an idea of how positional uncertainty varied throughout each entire cyclone, I also counted the number of times each position across the GBR was located inside an uncertainty circle (see Appendix 2), and thus may have been located near a cyclone eye. Areas

located inside many uncertainty circles were more likely to have had a cyclone pass nearby than otherwise.

Ivor

Uncertainty in the position of the eye for cyclone Ivor (Figure 4.5) varied considerably along its path.

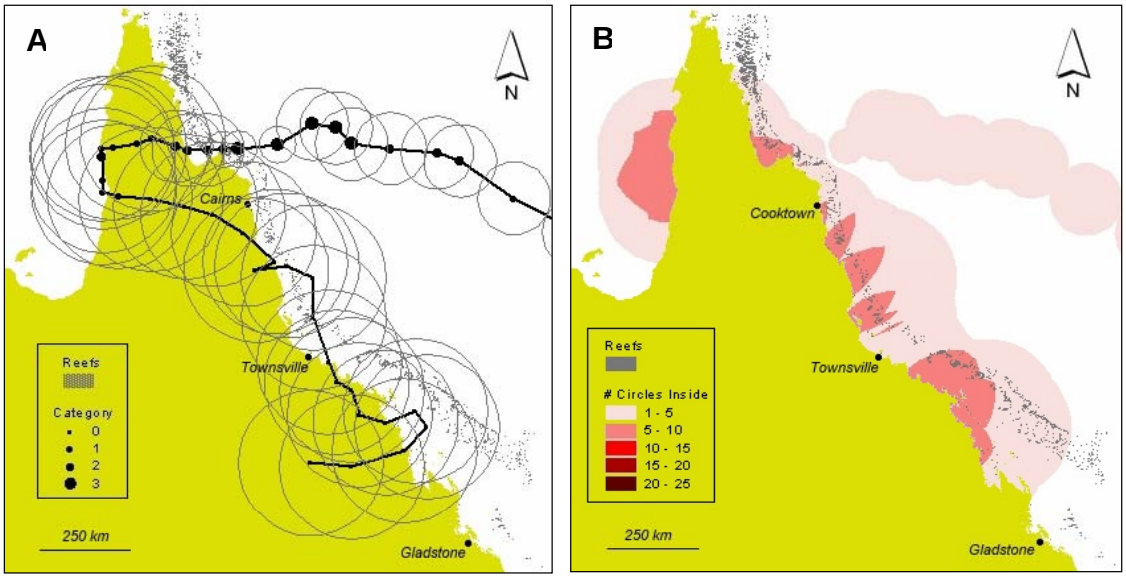

Figure 4.5: Positional uncertainty during cyclone Ivor (1990). Circles [A] define the area within which the eye could be located. Shading [B] indicates the frequency of location inside an uncertainty circle.

As it is typically more difficult to track cyclone positions far out to sea due to a lack of radar coverage, uncertainty in Ivor's eye positions decreased as it approached the north Queensland coast. The cyclone also intensified at this stage, which likely made it easier to define the eye on satellite images. It was also at this stage that reef sites surveyed following the cyclone were most likely to have been damaged. Interestingly, though, positional uncertainty increased after Ivor made landfall and remained high for the duration of its life. This may have occurred because it was

relatively weak at that stage, making the eye more difficult to pinpoint, or because it posed little threat to human populations.

Joy

Uncertainty in eye positions during cyclone Joy was also generally lower as the cyclone approached and reached maximum intensity (Figure 4.6), making it easier to define the eye on satellite imagery. The highest uncertainty occurred just after the cyclone made landfall near Townsville when it decreased rapidly in intensity. As was the case for cyclone Ivor, positional uncertainty was low at the time when reef sites surveyed following the cyclone were most likely to have been damaged.

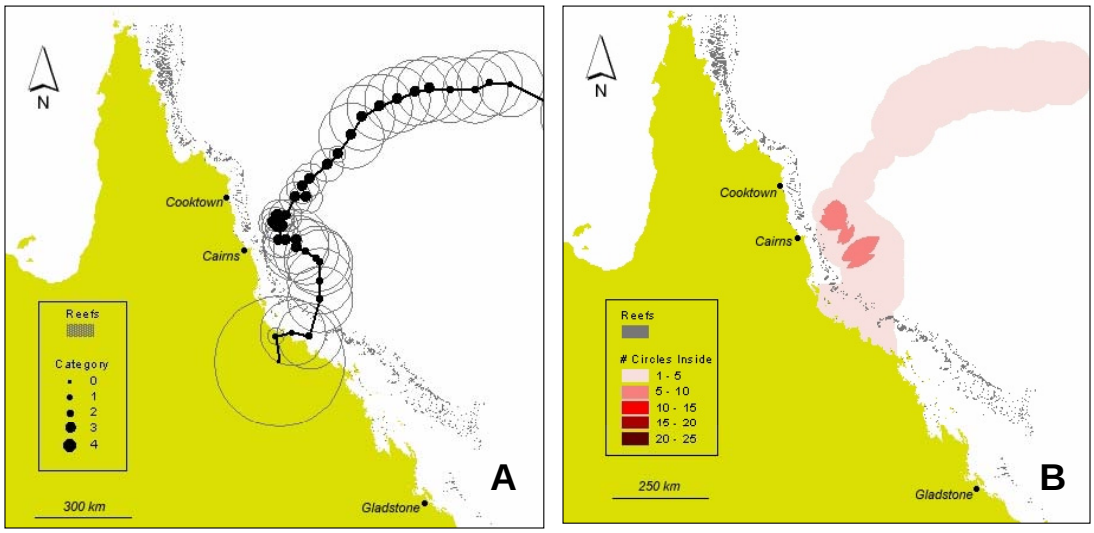

Figure 4.6: Positional uncertainty during cyclone Joy (1990). Circles [A] define the area within which the eye could be located. Shading [B] indicates the frequency of location inside an uncertainty circle.

Justin

In contrast, the location of cyclone Justin's eye was most uncertain when it was located far out to sea (Figure 4.7) transitioning between its initial stage, where it was

nearly stationary and unusually large, and its subsequent movement towards Papua New Guinea.

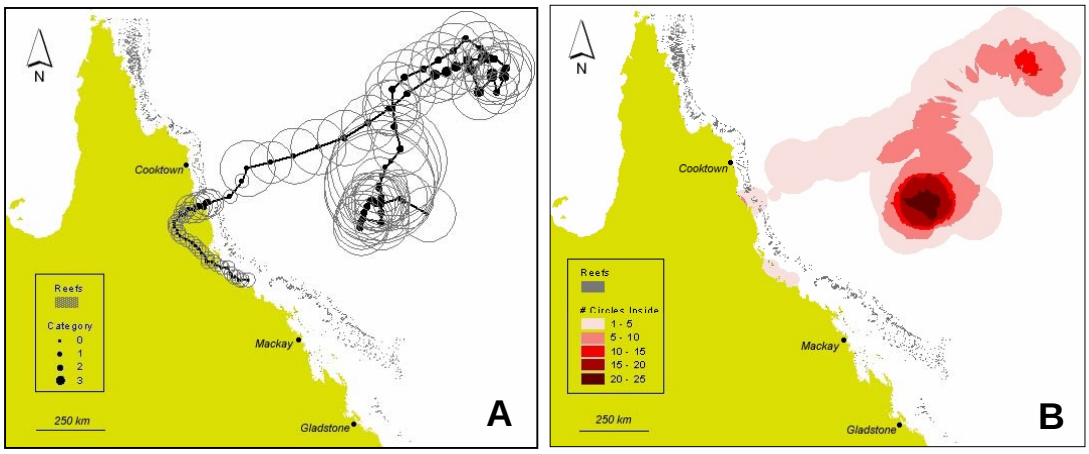

Figure 4.7: Positional uncertainty during cyclone Justin (1997). Circles [A] define the area within which the eye could be located. Shading [B] indicates the frequency of location inside an uncertainty circle.

Not only was Justin well beyond radar range at this time, but it also posed little threat to populated areas (thereby being tracked less frequently and intensively). And, as Justin was not very intense at this time (category 2), identifying the eye on satellite images was more difficult. As Justin entered its third phase, intensifying somewhat and approaching the coast at Cairns, meteorologists were able to pinpoint the eye much more effectively. Positional uncertainty was least while Justin tracked southward over Queensland to exit into the sea north of Townsville. Although the cyclone was very weak during this stage, it remained within radar range, which enabled more effective tracking.

Celeste

Positional uncertainty remained low throughout cyclone Celeste, even during its relatively weak initial stage (Figure 4.8).

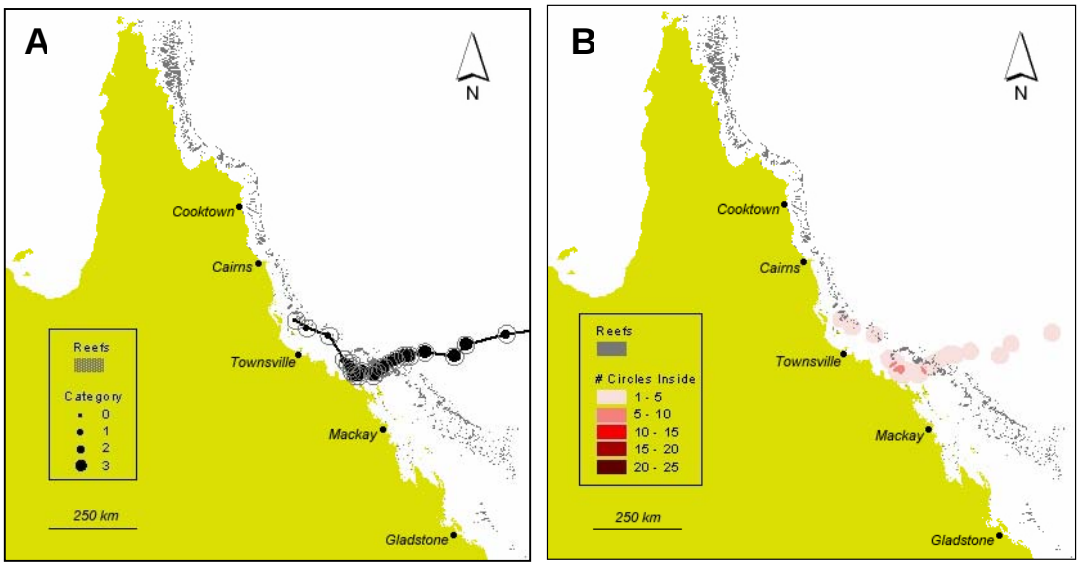

Figure 4.8: Positional uncertainty during cyclone Celeste (1996). Circles [A] define the area within which the eye could be located. Shading [B] indicates the frequency of location inside an uncertainty circle.

Celeste formed within the GBR and initially tracked southward quite close to the coast, during which time it moved within radar range. Once the cyclone turned westward and moved out of range, it had intensified to category 3, which made it easier to identify the eye on satellite images.

INTENSITY UNCERTAINTY

The intensity of a cyclone varies along its path, and the method(s) used to estimate it vary as the cyclone intensifies or weakens and/or moves within or beyond radar range. Because the method(s) used to estimate intensity are often recorded in the cyclone database, GIS can be used to visualise how intensity uncertainty varies over the life of the cyclone. Four qualitative categories of uncertainty were thus assigned based on methods reported in the cyclone database (Table 4.3).

Table 4.3: Categories of uncertainty in estimating cyclone intensity.

Category	Method of Intensity Estimation
Very Uncertain	Educated guess from opportunistic observations.
Uncertain	Pressure-wind relationship as per Holland 1980.
Certain	Satellite images are used as per Dvorak 1975.
Very Certain	Direct measurement taken of central pressure by an instrument.

The level of uncertainty in cyclone intensity varied within and between cyclones Ivor, Joy, Justin and Celeste (Figure 4.9).

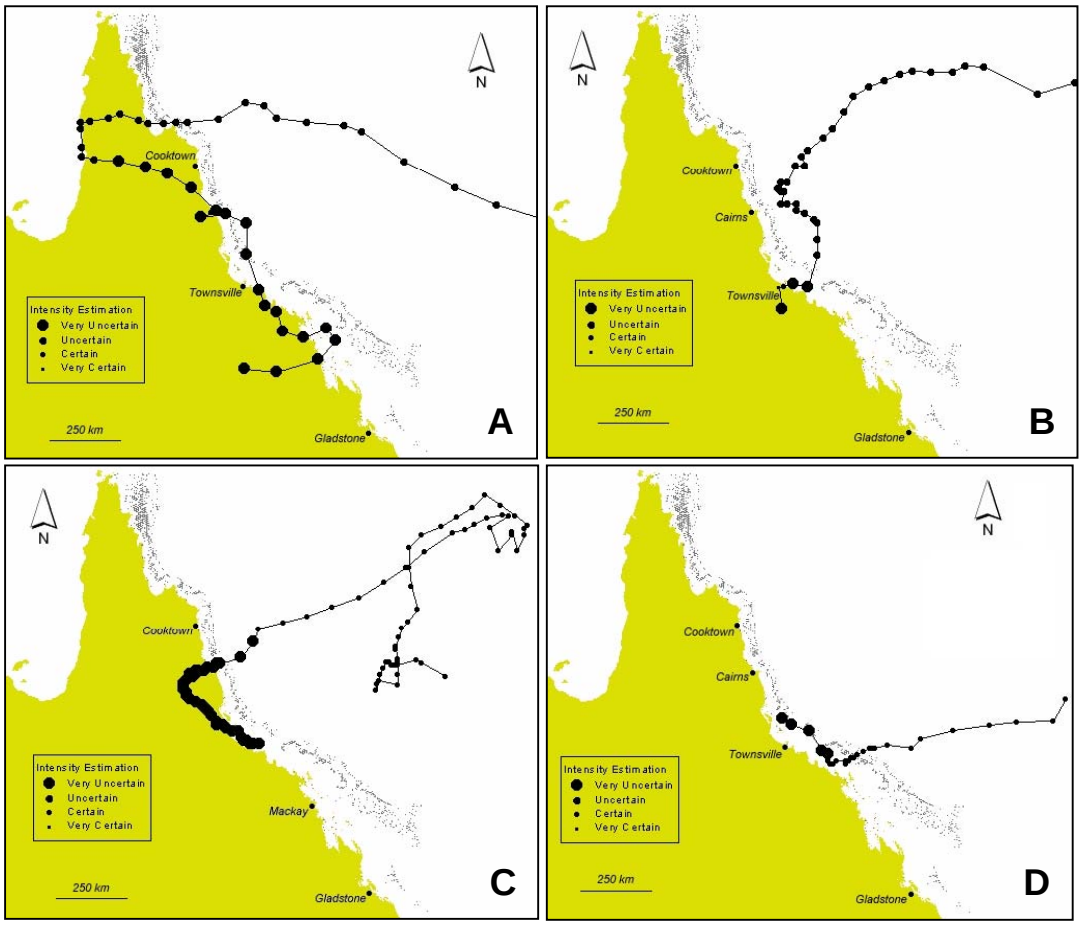

Figure 4.9: Predicted uncertainty in cyclone intensity estimates by eye position during cyclones Ivor [A], Joy [B], Justin [C] and Celeste [D].

The intensity of Celeste and Justin was generally more certain than for Ivor or Joy. In general, intensity estimates for eye positions located on or near the coast is less certain. For cyclones Ivor and Joy, positional uncertainty was also greater near the coast, while for cyclone Justin the opposite was true.

4.5 Hindcasting cyclone winds

A surface wind field was generated from the pressure profile at each interval (commonly one hourly) during the cyclone. In the southern hemisphere, cyclone winds spiral inward towards the eye in a clockwise direction, with the highest wind speeds found in a crescent shaped region in the front left quadrant at the radius of maximum winds (Figure 4.10).

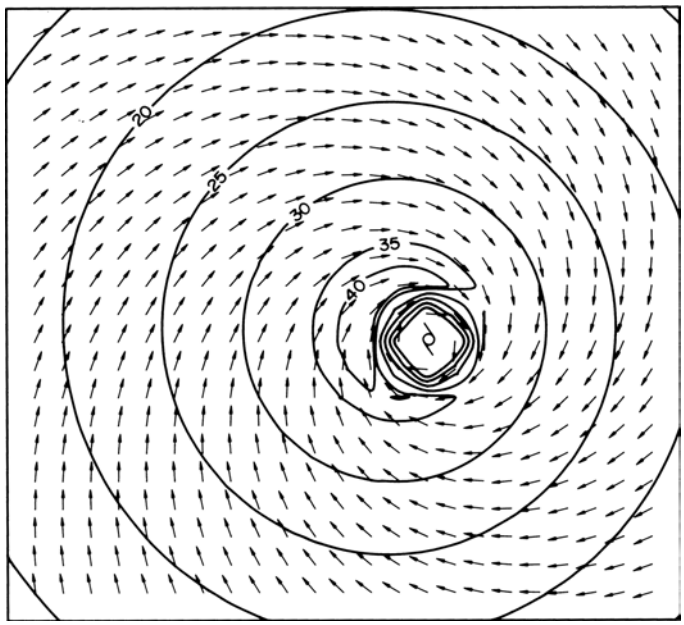

Figure 4.10: Typical hindcast cyclone wind field. The arrows indicate the direction to which the wind is blowing. The cyclone is moving towards the top of the page. (Source: Young and Hardy 1993).

While the most sophisticated cyclone wind models use numerical modelling techniques to solve the equations of motion using a planetary boundary layer model, a simpler and less computationally intensive analytic approach is also often used. The latter approach estimates cyclone wind speeds based on the air pressure gradients that drive the system, most often derived from the pressure field first defined by Holland (1980).

[1] $$P = P_o + \Delta P \cdot e^{-(R/r)^B}$$

where P = pressure at radius r
P_o = central pressure
R = radius of maximum winds (radius of eye)
r = distance from the centre of the eye
ΔP = ambient pressure - P_o
B = cyclone peakedness scaling parameter

Air pressure rises with distance from the boundary of the cyclone eye towards the ambient environment. The rate of this rise depends on the pressure difference between ambient and the eye, but also varies with the peakedness of the cyclone (size). Pressures rise very quickly with compact cyclones and rise very gradually with large systems. The peakedness parameter is defined by region, with values ranging between 1.5 and 2.5 (Holland 1980). As the value of B increases, the pressure profile declines more rapidly with distance from the eye wall (becomes more peaked). In this thesis, I defined B using the following relationship reported for the GBR by McConochie et al (1999).

[2] $B = B^1 - P_o / 160$

where B^1 = a constant set to 7.3.

Using equation [2], as the central pressure falls (and the cyclone becomes more intense), the value of B rises and the cyclone pressure field becomes more peaked. The reverse occurs as the central pressure rises (and the cyclone intensity falls). Using the above relationship is satisfactory except for the very rare occasions when a cyclone is both unusually large (less peaked than normal) and weak in intensity (for example, the early phase of cyclone Justin). Setting a large radius of maximum winds can partially counter this.

Cyclone wind fields (speeds) are predicted from the pressure profile described above and adjusted for the asymmetry caused by the forward motion of the cyclone (higher wind to the left of the cyclone path in the southern hemisphere).

Coral reef researchers have used simple, empirically driven versions of this approach to hindcast cyclone energy from single storms at particular reefs (Kjerfve and Dinnel 1983 - Hurricane Greta at Belize Barrier Reef; Kjerfve et al 1986 - Hurricane Allen at Discovery Bay, Jamaica; Done 1992b - Cyclone Ivor in the north-central GBR). None of these projects have implemented the hindcasting equations within a GIS environment. The only case described in the literature using GIS for hindcasting cyclone winds assessed hurricane wind damage to forests in Puerto Rico and New England, USA (Boose et al 1994).

McConochie et al's (1999) model was used to reconstruct local winds as they had adapted and enhanced Holland's basic model specifically for use in the Coral Sea. Their model provides the ability to incorporate both a primary vortex (which is what is described in [1] above) and a secondary vortex, as well as to approximate the high winds that can be generated outside the cyclone circulation (synoptic winds) from the interaction of the cyclone within the broader atmospheric environment. Energy parameters predicted by the model include 10 metre surface wind speeds (adjusted for the forward motion of the cyclone, the Coriolis effect and boundary layer effects) and wind direction (adjusted for surface friction). I used the McConochie model to hindcast cyclone wind speed and direction every hour for each of 85 cyclones in a grid spanning the entire GBR at a 1 km resolution. Initially, I completed hindcasts for the five cyclones for which field observations of reef damage exists (Althea, Ivor, Joy, Celeste and Justin) to test which parameters were significant in explaining damage (see Chapter 6). I modelled both a primary and primary + secondary vortex for each of these cyclones and compared the results with field data to assess whether or not to use the secondary vortex for the entire time series. Synoptic scale winds were not considered due to a lack of data and time, but more importantly to assess the efficacy of using a simple model based on local winds only. I implemented the equations from the model to run in workstation Arc-Info using an automated series of nested AMLs (see Appendix 2). A raster solution was used primarily, in order to enhance visualisation and testing of the results. A vector implementation was also developed for ease in extracting results for specific points of interest, such as the location of automatic weather stations and particular sites on reefs.

4.5.1 Hindcasting equations

The gradient winds (V_G) for each cyclone were calculated for each distance (r) from the centre of the cyclone as shown below (after McConochie et al 1999).

[3] $$V_G = [\ V_C^2 + (r^2 \cdot f^2) / 4\ ]^{0.5}$$

where V_G = gradient wind speed
V_C = cyclostrophic wind speed
f = Coriolis parameter

The Coriolis parameter takes into account the apparent motion of the earth as it spins on its axis and is defined by the following equation.

[4] $$f = 2 \cdot \text{angular velocity of the earth} \cdot \sin(\text{latitude})$$

where angular velocity of the earth = 0.0000729 radians / second

The cyclostrophic wind speed represents the cyclone wind field uncorrected for the Coriolis effect and is defined by the following equation.

[5] $$V_C = \left[\ \frac{(R / r)^B \cdot (B \cdot \Delta P) \cdot e^{-(R/r)^B}}{P_A}\ \right]^{0.5}$$

where P_A = air density = 0.0155 m / m^3

Equations 3-5 do not take into account the forward motion of the cyclone and produce a completely symmetrical wind field (Figure 4.11 - A). Introducing forward motion (Figure 4.11 - B) produces a more realistic asymmetrical wind field, with the strongest winds found in the front left quadrant with respect to the direction of movement of the cyclone.

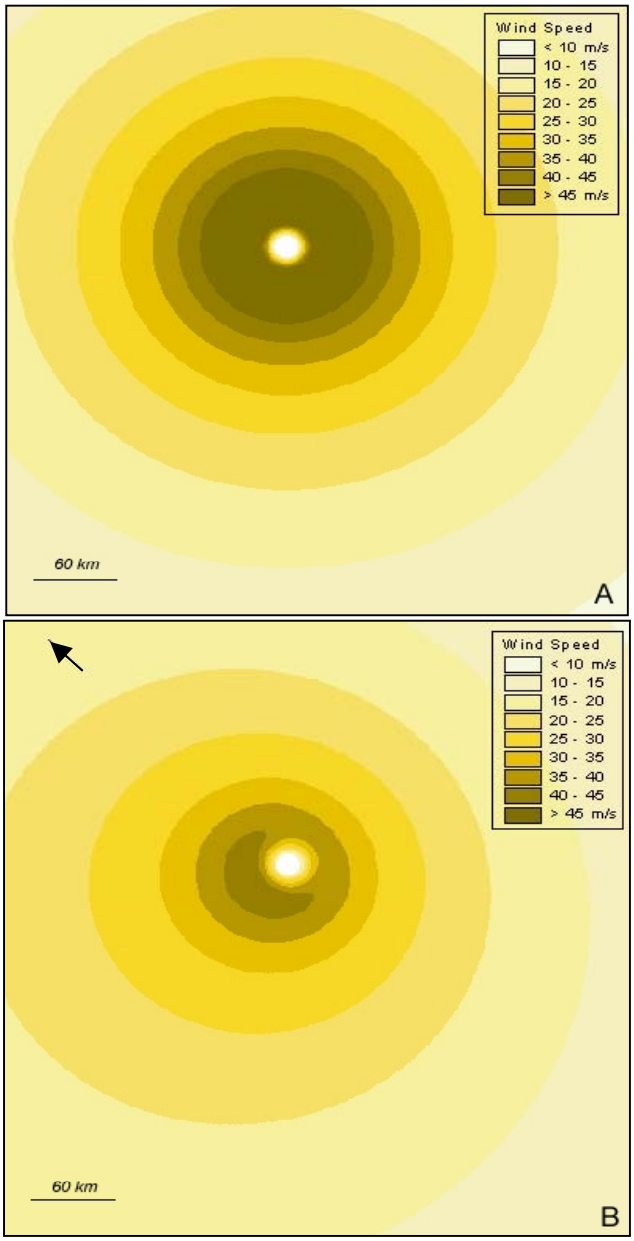

Figure 4.11. Extent and magnitude of 10 metre surface wind speeds during one eye position of cyclone Joy (1990) as if it were stationary (A) and corrected for the cyclone's forward motion (B). In B, the cyclone is moving at 10 km per hour in the direction of the arrow. The radius of maximum winds (eye) is set to 30 km.

Wind speeds are adjusted for the forward motion of the cyclone based on its speed and direction of movement, as described below.

[6] $V_{GF} = V_G + \alpha \cdot V_F$

where V_F = speed of cyclone forward motion

α = $0.5 (1 + \cos (\theta_F - 65))$

θ_F = anticlockwise angle between the point of interest and the cyclone eye with the direction of forward motion of the cyclone

Finally, wind speeds are adjusted for boundary layer effects, depending on predicted wind speed, using equation 7 below.

[7] $V = \gamma \cdot V_{GF}$

where $\gamma = 0.81$ when $V_{GF} < 6.0$

$\gamma = 0.81 - 2.93 * 10^{-3} \cdot (V_{GF} - 6)$ when $6.0 \leq V_{GF} < 19.5$

$\gamma = 0.77 - 4.31 * 10^{-3} \cdot (V_{GF} - 19.5)$ when $19.5 \leq V_{GF} < 45$

$\gamma = 0.66$ when $V_{GF} \geq 45.0$

The direction towards which cyclone generated wind was blowing was found for each time step by adding 90 degrees to the anti-clockwise angle between the site of interest and the direction of forward motion of the cyclone.

[8] $D^1 = \theta_F + 90$

This was then adjusted for the cross isobaric flow caused by surface friction, following Sobey et al (1977), as reported in McConochie et al (1999). The adjustment varies by the distance from the radius of maximum winds, with the largest adjustment carried out from the radius of maximum winds to 1.2 times that distance.

[9] $D = D^1 - B$

where $B = 10 \cdot r / R$ when $r < R$

$B = 75 \cdot r / R - 65$ when $R \leq r < 1.2 \cdot R$

$B = 25$ when $1.2 \cdot R \leq r$

After the correction, winds spiral inwards towards the eye more dramatically in close vicinity to it (Figure 4.12).

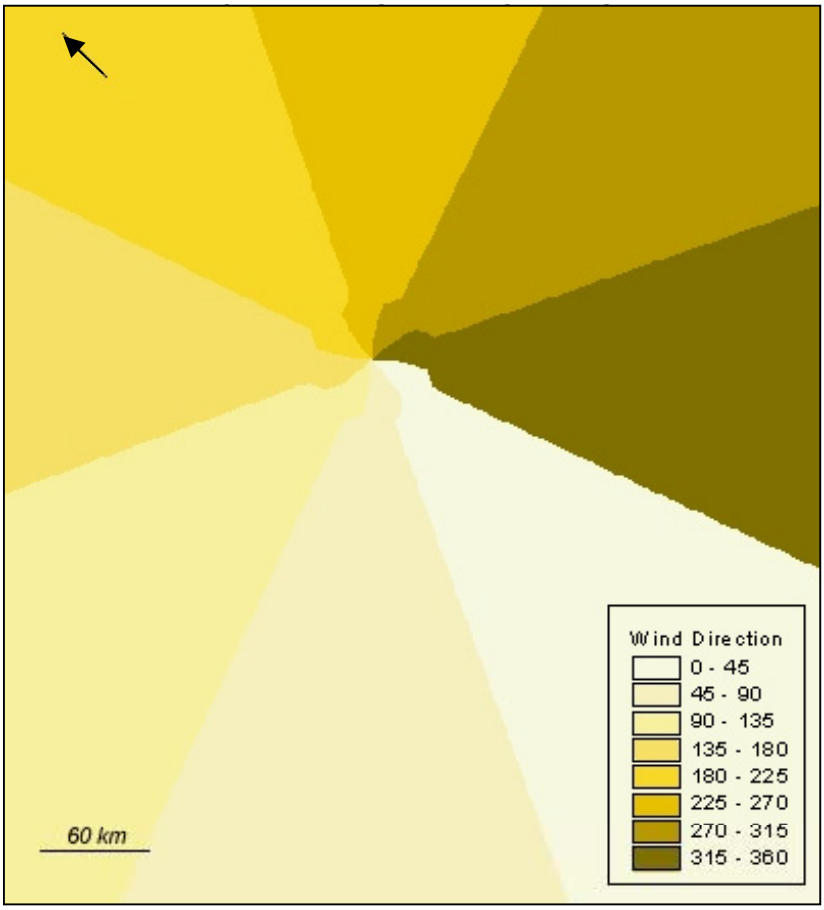

Figure 4.12. Direction from which surface winds originated during one eye position of cyclone Joy (1990). The cyclone is moving in the direction of the arrow. The radius of maximum winds is set to 30 km.

The resultant wind directions indicate the direction *towards which* the wind was blowing (Figure 4.13). However, automatic weather stations record the direction *from which* the wind blew. Thus 180 degrees was subtracted from the modelled directions to facilitate comparisons.

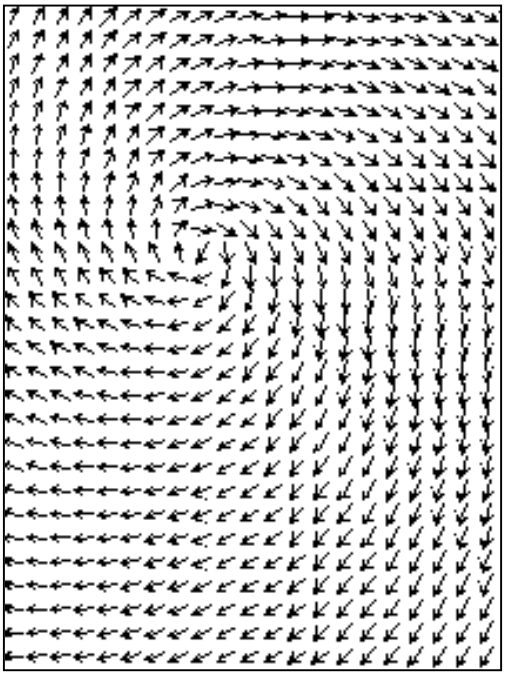

Figure 4.13. Wind direction during one eye position of cyclone Joy (1990). Arrows point in the direction towards which the wind was blowing. The cyclone is moving to the northwest at 10 km / hour. The radius of maximum winds is set to 30 km.

Over time, meteorologists have become aware that double, concentric eye walls can form during intense cyclones, producing a secondary as well as a primary wind maximum. Thompson and Cardone (1996) developed an extended wind model incorporating a second eye wall, or secondary vortex. Very little is known about the occurrence of secondary wind maxima in the Coral Sea region. However, McConochie et al (1999) found it useful to incorporate a secondary vortex to more effectively model the wind environment outside the primary vortex because Coral Sea cyclones are often embedded in a broader scale low pressure trough. Their secondary vortex is based on the results of Thompson and Cardone (1996). To incorporate the secondary vortex, the pressure profile must first be extended, as shown below.

$$[10] \qquad P = P^0 + \sum_{i=1}^{2} \Delta P_i \cdot e^{-(R/r)^{B_i}}$$

where $\sum_{i=1}^{2} \Delta P_i$ = ambient pressure - P^0

primary vortex: i = 1

secondary vortex: i = 2

Accordingly, finding V_G (wind speeds uncorrected for cyclone forward motion) requires finding the cyclostrophic wind speeds for each of the two vortices and then adding them together before applying corrections for the Coriolis effect, forward motion and boundary layer effects.

[11] $$V_G = \left(\sum_{i=1}^{2} V_{C_i}^{\,2} + (r^2 \cdot f^2) / 4 \right)^{0.5} - (r \cdot |f|) / 2$$

Following McConochie et al (1999), I set the radius of maximum winds for the second eye wall to 200 km and approximated the secondary pressure deficit using the following equation.

[12] $$\Delta P_2 = (1013 - 1005) + P^0 / 20$$

Incorporating the secondary vortex results in high wind speeds farther from the cyclone eye, as well as an enlarged crescent of maximum winds in the front left quadrant (Figure 4.14).

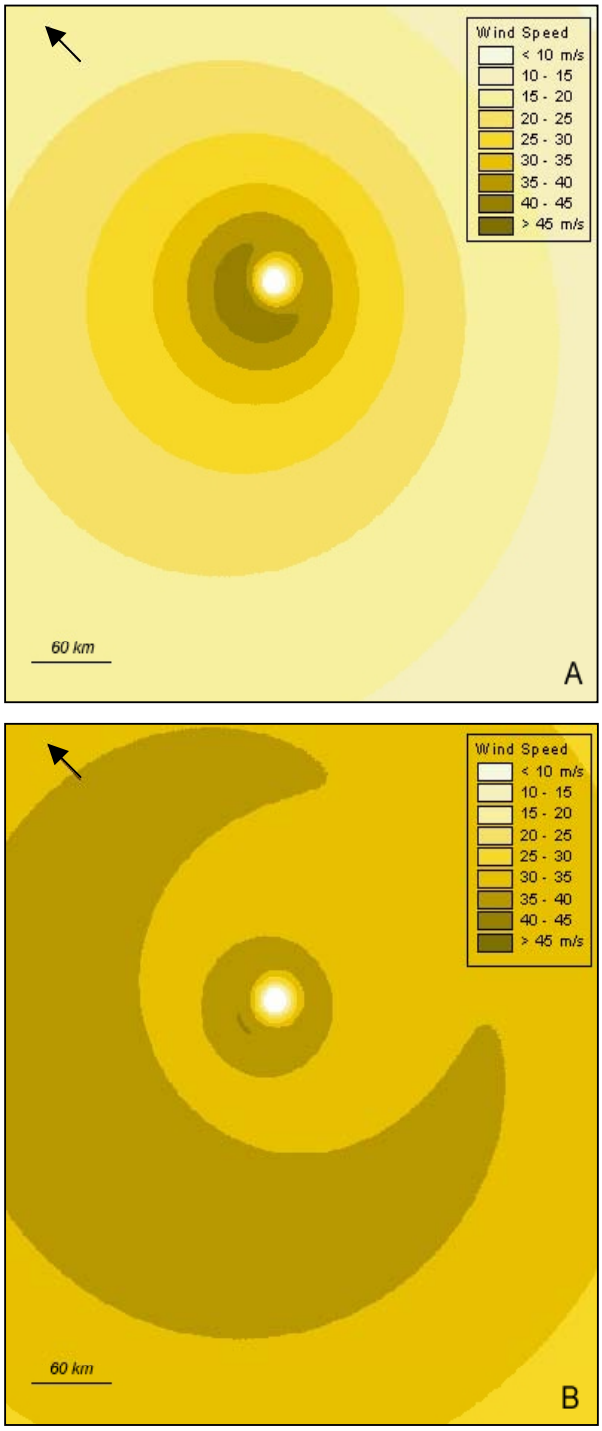

Figure 4.14. Extent and magnitude of 10 metre surface wind speeds during one eye position of cyclone Joy modelled with a primary vortex (A) and a primary + secondary vortex (B). The cyclone is moving at 10 km per hour in the direction of the arrow. The radius of maximum winds is set to 30 km.

4.5.2 Sensitivity of the model

The model results are sensitive to variation in several key input parameters, such as the speed of forward motion of the cyclone (V_F), the radius of maximum winds (R), and the intensity of the cyclone at each eye position. For example, the magnitude and

distribution of cyclone winds changes as a cyclone's forward speed changes (Figure 4.15). When a cyclone moves unusually slowly (less than 10 km / hour), the magnitude of cyclone winds is less, their distribution is more symmetrical and the crescent of highest winds nearly disappears. When cyclone translation speeds are closer to normal (10-20 km / hour), asymmetry becomes more marked, the magnitude of winds rises and the crescent of highest winds is distinct. As cyclone translation speeds rise above normal, these trends continue to the point where the wind speed predictions are in doubt - the threshold speed for this seems to be about 20 km / hour.

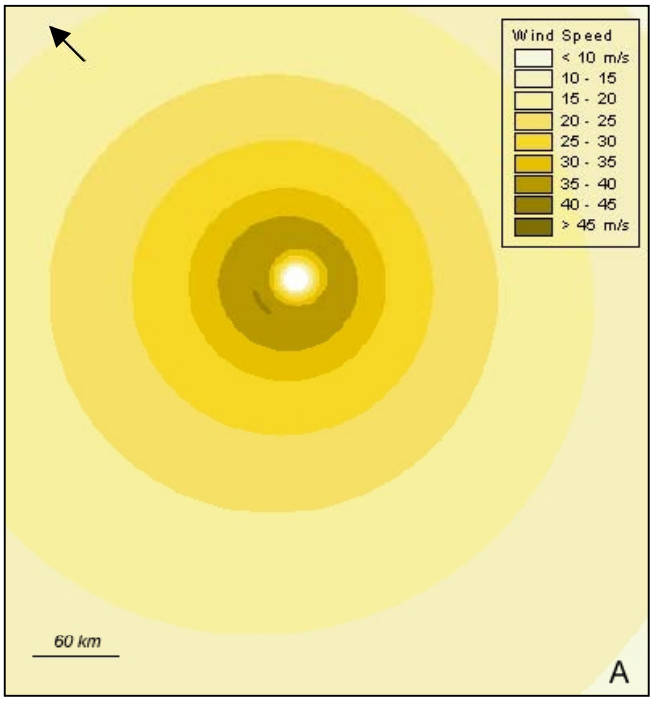

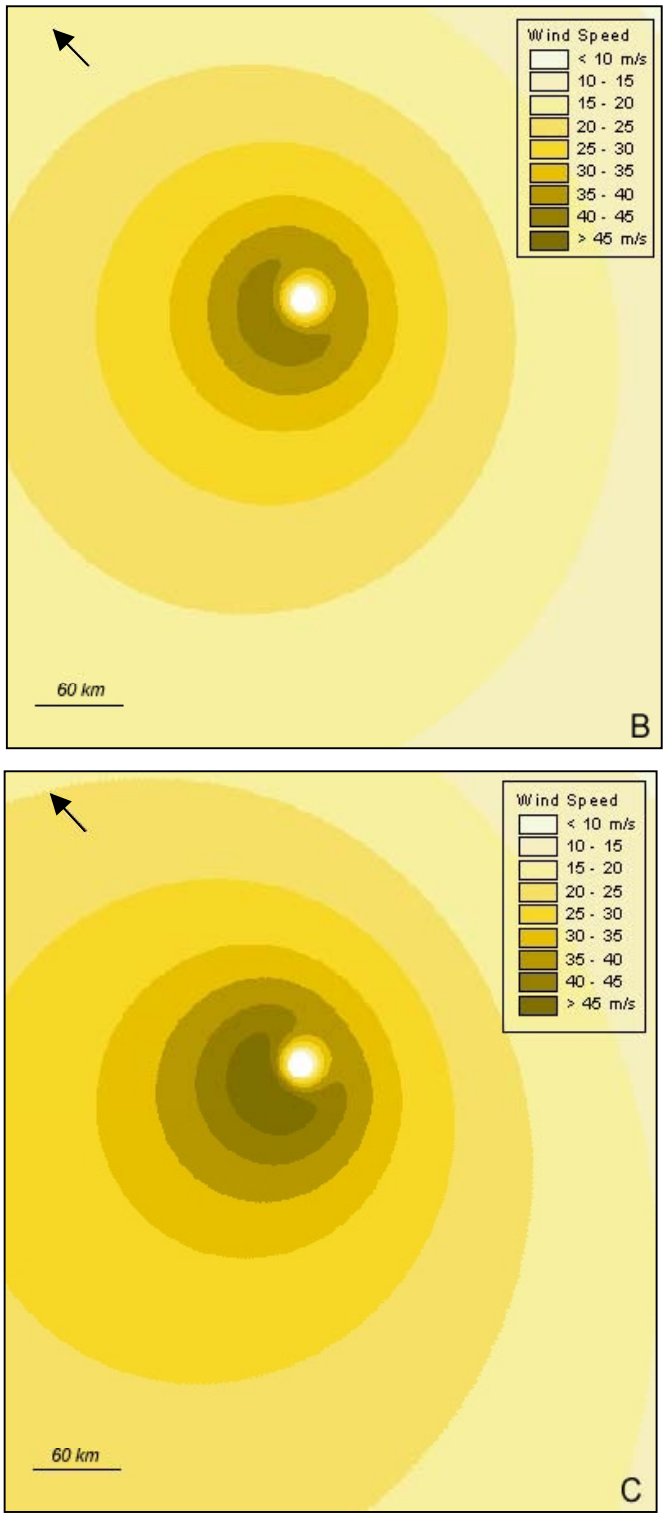

Figure 4.15. Effects of the rate of forward motion on the extent and magnitude of 10 metre surface wind speeds during one eye position of cyclone Joy. The cyclone is moving in the direction of the arrow at 5 km / hour [A], 10 km / hour [B] and 20 km / hour [C]. The radius of maximum winds (eye) is set to 30 km.

The predicted wind fields also differ considerably with changes in the radius of maximum winds (eye width), which is rarely measured. For example, when the cyclone eye is unusually wide (~100 km) rather than normal (~30 km), the highest predicted wind speeds extend further from the eye and the crescent of highest winds is enlarged (Figure 4.16).

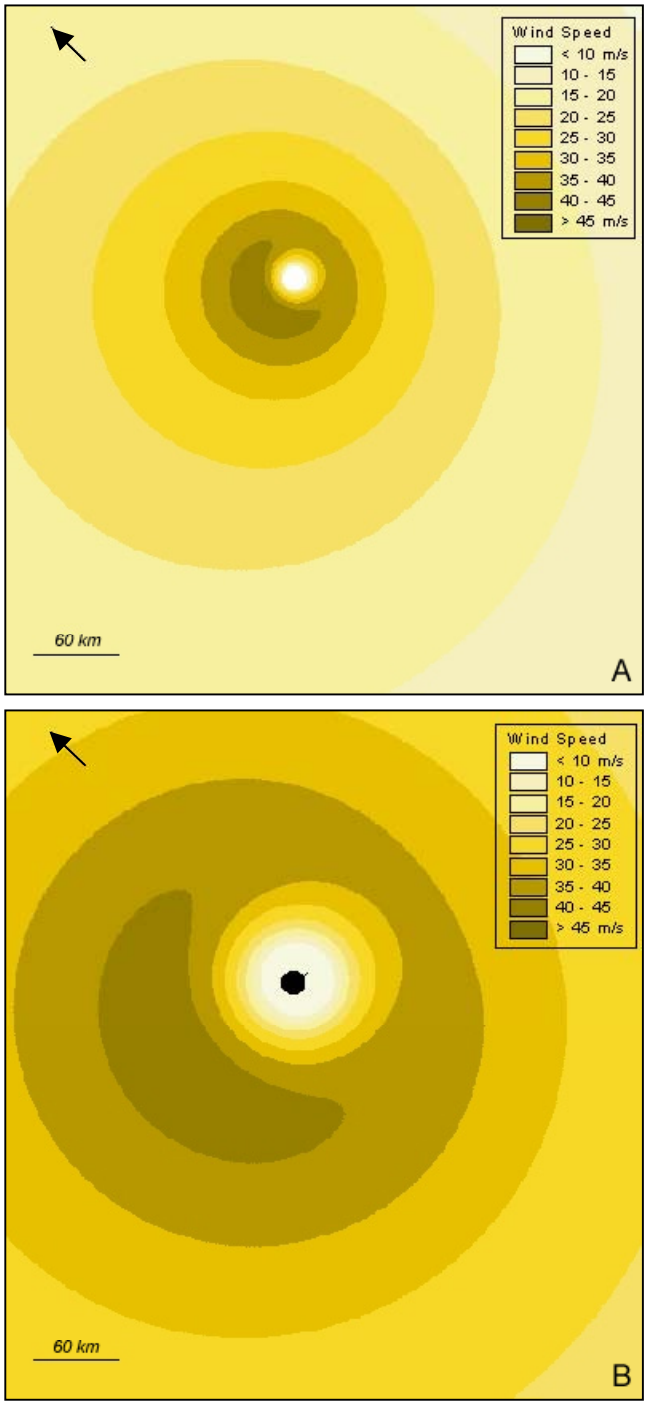

Figure 4.16. Extent and magnitude of 10 metre surface wind speeds during one eye position of cyclone Joy (1990) modelled with a primary vortex only for a typical radius of maximum winds - 30 km (A) and an unusually large radius of maximum winds - 100 km (B). The cyclone is moving at 10 km per hour in the direction of the arrow.

Finally, the hindcast wind fields also vary considerably with changes in the intensity of the cyclone. In general, the wind field becomes less clearly defined as the intensity of the cyclone decreases (Figure 4.17). Not only are the wind speeds in [B] lower overall, but the crescent of high winds is barely distinct. Further, wind speeds in [B] change more slowly with distance from the cyclone eye. The hindcast wind fields also vary with the spatial resolution at which they are calculated within the GIS. Cyclone processes and structures are not resolved in the meteorological model beyond a spatial resolution of about 1 to 2 km (Thompson and Cardone 1996). Using a finer (more detailed) resolution would vastly increase both computer disc space and processing times whilst adding no additional information for the purposes of this study. Using a coarser (less detailed) resolution results in a loss of detail - primarily due to decreasing levels of precision in measuring distances (a key input into the model). Automated scripts were written in AML (Appendix 2) to extract wind speed and direction predictions for specific points of interest to save as vector point coverages, after which the hindcast wind speed and direction grids were deleted. For the five test cyclones (Althea, Ivor, Joy, Celeste and Justin), these sites of interest included the location(s) of automated weather stations for validation, and the locations of sites visited during ecological surveys of wave damage. For all 85 cyclones, observations were extracted for points located every 1 km along the perimeter of each reef (n = 24,224).

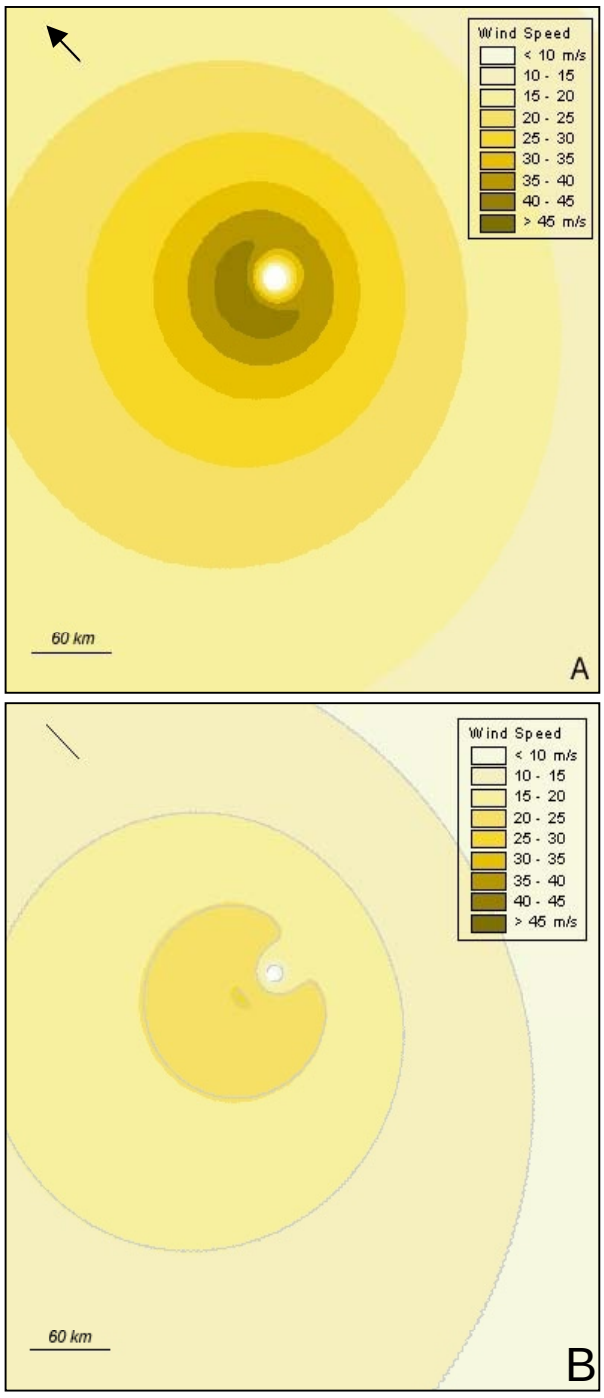

Figure 4.17. Extent and magnitude of 10 metre surface wind speeds during one eye position of cyclone Joy modelled with a primary vortex only when strong - intensity set to 940 hPa (A) and when weak - intensity set to 990 hPa (B). The cyclone is moving at 10 km per hour in the direction of the arrow. The radius of maximum winds (eye) is set to 30 km.

4.6 Comparison with field observations

Where possible, hindcast wind speeds and directions were compared to field observations to verify the model. Data was sought for as many weather stations as possible during each cyclone from the Australian Bureau of Meteorology. Not all

weather stations of interest were operational at the time of the cyclones. For example, data from Green Island would have been highly useful during cyclone Ivor but the station was not recording during that time. Further, weather station data were often incomplete and were rarely consistent in timing over the time series. This limited the ability to make detailed statistical comparisons between observed and modelled wind speeds and directions. Nonetheless, all relevant digital data that were reasonably available was used. At least one weather station recorded relevant observations for each of the cyclones for which reef damage data exists (Table 4.4). Some of the weather stations were located quite distant from the cyclone path at the time that measurements were made. For example, at its closest approach, cyclone Celeste was about 320 km away from Gannet Cay. In these cases, the modelled wind speeds and directions were less likely to match the observations as local factors become increasingly important to wind speeds with distance from the cyclone path. While cyclone Justin did not track very close to several of the stations, this was less problematic because of the unusually large extent of that storm. The height of the instruments above sea level at each station, particularly when located on an island with significant topography (Fitzroy, Hamilton and Hayman), also affected the match between observed and modelled winds. Local wind speeds and directions around high islands can be expected to vary a great deal due to local shelter effects (depending on the relative position of the cyclone) introducing noise into the observations. Additional wind data may also be available in non-digital form. For example, records of wind speed and direction were recorded on paper in Townsville during cyclone Althea (Oliver 1973). These observations were not used due to the difficulty of extracting accurate values from the reproduced instrument graphs.

Table 4.4. Locations of BOM weather stations that recorded relevant observed wind speed and direction data available during cyclones Althea, Ivor, Joy, Celeste, and Justin in digital form.

Station	Location		Station Height (m)	Cyclones (19xx)	Distance from cyclone path (km)
	Lat (^{0} S)	*Long (^{0} E)*			
Creal Reef	20.53	150.38	1.7	Celeste (96) Justin (97)	140, 315-365
Fitzroy Island	16.93	146.00	124.0	Ivor (90) Joy (90)	11, 75
Frederick Reef	20.94	154.40	12.8	Justin (97)	450
Gannet Cay	21.98	152.47	2.3	Celeste (96) Justin (97)	320, 510
Green Island	16.76	145.97	3.0	Celeste (96) Justin (97)	174, 30
Hamilton Island	20.35	148.95	22.6	Celeste (96) Justin (97)	30, 200-365
Hayman Island	20.06	148.95	2.4	Althea (71)	235
Holmes Reef	16.47	148.87	8.0	Justin (97)	63
Hook Reef	19.74	149.17	2.6	Justin (97)	200-300

Finally, these observations represent conditions at single points within the vast GBR (Figure 4.18), and thus provide only an indication of model performance because the cyclone wind field is known to be spatially variable within broad regions (McConochie et al 1999).

As is standard in the meteorological literature (for example, see Holland 1980, McConochie et al 1999, Thompson and Cardone 1996), time series plots were created to examine how the fit between the model predictions and station observations varied during each of the five test cyclones. Because station data was not available at each hourly interval modelled during the cyclones, comparisons could only be made at a sample of points along each time series. Modelled and observed wind speeds were

deemed to be in agreement if the former was within a threshold value of 10 $m.s^{-1}$ of the latter (differences within this range would have only a minor impact on the potential wave heights possible given the wind speed). Similarly, modelled wind directions were assumed to be reasonably accurate if found to be within 45 degrees of the observed values (wave directions are likely to vary from wind directions by at least this much). To assess this, the difference between the observed and predicted wind speed and direction

values was calculated and divided by the threshold value.

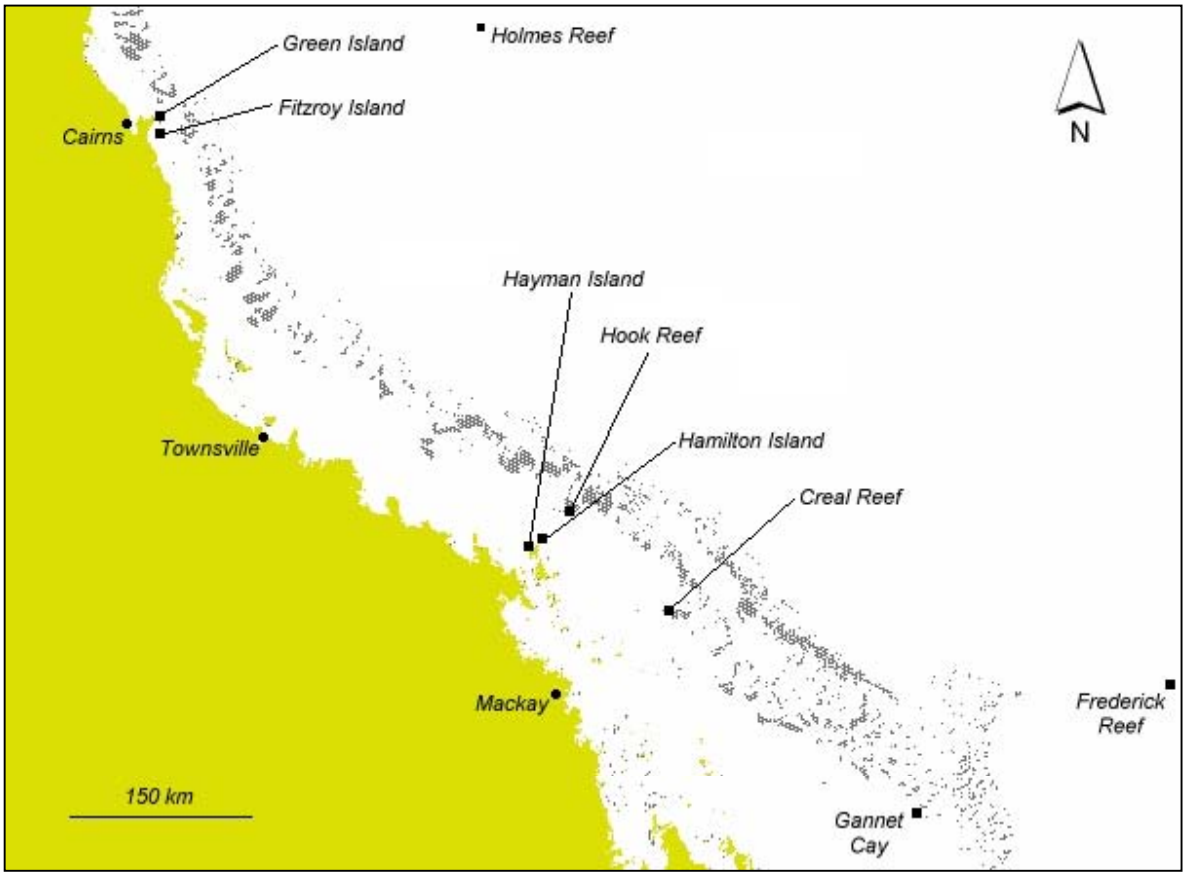

Figure 4.18. Location of automatic weather stations from which observations were used in this thesis.

The resultant **index of agreement** indicates the extent to which model results fell within the threshold of agreement (values of –1 to 1) for each point along the time

series for each set of weather station observations. Histograms were also created to show the number of comparisons for which the index of agreement fell within and beyond the threshold values for agreement.

4.6.1 Cyclone Ivor

Predictions for cyclone Ivor were compared to observations taken at the Fitzroy Island lighthouse (Figure 4.19).

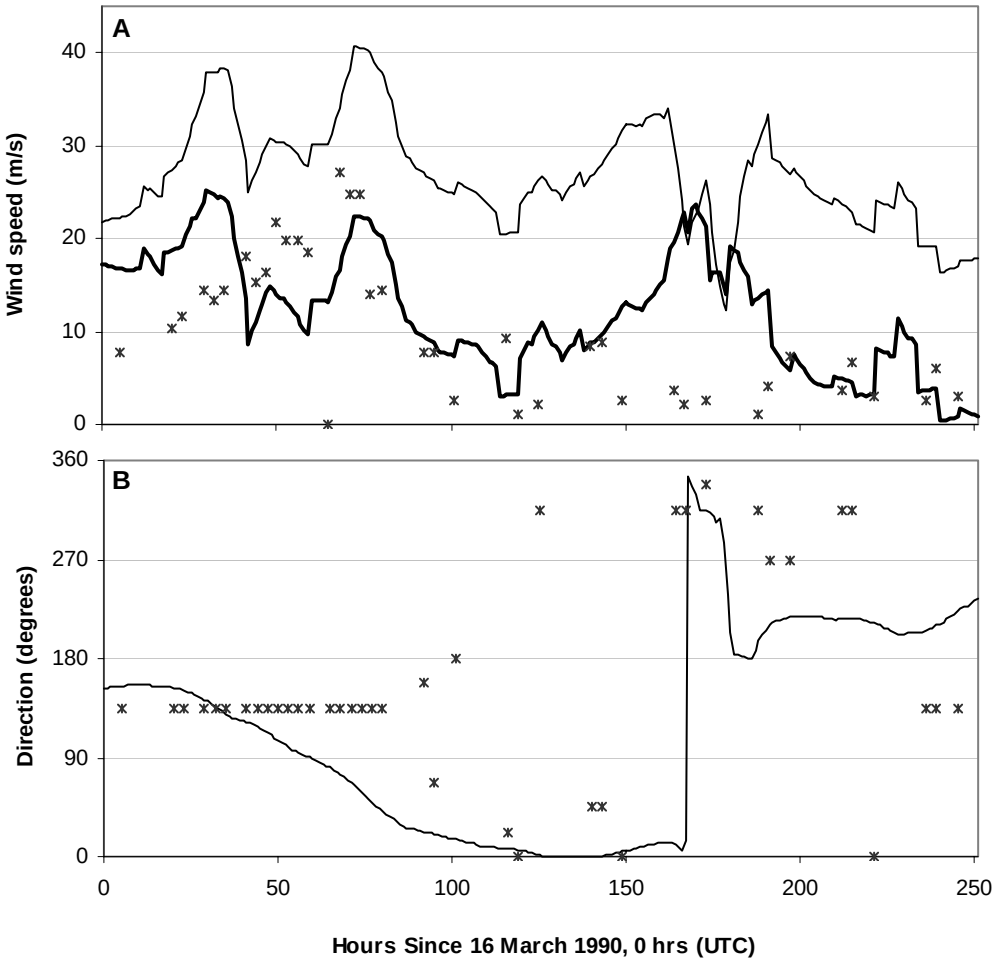

Figure 4.19. 10 metre surface wind speeds (A) and directions (B) during Cyclone Ivor (March 1990) at the Fitzroy Island Lighthouse (latitude: 16.93^0S, longitude: 146^0E). Asterisks show measurements taken by the Bureau of Meteorology weather station (altitude: 124 metres). The lines in (A) show winds predicted from the primary (thick) and primary + secondary (thin) vortices.

Though the cyclone passed very close (within 11 km) to the lighthouse, this occurred during the latter stages of the storm when the cyclone had weakened to below cyclone intensity (category 0). In its early stages, the cyclone was more than 300 km away from the station, reducing the expected accuracy of the model predictions. Inclusion of the secondary vortex over-predicted wind speeds for the entire storm. Between hours 150 and 200, observed wind speeds were near 0 while the model predicted a peak in speed approaching 25 $m.s^{-1}$. This disparity could be due to disruption of the wind field by the island's topography (maximum height = 269 metres, on a continental 'high' island). After about 100 hours, when winds approached from the south (the lighthouse is located on the north of the island), the observed directions became erratic. Also, the cyclone crossed the Queensland coast at about this time, after which the model performance would be expected to decline (it is designed for cyclone movement over water, not land). Further, the accuracy of cyclone eye positions and cyclone intensity estimates was poor once Ivor crossed the coast. However, wave damage to the surveyed reefs from the cyclone most likely occurred between 68 and 122 hours, when Ivor was located less than about 200 km away. Ten observations were available at the station during this time. These suggest that modelled wind speeds were reasonably accurate (90% of predictions were in agreement), with directions less so (only 20% of predictions within 45 degrees of the observed values).

Over the entire time series, comparisons of modelled versus observed wind speeds and directions were possible 39 times (Figure 4.20).

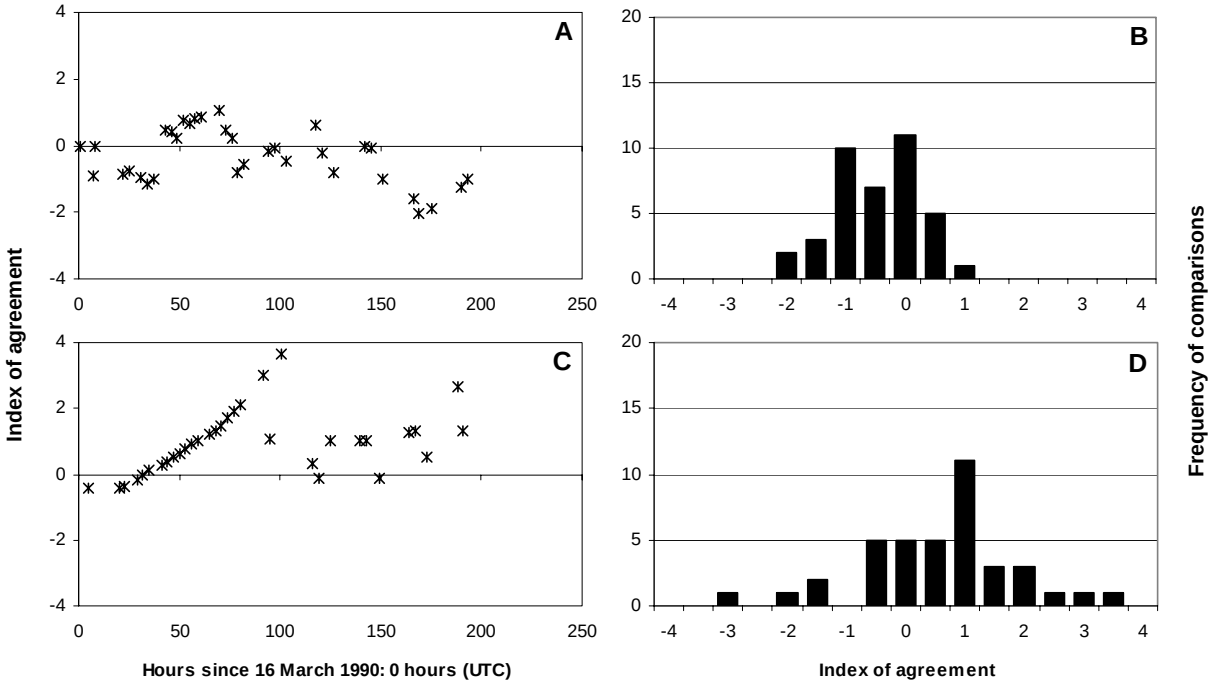

Figure 4.20. Index of agreement between wind speeds (A & B) and directions (C & D) observed at the Fitzroy Island Lighthouse and those predicted by the hindcasting model with a primary vortex only for selected points (n=39) during cyclone Ivor (March 1990). Index values were calculated by subtracting predicted from observed values and dividing by a threshold difference value (speed – 10 $m.s^{-1}$, direction – 45^0). Resultant values are plotted over the time series and tabulated by index value for: wind speed (A & B) and direction (C & D).

While most (82%) comparisons show agreement for wind speed, only just over half (51%) of predicted directions matched the observations. The maximum disagreement between modelled and observed winds was much more extreme for directions than winds. The slightly left skew in the wind speed histogram suggests that the model tended to over-predict wind speed (negative index values indicate modelled winds higher than observed winds). In contrast, the histogram of modelled wind directions shows a skew in the opposite direction, suggesting that modelled directions were under-predicted.

4.6.2 Cyclone Joy

Predictions for cyclone Joy (1990) were also compared to observations taken at the Fitzroy Island lighthouse (Figure 4.21).

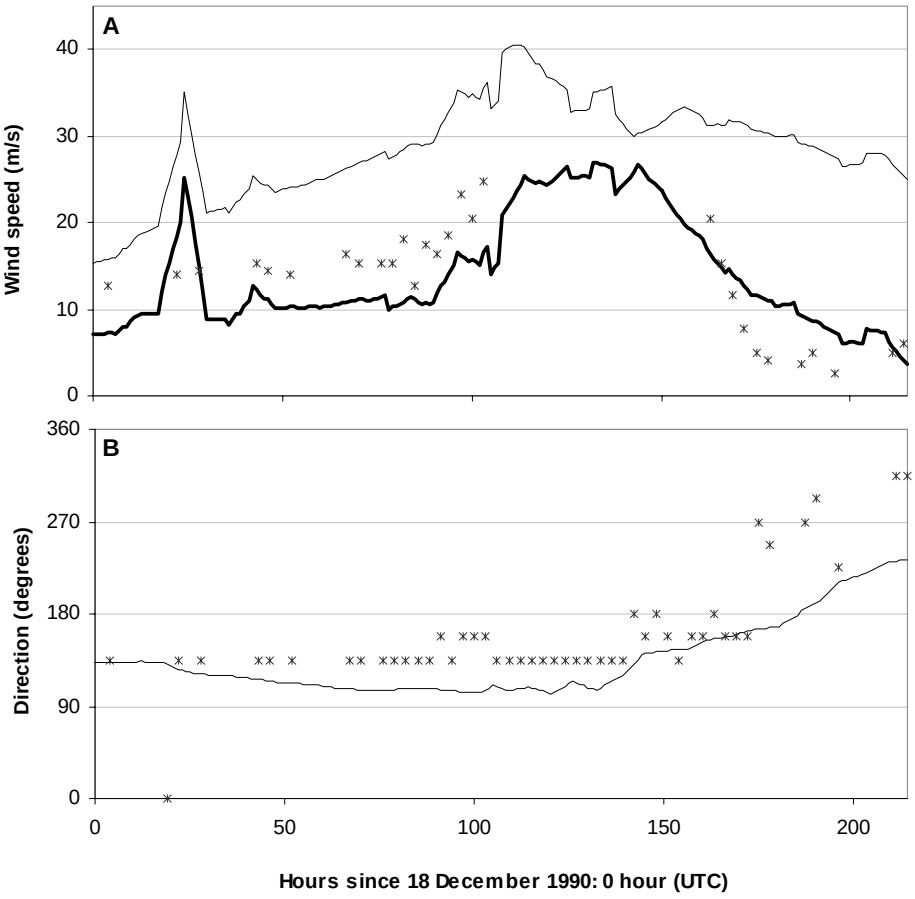

Figure 4.21. 10 metre surface wind speeds (A) and directions (B) during Cyclone Joy (December 1990) at the Fitzroy Island Lighthouse (latitude: 16.93^0S, longitude: 146^0E). Asterisks show measurements taken by the Bureau of Meteorology weather station (altitude: 124 metres). The lines in (A) show winds predicted from the primary (thick) and primary + secondary (thin) vortices.

When a secondary vortex was added to the simulation, winds were over-predicted, particularly towards the end of the storm. The primary vortex alone performed better, although it still over-predicted at the end of the storm and under predicted at the start. Unfortunately, observations were missing when the cyclone was most intense and

closest to the weather station (when the model was most likely to predict well). The predicted peak at about 25 hours from the start of observations resulted from the unusually fast speed of forward motion of the cyclone at this time (>20 km / hour). In contrast to cyclone Ivor, the predicted wind directions were good, falling within 45 degrees of the observed direction, except during the last 50 hours of the storm. In general, the model predicted winds to be more easterly than was observed. During this latter phase, the cyclone was located 100s of km away from the weather station. This was likely to reduce the quality of the model results at Fitzroy Island. Also, the model simulates conditions at 10 metres above sea level while the observations were recorded at 124 metres. Wave damage to the surveyed reefs from the cyclone most likely occurred between 102 and 213 hours, when Joy was located less than about 200 km away from the sites. Predicted wind speeds were in agreement for all observed speeds during this time. However, wind directions became slightly erratic towards the end of this period, but fit the observations more closely than was the case for cyclone Ivor. This may be partially due to the fact that the positional accuracy of the path worsened around this time.

Comparison of modelled versus observed wind speeds and directions was possible for 21 (speeds) and 40 (directions) times over the time series during cyclone Joy (Figure 4.22). These comparisons suggest that the model performed well, with agreement in wind speed and direction for 100% and nearly 75% of the cases, respectively. As was the case for cyclone Ivor, but to a lesser degree, the model tended to over-predict wind speeds and under-predict wind directions.

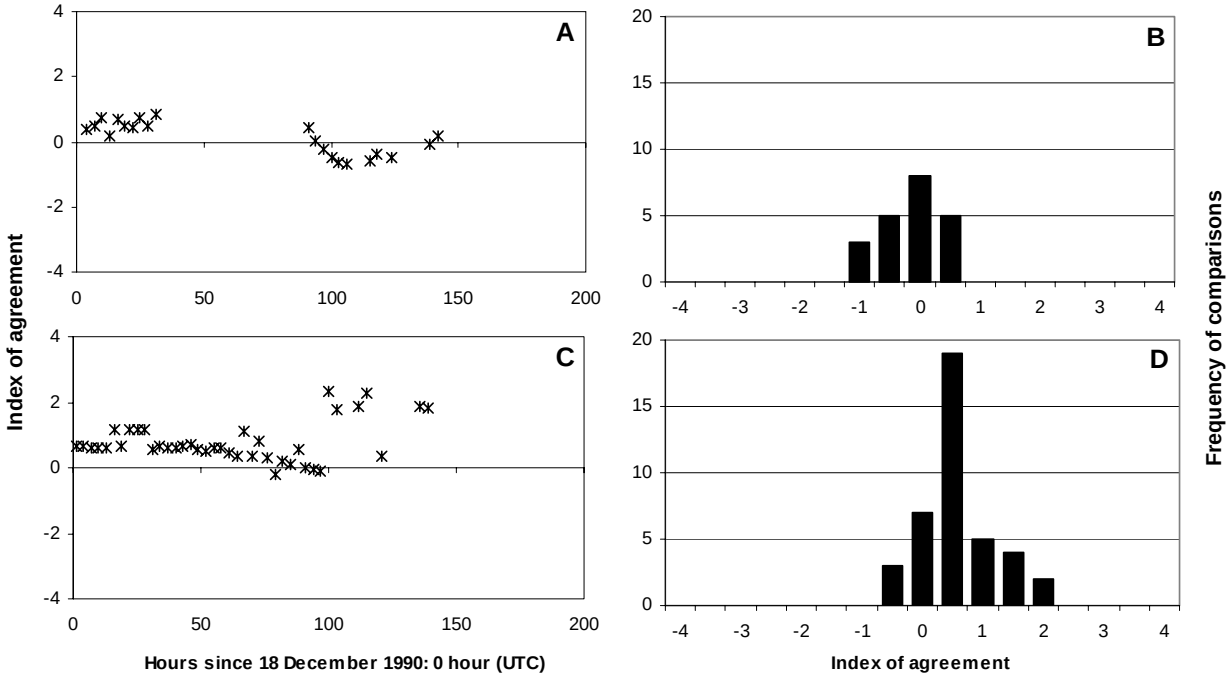

Figure 4.22. Index of agreement between wind speeds (A & B) and directions (C & D) observed at the Fitzroy Island Lighthouse and those predicted by the hindcasting model with a primary vortex only for selected points (speeds, n=21, directions, n=40) during cyclone Joy (December 1990). Index values were calculated by subtracting predicted from observed values and dividing by a threshold difference value (speed – 10 $m.s^{-1}$, direction – 45^0). Resultant values are plotted over the time series and tabulated by index value for: wind speed (A & B) and direction (C & D).

4.6.3 Cyclone Justin

Weather station data was available during cyclone Justin at seven locations - Holmes Reef, Green Island, Hook Reef, Hamilton Island, Creal Reef, Frederick Reef, and Gannet Cay Reef - that are spread across the southern two-thirds of the GBR. Of these, the results for Creal Reef are presented here (see Appendix 4 for results from the remaining stations). Because Justin was an unusually long lived cyclone, the time series of observations and model results was about twice as long as that for cyclones Ivor and Joy. Observed and modelled wind speeds during cyclone Justin matched most closely during the first ~75 hours of the storm at Creal Reef (Figure 4.23) – this was typical for most of the other weather stations.

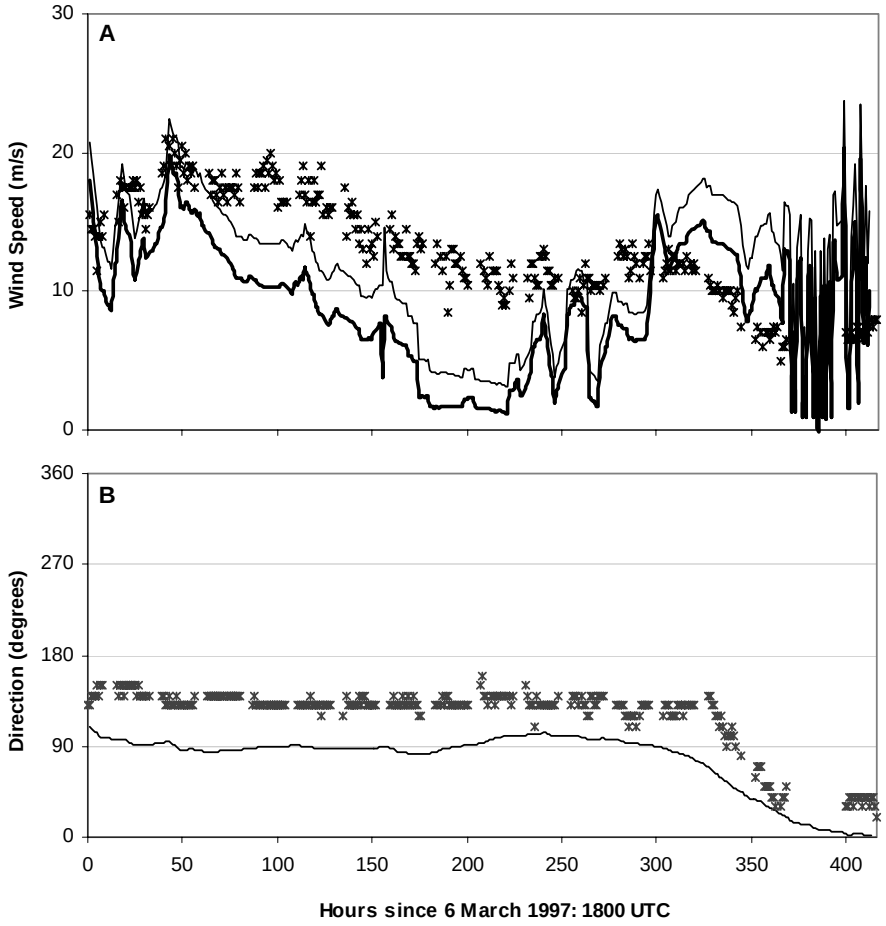

Figure 4.23. 10 metre surface wind speeds (A) and directions (B) during Cyclone Justin (March 1997) at Creal Reef (latitude: 20.53^0S, longitude: 150.38^0E). Asterisks show measurements taken by the Bureau of Meteorology weather station (altitude: 1.7 metres). The lines in (A) show winds predicted from the primary (thick) and primary + secondary (thin) vortices.

Both the primary and primary + secondary vortex under-predicted wind speeds from about 75 to just over 300 hours. Subsequently, they over-predicted until about 370 hours (when the cyclone crossed the coast at Cairns), at which time the modelled speeds became chaotic. Modelled wind directions consistently fell close to, though always more easterly than, the observed directions. This was also generally true for the remaining weather stations (see Appendix 4). The reef sites at which damage was measured after Justin were most likely impacted by waves generated during the first ~130 hours of the cyclone, when it was unusually large and nearly stationary and at

which time the model performed well – nearly all of the comparisons made between modelled and observed wind speeds during this time were in agreement (Figure 4.24). Because cyclone Justin was so long-lived and did not generate extreme conditions at the weather stations which could have disrupted observations, a nearly complete time series of observations was available for comparison with the modelled wind speed (n = 281) and direction (n = 280) data. Wind speeds were modelled quite well (nearly 96% of comparisons were in agreement), with directions less so (55% in agreement). However, the extent of disagreement in wind directions was not extreme, with index values limited to about 1.5 (predicted wind directions one and one-half times higher than observed).

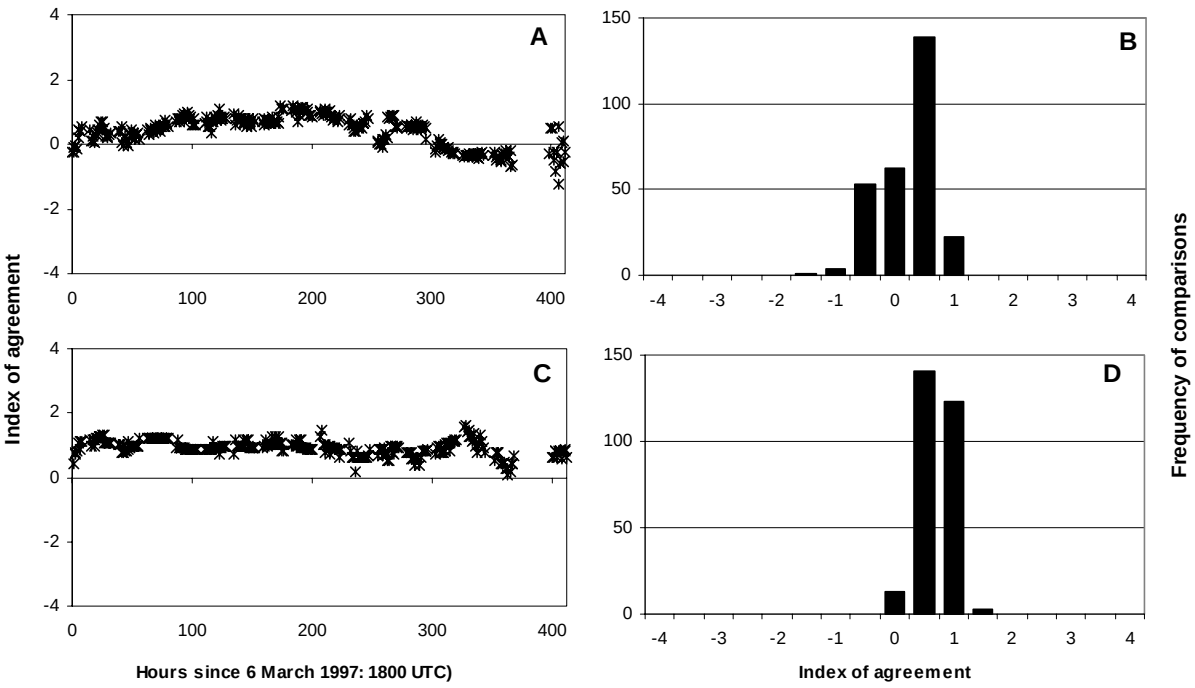

Figure 4.24. Index of agreement between wind speeds (A & B) and directions (C & D) observed at Creal Reef and those predicted by the hindcasting model with a primary vortex only for selected points (speeds, n=281, directions, n = 280) during cyclone Justin (March 1997). Index values were calculated by subtracting predicted from observed values and dividing by a threshold difference value (speed – 10 $m.s^{-1}$, direction – 45^0). Resultant values are plotted over the time series and tabulated by index value for: wind speed (A & B) and direction (C & D).

The worst fit between the modelled and observed wind speeds was found during the middle phase of the cyclone, when it had weakened and was moving northward in the Coral Sea. At this time, the position and size of the eye was very uncertain, which could have had a large effect on the subsequent wind fields. However, reef sites were unlikely to be affected by cyclone generated waves during this time as the cyclone was located more than 400 km away.

4.6.4 Cyclone Althea

Observed wind speeds and directions for cyclone Althea were only available for Hayman Island in a reasonably useable format (Figure 4.25). While it is difficult to make a judgement based on such scanty data (comparisons possible for wind speed = 12, direction = 11), it appears that both wind speeds and directions were modelled more successfully during the first half of the cyclone (up to ~100 hours). There was too little data to assess whether or not including the secondary vortex was worthwhile. In general, wind speeds were modelled more successfully than directions for the time series as a whole (67% versus 45% comparisons in agreement).

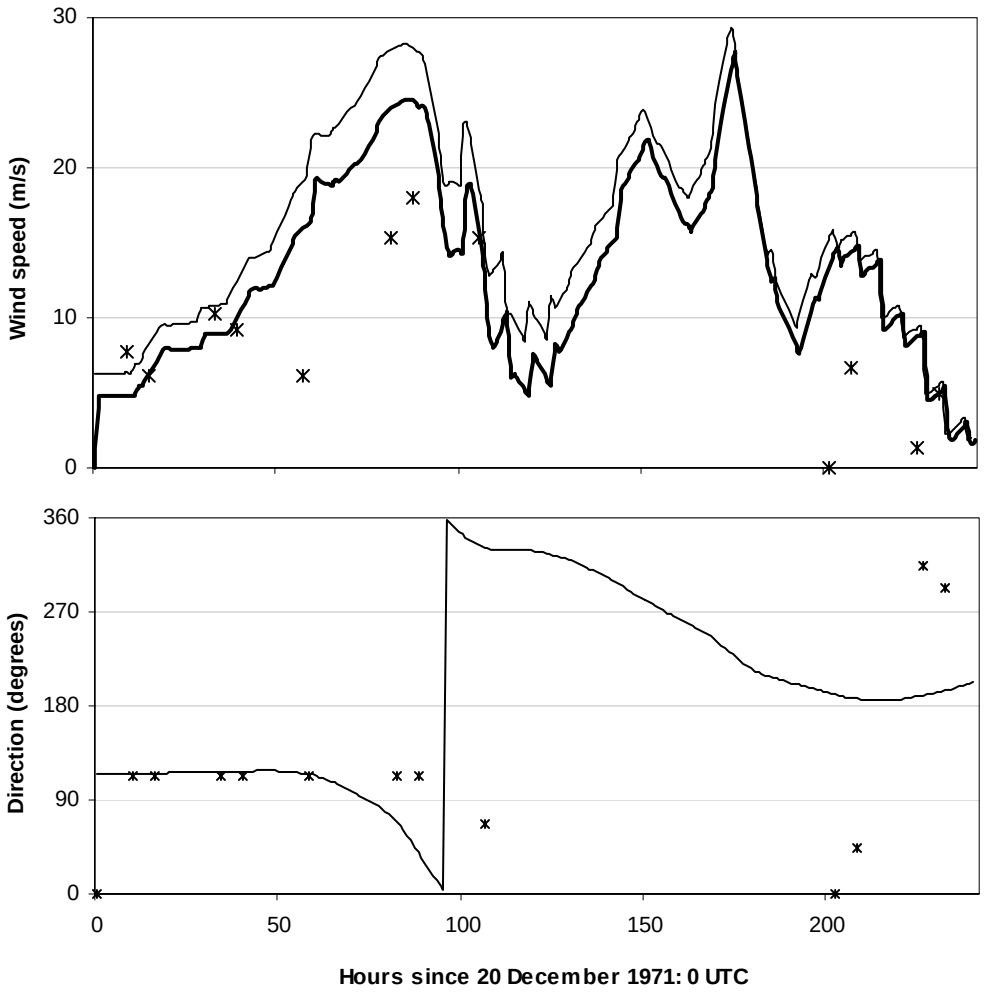

Figure 4.25. 10 metre surface wind speeds (A) and directions (B) during Cyclone Althea (1971) at the Hayman Island resort (latitude: 20.06^{0}S, longitude: 148.95^{0}E). Asterisks show measurements taken by the Bureau of Meteorology weather station (altitude: 2.4 metres). The lines in (A) show winds predicted from the primary (thick) and primary + secondary (thin) vortices.

However, this was not the case when the early part of the time series (0 to ~50 hours) was examined separately – in fact, modelled directions matched observations more closely that was the case for wind speeds (Figure 4.26). The histogram for wind directions illustrates the erratic nature of the observed directions during the latter part of the storm. These fluctuations were likely due to local-scale variation that the cyclone wind model would not be expected to resolve. In contrast, the histogram for

wind speeds is more compact, though skewed to the left, indicating that the model consistently over-predicted wind speeds.

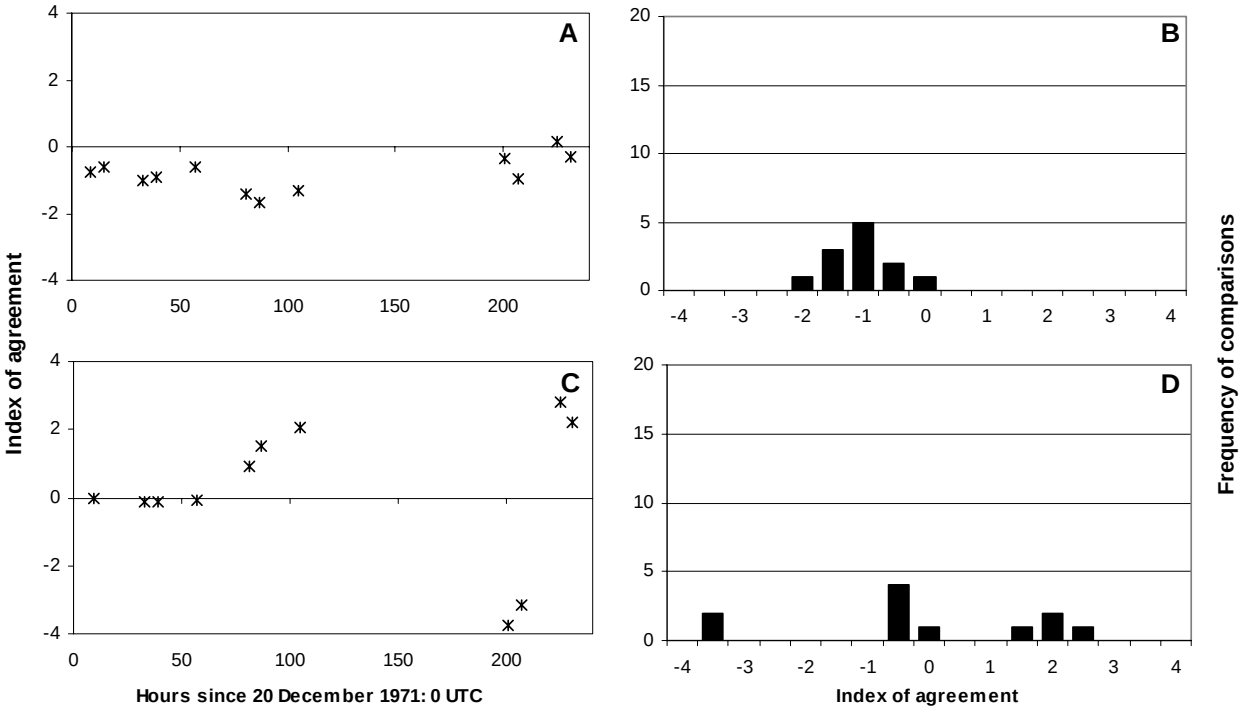

Figure 4.26. Index of agreement between wind speeds (A & B) and directions (C & D) observed at the Hayman Island resort and those predicted by the hindcasting model with a primary vortex only for selected points (speeds, n = 12, directions, n=11) during cyclone Althea (December 1971). Index values were calculated by subtracting predicted from observed values and dividing by a threshold difference value (speed – 10 $m.s^{-1}$, direction – 45^0). Resultant values are plotted over the time series and tabulated by index value for: wind speed (A & B) and direction (C & D).

4.6.5 Cyclone Celeste

Cyclone Celeste was very short lived, with observations spanning only half the time (~100 hours) of cyclones Ivor and Joy and one-fourth the time taken by Justin. Weather station data was available during cyclone Celeste at four stations: Green Island, Hamilton Island, Creal Reef, and Gannet Cay Reef. Of these, the results for Creal Reef are presented here (see Appendix 4 for results from the remaining stations).

Modelled and observed wind speeds matched best at Creal Reef at the beginning and end of the storm. Wind speeds were consistently over-predicted by both the primary and primary + secondary vortices (Figure 4.27).

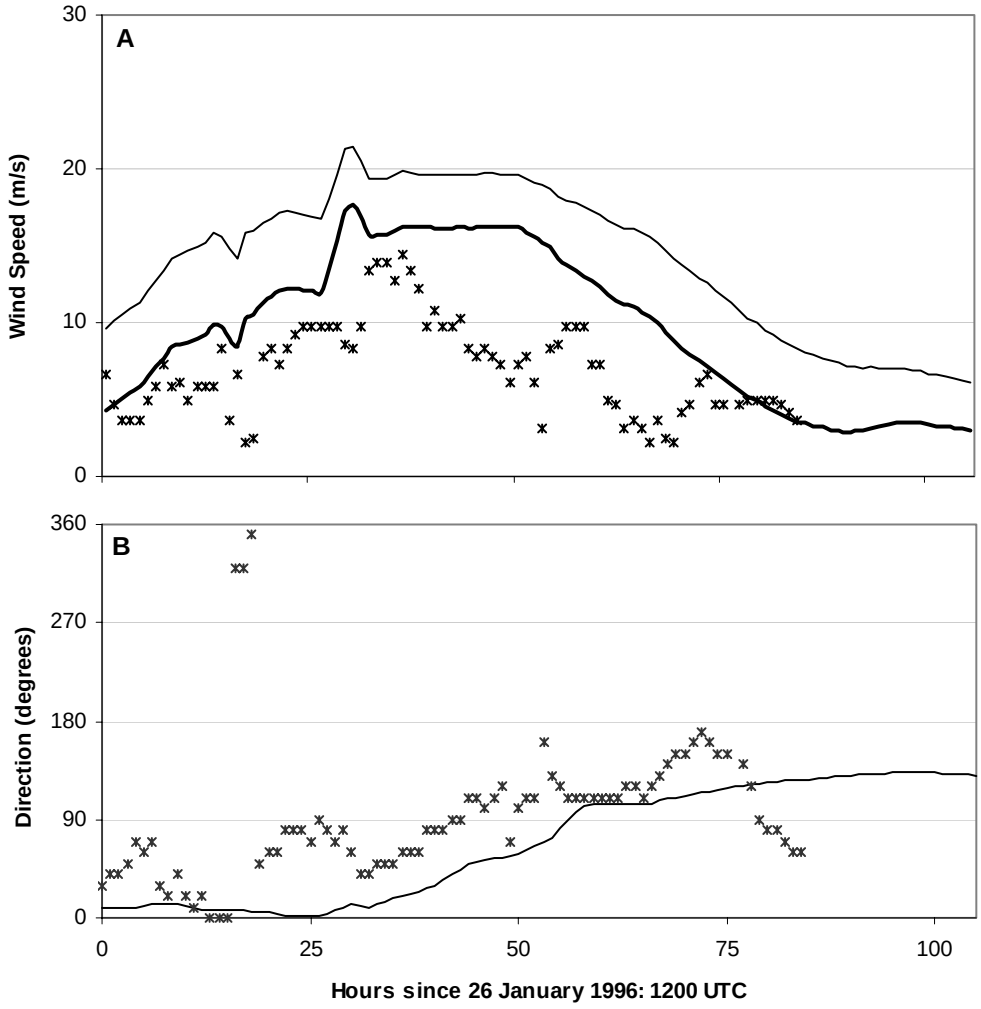

Figure 4.27. 10 metre surface wind speeds (A) and directions (B) during Cyclone Celeste (1996) at Creal Reef (latitude: 20.53^{0}S, longitude: 150.38^{0}E). Asterisks show measurements taken by the Bureau of Meteorology weather station (altitude = 1.7 m). The lines in (A) show winds predicted from the primary (thick) and primary + secondary (thin) vortices.

This was true for the other weather stations as well. The modelled wind directions, in contrast, both under-predicted and over-predicted actual wind directions because they did not track the periodic oscillations seen in the observed data. This suggests that local-scale processes affected wind directions but were not resolved by the model.

Using the primary vortex alone provided a better fit for wind speeds. As with cyclone Justin, nearly a complete time series of observations (n = 84) was available with which to compare modelled versus observed winds during cyclone Celeste (Figure 4.28).

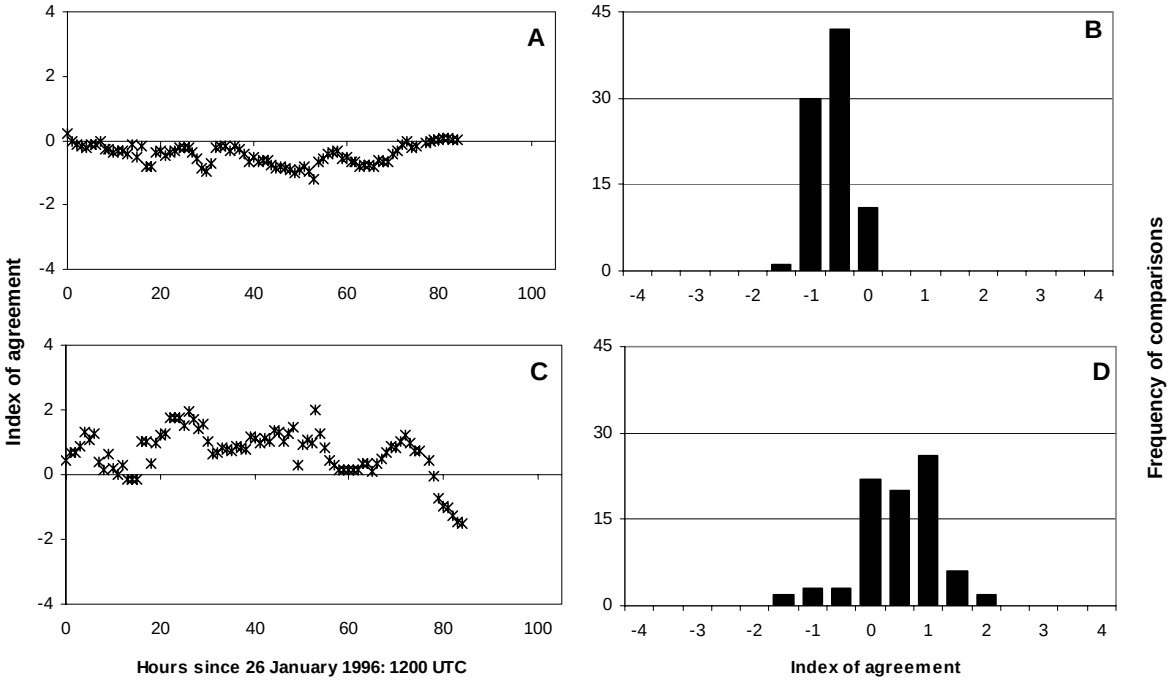

Figure 4.28. Index of agreement between wind speeds (A & B) and directions (C & D) observed at the Creal Reef and those predicted by the hindcasting model with a primary vortex only for selected points (n=84) during cyclone Celeste (January 1996). Index values were calculated by subtracting predicted from observed values and dividing by a threshold difference value (speed – 10 $m.s^{-1}$, direction – 45^0). Resultant values are plotted over the time series and tabulated by index value for: wind speed (A & B) and direction (C & D).

Observed wind directions were quite variable which was not reflected in the model results. However, they tended to oscillate within about 45 degrees of the predicted values. In fact, the modelled wind directions agreed with the observations most frequently for cyclone Celeste (88% agreement). The match between modelled and observed wind speeds was also quite good (nearly 100% agreement). This may be partly due to low positional error in cyclone Celeste's track, its high intensity (category 3) while located near the weather station (intense cyclones tend to be more

well organised and easier to model) and its relatively linear path once it tracked away from the coast offshore from Bowen.

4.6.6 Overall model performance

The purpose of using the hindcasting model was to estimate: 1) the direction from which the bulk of wind energy approached each reef site (an indication of the direction from which most waves would approach reef sites) and 2) the magnitude of that energy (a crude indication of the maximum wave heights that would be possible in the vicinity of reef sites). These estimates are based on predicted wind speeds and directions across the GBR every hour during each cyclone.

Comparing actual wind speeds and directions recorded at weather stations during each of the test cyclones provided a limited test of the quality of these estimates. It is important to realise, for example, that weather station data was recorded for only a sample of the time series for each cyclone and cannot be used to infer model fit at times where no data was recorded (most notably for cyclones Ivor, Joy and Althea, where observations are quite limited). In addition, the weather stations indicate model performance at single points, which cannot be extrapolated across the entire vast GBR. Further, the match between predicted and observed values is likely to vary over each time series, as each cyclone's position with respect to the weather station varied (a poor match is expected when a cyclone was distant from the weather station). Finally, the cyclone hindcasting model is designed to run at a spatial resolution of 1-2 km, which is insufficient to capture the local scale effects (some of which may be unrelated to the cyclone) likely to occur at weather stations that occupy a very small

proportion of that area. Given this, in all cases, wind speeds were modelled more successfully than wind directions (Table 4.5).

Table 4.5. Agreement between wind speeds (within 10 $m.s^{-1}$) and directions (within 45^0) observed at weather stations during cyclone Ivor, Joy, Justin, Althea and Celeste and those predicted by the McConochie et al 1999 model.

Cyclone	**Wind Speed**		**Direction**	
	Within 10 $m.s^{-1}$	*n*	*Within 45^0*	*n*
Ivor	82%	39	51%	39
Joy	100%	21	73%	40
Justin	96%	281	55%	280
Althea	67%	12	45%	11
Celeste	99%	84	88%	84

With the exception of cyclone Althea, modelled wind speeds matched the observations to within 10 $m.s^{-1}$ for the majority of the comparisons. For wind directions, this level of agreement was only found for cyclone Celeste (88% of comparisons matched within 45^0). The worst fit was found for cyclone Althea, with that of cyclones Ivor and Justin only marginally better. This disparity is not unexpected, however, as modelled wind directions are more sensitive to distance from the cyclone path (which is known to be uncertain) than is the case for wind speeds. Accordingly, the best model performance overall was achieved for cyclone Celeste, which also showed the least degree of positional uncertainty (see Figure 4.8).

4.7 Derived energy parameters

The potential for a cyclone to generate waves capable of damaging reefs depends on the intensity and duration of high wind energy. Assessing this potential thus requires parameters that reflect the potential for development of heavy local wind seas from the predicted wind speeds and directions over the entire cyclone. Thus, I calculated the maximum wind speed (MAX), the duration of gale force or higher winds (GALES), and the continuous duration of gale force or higher winds (CGALES) from the modelled hourly wind fields for each of the test cyclones (Althea, Ivor, Joy, Celeste, and Justin). I later tested their relative importance in explaining patterns of observed wave damage on the surveyed reefs (see Chapter 6). For ease in presenting maps, levels of MAX and GALES are classified into ranges. The original values, not these ranges, were used in building the statistical model testing the utility of the parameters to predicting wave damage, as reported in Chapter 6.

MAX estimates the maximum wind speed generated across the GBR *at any time* during each cyclone. MAX was calculated in GIS from the set of one-hourly wind speed grids using an automated AML (see Appendix 2). Values of MAX for specific sites of interest (surveyed reef sites) were extracted and imported into EXCEL for use in a model that predicts reef damage (see Chapter 6).

The formation of large waves requires sustained high wind conditions over an adequate expanse of deep water. Thus, the duration of high winds is just as important as their absolute magnitude. To measure the duration of high winds for each cyclone, I used GIS to count the number of hourly time periods each position across the GBR was predicted to experience cyclone winds of gale force (17 $m.s^{-1}$) or higher (GALES)

from the one-hourly wind speed grids (see Appendix 2). Values of GALES for specific sites of interest (surveyed reef sites) were extracted and imported into EXCEL for use in the predictive model of reef damage (see chapter 6). In contrast to MAX, the nature of the cyclone path and the speed of the cyclone's forward motion influenced GALES as much as the cyclone's intensity. For example, longer periods of gales were experienced in locations near the path when the cyclone was moving slowly or looped around within a small area. Similarly, some areas experienced gales from several eye positions along the path, particularly when the cyclone looped back and passed near where it had previously tracked.

The parameter GALES indicates the number of hours that winds were greater than or equal to gale force. However, waves build as winds blow *continuously* over an adequate stretch of open water (fetch). If the timing of gale force^{+} winds was intermittent rather than persistent, the potential wave climate that could form would be less than suggested by GALES. Thus, the longest continuous period during which winds met or exceeded gale force (CGALES) was found using an EXCEL spreadsheet of the hourly wind data for the surveyed reef sites. Where gale force^{+} winds were persistent rather than intermittent, values for CGALES are similar to those for GALES. The results for the five test cyclones are presented below.

4.7.1 Cyclone Ivor

During cyclone Ivor, the width of the maximum wind zone varied along the cyclone path as the intensity and speed of the cyclone changed (Figure 4.29-A). For example, maximum wind speeds greater than 30 m.s^{-1} were predicted only while Ivor was

intense (category 3). No distinct zone of maximum winds was present around the path when it tracked south, as the cyclone was weak at that time. Because of the asymmetry in the wind field at each eye position (higher wind in the front left quadrant with respect to the cyclone forward motion), more of the areas of highest wind speed (30^{+}m.s^{-1}) are located to the left of the path. All of the reef sites surveyed by Done et al (1991) were located within the 25 m.s^{-1} zone or higher, with 45% of them found inside the 35^{+}m.s^{-1} zone.

A broad area of the GBR experienced gale force or higher winds for more than 2.5 days during cyclone Ivor (Figure 4.29 - B). All of the reef sites surveyed by Done et al (1991), several of which sustained considerable high-energy wave impacts (dislodgment of massive corals and exfoliation of the reef matrix), fell within the 2^{+}day gales zone. The most consistently persistent high winds, lasting for up to two days, occurred on outer reef sites to the southeast of the path (Figure 4.29 - C). The least persistent high winds, lasting up to a day, occurred just to the north of the path and at ~ 100 km to the south.

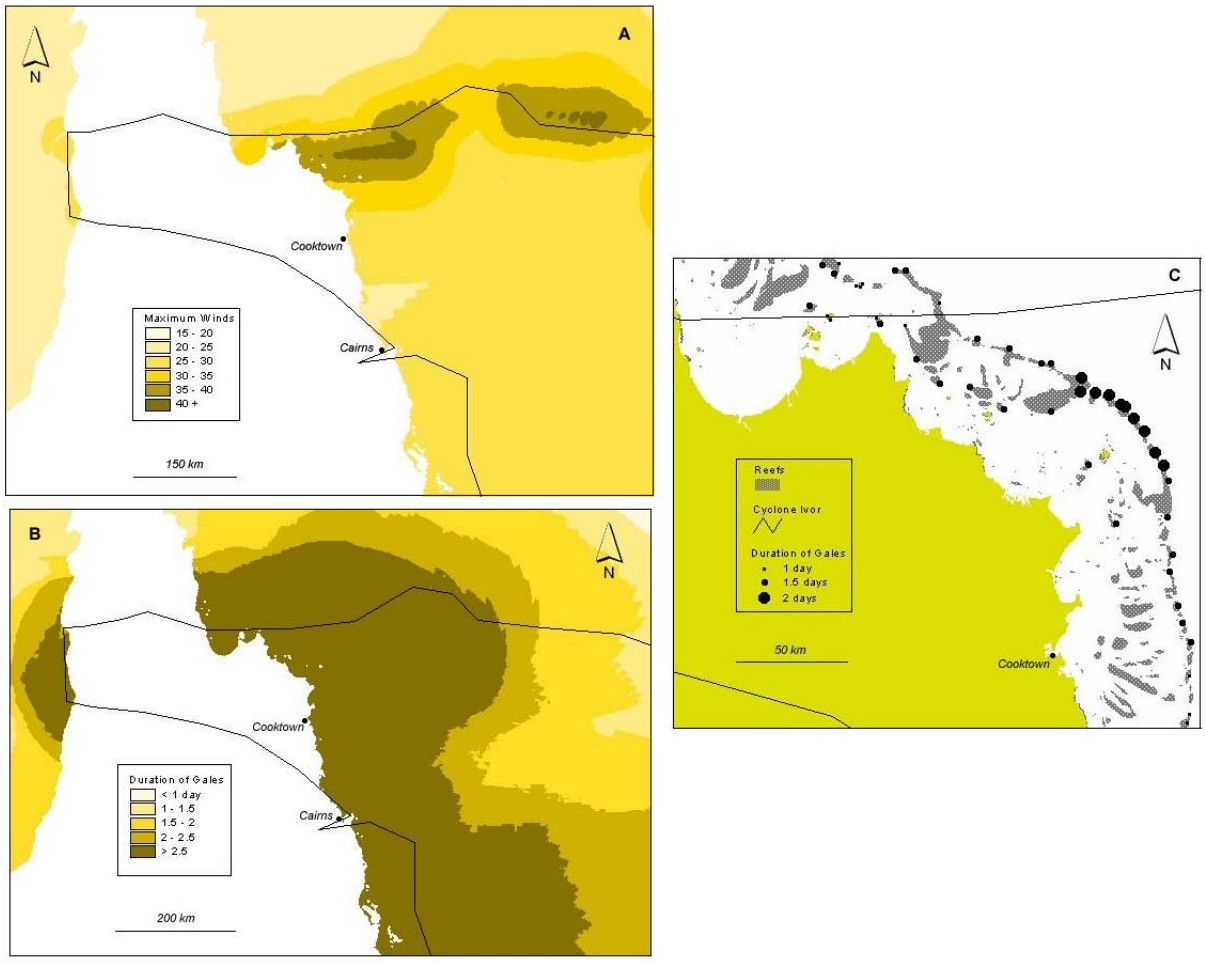

Figure 4.29. Cyclone energy parameters hindcast for cyclone Ivor: A- maximum 10 metre surface wind speeds, B – duration of winds ≥ gale force (17 $m.s^{-1}$), and C – continuous duration of high-energy winds at reef sites surveyed by Ayling 1991. The thin line shows the cyclone's path.

4.7.2 Cyclone Joy

During cyclone Joy, maximum wind speeds were concentrated around the section of the cyclone path nearest to Cairns, where the cyclone reached maximum intensity (Figure 4.30 - A). As with Ivor, the majority of reef sites (84%) surveyed by Ayling (1991) were located within the $25^{+}m.s^{-1}$ maximum wind zone. However, very few (2%) of the sites were found within the 35^{+}m.s-1 zone, largely because Joy approached, but did not cross, the GBR reef matrix while at high intensity. No zones

of highest winds are found southward along the path when the cyclone actually crossed the GBR because the cyclone was weak at that time.

GALES were widely distributed around the path of cyclone Joy (Figure 4.30 - B). The swath of most persistent gales (2.5^{+}days) was widest when Joy's path approached closest to Cairns, as it was then that the cyclone reached peak intensity (category 4), was moving slowly, and followed a convoluted path that further slowed its movement through the area. As with Ivor, most (93%) of the reef sites surveyed for wave damage following cyclone Joy were located within the 2.5^{+}day GALES zone. Many of these sites were damaged, some of them by high-energy impacts (dislodgment of massives and stripping of the reef matrix). About 5% of the sites, located ~200 km north of the cyclone's path, were found within the 1^{+}day GALES zone – none of these sites were damaged.

As might be expected, the least persistent high winds during cyclone Joy, lasting up to 1 day, occurred far from the cyclone's path (Figure 4.30 - C) - to the north of Cooktown. The duration of continuous gales gradually increased with distance southward (and proximity to the cyclone path). For example, sites located offshore from Cooktown experienced 1-2 days of continuous gales, while sites located southwards to Cairns experienced 2-3 days. The most persistent gales were found at only a few sites south of Cairns, where gales lasted up to 4 days.

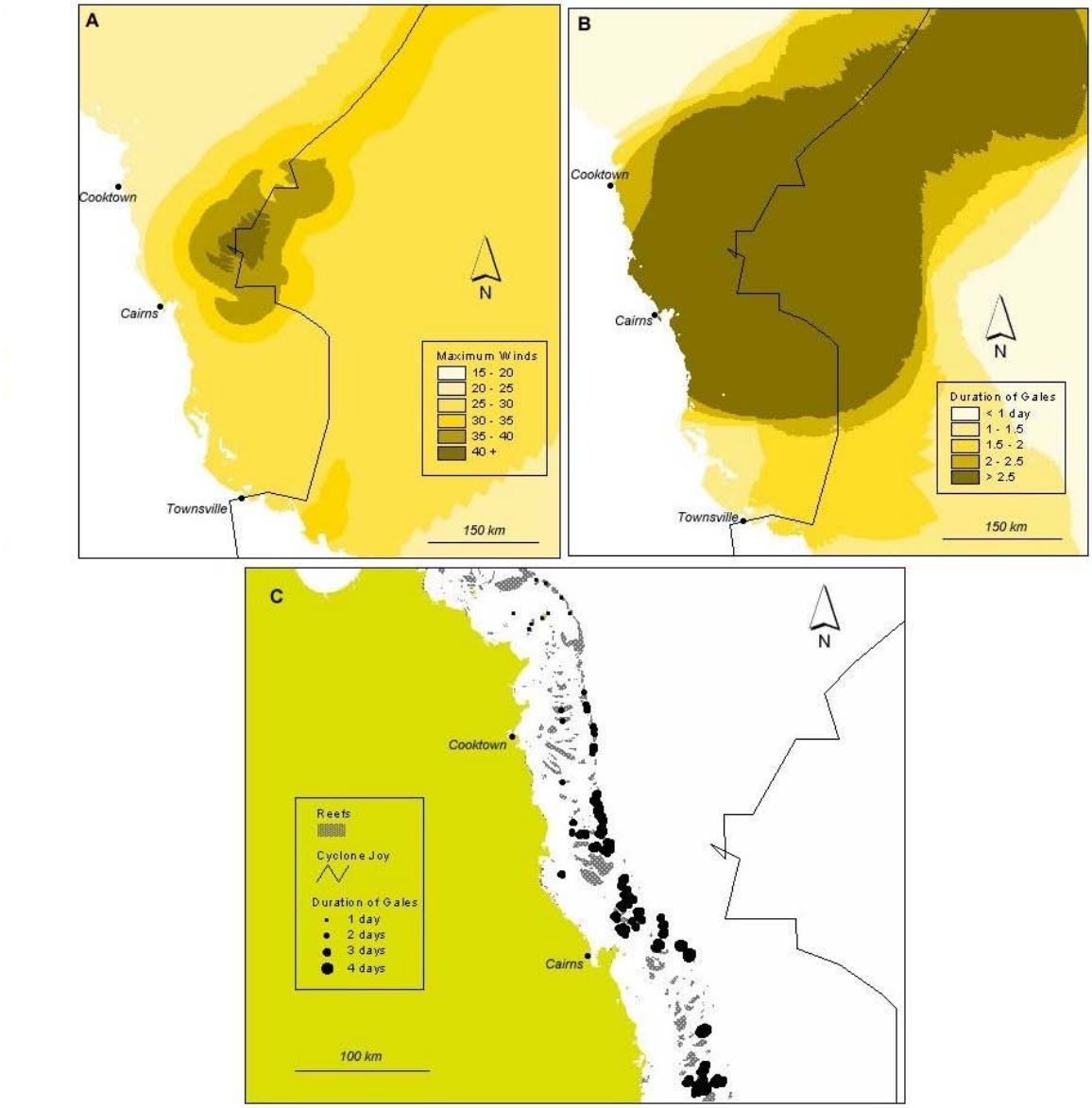

Figure 4.30. Cyclone energy parameters hindcast for cyclone Joy: A- maximum 10 metre surface wind speeds, B – duration of winds $\geq$ gale force (17 $m.s^{-1}$), and C – continuous duration of high-energy winds at reef sites surveyed by Done et al 1991. The thin line shows the cyclone's path.

4.7.3 Cyclone Justin

Cyclone Justin was nearly stationary for much of its early phase when it was unusually large in extent, causing high winds ($25^{+}m.s^{-1}$) in a roughly circular region around its path while in the Coral Sea (Figure 4.31 - A).

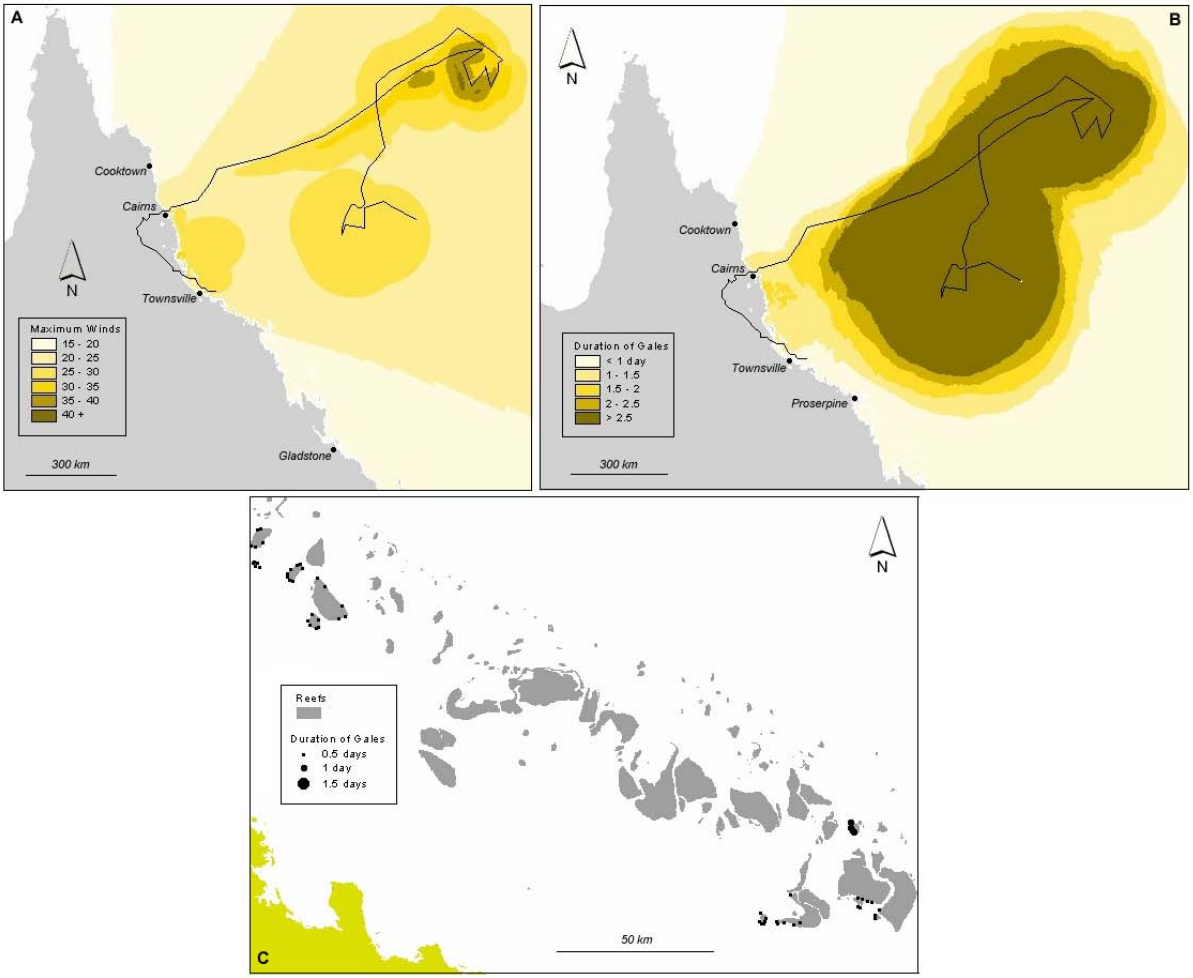

Figure 4.31. Cyclone energy parameters hindcast for cyclone Justin: A- maximum 10 metre surface wind speeds, B – duration of winds ≥ gale force (17 $m.s^{-1}$), and C – continuous duration of high-energy winds at reef sites surveyed by this author. The thin line shows the cyclone's path.

As the cyclone moved north, it weakened considerably. After turning northwest, it then intensified to category 4 and reached the highest maximum winds of $35\text{-}40^{+}m.s^{-1}$. The magnitude and width of the maximum wind zone decreased as Justin approached Cairns and weakened. As it crossed land, it intensified slightly, generating a zone of $25^{+}m.s^{-1}$ winds offshore. Less that half (48%) of the reef sites surveyed by this author were located inside the $25^{+}m.s^{-1}$ zone and none were located in the $35^{+}m.s^{-1}$ zone.

Cyclone Justin also generated a broad area of gales that persisted for more than 2 days (Figure 4.31 - B), though it was located farther out to sea than was the case for

cyclones Ivor or Joy. While nearly three-fourths of the GBR experienced gale force^{+} winds for at least one half of a day, only a small region located just south of Cairns saw these winds persist for longer than a day and a half. A zone of gales that lasted more than one day extended offshore through the GBR between Cairns and Townsville and along the outer reefs southwards towards the Swains reef complex in the southern GBR. Thus, none of the reef sites surveyed following cyclone Justin were located within the 2.5^{+}day zone, and only 7% were found within the 1^{+}day zone. Included in the latter was the site at Oublier Reef that sustained severe, high-energy wave damage. It is important to note that the 2.5+ day zone was located only about 100 km seaward of these sites – it is feasible that some large swell generated by the cyclone may have propagated into the area and impacted outer reef sites, which were not surveyed. While the extent of gales at any time during cyclone Justin covered nearly two-thirds of the GBR, the high wind conditions were not as continuously persistent (Figure 4.31 - C) as was the case for cyclones Ivor or Joy. The most persistent gales were found at Oublier Reef, where the only observations of significant wave damage was also found. At this site, continuous gales persisted for up to 1 day. For the rest of the sites, continuous gales persisted for only up to twelve hours.

4.7.4 Cyclone Althea

Cyclone Althea followed a relatively straight path towards landfall at Townsville while intense, resulting in a clear band of very high maximum winds (40^{+}m.s^{-1}) along the path (Figure 4.32 - A). A second band of highest winds is evident as the cyclone headed out of sea south of Gladstone again at high intensity. The ellipse of high

winds ($25^{+}m.s^{-1}$) evident offshore from Gladstone is due to the cyclone attaining high translation speeds (over 25 km/hr) at which model predictions become unrealistic (see section 4.5.2). In general, Althea had the highest and most widespread zone of maximum winds of the five test cyclones due to its long path and high intensity. Most of the reef sites (68%) for which records of likely wave damage exist from Althea were located inside the $25^{+}m.s^{-1}$ zone. More than half (59%) of the sites were found within the $35^{+}m.s^{-1}$ zone. The distribution of GALES for cyclone Althea, like that of cyclones Ivor and Joy, covered a huge area near the coast (Figure 4.32 - B). The 2.5^{+} day zone extended across the entire GBR, from just north of Townsville to well past Gladstone. Althea generated persistent gales over such a large area because it tracked back along a similar, but more southerly path seawards after crossing the coast just north of Townsville, and because the cyclone maintained intensity (category 3) along much of the path. Consequently, all the sites for which wave damage was recorded were located inside the 2.5^{+} day zone. The most persistent gales predicted during cyclone Althea lasted only up to 2 days, but were found more at sites located more than 200 km south of the cyclone's path (Figure 4.32 - C). These sites were situated on the left (strong) side of the path when the cyclone was intense (category 4). Gales that were sustained at sites situated closer to the path, though less persistent, still lasted for up to 1.5 days.

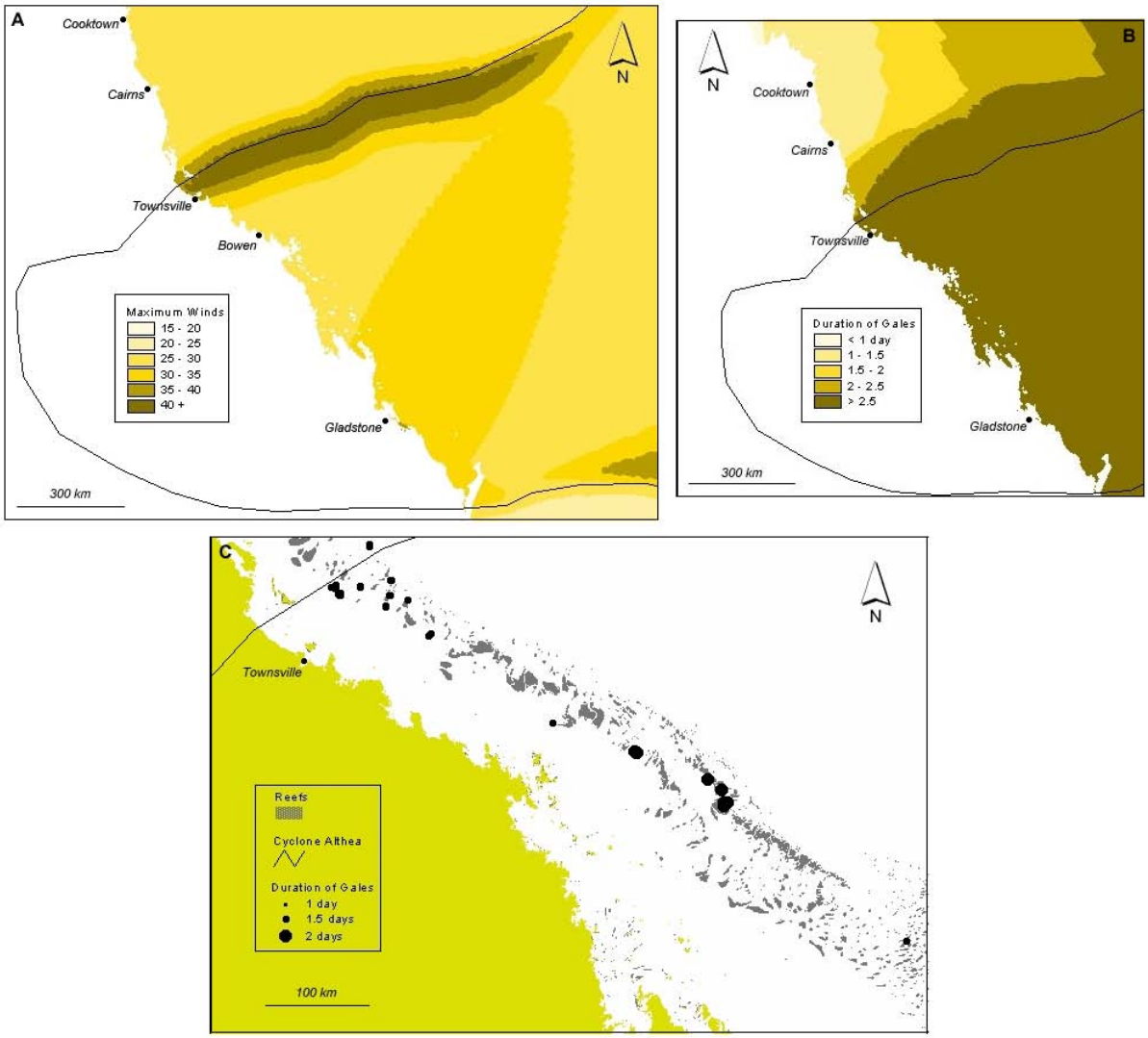

Figure 4.32. Cyclone energy parameters hindcast for cyclone Althea: A- maximum 10 metre surface wind speeds, B – duration of winds ≥ gale force (17 $m.s^{-1}$), and C – continuous duration of high-energy winds at reef sites surveyed by Pearson 1974. The thin line shows the cyclone's path.

4.7.5 Cyclone Celeste

The highest maximum winds ($25^{+}m.s^{-1}$) during cyclone Celeste were predicted to occur on the left side of the path just after the cyclone turned east, when it reached maximum intensity but before its speed increased (Figure 4.33 - A). All but one of the reef sites surveyed by Malcolm et al (1996) following cyclone Celeste were located within the $25^{+}m.s^{-1}$ zone, but none were found in areas of $35^{+}m.s^{-1}$ winds. Gale force winds covered a much smaller area during cyclone Celeste (Figure 4.33 –

B) and dissipated more quickly. The most persistent gales, located offshore between Townsville and Bowen, lasted for up to 2 days.

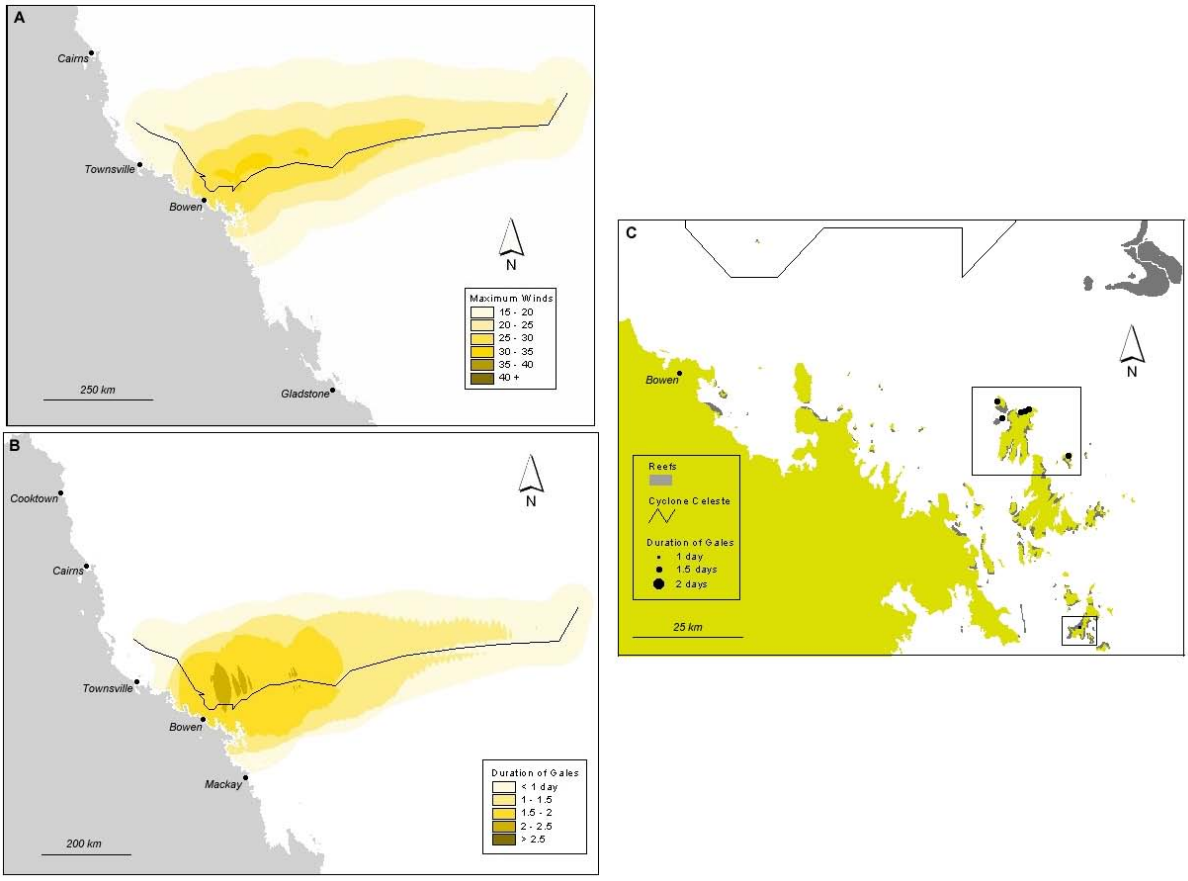

Figure 4.33. Cyclone energy parameters hindcast for cyclone Celeste: A- maximum 10 metre surface wind speeds, B – duration of winds $\geq$ gale force (17 $m.s^{-1}$), and C – continuous duration of high-energy winds at reef sites surveyed by Malcolm et al 1996. The thin line shows the cyclone's path.

The region in which gales persisted for a day or longer was concentrated around the cyclone's path and varied in width according to the speed of the cyclone and smoothness of the path. Close to the coast at Bowen, where the cyclone turned, followed a convoluted path and moved relatively slowly, the 1^{+}day zone was wider. This zone narrowed as the path tracked eastward because the cyclone picked up speed and followed a smoother path. All but one of the reef sites surveyed by Malcolm et al 1996 following the cyclone were located within the 1^{+}day zone. All of these sites

sustained some form of low energy wave damage. The remaining site was found in the 0.5 day zone and was not affected. Although the study sites were located close to the cyclone, they were on the right (weak) side of its path. Further, Celeste was an unusually compact and fast moving cyclone, which reduced the spread and duration of gales around the path even though it was intense (category 3). Finally, the duration of continuous gales was greater for the sites located closer to the path of cyclone Celeste (Figure 4.33 - C). For these sites, gales persisted for up to 1.5 days, while they persisted for less than a day at the most southerly site.

4.7.6 Summary

Both the absolute magnitude of wind energy and its duration are important for predicting the size and distribution of heavy local wind sea that can form during a cyclone. Thus, the three parameters (MAX, GALES and CGALES) derived from the series of wind speed grids were instructive as a proxy for the potential for development of local wind-sea capable of damaging reefs.

The cyclones varied considerably in the absolute magnitude and distribution of these parameters. All but Celeste generated maximum wind speeds over 40 $m.s^{-1}$, though for Justin these were located far out to sea near Papua New Guinea. Celeste was intense but unusually small, which limited the maximum wind speeds reached. Where cyclones followed a relatively straight path at high intensity (parts of Ivor, Althea and to a lesser degree, Celeste), a zone of highest winds was generated mainly to the left side of the path due to asymmetry in the cyclone wind field (see section 4.5.1). Where a cyclone's path was irregular and/or the cyclone moved slowly, the

zone of highest winds was more symmetrical around the path (parts of Joy, Justin and Celeste). Of the reefs surveyed following the cyclones, more of the Ivor sites were found in the highest wind zones.

All of the cyclones except Celeste produced broad regions of gales persisting for more than 2.5 days, though these areas were located more offshore during cyclone Justin. Celeste's extent and duration of gales was reduced due to its unusually small size and fast movement along its track. Most of the reef sites surveyed for cyclones Ivor, Joy and Althea were located in areas where gales persisted for more than 2.5 days. In contrast, only a few reef sites were located in areas where gales persisted more than a day during cyclone Justin – these sites were at Oublier Reef, where the only high-energy impacts were observed. Similar patterns were found for continuous gales.

In Chapter 6, I investigate the extent to which each of these parameters is useful for predicting wave damage on reefs.

4.8 Conclusions

This chapter has shown that a simple wind model can adequately characterise conditions at weather stations, and by implication, at reef sites of interest. Application of this approach to all 85 cyclones in the database from 1969 to 2003 therefore appears warranted. The test of the five cyclones showed that the hindcast wind speeds and directions do not perfectly match the observed field data that was available on an hourly basis. This is to be expected given that many of the stations were located quite distant from the cyclone paths, and complex topography on the island stations likely altered wind speeds and directions. Further, local-scale effects

within the cyclone circulation (such as the dynamics within rainbands) cannot be modelled at present, but could affect the measurements. Despite this, wind speeds were mostly (greater than 80% of the comparisons) modelled to within 10 $m.s^{-1}$ of the observed values (with the exception of cyclone Althea, for which a very limited time series of observations was available). Modelled wind directions were less successful in matching the observations for cyclones Ivor, Justin and Althea (within 45^0 for 45-55% of the comparisons), during which positional uncertainty in the cyclone paths is estimated to be high (see Figures 4.5 - 4.9). The secondary vortex used by McConochie et al (1999) did not perform as well as using the primary vortex alone for the five test cyclones. Thus, a secondary vortex was not used to hindcast the remaining 80 cyclones. While synoptic scale winds were likely important for some cyclones (for example, cyclone Justin), a lack of data and time meant they were not incorporated into this study. Further, although it is waves that actually damage coral communities, given the spatial and temporal scale of this study, the uncertainties and the lack of necessary data, wave heights were not predicted (see Chapter 1).

Finally, representing the cyclone eye positions in a GIS made it easy to build the paths they form and to visualise uncertainty in the data. GIS also provided an effective platform through which to implement the equations necessary to hindcast cyclone winds, and to analyse and visualise the results.

CHAPTER 5: Modelling reef site exposure and vulnerability

5.1 Overview

The purpose of this chapter is to develop a system to classify reef sites based on the two complex determinants of their vulnerability to wave damage from cyclones: 1) their level of exposure to waves during individual cyclones, and 2) their site-specific susceptibility to structural damage from waves (Figure 5.1).

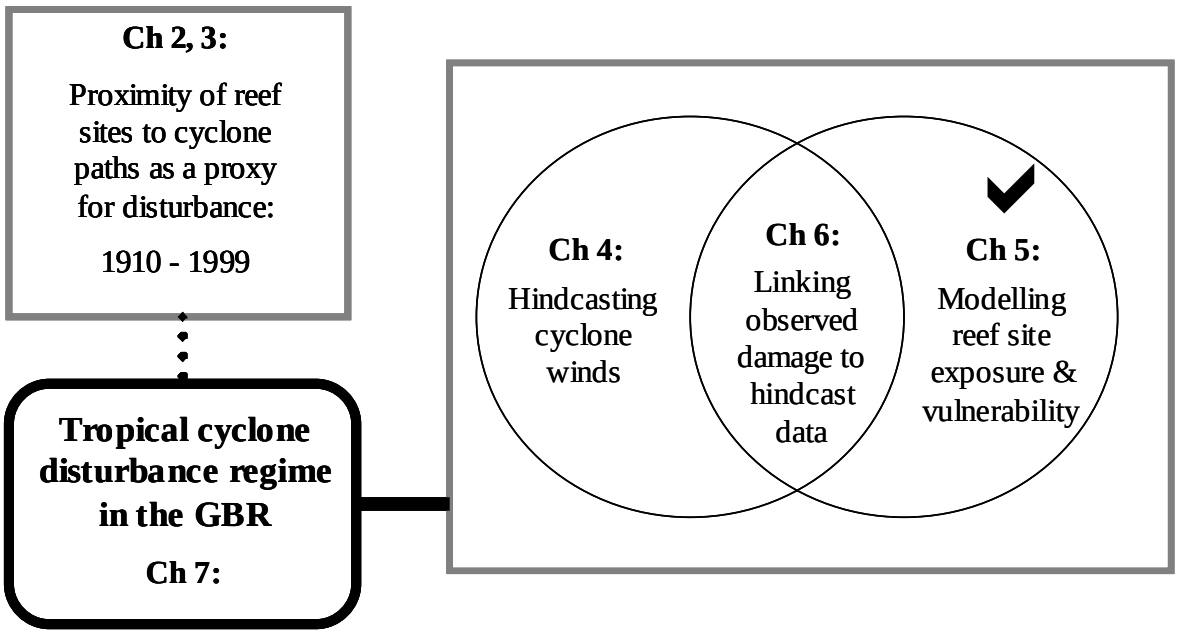

Figure 5.1. Overview diagram of this thesis. The check mark indicates the current chapter.

A degree of uncertainty in predicting the distribution of cyclone damage on reefs will always remain due to the lack of fine scale ecological data and the complex mix of interrelated factors that influence patterns of exposure and vulnerability. Here, simple and intuitive measures are developed to approximate these poorly understood phenomena, with the aim of reducing the variability within the potential damage zone that can be predicted for each cyclone based on the magnitude and duration of high

winds (see Chapter 4). The chapter demonstrates these measures using case studies of five cyclones for which detailed field data of wave damage was available (Ivor, Joy, Justin, Althea and Celeste). Tested individually, they are shown to have little explanatory power. However, these results do warrant further examination of their performance in combination with each other and with cyclone wind parameters (see Chapter 6).

5.2 Introduction

The intensity and duration of heavy seas generated by a cyclone in the vicinity of a reef site only partially explains the likelihood of damage. Also important is the level of exposure of the site to waves generated by the cyclone, and its inherent vulnerability to structural damage. Both of these depend on a range of interrelated and highly variable factors, such as the nature and state of the coral communities, the strength of the reef framework and the micro-topography upwind of the reef, that are unknowable in advance. As a result, the spatial distribution of cyclone damage is highly patchy (Harmelin-Vivien 1994) at a range of spatial scales: between reef complexes (~100 km), between reefs (~10 km), within reefs (~1 km) and within reef sites (>0.5 km) (Puotinen et al 1997). For example, damage observed on Oublier Reef (in the Whitsunday region of the GBR) following cyclone Justin ranged from complete devastation on the south face of the reef to none just a few hundred metres away (see Chapter 3).

5.2.1 Exposure

Waves lose much of their energy when breaking at the leading edge of the first reef (or other shallow water obstacle) they encounter (Young and Hardy 1993). This creates a *within-reef shelter* effect, where the lee side of the reef receives relatively little wave energy, and a *between-reef shelter* effect, where reefs beyond the first obstacle lie within a long energy 'wave shadow'.

BETWEEN REEF SHELTER

The magnitude of the between-reef shelter effect at a given reef site depends on the size, shape and orientation of the reef on which the site is situated with respect to incoming waves, as well as the density of nearby reefs and other wave-blocking obstacles (islands, coastline).

Waves passing over reefs lose energy due to changes in water depth, friction from interaction with the sea bottom, and breaking (Lugo-Fernandez et al 1998). For example, Gourlay (1994) suggests that waves that reform after encountering reefs in the GBR retain only about 5% of their original energy. Studies elsewhere also report similar dissipation (from 50-90% - Lugo-Fernandez et al 1998). In general, long period waves are more severely attenuated by reefs than short period waves - research suggests that the GBR acts as almost a complete barrier to waves generated seaward of the complex, even at high tide (Young and Hardy 1993), regardless of differences in the density of reefs (Young 1989). Thus, the long period swells that can propagate towards the GBR from a distant cyclone are unlikely to damage any but the outermost reefs they first encounter. For example, although cyclone Pam generated storm surge along the entire Queensland coast south of Cairns (Hopley and Harvey 1974), reef

damage was probably limited to sites located on the outer continental shelf because the cyclone's nearest approach to the GBR was hundreds of kilometres away. Most reefs, therefore, are probably damaged during cyclones by heavy local wind-sea (seas built by local winds while a cyclone passes in their vicinity). For this reason, I have ignored the potential contribution of long period swell by using locally generated cyclone winds as a proxy for waves (see Chapter 4).

WITHIN REEF SHELTER

As waves approach a reef (or other shallow water obstacle), those that directly encounter the reef lose energy and slow down. Since the remainder of the wave train maintains a constant speed, the wave front appears to bend around the obstacle (Denny 1988). Subsequently, waves that reach the lee side of the reef are less energetic, creating a 'within reef' shelter effect. The extent to which wave energy dissipates at the leading edge of a reef depends on factors such as the size and shape of the reef, and its orientation with respect to incoming waves. Waves do not have to travel as far when they encounter a small reef, thus retaining more wave energy at the lee side. For a reef that is a simple circular shape, wave heights are highest in bands around the leading edge due to reflection. Heights are lowest (down to 1% of the original wave height) on the lee side of the barrier (Figure 5.2). Only occasionally do cyclone generated waves approach reefs in a manner such that they reach areas normally sheltered from heavy wave action at full strength. In these cases, particularly severe damage can result (Harmelin-Vivien 1994).

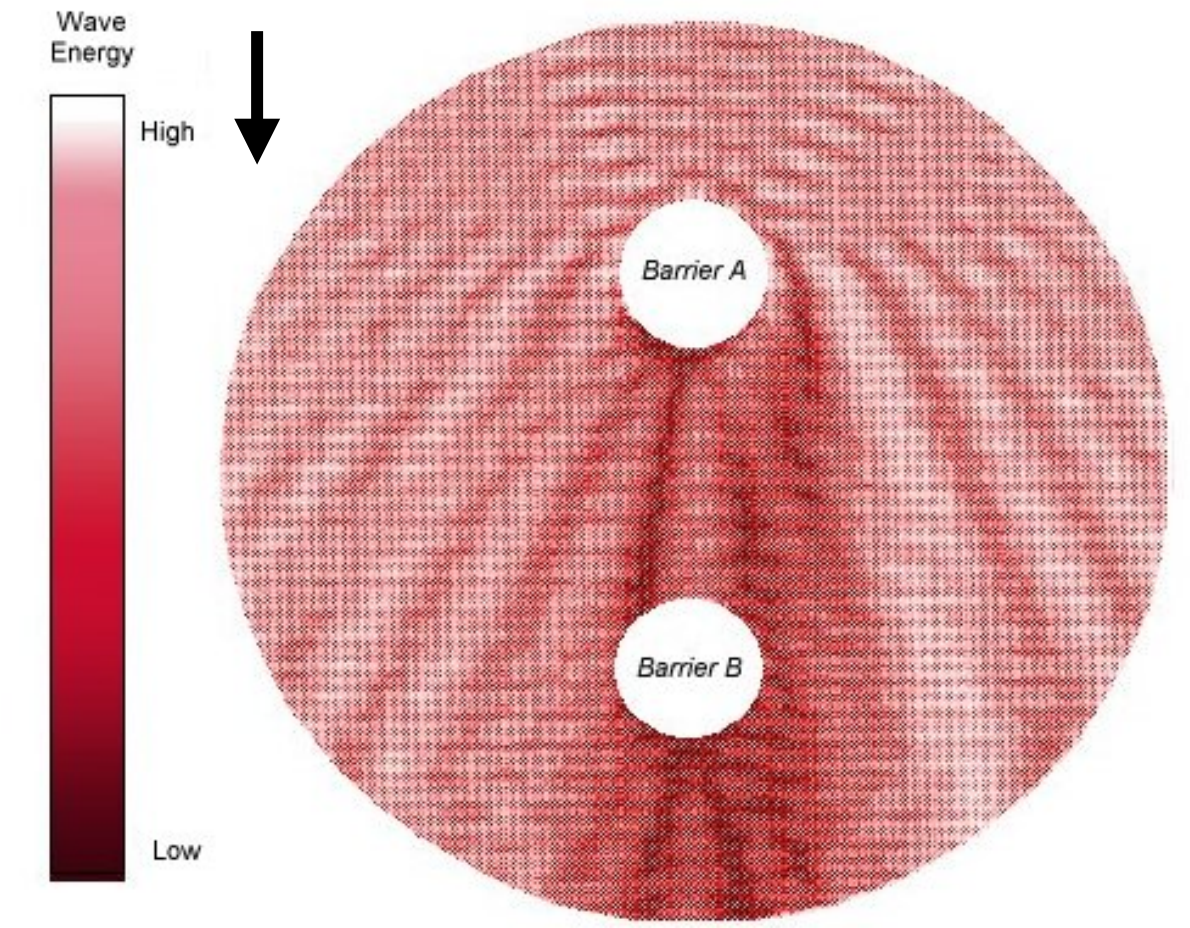

Figure 5.2: Example of the effect of two round obstacles on wave flows, as predicted by Massel 1996. Shading indicates the extent to which wave energy is dissipated (darker colours) or augmented from reflection (lighter colours). Waves are approaching the barriers in the direction of the arrow.

For example, waves generated by cyclone Althea approached Palm Island (offshore from Townsville) along the normally sheltered lee side, which caused severe damage to fringing reefs (Hopley 1972). Nearby areas where energy levels were higher, but approached from a more typical direction were much less affected. Further, the devastation observed on Oublier Reef following cyclone Justin occurred along a section of the south face, which is normally sheltered from waves by nearby reefs.

5.2.2 Vulnerability

The vulnerability of individual coral colonies to cyclone wave damage depends on a great many factors that are highly variable over short time periods and across small distances (Done 1992b, Harmelin-Vivien 1994). Thus, the severity of cyclone damage across one small area of a reef may range from complete devastation to none. These factors are based largely on the nature of the resident coral communities as well as the history of disturbances.

NATURE OF CORAL COMMUNITIES

Local-scale, site-specific characteristics of the coral communities found on a reef influence its vulnerability to wave damage (Table 5.1).

Colony integrity

Coral colonies can sustain structural damage from many sources, such as competition and predation (Hughes and Connell 1999). This damage, even if the colony is not killed outright, reduces its structural integrity as a wave resistant object. For example, corals that are damaged or killed by crown-of-thorns starfish predation become more vulnerable to wave damage (Rogers et al 1982), as the removal of live tissue from the coral skeleton increases its exposure to various forms of bioerosion that ultimately compromise its structural integrity.

Table 5. 1: Major site-specific factors that influence reef vulnerability to cyclone wave damage**.**

Factor	Impact on Vulnerability
Colony integrity	Coral colonies that have been partially damaged (by bioerosion, predation, etc) are at greater risk from damage.
Strength of coral attachment to the substratum	Corals that are firmly attached are difficult to dislodge. Most corals are not firmly attached in the GBR.
Nature of the substratum	Firmly consolidated limestone substrates are more resistant to waves than loose rubble. With the latter, waves may dislodge entire sections of substratum instead of individual corals.
Dominant growth forms	Some forms (branching) are more vulnerable to waves than others (massives, encrusting).
Community size structure	Very small and very large coral colonies are more resistant to dislodgement than medium sized corals.
Routine wave climate	Corals adapt to persistant high wave conditions, which makes them less vulnerable to cyclone damage.
Reef geomorphology	Juvenile reefs are more vulnerable than mature reefs, unless the latter are exposed on their lee side. Fringing and ribbon reefs are wave adapted.
Depth	Colonies positioned along reef flats and deep slopes are generally less vulnerable to damage than those on the upper slope.
Slope	Colonies positioned along very flat or very steep slopes are generally at less risk from damage.

Strength of attachment

Coral colonies that are firmly anchored to immovable substratum are more resistant to dislodgement by waves. For example, wave energy expected to occur within the GBR, even during intense cyclones, is insufficient to dislodge massive corals (eg, *Porites spp*) when firmly attached to immovable substratum (Massel and Done 1993). The fact that dislodged massive corals have been periodically observed on the GBR

(for example, during cyclones Ivor, Joy and Justin as described in Chapter 3) indicates that colonies are often not firmly attached and/or that the substrate is not immovable. Many factors can affect the nature of the substratum and a colony's attachment to it. For example, bioerosion - grazing by fish, urchins, gastropods, limpets and chiton; etching by bacteria, fungi and algae; and boring by sponges, molluscs and worms in the basal region (Tunnicliffe 1982) - can weaken colonies (Hutchings 1986), which increases their vulnerability to wave damage. Further, standing skeletons of corals that provide stable substrate for coral colonies weighing only grams or less can collapse as the colonies grow to weigh tens to thousands of kilograms.

Nature of substratum

High-energy waves can damage the reef substratum. For example, as observed by Done et al 1991 after cyclone Ivor, sustained wave impacts can dislodge entire slabs of the substratum or peel it away in layers (exfoliation). A substratum that is firmly consolidated will resist wave energy for longer than a loose formation of rubble. Under relatively low energy conditions, such as during cyclone Justin in 1997, entire small to medium sized colonies were dislodged while still attached to the substratum. This indicates that the substratum was poorly consolidated. Standing dead corals cemented together by coralline algae help form the substratum. Recent disturbance at a site may therefore indicate a less consolidated, and more vulnerable, substratum (piles of dead coral not yet fully cemented together).

Dominant growth forms and community size structure

Corals become more vulnerable to wave damage as they grow in size because the force due to water acceleration increases faster with increased coral size than the coral's strength increases (Denny et al 1985). In addition, vulnerability varies with growth form - tall and thin forms are more vulnerable to wave action than short and squat forms (Koehl 1984, Tunnicliffe 1982). Thus, large branching forms are the most vulnerable (Figure 5.3), while small encrusting and massive forms are the least vulnerable (Done 1992b, Harmelin-Vivien 1994). For example, differential mortality by growth form was evident on the reef crest at Heron Island following a 1967 cyclone. Coverage of tabular forms decreased by more than 40%, bush forms by just under 30%, encrusting forms by less than 10% and massive forms by less than 5% (Hughes and Connell 1999).

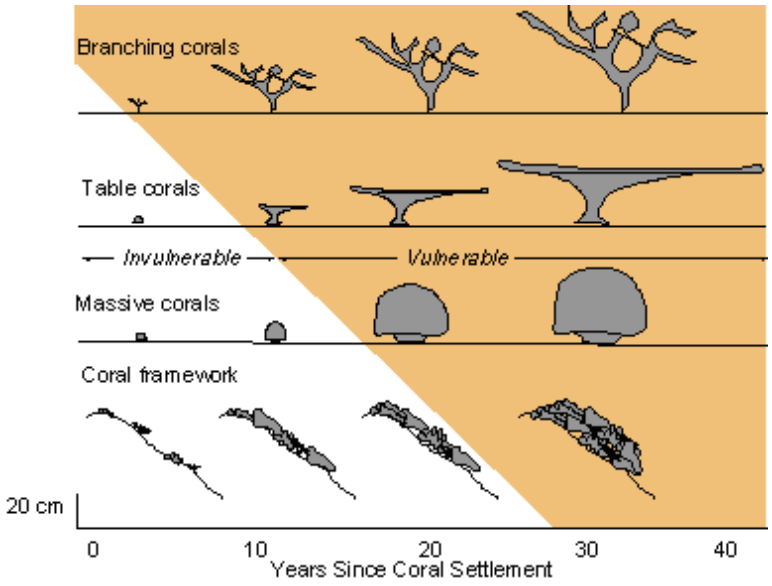

Figure 5.3: Diagram showing postulated differences in time to vulnerability to storm waves of different coral growth forms and structures, assuming area was denuded in 1950. Adapted from Done 1992b.

As colonies grow larger, they present more drag to incident wave energy (Denny 1988). However, Massel and Done (1993) found that massive forms can reach a size large enough to render them virtually invulnerable to wave damage. These colonies, often many metres in diameter, are primarily damaged due to failure of the substratum to which they are attached or are scarred by impacts with wave-born debris.

Gradients in water movement and light (which vary with depth) largely determine the distribution of dominant growth forms across a reef (Done 1983). For example, in the Caribbean, Roberts et al (1977) found that wave-dominated parts of the reef contained mostly thickly branched, bladed and encrusting growth forms. In contrast, deeper current-dominated areas contained mostly delicately branched, platelike and massive forms. In the central GBR, Done (1983) identified assemblages (coral growth forms and species) characteristic of various positions along the water-light-depth gradient (zones). Vulnerability to wave damage thus varies within a reef by these zones.

Routine wave climate

Coral colonies at sites that are normally exposed to high levels of wave energy can adapt to reduce their vulnerability to damage by adopting stream-lined shapes or orientating themselves in the most frequent flow direction (Koehl 1984, Tunnicliffe 1982). High routine wave exposure may favour growth forms that are more resistant to dislodgment by waves, such as massive and encrusting corals (Chappell 1980). Based on this, these sites would be more resistant to damage from cyclone waves than normally sheltered sites. One indication of a high routine wave climate is the development of a wave hardened reef ‘front’ habitat (versus more fragile forms in relatively sheltered ‘backs’). Where these habitats have been mapped, they can be used as a proxy for the level of routine exposure as well as dominant colony growth

forms and size classes. Because routine wave energy typically approaches GBR reefs from the southeast, reef habitat can be crudely mapped based on the position of a site within the reef - most fronts form in the southeast section, while most backs form in the northwest section.

Reef geomorphology

The stage of development of a reef may influence its vulnerability to cyclone damage. Hopley (1982) defined three basic stages of reef development and nine basic geomorphologic reef types for the Great Barrier Reef (Table 5.2). This classification may not apply in other areas, most notably the windward fringing reefs of the Caribbean islands. Over time, continued wave action on reefs promotes the development of geomorphologic features such as algal pavement, rubble zones, and shingle ramparts where exposure to wave energy is highest (Hopley 1983). These features subsequently dissipate much of the incoming wave energy, creating a relatively sheltered lagoon on the leeward side. For this reason, mature and senile forms are usually only vulnerable to cyclone damage if waves reach the normally protected lee side (the back reef lagoon). This can happen if a cyclone, such as Althea in 1971, generates waves that approach from an unusual direction (Hopley 1972). It can also happen if the water level over the reef is unusually high at the time of the cyclone (due to extreme high tide and/or surge). In contrast, juvenile reefs have yet to develop these protective features and are much more exposed to wave action from all directions. On the other hand, ribbon reefs are highly adapted to heavy seas and are protected by an extensive algal pavement and rubble zone on their windward margins.

Table 5.2: Stages of reef development and geomorphologic types defined by Hopley (1982) for the Great Barrier Reef.

Stage of Development	Reef Type	Relevant Characteristics	Implications for Vulnerability
Juvenile	Unmodified antecedent platform	Below modern sea level.	None.
	Submerged reefs	Below modern sea level.	Not adapted to high energy conditions - high risk.
	Irregular patch reefs	Approaching modern sea level.	
Mature	Crescentic reefs	At modern sea level. Orientated to windward margin with open back reef area.	Adapted to high energy conditions. Back reef well protected by reef structure. Back reef at risk if cyclone waves approach from an atypical direction.
	Lagoonal reefs	At modern sea level. Extended reef flat enclosing back reef lagoon(s).	
Senile	Planar reef	At modern sea level. Extensive reef flat, infilled lagoon(s).	
Other	Ribbon reefs	At modern sea level. Linear reefs along outer shelf.	Adapted to high energy conditions - low risk.
	Incipient fringing reefs	Along mainland or islands, mostly below low tide. Minimal reef flat.	None.
	Fringing reef	Along mainland or islands. Identifiable reef flat.	Mostly found on the lee side of high islands - very protected with low risk.

Further, they tend to be wave-hardened due to their placement on the high-energy outer continental shelf of the GBR. For fringing reefs, it is their typical position on the lee side of high continental islands that usually protects them from wave energy.

Depth

The water depth over a reef greatly influences how much energy is retained by waves passing over it (Young and Hardy 1993, Lugo-Fernandez et al 1998) – more wave energy is retained when there is a greater depth of water above the reef. This water level changes with the tide. In general, reefs block the most energy when waves approach at low tide (Hardy et al 2001). The extent of this difference depends on the tidal range, though even a reef with a small tidal range (< 2 m) showed a 15% difference in wave attenuation between low and high tide (Lugo-Fernandez et al 1998). Given that the GBR exhibits a large tidal range (2.35 to 10.36 m - Maxwell 1968), the extent to which reefs attenuate short period wave energy (which dominates local wind-sea) may vary considerably given the timing of the cyclone with respect to the tidal cycle. Adding to this variability is the heightened sea level in the front left quadrant of the cyclone (southern hemisphere) associated with storm surge, the magnitude of which increases with the intensity of the cyclone (Hopley 1974b). In general, cyclone wave damage decreases with a greater depth of water over the site (Harmelien-Vivien 1994), usually not extending below about 20 metres from the surface (Scoffin 1993).

Also important is the depth of water in the general vicinity of a reef. Waves that pass through relatively shallow water before reaching a reef will lose energy to bottom friction before breaking (Denny 1988). In contrast, waves that break on reefs situated in relatively deep water will do so at full force. Defining the threshold between shallow and deep water depends on the nature of the waves. Waves interact with the sea bottom when the water depth is less than one-half of the typical wave's length (Denny 1988). Wave length, in turn, depends on the wave period (level of energy in

the wave). Most reefs in the GBR are impacted by highly energetic short period waves (5-10 s) because fetches within the lagoon are too short for the development of long period swell and the outermost reefs of the GBR largely block it from entering from outside (Young and Hardy 1993). A very short period wave (5 s) 'feels the bottom' at a water depth of just under 20 m (Table 5.3), while a longer period wave (10 s) begins to interact with the bottom at a depth of 78 m. Since cyclone waves on the GBR fall within this range (Young and Hardy 1993), I assumed that, on average, cyclone waves would be affected by the sea bottom at depths of about 50 m.

Table 5.3: Periods for surface waves and their associated lengths and interaction depths. Adapted from Denny 1988.

Wave Period (seconds)	Wave Length (metres)	Interaction Depth (metres)
5	39	19.5
10	156.1	78
15	351.2	175.6

Slope

Sites situated along a part of a reef where the slope is neither very flat nor very steep often sustain greater cyclone wave damage (Scoffin 1993). Initial wave impacts create debris (broken and dislodged corals, sand and rubble) that, where unlikely to quickly move down slope, is reworked by subsequent waves greatly increasing the potential for further damage. Indeed, most damage reported on very steep slopes results from 'avalanches' of debris loosened by wave action. The likelihood of this depends on the local reef topography. In general, reefs typically exhibit very complex

topography, which alters incoming waves and currents (Roberts et al 1975) and has been shown to contribute considerably to the patchiness of cyclone damage (Kjerfve et al 1986). This micro-topography is rarely mapped in detail, except at very local scales.

HISTORY OF DISTURBANCES

The impact of a particular cyclone on a given reef site often depends just as much on the history of previous cyclones as on the characteristics of the cyclone itself (Hughes and Connell 1999, Harmelin-Vivien 1994, Scoffin 1993). For example, individual corals on reefs become more vulnerable to dislodgment by storm waves as they grow larger in size (Figure 5.3 above), although massive corals (eg, *Porites spp*.) may remain undisturbed so long that they reach a size that is essentially invulnerable to normal cyclone-generated waves (Massel and Done 1993). Thus, corals at reef sites recently damaged by cyclones (less time to grow bigger) tend to be less vulnerable to further damage. In contrast, the longer a site remains undisturbed, the more likely it is to contain a greater proportion of large and more fragile colonies (within the constraints of the routine wave climate), and the more vulnerable it becomes to wave damage. In other words, long-lived large and fragile colonies are less likely to persist at sites that are frequently disturbed by severe cyclones (Done 1997). Thus, with the exception of massive corals that have reached very large size (metres across, tonnes in weight), vulnerability to future cyclone damage increases with time since the last major cyclone event and with longer average return periods between past events.

5.3 Modelling reef exposure and vulnerability

This section describes the methods used in this thesis to codify each reef site's exposure to cyclone waves and vulnerability to damage, using data from the five test cyclones (Ivor, Joy, Justin, Althea and Celeste).

5.3.1 Exposure

The exposure of a site to local wind-sea approaching from a given direction depends largely on the distance of water over which winds can blow uninterrupted to the site in that direction (fetch). To estimate this, I calculated the distance between each reef site and the nearest obstacle in all directions at intervals of 7.5 degrees (see Appendix 2) following Ekebom et al (2003). There are thus 48 measures of fetch for each of the case study sites. The fetch length was limited to 50 km to ensure that computer processing could be completed within a reasonable time (processing time increases exponentially with the search distance). For each site, this generated an array of fetch lines in all directions (Figure 5.4). Every site on a reef perimeter has a fetch of zero for all those fetch lines that lie across the body of the reef (and/or nearby land in the case of fringing reefs). Fetch lengths greater than or equal to 50 km were all set to 50 km, which was assumed to represent unlimited fetch.

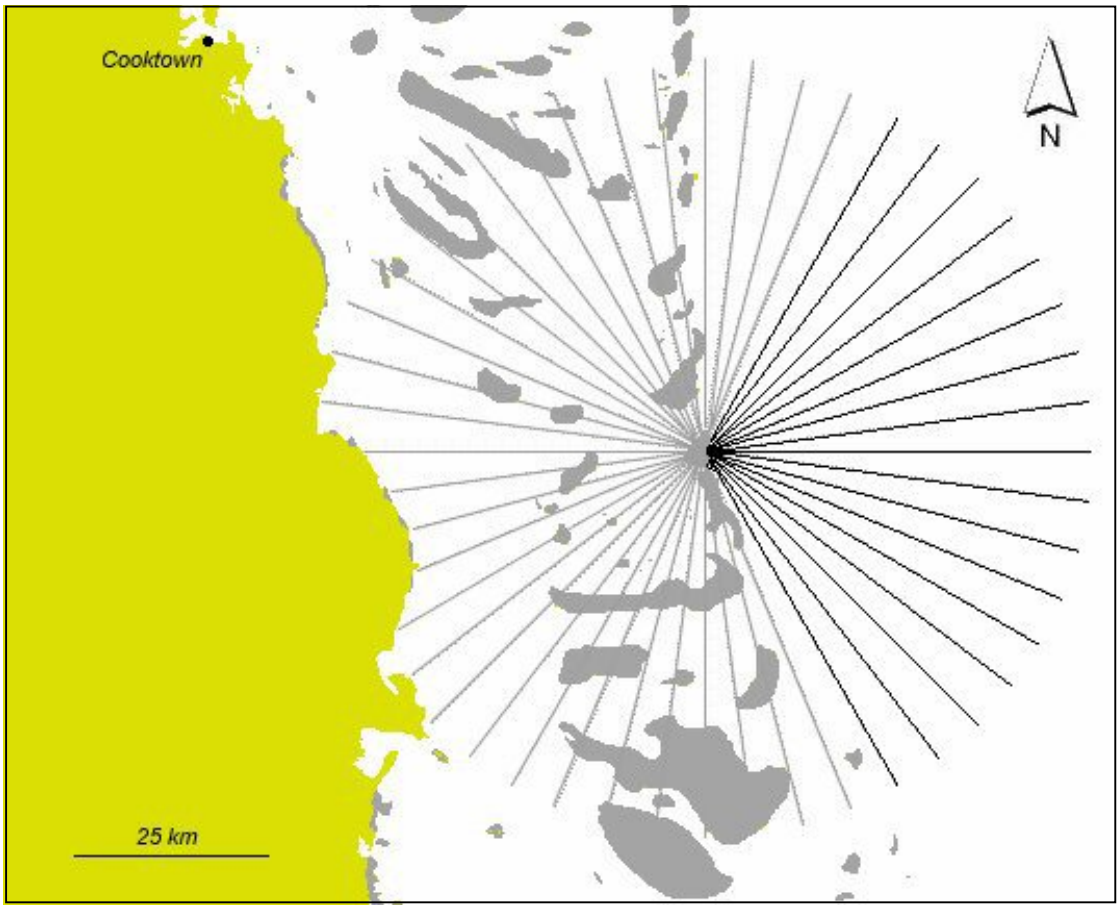

Figure 5.4. Example of an array of fetch lines around a reef site. The maximum line length is 50 km, after which fetch is considered unlimited. Black lines indicate directions from the site which are unobstructed by barriers. Gray lines indicate directions in which the site is completely blocked by barriers (zero fetch). Barriers include land, island, and reef.

The resultant array of fetch lines varied by the relative position of the site within the surrounding reef matrix (Figure 5.5).

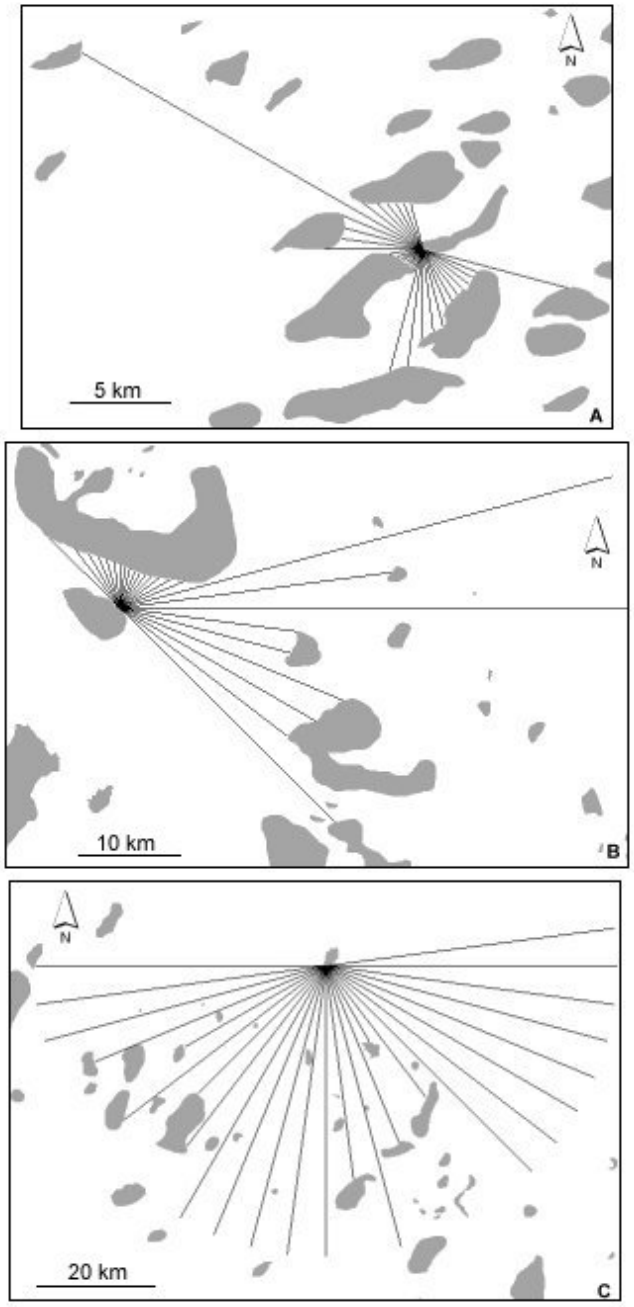

Figure 5.5. Indicative array of fetch lines around a reef site that is [A] – very sheltered, [B] – somewhat exposed and [C] – very exposed to local wind-sea. Note the differences between the scale bars.

CYCLONE EXPOSURE

The longest unbroken period during which winds exceeded gale force (CGALES) was found using an excel spreadsheet (see chapter 4). Exposure during the cyclone for

each site was subsequently calculated as the average length of the fetch lines from that site in directions ranging ±45 degrees from the average wind direction during the CGALES period. Fetch lines were averaged in this way to minimise the impact of known uncertainty in the modelled wind directions (see Chapter 4) and to account for the imperfect correlation between wind and wave directions (Denny 1988). The relationship between the level of exposure (average fetch) and total damage recorded following the cyclones (Ivor, Joy and Justin combined) was understandably noisy even when fetch was averaged by damage score (Figure 5.6), as it takes no account of the magnitude or duration of cyclone energy, or of site vulnerability. In general, the total damage score does rise with greater exposure during the cyclones, but several outliers show high damage with low exposure (top left of Figure 5.6).

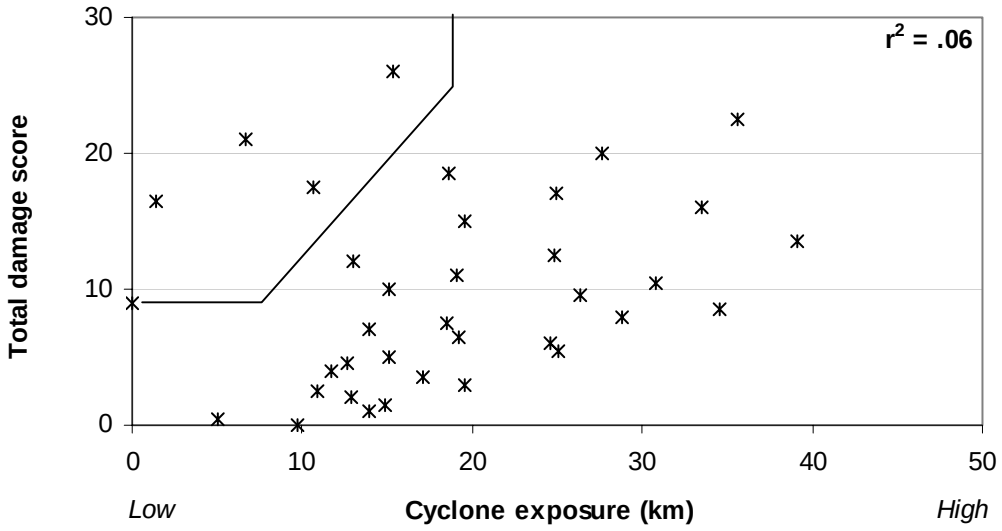

Figure 5.6: Mean predicted exposure of surveyed reef sites to waves during cyclones Ivor, Joy and Justin combined (cyclone exposure), plotted against total recorded damage. The average fetch distances for all surveyed points were averaged by damage score to highlight general trends.

For example, the highest damage recorded (26) was along the high-energy reef front at Jewell Reef following cyclone Ivor. This site was predicted to be exposed in the direction of the incoming wind for a distance of only ~15 km. However, wind

directions were not modelled well during cyclone Ivor – it is possible that waves actually approached the site from a much more exposed direction (fetch at the site is >50 km along its entire eastern flank). There is also some suggestion that the reported track of cyclone Ivor is in error (T. Done, AIMS, pers comm). Similarly, the south face of Oublier Reef sustained severe damage (21) during cyclone Justin, but was predicted to be exposed to incoming winds along a stretch of water less than 10 km long. Wind directions in this region were modelled reasonably well, but it is possible that wave heights were magnified by passing through the narrow channel between Hook and Black Reefs to the immediate south of the site.

5.3.2 Vulnerability

Coral community vulnerability to cyclone damage depends on the nature of the coral communities themselves (Table 5.1) as well as the history of disturbances, at each site. Practical limitations prevented modelling all of the relevant factors for this thesis. For example, the strength of attachment of individual coral colonies to the substratum and detailed micro-topography of the substratum itself are unknowable at present, much less at the time of past cyclone impacts. Further, the timing, frequency and magnitude of prior cyclone disturbance at each site at the time of each cyclone (cyclone disturbance regime) undoubtedly influenced its vulnerability to damage from that cyclone. In the absence of field data at the start of the time series (to provide a baseline for reef condition), it was not possible to consider the role of the cyclone disturbance history at the same time that history was being constructed (a major objective of this thesis). Of the ten factors described in section 5.3.1, five are modelled in this thesis: routine exposure (magnitude of typical wave climate), reef

geomorphology, habitat (an indication of typical wave climate and the dominant size and growth forms at the site), depth and slope.

ROUTINE EXPOSURE

For much of the year, winds in the GBR region (and thus local wind-sea) predominantly approach from the southeast (Orpin et al 1999, Hopley 1982). Sites with a long fetch in these directions may be more wave adapted and less vulnerable to cyclone wave damage. To estimate the routine exposure for each site, I averaged the set of distances from that site to the nearest obstacle in the 90-degree arc centred on 135 degrees (southeast). Lewis (2001) calculated a similar index, but based his on a raster depth model of the GBR at a relatively coarse resolution (500 m). Delineating the exposure differences between reef sites from local scale features, which can be quite significant, would be impossible at such a coarse resolution. Therefore it was necessary to measure the fetch distances using the computationally intensive, but more precise, vector approach I developed.

A priori, one would expect that the total wave damage from a cyclone would be higher at reef sites that are sheltered from waves under routine conditions. However, this generally proved not to be the case during cyclones Ivor, Joy and Justin, even when routine exposure was averaged by damage score (Figure 5.7). With only a few exceptions, the total recorded damage was higher for sites that are normally highly exposed. This suggests that the largest waves generated during the cyclones predominantly approached the surveyed sites from the southeast (normal for routine incoming waves). In other words, the normally sheltered sites on reefs were generally not exposed to cyclone energy. This seems likely given that, on average, winds

during the cyclones were estimated to approach the surveyed reef sites from the east-southeast (mean incoming direction for all sites during cyclone Ivor - 114 $\pm$ 9^0, Joy - 118 $\pm$ 76^0, and Justin - 120 $\pm$ 12^0, summarised from wind model results described in Chapter 4).

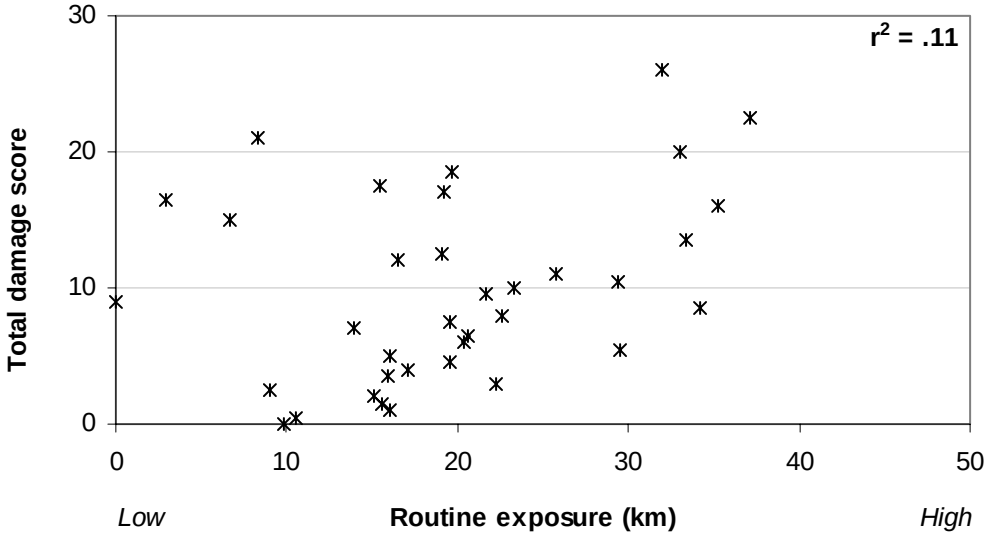

Figure 5.7: Mean predicted mean exposure of surveyed reef sites to waves under routine conditions (routine exposure) plotted against total recorded damage following cyclones Ivor, Joy and Justin. The average fetch distances for all surveyed points were averaged by damage score to highlight general trends.

However, as discussed in chapter 4, the predicted wind directions were not always accurate to within 45 degrees as compared to direct observations recorded by the weather stations. Nonetheless, a few cases of high total damage (total damage score $\geq$ 10) were observed at sites with low routine exposure in the direction of likely wave approach during the cyclone (< 10 km). Notable examples include Scooterboot (routine exposure ~7 km) and Davis (~4 km) reefs during cyclone Ivor; Moore (~6 km), Hastings (~2 km), and Euston (~3 km) reefs during cyclone Joy; and Oublier reef (~8 km) during cyclone Justin. Additional observations of reef damage at

normally sheltered sites that were exposed to waves during cyclones are required to further test the utility of the routine exposure parameter.

RELATIVE EXPOSURE

If coral colonies are sheltered from large breaking waves for long enough, they can become very large (Done 1992b, Scoffin 1993). Thus, holding other factors constant, reef sites that are normally highly sheltered from waves could be expected to contain larger coral colonies exhibiting more fragile growth forms than otherwise. The greatest potential for physical damage from waves occurs when these normally sheltered sites are exposed to sustained high levels of cyclone energy. I approximated this by subtracting the exposure of each site during the cyclone from its exposure under normal conditions. A highly negative value of this index indicates that a site was much more exposed during the cyclone than normal, and thus may have been more vulnerable to wave damage.

Examining this for sites surveyed following cyclones Ivor, Joy and Justin (averaged by total damage score) showed a clear increase in total damage as the index became more negative (Figure 5.8). However, this relationship did not hold for positive values of the index. In other words, there were a number of reef sites that sustained high damage even though they were less exposed during the cyclone than normal. One possible explanation for this is due to error in the polygons that describe the reefs or in the positions of the sites along them. For example, Jewell Reef sustained the highest total damage of any site during cyclones Ivor, Joy or Justin. Based on its position along the Jewell Reef polygon, the site appears to be highly exposed under routine conditions, and thus less exposed during cyclone Ivor than normal. However, it is actually highly sheltered within a bay not captured by the reef polygon (T. Done,

AIMS, pers comm), and was thus much more exposed during the cyclone than normal.

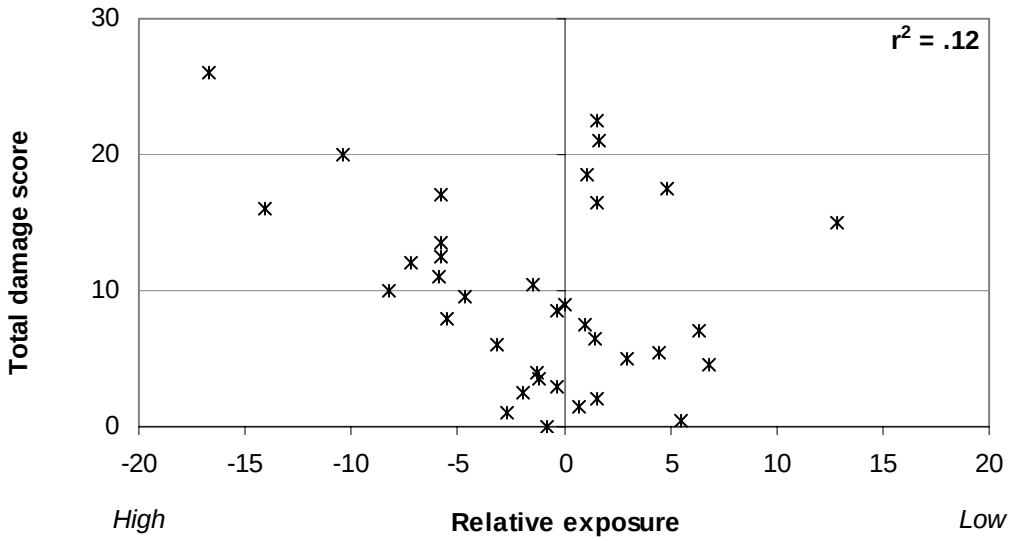

Figure 5.8: Predicted mean difference between the exposure of surveyed reef sites to waves during cyclones Ivor, Joy and Justin versus their exposure under routine conditions (relative exposure), plotted against total recorded damage (index values were averaged by total damage score). Negative values indicate that the sites were more exposed during the cyclone than normal. Positive values indicate the reverse. The values for all surveyed points were averaged by damage score to highlight general trends.

REEF GEOMORPHOLOGY

Sites surveyed following cyclones Ivor, Joy and Justin were classified into the seven geomorphologic types (after Hopley (1982) predicted to affect vulnerability to cyclone wave damage based on a GIS database provided by GBRMPA. In general, juvenile reefs (submerged and patches) are expected to be most vulnerable to wave damage, while ribbon and fringing reefs should be least vulnerable (Table 5.2). The vulnerability of mature (crescentic and lagoonal) and senile (planar) types depends on the angle of wave approach. To test whether this was true for the GBR during cyclones Ivor, Joy and Justin, the mean and maximum total damage score for each

reef type was calculated (Figure 5.9). As expected, mean total damage was highest for sites located on patch reefs (4.5) and lowest for those located on ribbon reefs (1.45). Although the mean total damage was the second lowest for submerged reefs, their maximum damage score was the highest. Similarly, though the mean total damage score for fringing reefs was the second highest, their maximum damage score was the third lowest (though it was still quite high). On average, crescentic, lagoonal and planar reefs experienced relatively minor damage (mean score < 5).

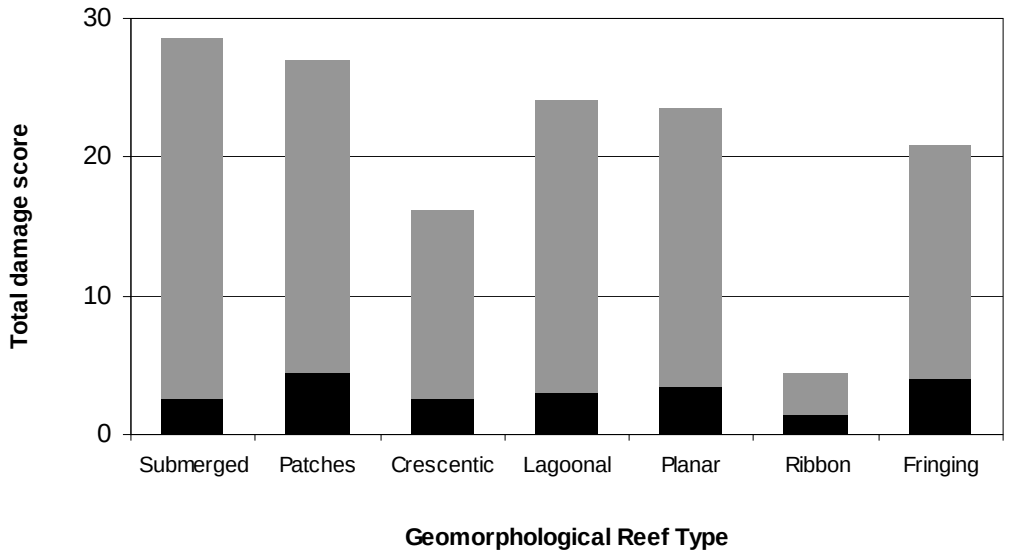

Figure 5.9: The mean (black bars) and maximum (grey bars) total damage score for reef sites surveyed following cyclones Ivor, Joy and Justin, plotted by geomorphologic reef type (as defined by Hopley 1982): submerged (mean = 2.6, n = 51), patches (mean = 4.5, n = 36), crescentic (mean = 2.6, n = 33), lagoonal (mean = 3.1, n = 20), planar (mean = 3.5, n = 51, ribbon (mean = 1.45, n = 10), and fringing (mean = 3.9, n = 55).

However, it is clear from the highest maximum damage scores (> 20), that particular sites found on these reef types were severely damaged. Given that waves were unlikely to approach the reefs from an unusual direction during cyclones Ivor, Joy or Justin (see Chapter 4), this is probably due to cyclone waves approaching the sites at high tide combined with storm surge. This would have allowed waves to reach

normally protected areas. Alternatively, wave energy may have been sufficient to damage even wave-hardened sites exposed during the cyclones. These results suggest that geomorphologic reef type alone is insufficient to explain patterns of damage sustained by reef sites during cyclones. However, the geomorphologic reef type may be more valuable for examining particular types of damage, most notably sand movement.

HABITAT

A range of zones defined by gradients of depth, light and wave energy can be defined on a given reef (Done 1983), with the most obvious differences being between wave-adapted reef fronts and the sheltered reef backs. Classifying a reef site as a front or a back habitat provides an indication of the level of routine exposure to waves (fronts are exposed, backs are not) as well as the probable dominant growth forms (branching and encrusting corals on fronts, massive and tabular corals on backs) and community size structure (smaller, more stream-lined colonies on fronts). Based on this, reef sites at the reef back have the greatest potential for damage, but only if waves can actually reach them (waves approach from an unusual direction, or tides/storm surge reduce the normal within-reef shelter effect). Otherwise, sites at the reef front are vulnerable to damage given that wave energy is sufficient to overcome their wave-adapted nature.

It seems improbable that the largest waves generated by cyclones Ivor, Joy and Justin approached reef sites from an unusual direction. For example, the mean incoming wind direction predicted for cyclone Ivor was to the east - southeast (114^0, $\pm$ 9). Consequently, damage during these cyclones would be expected to be greatest at sites

located along the reef front. Comparing the habitat of each reef site surveyed during the three cyclones with the frequency of damage confirms this (Table 5.4).

Table 5.4: Habitat (reef front versus back) and the frequency of wave damage at sites surveyed following cyclones Ivor, Joy, and Justin.

Cyclone	Habitat	Damage?				Summary
		No		**Yes**		
		#	%	#	%	
Ivor	*Back*	4	57	3	43	Fronts surveyed the most. Mostly fronts were damaged.
	Front	12	24	38	76	
	Other	0	0	6	100	
Joy	*Back*	76	72	30	28	Fronts and backs surveyed equally. Mostly fronts were damaged.
	Front	44	42	62	58	
Justin	*Back*	14	58	10	42	Slightly more fronts surveyed. Mostly fronts were damaged.
	Front	10	33	20	67	

For example, during cyclone Ivor, all of the sites located on the reef fronts, but less than half of those along the backs, were damaged.

DEPTH

All the surveyed reef sites were located in the top 10-12 metres of water. The average depth in the vicinity of each reef site was estimated using a digital depth model of the GBR at a 500 m resolution (Lewis 2001). This depth value was classified as deep (> 50 m), shallow (0-50 m) or dry (above mean sea level, which means the site is adjacent to land). The 50 metre cut-off is based on the depth at which waves of typical periods in the GBR (5-10 s) begin to interact with the sea floor.

About twice as many of the surveyed sites were located near mostly deep water (Table 5.5). Of these, most (~76%) suffered some damage. Sites located in a generally very shallow area (near the coast or islands) were impacted the least. These results could be very different, however, for a cyclone that generates waves that approach reef sites from normally sheltered directions. In that case, sites located in shallow areas (such as fringing reefs normally protected by high continental islands) would be very vulnerable to damage. For example, at Palm Island during cyclone Althea, waves approached from the lee side and caused severe damage to fringing reefs (Hopley 1972).

Table 5.5: Average depth around reef sites surveyed following cyclones Ivor, Joy, Justin, Althea and Celeste.

	Damage?		
Local Water Depth	*% Yes*	*% No*	n
Deep	76.1	23.9	255
Shallow	56.8	43.2	81
Dry	54.2	45.8	24

SLOPE

The slope of the reef was recorded at sites surveyed following cyclone Ivor (Done 1992b). These measurements represent the slope at a very local scale (~100 m) within each site. To test the expectation that damage would be most severe on moderate slopes (Harmelin-Vivien 1992), slope values were standardised into four qualitative categories: gradual (0-20 degrees), moderate (20-45 degrees), steep (45-70 degrees) and nearly vertical (70-90 degrees) and compared to total damage scores.

Most of the sites (~75%) were situated on a section of the reef with a gradual (up to 20%) slope (Table 5.6).

Table 5.6. Slope and total cyclone damage recorded at reef sites surveyed following cyclone Ivor.

Slope	**% of Sites Surveyed**				*n*
	Total Damage				
	0	*1-5*	*6-10*	*11-26*	
Gradual	23.4	57.4	8.5	10.6	47
Moderate	0	28.6	14.3	57.1	7
Steep	50	50	0	0	2
Nearly Vertical	66.7	33.3	0	0	6

The greatest proportion of sites left undamaged were those surveyed along nearly vertical slopes (~67%), where no severe damage was found. In contrast, all sites surveyed along moderate slopes were damaged to some degree, and sustained the highest percentage of severe damage. While some severe damage was found on sites of gradual slope, none was recorded at sites of steep slope. These results support the prediction that intermediate slopes would be damaged the most, although more data is needed to confirm this.

5.4 Conclusions

Modelling the intensity and duration of cyclone energy near a reef site establishes an impact zone of potential wave damage, within which the development of heavy seas capable of damaging coral communities is possible (see Chapter 4). To explain the

patchiness of actual reef damage within this impact zone, I estimated the level of exposure of reef sites to cyclone waves and their vulnerability to wave damage using seven potentially explanatory variables: 1) exposure during the cyclone, 2) routine exposure, 3) relative exposure, 4) geomorphologic reef type, 5) habitat (reef front versus back), 6) average depth near sites, and 7) slope. Used singly, these variables had little explanatory power for predicting the patterns of damage observed following the five test cyclones. Their efficacy when used in combination with each other and with hindcast cyclone wind parameters is explored in Chapter 6.

CHAPTER 6: Linking observed damage to hindcast data

6.1 Overview

The purpose of this chapter is to explore the degree to which the hindcast cyclone energy (see Chapter 4) and reef site exposure and vulnerability (see Chapter 5) factors, when used in combination, can explain cyclone damage observed in the field following cyclones Ivor, Joy, Justin, Althea and Celeste (Figure 6.1).

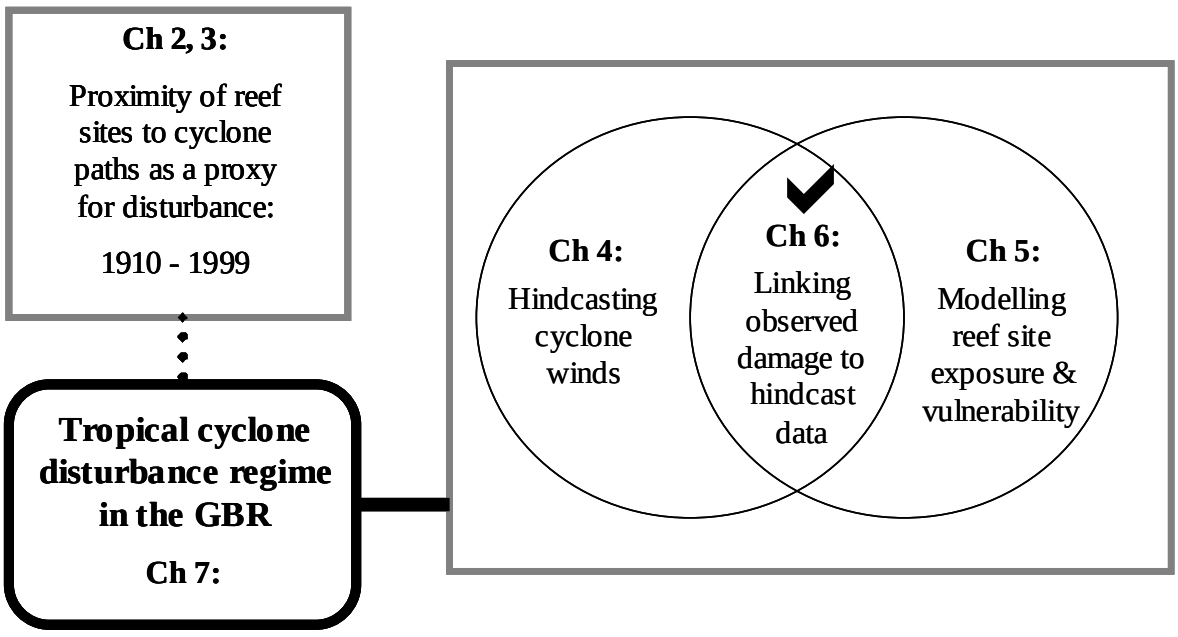

Figure 6.1. Overview diagram of this thesis. The check mark indicates the current chapter.

Based on the results, I devised decision rules to predict, in relation to cyclones from 1969 to 2003, the occurrence of four types of damage: severe damage of any type; breakage; dislodgement; and exfoliation. This reconstructed cyclone history is the basis for characterising the cyclone disturbance regime for the GBR (see Chapter 7).

6.2 Introduction

Many researchers have examined cyclone damage on reefs through field surveys (see Chapter 1). However, high variability in the spatial distribution of damage (patchiness) has limited attempts to use these findings to predict the spread of damage from other cyclones. Done (1992b) used linear regression to link observations of wave damage of several types to wind speeds and directions hindcast for cyclone Ivor. After log transforming an index of severity of exfoliation, he established a positive correlation between it and the total summed value of wind speed incident to each reef site during the cyclone. Given the log transform, however, considerable variability remained inherent in this model.

An alternate approach is to use logistic regression analysis, which is designed to predict values of a binary dependent variable, such as the presence or absence of damage or high versus low severity of damage. Logistic regression has been widely used in ecological studies, where presence / absence data is common. For example, Turner et al (2003) used logistic regression to identify factors influencing the spatial distribution of aspen seedlings after a recruitment event across the Yellowstone National Park. Lawler and Edwards (2003) used it to model nesting habitat of several species of birds in the Uinta Mountains of Utah. And Van Horssen et al (2003) used logistic regression combined with GIS to predict the presence or absence of 78 wetland plant species in coastal areas of the Netherlands. However, logistic regression is a parametric approach, requiring data to meet assumptions (independence, normality, stable variance structure) that do not hold for much of the data relevant to this project. Further, it excels at delineating linear relationships between variables, while the links between observed cyclone damage and hindcast

variables are more complex than this. Lengthy experiments with linear and logistic regression confirmed that identifying linear relationships in the data used in this project would be very difficult, if even possible. However, a relatively new technique – classification and regression tree analysis (CART) – proved to be far more useful.

6.3 Classification and regression tree (CART)

CART has had much use among medical researchers developing decision rules for classifying patients into risk categories for appropriate treatment (Lewis 2000). In recent years, researchers in other disciplinary areas, such as ecology, where classification problems are common and data sets are not suited to standard approaches, have begun to use CART. For example, Sutherland et al (1999) used classification trees to explore factors influencing the presence or absence of frogs in British Columbia. De'ath and Fabricius (2000) used both classification and regression trees to define habitat types for soft coral species on the GBR based on a range of physical and spatial variables. Marshall (2000) used regression trees to identify a relationship between coral colony morphology and resistance to breakage from mechanical force. In 2002, Feldesman tested the performance of CART against linear discriminant analysis (LDA), which is commonly used for classification problems, to classify hominid skulls into species based on various characteristics of their components. He found that CART performed equally as well as LDA for complete data sets, and was more effective than LDA when important data variables contained missing values.

CART is used in this study to determine how well observed patterns in wave damage can be explained by hindcast cyclone winds (maximum wind speed, duration of gales,

duration of continuous gales), reef exposure (during the cyclone, during routine conditions and the ratio between these) and reef site vulnerability (geomorphologic reef type, habitat, slope and depth nearby) factors. CART was ideal for this task because it can handle both numeric and categorical data, it allows for multi-level categorical variables, it deals effectively with missing observations, and it is non-parametric (De'ath and Fabricius 2000). The ultimate reasons for building the trees were to search for meaningful structure in the data, and to classify reef sites by predicted levels and types of wave damage (to build the likely cyclone history). Simple decision rules were then programmed into GIS to automate the process of predicting the occurrence of different types of damage across the GBR (see Appendix 2). Automating this process is quite important, considering that the GBR is examined at 24,224 individual reef sites for four damage types for each of 85 cyclones.

CART splits the initial data set into two classes, with the aim of making each resultant node as 'pure' (for example, wave damage = mostly yes versus wave damage = mostly no) as possible. It continues to divide the resulting data sets until no more splits can be made and a tree is created. Because the resultant tree very likely represents an 'overfit' of the data (explaining 'noise' variation that would be irrelevant when using the tree on another data set), CART systematically 'prunes' the tree until an optimal balance between the classification power of the tree and its complexity is reached. Using this approach, none of the classic parametric assumptions (eg, normality, stable variance structure) are required, and no data transformations are necessary. This is particularly important for this project as the field data is typically not normally distributed, has unstable variances, consists of small sample sizes, and is not independent in distribution.

One limitation of CART is its relative inability to extract linear relationships compared to other data mining techniques (Hastie et al 2001). However, experiments with linear and logistic regression showed that linear relationships are not a key feature of the cyclone data sets. Another limitation is that the predictive power of CART is lower than other techniques, such as neural networks (Hastie et al 2001). This was not a major problem in this study because the high level of uncertainty inherent in any model that could be devised and the low sample size of the ecological database precluded very high predictability regardless of the method chosen.

In this project, a series of classification and regression trees were fitted to search for linkages between hindcast cyclone energy, reef exposure, and reef vulnerability parameters and field observations of wave damage from cyclones Ivor, Joy, Justin, Althea and Celeste (Table 6.1). Field data for cyclones Celeste and Althea do not include detailed observations about particular types of damage or their severity. Thus, trees including them are limited to examining the occurrence of damage of any type or severity. Of the five test cyclones, Justin persisted longer than normal, and was unusually large during its initial phase. Subsequently, sites located far from the track (when the cyclone was large and stationary) were affected, but sites located close to the track (when the cyclone was normal in size and weaker) were not. Therefore, trees were fitted with and without cyclone Justin to test the influence of this.

CART searches for linkages between data variables. However, as with any statistical technique, it is vital to consider whether or not these linkages could have a real world meaning. Thus, classification trees were assessed based on their classification accuracy, the extent to which nodes could distinguish between presence and absence

of damage (node purity), and the degree to which the tree structure was meaningful from an ecological standpoint (De'ath and Fabricius 2000).

Table 6.1. Classification and regression trees built using CART. Quantitative dependent variables (maximum, total, total low, and total high) were modelled using regression trees. All others, based on presence versus absence data, were modelled using classification trees. Severe damage was defined by a maximum damage score of 3 or above for at least one type of damage.

	Cyclone Field Survey Data						
Dependent Variable	Ivor, Joy, Justin, Celeste, Althea	Ivor, Joy, Celeste, Althea	Ivor, Joy, Justin	Ivor, Joy	Ivor	Joy	Justin
Damage of any type	✔	✔	✔	✔	✔	✔	✔
Severe damage of any type			✔	✔	✔	✔	✔
Maximum damage of any type			✔	✔	✔	✔	✔
Total damage			✔	✔	✔	✔	✔
Total low energy damage			✔	✔	✔	✔	✔
Total high energy damage			✔	✔	✔	✔	✔
Breakage			✔	✔	✔	✔	✔
Debris scars			✔	✔	✔	✔	✔
Dislodgement of massives			✔	✔	✔	✔	✔
Exfoliation			✔	✔	✔	✔	✔
Fallen slabs			✔	✔	✔	✔	✔
Sand movement			✔	✔	✔	✔	✔
Soft corals stripped			✔	✔	✔	✔	✔
Trenching			✔	✔	✔	✔	✔

For example, the degree to which the presence versus absence of damage can be predicted within a section of a tree depends on the purity of the relevant splitting node. Node purity of 50% (very poor) indicates that presence or absence of damage is equally likely. Nodes were considered to be reasonably pure (and suitable for prediction) if the binary split was at least ~60/40. However, the importance of the

purity of each node to the overall tree depended on its relative contribution to splitting the data – purity was most important for nodes that split a large proportion of the data. Trees were considered to be ecologically relevant if the combination of decision rules generated for each / most splitting node made ecological sense. Trees that met these conditions are described in detail below. The remaining trees are provided in Appendix 5.

6.4 Damage of any type or severity

The simplest possible model predicted the occurrence of cyclone damage of any type or severity given the hindcast variables. Seven trees were fitted, each for a different combination of cyclones (Table 6.2). The factors chosen by CART to build the trees differed between the data sets. For cyclones Ivor (5) and Justin (7), reef type was the sole factor chosen to explain the presence or absence of damage.

In contrast, measures of cyclone energy (duration of gales and maximum wind speed), as well as the routine exposure of each site to wave energy, were selected for cyclone Joy (6). When data for cyclones Althea and Celeste were included (1, 2), the distance of each site to the cyclone track was also relevant.

The tree that included all of the cyclones except Justin (2) yielded the highest classification accuracy balanced across both presence and absence, although the purity of the nodes (how distinctly presence versus absence are distinguished from one another) was only fair. Nodes were most distinct for cyclone Justin alone (7), although the classification accuracy was less balanced in that case. The tree fitted for cyclone Ivor alone (5) performed the worst, with the classification accuracy for the

presence of damage less than that achieved by chance. This may be due to error in the position of cyclone Ivor's path.

Table 6.2. Key features of classification trees modelling the occurrence of any type or severity of cyclone damage given the hindcast variables. See Appendix 5 for a description of trees not discussed in the text.

	Data Set	Factors used to build the tree	Classification accuracy (% correct)		Node purity	Ecological relevance
			Yes	*No*		
1	Ivor, Joy, Justin, Althea, Celeste	Ambient exposure, Distance, Duration of Gales	66.0	75.5	Fair	Moderate
2	Ivor, Joy, Althea, Celeste	Ambient exposure, Distance, Duration of Gales	69.2	76.2	Fair	High
3	Ivor, Joy, Justin	Ambient exposure, Reef type, Duration of Gales	60.0	77.4	Good	Low
4	Ivor, Joy	Ambient exposure, Slope, Reef type, Duration of Gales	69.1	71.4	Good	Moderate
5	Ivor	Reef type	48.9	81.3	Poor	Low
6	Joy	Ambient exposure, Duration of Gales, Maximum Wind Speed	66.4	83.8	Good	High
7	Justin	Reef type	87.5	59.1	Very Good	Low

For cyclones Ivor, Joy, Althea and Celeste combined (2), all reef sites normally sheltered from waves (routine exposure $\leq$ ~4.0 km) that were located within 21 km of the cyclone path were damaged (Figure 6.2 - A). In contrast, wave damage was recorded for only about half of the sheltered sites located beyond that distance. For

normally exposed sites, most wave damage occurred where gale force winds persisted for longer than 57 hours.

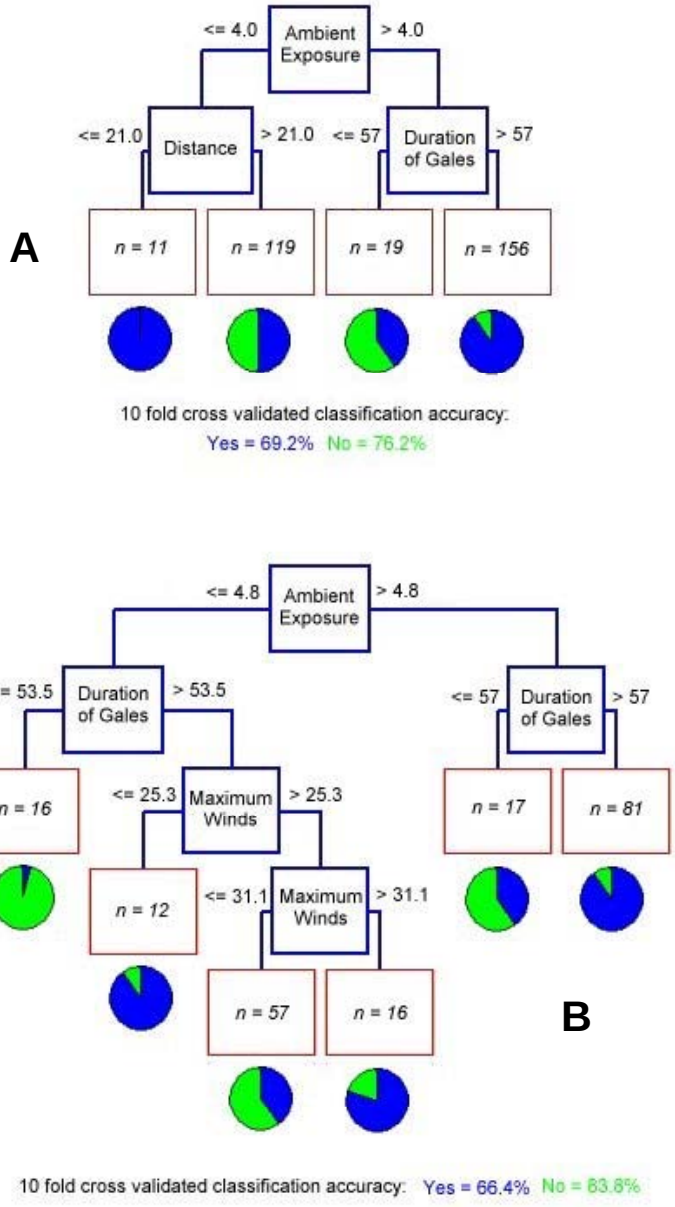

Figure 6.2. Classification tree fitted for the occurrence of any type or severity of damage for cyclones: A - Ivor, Joy, Althea and Celeste, and B - Joy. The relative purity of the terminal nodes (as shown by the pie diagrams, where black = damaged and grey = not damaged) and the classification accuracy indicate the success of the tree.

The tree for cyclone Joy alone (6) was dominated by routine exposure, the duration of gales, and maximum winds (Figure 6.2 - B). Some form of damage was most likely

at sites that are exposed to wave action under normal conditions and that experienced persistent gale force winds (>57 hours) during the cyclone. Although normally exposed sites may be more wave-adapted, prolonged exposure to high-energy conditions was enough to overcome this. In contrast, for sites normally sheltered from waves, the situation is more complex. Normally sheltered sites were less affected because Joy's winds approached largely from a typical direction (the south and east) and thus were less likely to reach these sites. There was an absence of damage at sites where gales were persistent (>53.5 hours), but weak (< 31.1 $m.s^{-1}$). Damage was also unlikely when gales were short-lived (<53.5 hours).

6.5 Severe damage of any type

Minor, low-energy damage can sometimes be difficult to identify in the field. Therefore, predicting the location of severe damage of any type may be more effective. To this end, four trees were fitted (Table 6.3), with the most complex for cyclone Joy (4) and the rest equally simple. Both exposure and vulnerability variables were invoked to explain the distribution of severe damage from the test cyclones. Exposure and vulnerability factors that were important in explaining the likelihood of severe damage included: habitat (front versus back); the slope; and the exposure during the cyclone. The duration of continuous gales was the most relevant hindcast wind factor.

Table 6.3. Key features of classification trees modelling the occurrence of severe damage of any type given the hindcast variables. See Appendix 5 for a description of trees not discussed in the text.

	Data Set	Factors used to build the tree	Classification accuracy (% correct)		Node purity	Ecological relevance
			Yes	*No*		
1	Ivor, Joy, Justin	Duration of continuous gales	91.8	58.3	Good	Moderate
2	Ivor, Joy	Duration of continuous gales, Slope, Front vs/ back habitat	75.0	67.2	Fair	High
3	Ivor	Reef type	50.0	74.5	Good	Low
4	Joy	Front vs/ back habitat, Distance, Cyclone exposure, Relative exposure	70.8	82.8	Good	Moderate
5	Justin	No tree possible	n/a	n/a	n/a	n/a

When cyclones Ivor, Joy and Justin were combined (1), the duration of continuous gales was the sole variable chosen to predict the severity of damage for (Figure 6.3 - A). Very little severe damage occurred at sites where gales persisted uninterrupted for less than 38.5 hours. About forty percent of sites sustained severe damage when gales persisted beyond this threshold. When cyclone Justin was removed from the data set (2), slope and habitat were added to the tree (Figure 6.3 - B). As with the previous tree, severe damage was rare where gale force winds did not persist for at least 38.5 hours. However, for sites where gales lasted beyond this threshold, severe damage did not occur if the slope was near vertical, or rarely occurred if the site was located along the sheltered back side of a reef.

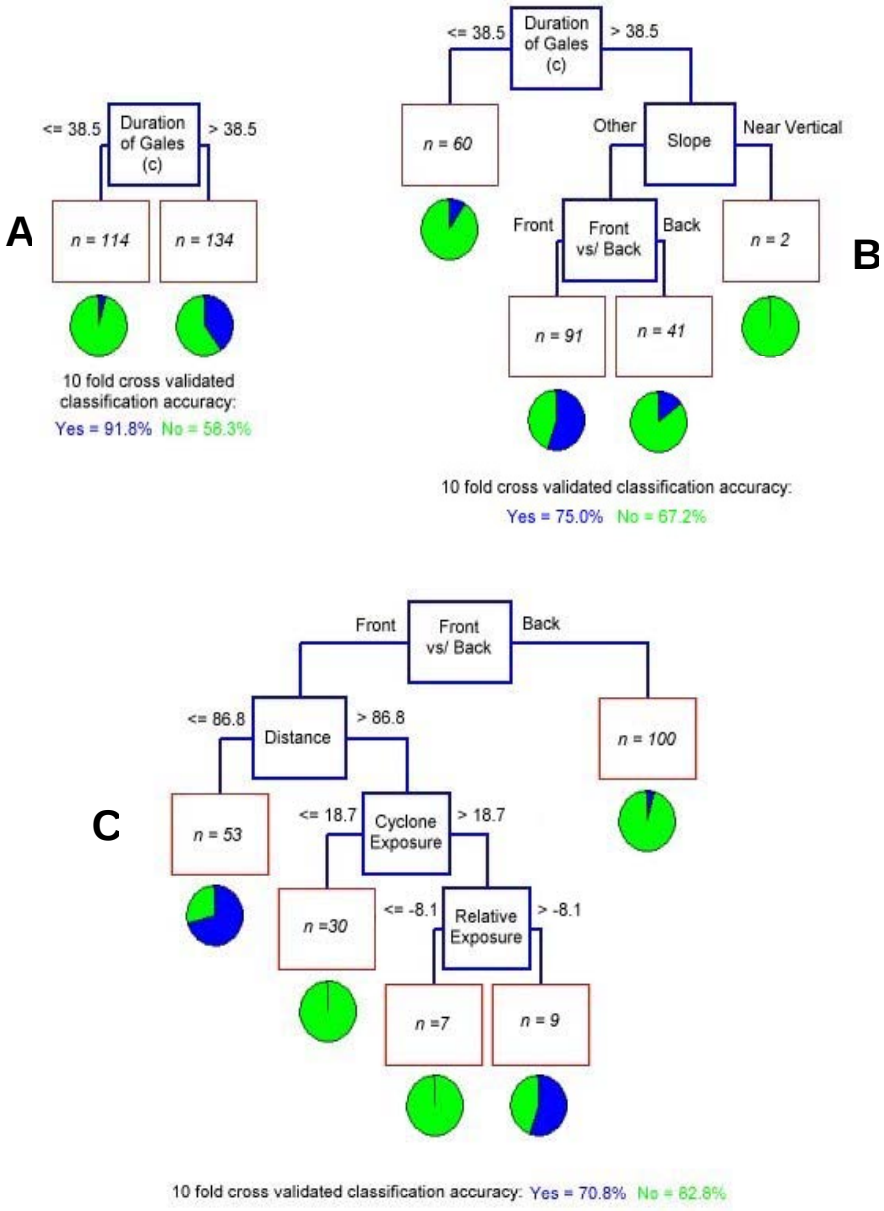

Figure 6.3. Classification tree fitted for the occurrence of severe damage of any type for cyclones: A - Ivor, Joy, and Justin, B – Ivor and Joy, and C - Joy. The relative purity of the terminal nodes (as shown by the pie diagrams, where black = severely damaged and grey = not severely damaged) and the classification accuracy indicate the success of the tree.

In contrast, for cyclone Joy alone (4), the tree was dominated by exposure and vulnerability (front versus back habitat, cyclone exposure, relative exposure) rather than cyclone energy factors (Figure 6.3 - C). For example, very few sites located on sheltered back reef sites sustained severe damage. Although normally sheltered sites

along the back reef would be more vulnerable to impacts from waves, waves did not reach those sites because they predominantly approached from the south and east. For front reef sites, severe damage was much more likely if the site was located near (>~86 km) the cyclone track. Some sites located beyond this distance were severely damaged, but only if the site was highly exposed during the cyclone.

6.6 Maximum and total severity of damage

Regression trees were used to explore quantitative measures of the severity of damage: maximum severity of any type of damage; total severity of all damage; total severity of low-energy types of damage; and total severity of high-energy types of damage (see chapter 1 for an explanation of low versus high energy types). Three trees were fitted for each of these, with each of the three using a combination of cyclones Ivor, Joy and Justin (Table 6.4). For the combined trees (1-2), the duration of gales was the first splitter for maximum damage of any type and total low-energy damage, while maximum wind speed was the first splitter for total damage and total high-energy damage. In other words, the most important driver of low-level damage is a sufficient period above a threshold level (gale force winds), whereas for high-energy damage to occur, it is the surpassing of an energy threshold. None of the regression trees are suitable for prediction due to overlapping nodes (see Appendix 5).

Table 6.4: Key features of regression trees modelling the severity of cyclone damage given the hindcast variables. See Appendix 5 for a description of trees not discussed in the text.

Data Set	Factors used to build the tree				Ecological Relevance
	Maximum Damage	*Total Damage*	*Total Low Energy Damage*	*Total High Energy Damage*	
Ivor, Joy, Justin **1**	Duration of continuous gales	Maximum wind speed, Front vs/ back habitat, Reef type, Duration of continuous gales	Duration of gales	Maximum wind speed	Low High Low Low
Ivor, Joy **2**	Duration of continuous gales	Maximum wind speed	Duration of gales	Maximum wind speed	Low Low Low Low
3 Ivor	Reef type	No tree possible	No tree possible	No tree possible	n/a
4 Joy	No tree possible	Maximum wind speed, Front vs/ back habitat	Front vs/ back habitat, Maximum wind speed, Cyclone exposure	Front vs/ back habitat, Maximum wind speed	n/a Moderate Moderate Moderate
5 Justin	No tree possible	No tree possible	No tree possible	No tree possible	n/a

The clearest tree was generated for total damage for cyclones Ivor, Joy and Justin combined (Figure 6.4). In this tree, the majority of sites surveyed sustained damage of low severity. Most were grouped together in node 1, where maximum winds failed to exceed 30.2 m.s-1. However, some sites were undamaged (nodes 2 and 3) even when winds exceeded this threshold: in sheltered back reefs (node 2) or at reef fronts where gales were less persistent (< 39.5 hrs – node 3). The highest total damage in general was recorded at those sites located on patch reefs (node 5).

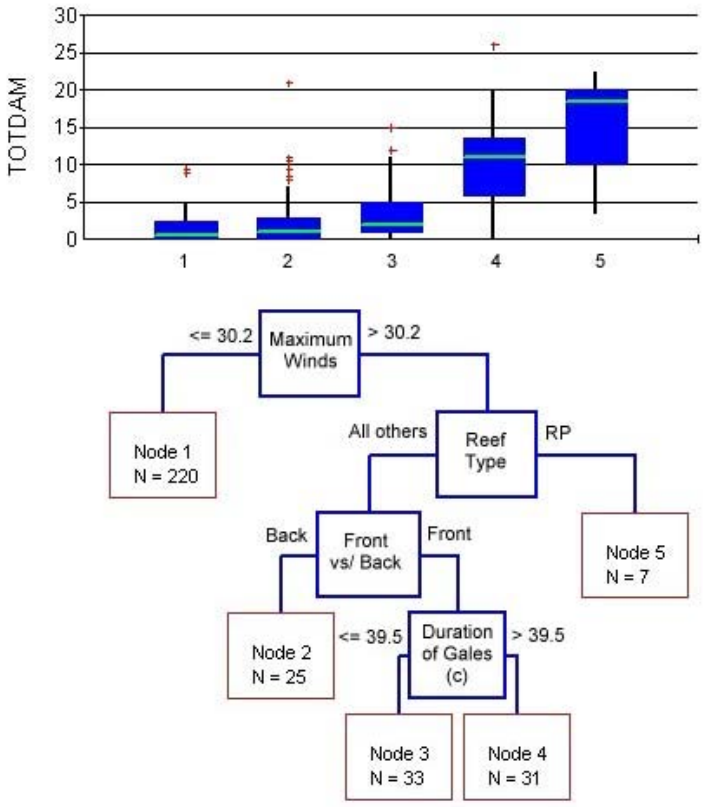

Figure 6.4. Regression tree fitted for the total severity of damage of all types for cyclone Ivor, Joy and Justin combined. The box plot indicates the success of the tree. Reef type code C = Crescentic, CF = Coastal Fringing, F = Fringing, IF = Incipient Fringing, L = Lagoonal, P = Planar, R = Ribbon, RP = Reef Patches, and S = Submerged.

6.7 Coral breakage

Different variables best explained patterns of coral breakage for the three cyclones (Table 6.5). When the cyclones were combined, complex trees were needed to explain the highly variable patterns in the distribution of breakage. The most balanced classification accuracy was achieved when cyclones Ivor and Joy were combined (2), and the least for cyclone Justin alone (5). Node purity was high for the combined cyclones (1,2) but only fair for cyclone Ivor alone (5). The combined tree of cyclones Ivor and Joy (2) performed best overall.

Table 6.5. Key features of classification trees modelling coral breakage given the hindcast variables. See Appendix 5 for a description of trees not discussed in the text.

Data Set	Factors used to build the tree	Classification accuracy (% correct)		Node purity	Ecological relevance
		Yes	*No*		
1 Ivor, Joy, Justin	Slope, Reef type, Duration of continuous gales, Relative exposure, Maximum wind speed, Front vs/ back habitat	71.4	73.7	Very Good	Low
2 Ivor, Joy	Duration of continuous gales, Front vs/ back habitat, Reef type, Relative exposure	71.7	80.5	Very Good	High
3 Ivor	Distance	80.0	64.6	Fair	High
4 Joy	Ambient exposure, Duration of Gales	60.5	87.5	Good	High
5 Justin	Reef type	90.0	54.2	Good	Moderate

A mixture of exposure, vulnerability and cyclone wind parameters best explained patterns in breakage observed following cyclones Ivor and Joy (Figure 6.5 - A). Breakage was unlikely if gales persisted for less than about 39 hours. For sites with more persistent gales, breakage was very likely at sites on the exposed reef fronts, and also on the reef backs of crescentic, incipient fringing, ribbon or submerged reefs. Reefs of the first three types are typically wave-hardened along their fronts, which protect a sheltered back reef zone that would be at greater risk of damage. Submerged reefs, if located sufficiently near the sea surface would be at risk from any direction. Finally, for other reef types, breakage was less prevalent at sites that were more exposed during the cyclone than normal (negative values for relative exposure). This

seemingly counter-intuitive result is probably due to the fact that many sites that are normally very exposed under normal conditions were surveyed. Given the spatial arrangement of the reefs, it may not have been possible for cyclone waves to approach these sites from a direction where they could be more exposed than normal.

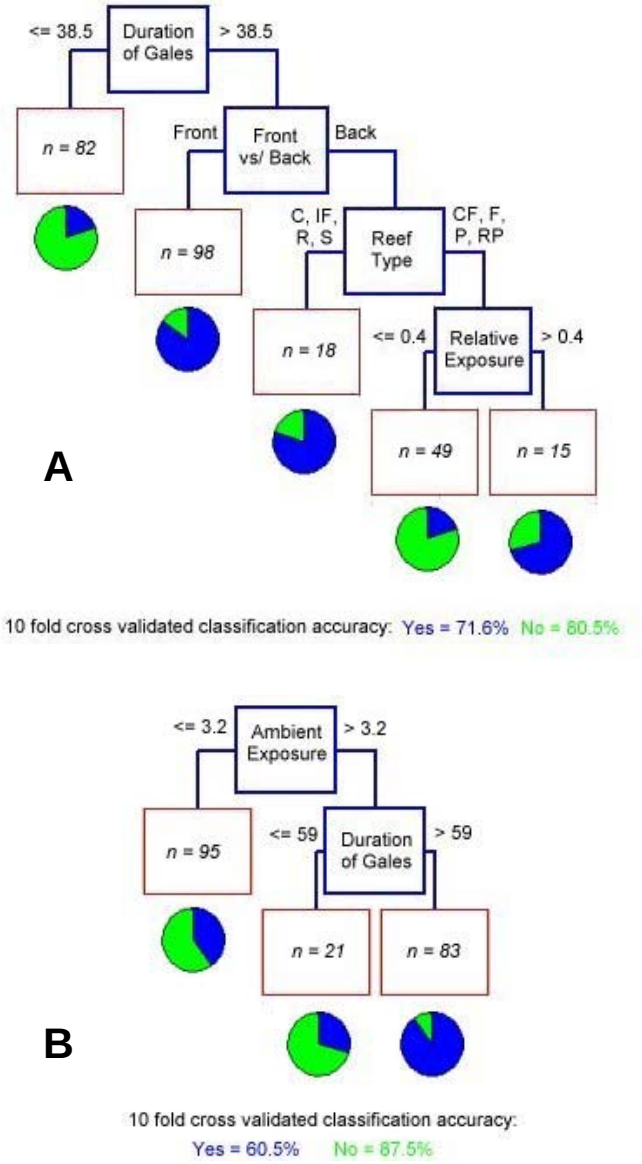

Figure 6.5. Classification tree fitted for the occurrence of coral breakage for cyclones: A - Ivor and Joy, and B - Joy. The relative purity of the terminal nodes (as shown by the pie diagrams, where black = damaged and grey = not damaged) and the classification accuracy indicate the success of the tree. Reef type code C = Crescentic, CF = Coastal Fringing, F = Fringing, IF = Incipient Fringing, L = Lagoonal, P = Planar, R = Ribbon, RP = Reef Patches, and S = Submerged.

Alternately, errors associated with the position of the cyclone path may have affected the estimates of reef site exposure during the cyclone.

Routine exposure and duration of gale force winds best explained the incidence of breakage during cyclone Joy (Figure 6.5 - B). Breakage was very likely at sites where gales persisted longer than 59 hours and where the position of the site is generally exposed under normal conditions (fetch > ~3 km). However, some breakage did occur below the gale force wind threshold, particularly at normally sheltered sites – perhaps because coral colonies at reef communities that are normally sheltered from waves require less energy to break.

6.8 Debris scars

For damage to coral colonies from wave-borne debris (as evidenced by debris scars), five trees were fitted, each for a different combination of cyclones (Table 6.6). The distance of a reef site to the cyclone track was a key factor for predicting the presence or absence of debris scars for most of the trees. The tree that combined cyclones Ivor, Joy and Justin (1) used completely different factors than were found in the trees fitted for each cyclone individually (3, 4, 5). This apparent instability may be due to the low incidence of debris scars observed throughout the field surveys (the high prevalence of poorly consolidated substratum in the GBR makes the occurrence of debris scars less likely). The tree for cyclone Justin (5) generated the most balanced classification accuracy, and the purest nodes. In general, these trees were unsuccessful for prediction because classification accuracies were not well balanced and nodes were indistinct.

Table 6.6. Key features of classification trees modelling debris scars given the hindcast variables. See Appendix 5 for a description of trees not discussed in the text.

	Data Set	Factors used to build the tree	Classification accuracy (% correct)		Node purity	Ecological relevance
			Yes	*No*		
1	Ivor, Joy, Justin	Ambient exposure, Reef type, Duration of Gales	62.5	73.3	Poor	Moderate
2	Ivor, Joy	Distance	95.0	52.5	Poor	Moderate
3	Ivor	Cyclone exposure, Distance	50.0	68.4	Poor	Low
4	Joy	Distance	92.9	62.2	Poor	Moderate
5	Justin	Maximum wind speed	75.0	94.0	Good	Moderate

For cyclone Justin alone (5), debris scars were only found at sites where maximum winds exceeded 20.7 $m.s^{-1}$ (Figure 6.6).

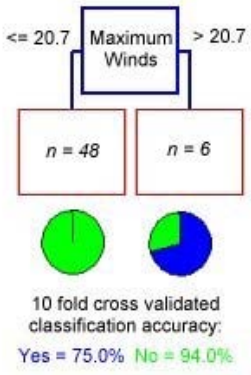

Figure 6.6. Classification tree fitted for the occurrence of debris scars for cyclone Justin. The relative purity of the terminal nodes (as shown by the pie diagrams, where black = damaged and grey = not damaged) and the classification accuracy indicate the success of the tree.

This tree would be useful for prediction, but only for cyclones similar to Justin (i.e. unusually large, persistent, and slow-moving).

6.9 Dislodgement of massives

For the dislodgement of massive corals (e.g. *Porites spp*), five trees were fitted, each for a different combination of cyclones (Table 6.7). Of the individual cyclones, the most complex tree was produced for cyclone Joy and the simplest for Justin. Distance was a useful factor in explaining the presence or absence of dislodged massives for both cyclones Ivor and Joy, but not for Justin. In contrast, the duration of gales was relevant for cyclones Joy and Justin, but not Ivor. Classification accuracy was most balanced for cyclone Ivor, but ecological relevance was low (see Appendix 5). Nodes were most and least pure for cyclones Joy and Justin respectively. Overall, combining Ivor and Joy yielded the most effective tree (2), which was suitable for prediction.

Table 6.7. Key features of classification trees modelling dislodged massives given the hindcast variables. See Appendix 5 for a description of trees not discussed in the text.

Data Set	Factors used to build the tree	Classification accuracy (% correct)		Node purity	Ecological relevance
		Yes	*No*		
1 Ivor, Joy, Justin	Duration of gales, Distance, Cyclone exposure, Slope, Relative exposure, Reef type	80.9	66.5	Good	Low
2 Ivor, Joy	Distance	64.5	67.1	Good	Moderate
3 Ivor	Distance, Reef type	69.2	78.4	Good	Low
4 Joy	Distance, Cyclone exposure, Maximum wind speed, Reef size, Duration of gales	65.4	70.3	Very Good	Moderate
5 Justin	Duration of gales	66.7	94.1	Fair	Moderate

Combining data from cyclones Ivor and Joy (2) resulted in a very simple tree with reasonably distinct nodes (Figure 6.7 - A). Sites located beyond about 78 km of the cyclone track were much less likely to contain dislodged massives than those near the track. However, nearly forty percent of sites located near the track did not contain dislodged massives. This could be due to a lack of massive corals in existence at those sites, the massives present could be of a less vulnerable size, or they could be strongly cemented to the reef substratum.

Dislodgement of massives was relatively rare during cyclone Justin (n = 3), and was limited to sites that sustained gales for more than 19.5 hours (Figure 6.7 - B). No sites with less persistent gales contained dislodged massives.

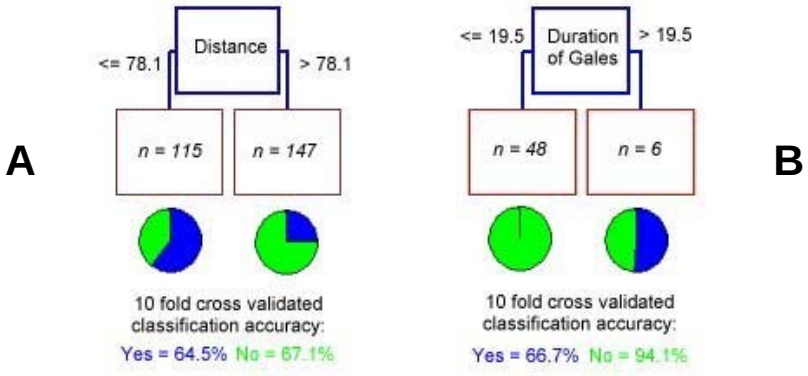

Figure 6.7. Classification tree fitted for the occurrence of dislodged massives for cyclones: A - Ivor and Joy, B – Justin. The relative purity of the terminal nodes (as shown by the pie diagrams, where black = damaged and grey = not damaged) and the classification accuracy indicate the success of the tree.

6.10 Exfoliation

For exfoliation (removal of reef framework to a thickness of about 1 m), four trees were fitted, each for a different combination of cyclones (Table 6.8).

Table 6.8. Key features of classification trees modelling exfoliation given the hindcast variables. See Appendix 5 for a description of trees not discussed in the text.

Data Set	Factors used to build the tree	Classification accuracy (% correct)		Node purity	Ecological relevance
		Yes	*No*		
1 Ivor, Joy, Justin	Maximum wind speed, Front vs/ back habitat	88.2	76.2	Good	High
2 Ivor, Joy	Front vs/ back habitat, Duration of continuous gales, Reef type	82.4	76.9	Very Good	High
3 Ivor	Reef type	50.0	77.1	Very Good	Moderate
4 Joy	Front vs/ back habitat, Duration of gales, Ambient exposure, Distance, Cyclone exposure, Maximum wind speed	79.7	86.4	Very Good	Moderate
5 Justin	None observed.	n/a	n/a	n/a	n/a

No tree was possible for cyclone Justin because no exfoliation was observed during the field surveys.

For cyclone Joy alone (4), a mixture of both exposure (habitat, routine exposure, cyclone exposure) and cyclone energy (duration of gales, distance, maximum winds) best explained the presence or absence of exfoliation. In stark contrast, for cyclone Ivor (3), reef type was the only factor chosen. When Ivor and Joy were combined (2), one exposure factor (habitat) and one energy factor (duration of continuous gales) were used to build the tree. When Justin was added to the analysis (1), this simplified

to maximum winds and habitat. All of the trees were reasonably successful. The best balance in classification accuracy between presence and absence was for cyclone Joy. Node purity was high for all trees. Given this, these trees are suitable to use for prediction.

For cyclones Ivor, Joy and Justin combined (1), exfoliation did not occur unless maximum winds were greater than about 25 $m.s^{-1}$ (Figure 6.8 - A). It was most common for sites along the high-energy reef front where winds exceeded this threshold. Exfoliation is primarily a reef front phenomenon because high-energy routine conditions are needed to develop the consolidated substratum that is stripped away with this type of damage. However, it can occur at the margins of back reef areas where enough wave energy persists for a consolidated framework to develop. Given that exfoliation requires high-energy conditions, the threshold identified (25 $m.s^{-1}$) may seem somewhat low. However, it is the persistence rather than the magnitude of winds that are stronger than normal (gale force [17 $m.s^{-1}$] or above) that enables the generation of large waves capable of exfoliation.

For cyclones Ivor and Joy combined (2), exfoliation was also much less likely to occur at sites located along the reef backs (Figure 6.8 - B). Of the sites located at reef fronts, exfoliation was present at most of those that sustained continuous gales for longer than 37.5 hours. Of the sites with less persistent gales, nearly all sites located on fringing, lagoonal, ribbon or patch reefs sustained exfoliation. These reef types all typically contain well-developed front habitats that are wave adapted – in other words, a consolidated reef framework is very likely to be present (and thus exfoliation is possible).

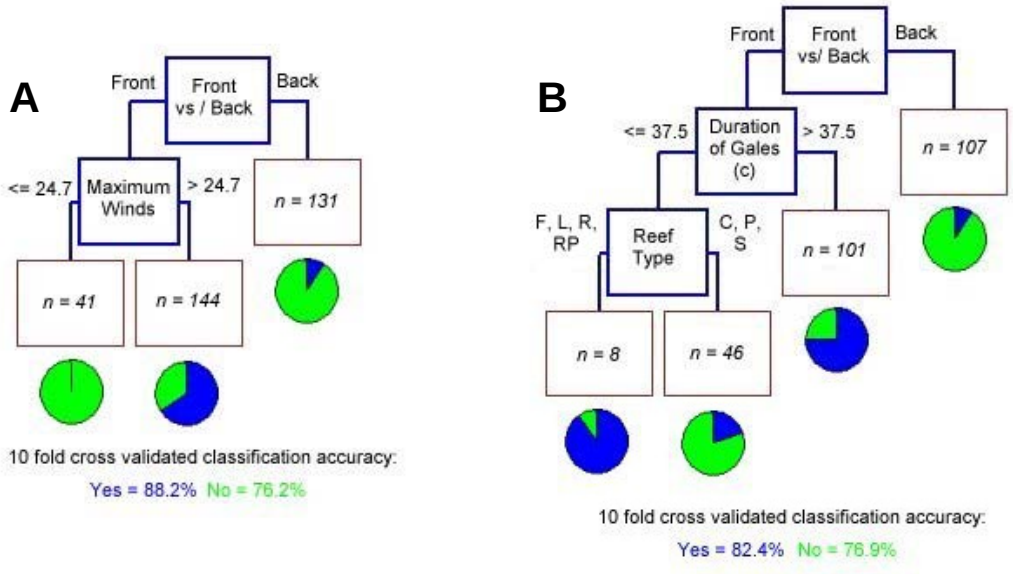

Figure 6.8. Classification tree fitted for the occurrence of exfoliation for cyclones: A - Ivor, Joy, and Justin, and B – Ivor and Joy. The relative purity of the terminal nodes (as shown by the pie diagrams, where black = damaged and grey = not damaged) and the classification accuracy indicate the success of the tree.

6.11 Fallen intact slabs

For fallen intact slabs of the reef matrix, four trees were fitted, each for a different combination of cyclones (Table 6.9). Although distance was the primary splitter chosen for cyclone Justin (5), it was not relevant to any of the other trees, which were dominated by the persistence of gales and habitat. In general, the presence versus absence of fallen intact slabs was poorly modelled. Although classification accuracy was quite high and well balanced for cyclone Joy (4), node purity was poor, as was the case for all the trees. No tree was possible for cyclone Ivor (3).

Table 6.9. Key features of classification trees modelling fallen intact slabs given the hindcast variables. See Appendix 5 for a description of trees not discussed in the text.

	Data Set	Factors used to build the tree	Classification accuracy (% correct)		Node purity	Ecological relevance
			Yes	*No*		
1	Ivor, Joy, Justin	Front vs/ back habitat	100.0	46.5	Poor	High
2	Ivor, Joy	Duration of gales, Duration of continuous gales, Front vs/ back habitat	65.5	81.1	Fair	Moderate
3	Ivor	No tree possible	n/a	n/a	n/a	n/a
4	Joy	Duration of continuous gales, Front vs/ back habitat	89.5	93.9	Poor	High
5	Justin	Distance	50.0	73.5	Poor	Moderate

6.12 Sand movement

For the presence or absence of redistribution of sand, three trees were fitted, each for a different combination of cyclones (Table 6.10). This type of damage was also very poorly modelled. No tree was possible for either cyclone Ivor (3) or Justin (5). While the combined trees show a reasonably high and balanced classification accuracy (1, 2), node purity was poor for all trees. Despite this, the linkages identified by the trees seem relevant and are worthy of further investigation should more damage survey data become available.

Table 6.10. Key features of classification trees modelling sand movement given the hindcast variables. See Appendix 5 for a description of trees not discussed in the text.

Data Set	Factors used to build the tree	Classification accuracy (% correct)		Node purity	Ecological relevance
		Yes	*No*		
1 Ivor, Joy, Justin	Front vs/ back habitat, Slope, Reef type, Maximum wind speed	70.0	72.6	Poor	High
2 Ivor, Joy	Maximum wind speed, Reef type	85.7	73.8	Poor	High
3 Ivor	No tree possible	n/a	n/a	n/a	n/a
4 Joy	Reef type	100.0	78.1	Poor	High
5 Justin	No tree possible	n/a	n/a	n/a	n/a

For cyclones Ivor, Joy and Justin combined (1), reef type was the initial factor chosen to classify sites based on the presence or absence of sand movement (Figure 6.9 - A). Reef types and reef habitats both vary in the amount of sand they typically retain. For example, planar reefs, which often contain sand cays, by far retain the most sand (Hopley et al 1989). Patch reefs, in contrast, normally retain only about one-fourth the amount of sand found on planar reefs, but much more than on other types (i.e. ribbon or submerged). Thus, planar and patch reefs would be most likely to exhibit sand movement, though it would be possible on other types. Accordingly, the tree found that the most sand movement (though it was relatively rare) occurred at sites located on incipient fringing, lagoonal, planar, or patch reefs. For these sites, no sand movement occurred unless the slope at the site was flat, and very little occurred along back reef habitats. For other reef types, sand movement was very rare and only occurred where maximum winds exceeded about 35 $m.s^{-1}$.

When cyclone Justin was removed from the analysis (2), the maximum wind speed became the primary splitter in the resultant tree, though reef type was still important (Figure 6.9 - B).

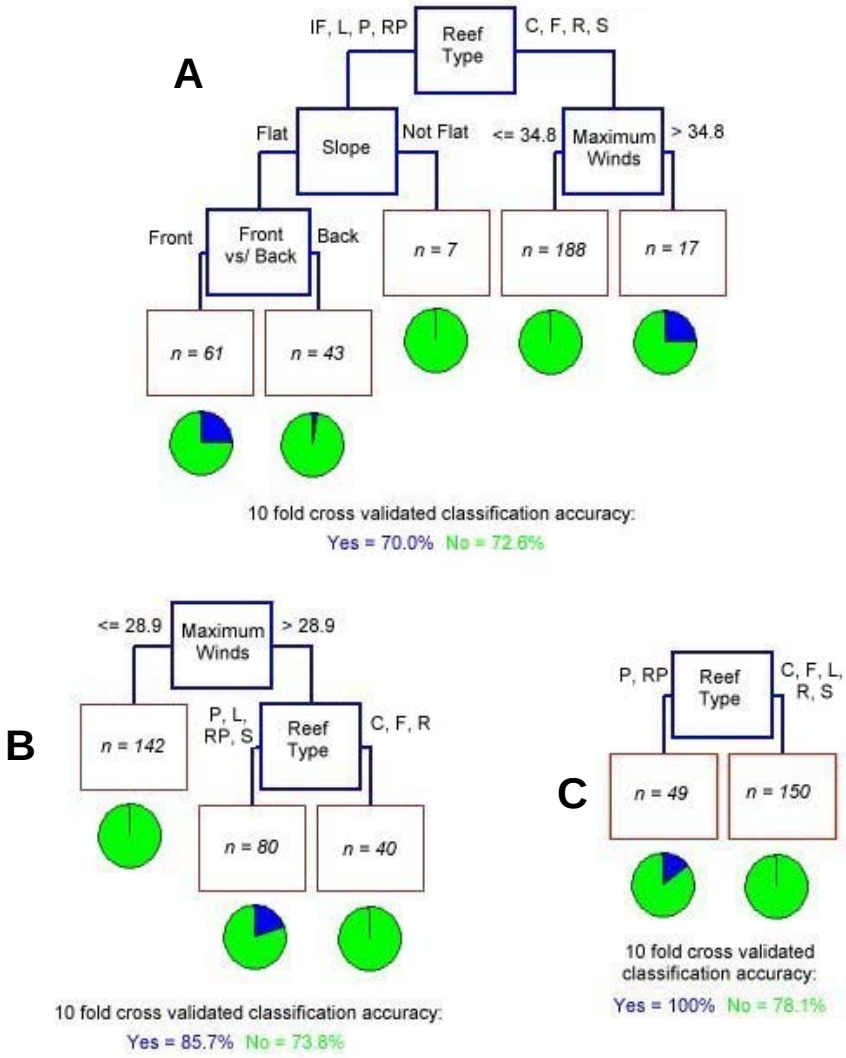

Figure 6.9. Classification tree fitted for the occurrence of sand movement for cyclones: A - Ivor, Joy, and Justin, B – Ivor and Joy, and C - Joy. The relative purity of the terminal nodes (as shown by the pie diagrams, where black = damaged and grey = not damaged) and the classification accuracy indicate the success of the tree. Reef type code C = Crescentic, CF = Coastal Fringing, F = Fringing, IF = Incipient Fringing, L = Lagoonal, P = Planar, R = Ribbon, RP = Reef Patches, and S = Submerged.

No sand movement occurred if sites were located on crescentic, fringing or ribbon reefs, all of which are likely to contain very little sand. Where sand movement did occur on the other reef types, it required maximum winds greater than about 29 $m.s^{-1}$.

When cyclone Joy was modelled alone (4), reef type was the sole factor chosen for the tree generated (Figure 6.9 - C). Sand movement was only observed at sites located on planar or patch reefs where sand is likely to be quite abundant.

6.13 Soft coral stripping

For the stripping of soft corals from the reef, four trees were fitted, each for a different combination of cyclones (Table 6.11).

Table 6.11. Key features of classification trees modelling soft coral stripping given the hindcast variables. See Appendix 5 for a description of trees not discussed in the text.

Data Set	Factors used to build the tree	Classification accuracy (% correct)		Node purity	Ecological relevance
		Yes	*No*		
1 Ivor, Joy, Justin	Duration of continuous gales, Nearby depth	83.3	73.0	Poor	High
2 Ivor, Joy	Duration of continuous gales, Nearby depth	88.1	62.7	Poor	High
3 Ivor	Relative exposure, Reef type	71.4	87.5	Poor	Moderate
4 Joy	Nearby depth, Distance	74.3	77.4	Poor	High
5 Justin	No tree possible	n/a	n/a	n/a	n/a

The presence versus absence of soft coral stripping was poorly modelled. Although classification accuracies were reasonably high and well balanced, node purity was poor for all cyclones. No tree was possible for cyclone Justin, probably because evidence of soft coral stripping was extremely rare. Although the trees are not

suitable for prediction, the linkages they identify are worthy of further investigation. For example, the typical water depth in the area surrounding each site was an important factor in three of the four trees.

When cyclones Ivor, Joy and Justin were combined (1), the duration of continuous gales was the primary splitter in the resulting tree (Figure 6.10 - A).

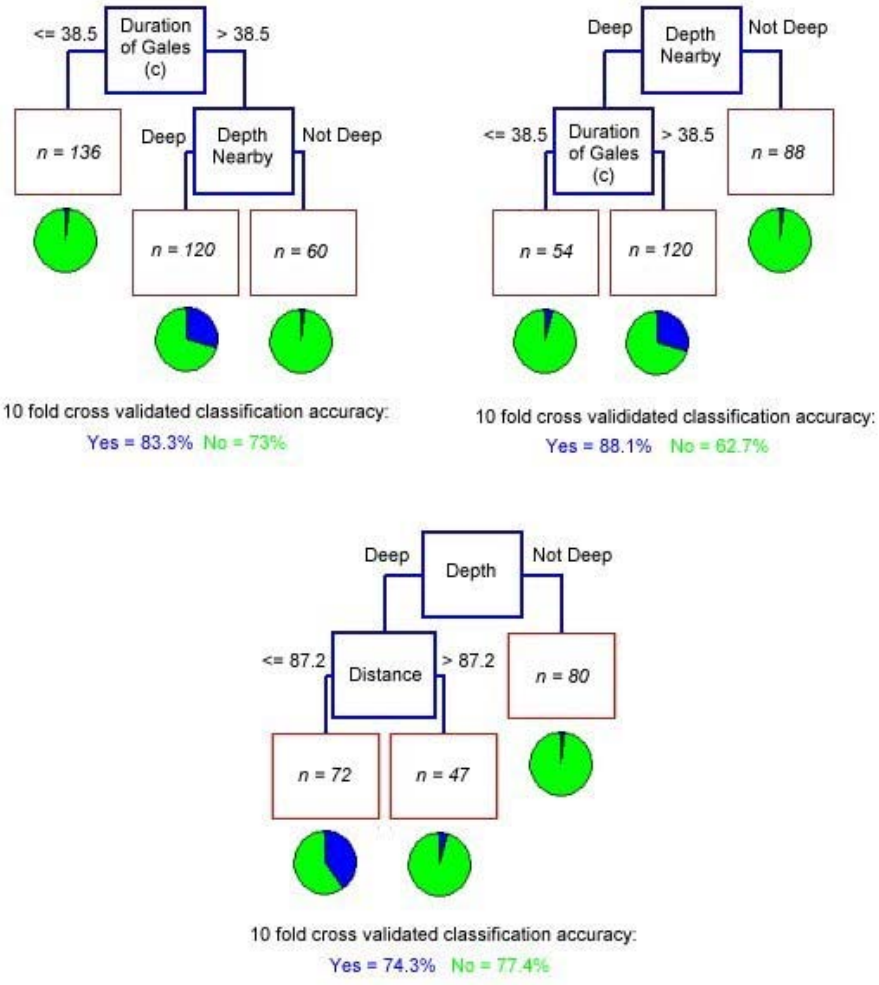

Figure 6.10. Classification tree fitted for the occurrence of stripped soft corals for cyclones: A - Ivor, Joy, and Justin, B – Ivor and Joy, and C - Joy. The relative purity of the terminal nodes (as shown by the pie diagrams, where black = damaged and grey = not damaged) and the classification accuracy indicate the success of the tree.

Soft coral stripping was very unlikely at sites where gales did not continue uninterrupted for at least 38.5 hours. Where gales persisted beyond this threshold,

stripping was least likely for sites near shallow water. Soft corals are less prevalent in the highest energy environments (Dineson 1983), which are more likely to be located in the relatively shallow water (< 20 m deep) in which all surveyed sites were located. Thus, evidence of coral stripping was likely rare because few soft corals were present at the surveyed sites. For those that were present, stripping was more likely at sites where waves approached at full force (i.e. close to deep water which did not dissipate the waves before they approached the site). A similar tree resulted when cyclone Justin was removed from the analysis (2), except that the depth nearby became the primary splitter (Figure 6.10 - B). Stripping was most likely when water nearby was deep (waves hit the shallow sites at full force) and gales continued uninterrupted for more than 38.5 hours.

For cyclone Joy alone (4), depth in the vicinity of each site was again a key factor (Figure 6.10 - C). Very little soft coral stripping occurred at sites not located near an area of relatively deep water. Of the others, those located relatively near the cyclone track (within ~87 km), were much more likely to sustain this type of damage.

6.14 Trenching

For trenching (superficial trenches through the substratum usually about 1 m across and deep), four trees were fitted, each for a different combination of cyclones (Table 6.12). Although no tree was possible for cyclone Joy (4) and node purity was poor for Justin (5), the combined tree of cyclones Ivor and Joy (2) did a reasonably good job of explaining patterns in the presence versus absence of trenching, and it is suitable for use in prediction. Although Ivor (3) and Justin (5) alone used single factors (duration of continuous gales and distance, respectively), when Joy was added to the analysis

(1), several factors in addition to those two became relevant, most notably the reef slope.

Table 6.12. Key features of classification trees modelling trenching given the hindcast variables. See Appendix 5 for a description of trees not discussed in the text.

Data Set	Factors used to build the tree	Classification accuracy (% correct)		Node purity	Ecological relevance
		Yes	*No*		
1 Ivor, Joy, Justin	Slope, Reef type, Reef shape, Duration of continuous gales, Front vs/ back habitat, Distance	65.7	79.9	Good	Low
2 Ivor, Joy	Duration of continuous gales	66.7	84.3	Good	High
3 Ivor	Duration of continuous gales	58.3	90.0	Good	Moderate
4 Joy	No tree possible	n/a	n/a	n/a	n/a
5 Justin	Distance	75.0	71.4	Poor	Moderate

For cyclones Ivor and Joy (2), the continuous duration of gales and the habitat (front versus back) were chosen as splitters to explain patterns in trenching (Figure 6.11). As might be expected, trenching was very unlikely unless there was a sustained period of uninterrupted gale force winds. Trenching requires repeated wave impacts to scrape and scour corals and framework from the reef matrix. As with exfoliation, trenching was much less likely at sites along back reef habitats, where the reef substratum is typically less consolidated.

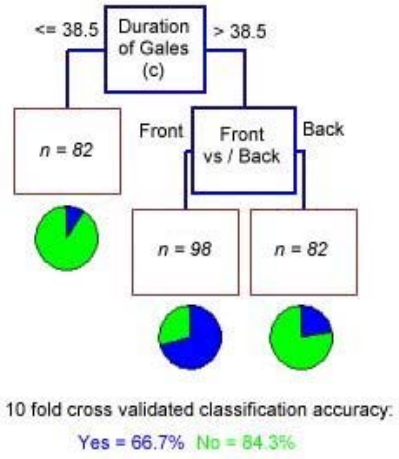

Figure 6.11. Classification tree fitted for the occurrence of trenching for cyclones Ivor and Joy. The relative purity of the terminal nodes (as shown by the pie diagrams, where black = damaged and grey = not damaged) and the classification accuracy indicate the success of the tree.

6.15 Conclusions

Waves capable of physically damaging reef communities can propagate across large areas (100s of km). However, the resultant wave damage is typically very patchy in distribution across small distances (100s of m). This occurs because the local scale factors that affect reef exposure and vulnerability to wave damage (proximity and orientation with respect to nearby wave-blocking obstacles, local topography, water depth, slope, colony size, growth form and orientation, and so on) are highly variable over time and across space.

The most useful classification trees for predicting the occurrence of damage were those with a reasonably high classification accuracy balanced between presence versus absence of damage, with nodes that clearly distinguished between presence and absence, and that were defensible ecologically (De'ath and Fabricius 2000). The four trees that satisfied these conditions, and thus will be used to build predictive decision rules in GIS, were: severe damage of any type, breakage, dislodgement and

exfoliation (Table 6.13). These trees are based on varying combinations of cyclone survey data that were fitted by CART and assessed for utility (based on classification accuracy, node purity, and ecological relevance) by the author.

For two of the trees (breakage and dislodgement), the unusual nature of cyclone Justin required that risk predictions for cyclone Justin be made separately from the remaining 84 cyclones.

Table 6.13. CART trees chosen to predict the occurrence of wave damage across the GBR from 1969 to 2003.

	Cyclone Field Survey Data						
Dependent Variable	Ivor, Joy, Justin, Celeste, Althea	Ivor, Joy, Celeste, Althea	Ivor, Joy, Justin	Ivor, Joy	Ivor	Joy	Justin
Any damage							
Severe damage of any type			✔				
Maximum damage of any type							
Total damage							
Total low energy damage							
Total high energy damage							
Coral breakage				✔			✔
Debris scars							
Dislodgement of massives				✔			✔
Exfoliation			✔				
Fallen slabs							
Sand movement							
Soft corals stripped							
Trenching							

For two of the selected trees, practical considerations (model uncertainty and computer processing time) precluded the use of certain factors chosen as relevant in the analysis. For example, factors that rely on modelled cyclone wind directions

(cyclone exposure, relative exposure) are of uncertain quality because wind directions were sometimes poorly modelled (see chapter 4). This uncertainty is reflected in the fact that these factors were rarely chosen as splitters in the classification and regression trees despite being of obvious importance to the presence, severity and type of damage. Further, calculating the duration of *continuous* gales (done manually within a spreadsheet for each cyclone) was too time consuming to repeat for each of the 85 cyclones across 24,224 individual reef sites within the time frame of this thesis.

Removing these factors from the analysis altered these trees. For example, for the occurrence of severe damage of any type (case 1 – Ivor, Joy and Justin in Table 6.3), this resulted in a more complex, but nearly as effective tree, where the maximum wind speed replaced the duration of continuous gales as the primary splitter (Figure 6.12). Further, slope was relevant in the new tree, with sites of moderate and flat slopes more likely to sustain severe damage. The classification accuracy was slightly less balanced than the original tree, but the nodes remained reasonably distinct.

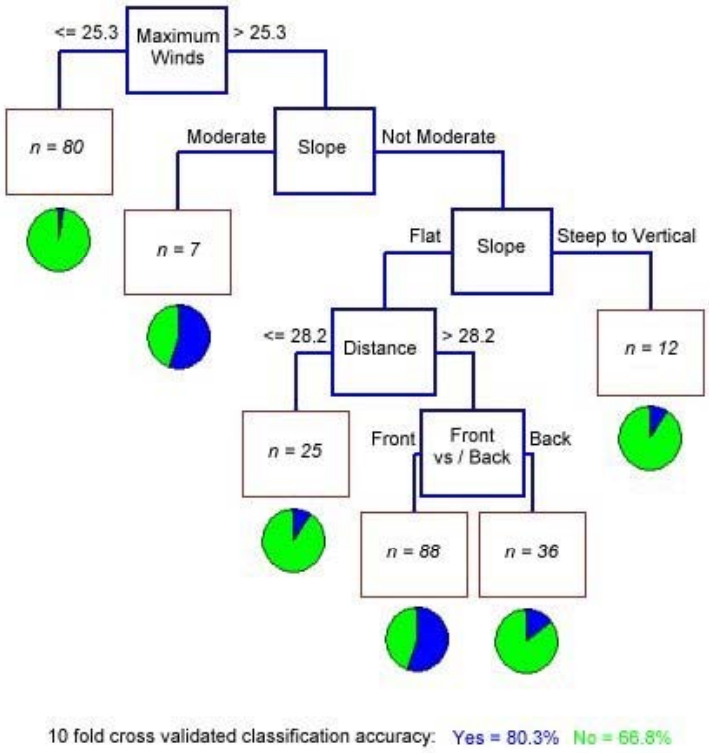

Figure 6.12. Revised classification tree fitted for the occurrence of severe damage of any type for cyclones Ivor, Joy and Justin combined. The relative purity of the terminal nodes (as shown by the pie diagrams) and the classification accuracy indicate the success of the tree.

The second tree affected was breakage for cyclones Ivor and Joy combined (2 in Table 6.5). While the basic form of the tree remained the same, the classification accuracy declined to a minor degree (Figure 6.13). However, the nodes remained quite distinct and useful for prediction. Relative exposure was replaced by reef type, and distance became the new primary splitter.

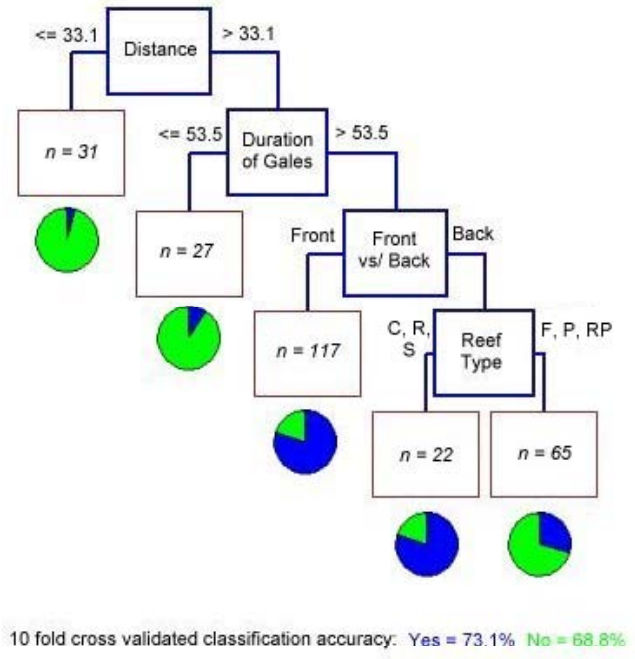

Figure 6.13. Revised classification tree fitted for the occurrence of breakage for cyclones Ivor and Joy combined. The relative purity of the terminal nodes (as shown by the pie diagrams) and the classification accuracy indicate the success of the tree.

Given these changes, a final set of decision rules for predicting the distribution of cyclone damage across the GBR for each cyclone from 1969 to 2003 was produced from the selected classification trees (Table 6.14). The subsequent predictions were used to generate a time series (1969-2003) of the presence versus absence of cyclone disturbance of the four types on a yearly basis across the GBR at each site (n = 24,244). This cyclone history is summarised and discussed in Chapter 7.

Some of the trees that were not useful for prediction were valuable in identifying possible ecological factors that influence the likelihood of damage. For example, the geomorphologic reef type appears to influence sand movement, and the water depth in the vicinity of a site seems important for potential damage to soft corals. These

relationships identified by the CART analysis should be explored further as more damage surveys are conducted following future cyclones.

Table 6.14. Decision rules for predicting the occurrence of four types of cyclone damage across the GBR from 1969-2003.

Type of damage	Data set(s)	Decision Rules
Presence or absence of severe damage of any type	Ivor, Joy, Justin	Impacts are severe IF: maximum winds > 25.3 m/s and slope = moderate; or IF: maximum winds > 25.3 m/s and slope = flat and distance > 28.2 and habitat = front.
Presence versus absence of coral breakage	Ivor and Joy	Breakage is present IF: distance > 33.1 km, and duration of gales > 53.5 hours and habitat = front; or IF: distance > 33.1 km and duration of gales > 33.5 hours and habitat = back and reef type = crescentic, incipient fringing, ribbon or submerged.
	Justin	Breakage is present IF: reef type = crescentic, crescentic / fringing, fringing, incipient fringing, ribbon or submerged.
Presence versus absence of dislodgement of massives	Ivor and Joy	Dislodgement is present IF: distance $\leq$ 78.1 km.
	Justin	Dislodgement is present IF: duration of gales > 19.5 hours.
Presence versus absence of exfoliation	Ivor, Joy, Justin	Exfoliation is present IF: habitat = front and maximum winds > 24.7 m/s.

CHAPTER 7: Tropical cyclone disturbance regime in the GBR, 1969-2003

7.1 Overview

Over the past 35 years (1969-2003), waves generated by 85 cyclones had the potential to damage each of the more than 2,700 reefs of the GBR. The intensity and timing of damage has helped shape the structure and function of the coral communities present at each site. The aim of this chapter is to characterise the cyclone disturbance regime across the region, based on the occurrence of four measures of disturbance: 1) breakage of coral colonies, 2) dislodgement of massive coral colonies, 3) exfoliation, and 4) severe (widespread) damage of any type (Figure 7.1).

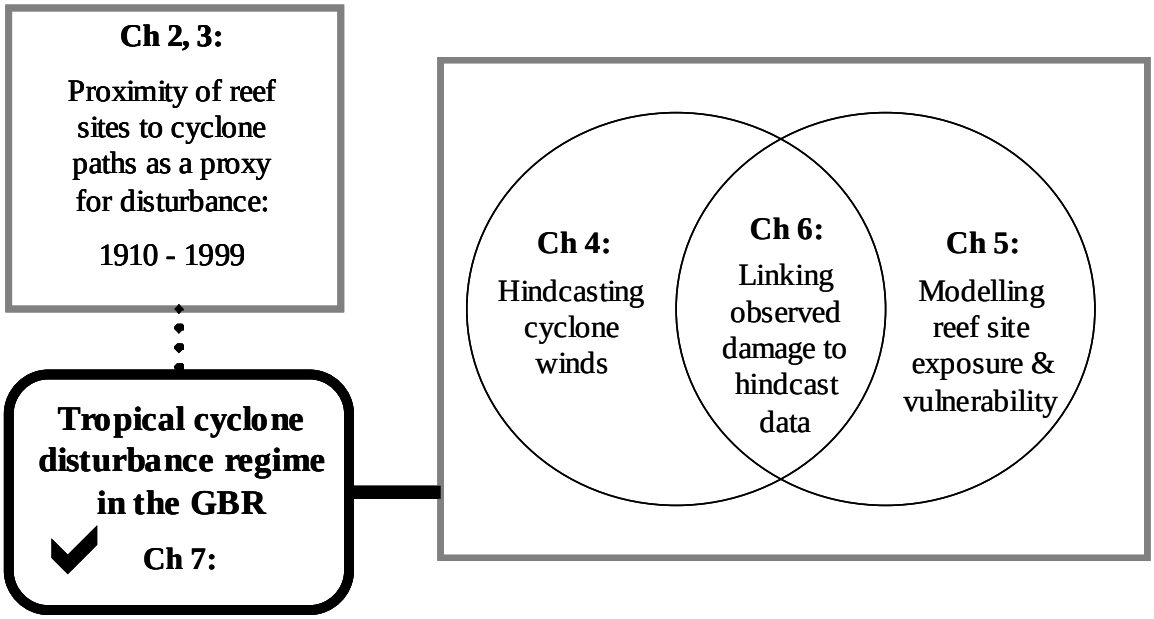

Figure 7.1. Overview diagram of this thesis. The check mark indicates the current chapter.

7.2 Introduction

White and Pickett (1985) define a disturbance as "any relatively discrete event in time that disrupts ecosystem, community, or population structure and changes resources,

substrate availability, or the physical environment." The nature of a given disturbance depends on the spatial and temporal perspective from which it is viewed (White and Pickett 1985). The primary building block of coral reef ecosystems, whether an isolated mid-ocean atoll or a complex system of thousands of reefs (like the GBR), are the individual coral colonies that combine to form reef structures. While disturbances such as mass bleaching, crown-of-thorns starfish predation and tropical cyclones can affect large areas with a single event, damage is invariably patchy in distribution because vulnerability varies at many scales, from individual coral colonies upwards. Disturbance regimes need to be understood at regional scales (100s of km) to capture their full extent, and at very local scales (10s of m) to assess their potential impacts. For example, patches of coral damage range in size from less than a metre (selective death of polyps within a single colony) to whole sections of reefs (Connell and Keough 1985). Further, the recovery of reef communities from disturbance and their resilience to repeated impacts depends in part on the species richness and diversity at the sub-reef scale as well as the interconnectivity between individual reefs across 100s of km (Done et al 1996).

7.2.1 Defining reef sites

To characterise the tropical cyclone disturbance regime in the GBR, I modelled the distribution of cyclone energy at broad scales (100s of km at a 1 km resolution) and the vulnerability of coral communities at local scales (individual sites within each reef). Vulnerability to cyclone damage can vary between sites located only hundreds of metres apart, such as at Oublier Reef during cyclone Justin where damage severity ranged from devastation to none over this distance. To capture this local scale

variability, I defined a series of 'sites' around the perimeter of each reef at a 1 km interval (Figure 7.2) at which to model the cyclone disturbance regime. For the 2,728 individual reefs of the GBR, this produced a total of 24,224 individual sites. Although each site is indicative of the local exposure conditions in its vicinity, high variability in vulnerability across very small distances means that it is not representative of the entire 1 km area.

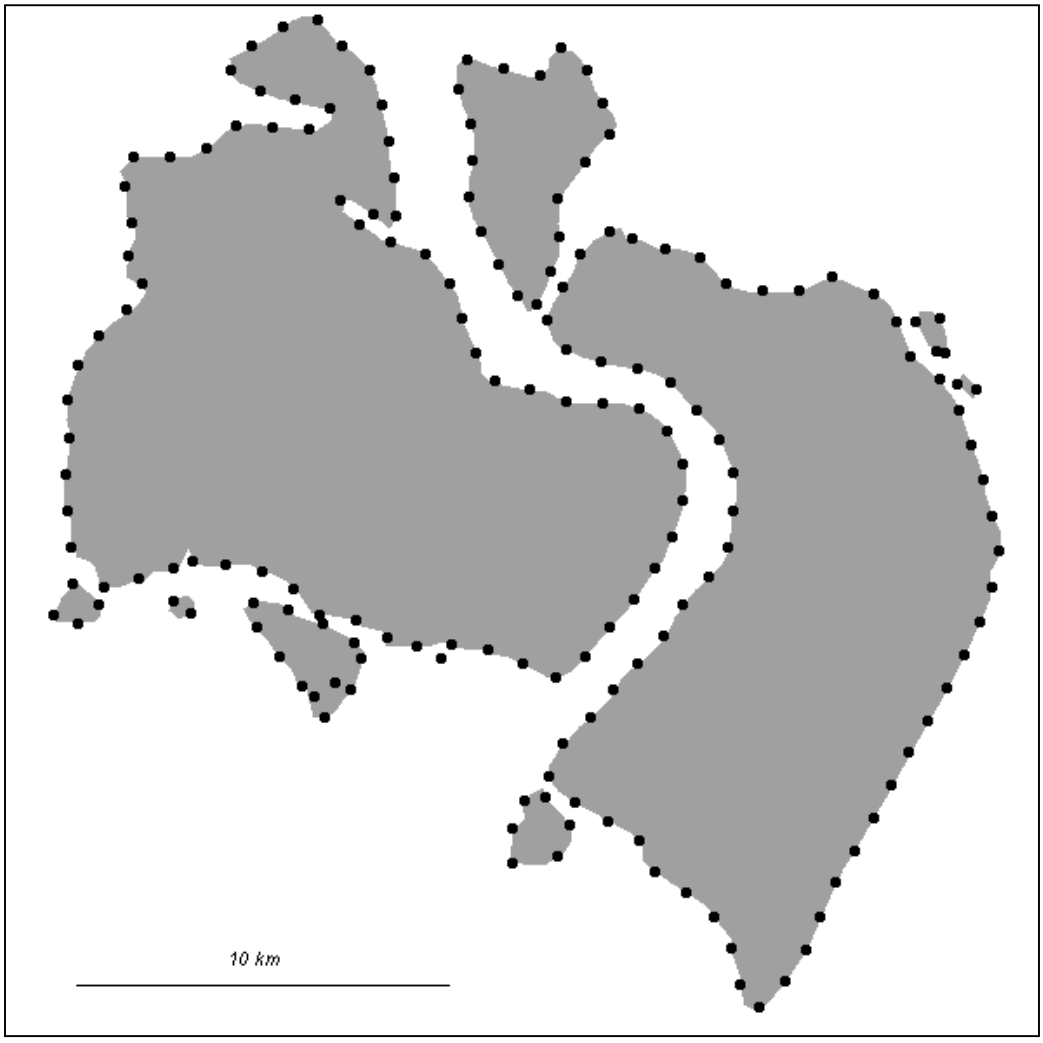

Figure 7.2. Spacing of reef sites (black circles) along GBR reefs (gray polygons). A reef site was placed every 1 km around the perimeter of each reef. Although each site is indicative of the local shelter conditions in its vicinity, it is not assumed to represent the entire 1 km area.

7.2.2 Predicting reef damage

I estimated cyclone winds (maximum wind speed and duration of gales), exposure (under routine conditions, during the cyclone, and the difference between the two), and vulnerability (geomorphologic reef type, depth nearby) for each site. Slope and habitat (front versus back) values were taken from field data.

Based on the decision rules derived in Chapter 6 (Table 6.14), the occurrence of breakage, dislodgement, exfoliation and severe (widespread) damage of any type was predicted for each site during each cyclone. Subsequently, descriptors of the cyclone disturbance regime (described in next section) were calculated for each site. To identify broad trends in the latter, the GBR was divided into one-degree latitude by one-degree longitude blocks (Figure 7.3), within which values for the reef sites were averaged. The highest concentration of reef sites by latitude is located in the far north (10^0-11^0S) and in the Townsville and Whitsunday region (19^0-21^0S). By far, the highest concentration of sites by longitude (three-fold more) is located at 143^0-144^0E (close to land in the far north). Thus, in general, more reef sites are likely to be damaged by cyclones that pass through these areas. In contrast, relatively few sites are found at 17^0-18^0S, 146^0-147^0E where the continental shelf is narrowest, and in the far southern GBR (24^0-25^0S) where reefs are few and widely scattered. In these areas, less reef sites are likely to be damaged by cyclones that pass through these areas.

	Longitude												
Latitude	142	143	144	145	146	147	148	149	150	151	152	153	*Total*
10	861	1160	142										2163
11	192	2378	277										2847
12		1706											1706
13		1203	383										1586
14		94	629	671									1394
15				969									969
16				562	266								828
17					781								781
18					536	551	52						1139
19					43	29	840	1114	240				2266
20							363	438	1763	540	35		3139
21								589	454	1463	1411		3917
22								119	159	36	470		784
23									113	377	125		615
24										8	40	42	90
Total	1053	6541	1431	2202	1626	580	1255	2260	2729	2424	2081	42	24224

Figure 7.3. The Great Barrier Reef divided into one-degree latitude by one-degree longitude blocks. The number within each block indicates the number of reef sites (spaced every 1 km along the perimeter of each reef) located therein: white = < 1,000, light grey = 1,000-2,000, dark grey = 2,000-3,000 and black = >3,000.

7.2.3 Characterising the disturbance regime

The dynamics of a disturbance regime can be described using a range of interrelated descriptors, such as the frequency, return interval, and magnitude of the disturbance (White and Pickett 1985). For this study, four basic descriptors (intensity, incidence, timing and synergism) illustrated by seven calculated parameters (max, gales, time series plots, number of disturbance-free periods, mean length of disturbance-free

periods, maximum length of disturbance-free periods, time since last event) are used to characterise tropical cyclone disturbance of the GBR (Table 7.1).

Table 7.1. Descriptors of the tropical cyclone disturbance regime in the Great Barrier Reef Region from 1969 to 2003. Adapted from White and Pickett 1985 and Woodley 1992.

Descriptor	Parameter	Definition
Intensity	*Max*	Frequency of maximum wind speeds > 24.7 m/s from 1969 to 2003 across the GBR (resolution = 1 km).
	Gales	Frequency of gale force wind periods > 19.5 hours from 1969 to 2003 across the GBR (resolution = 1 km).
Incidence	*Time series plots*	Percentage of GBR reef sites predicted to be disturbed by cyclone waves during each cyclone from 1969 to 2003.
Timing	*Disturbance-free periods*	Number of intervals during which reef sites were predicted to be undisturbed by cyclone waves, averaged by 1^0 latitude by 1^0 longitude cells.
	Length of disturbance-free periods	Average number of years expected between successive disturbance events (calculated based on a geometric distribution) for each 1^0 latitude by 1^0 longitude cell.
		Maximum length of disturbance-free intervals at each reef site, averaged by 1^0 latitude by 1^0 longitude cells.
	Time Since Last Event	Number of contiguous years (as of 2003) since the last event predicted to disturb each reef site, averaged by 1^0 latitude by 1^0 longitude cells.
Synergism	-	Discussion of potential effects of cyclone damage on other disturbances.

The intensity of each cyclone was examined from the point of view of individual coral colonies by using hindcast wind speeds as a proxy for locally generated sea state. Although long period swells can occasionally affect outer reef sites not protected within the GBR matrix (such as was probable during cyclone Pam in 1974), most damage to most sites is probably caused by locally generated waves in the vicinity of the cyclone (Van Woesik 1992). Thresholds in **maximum wind speed** (Max) and the **duration of winds exceeding gale force** (Gales - as derived in Chapter 6) were used

to approximate the potential for development of waves capable of damaging coral reef communities. The spread of potentially damaging wave energy also depends on the cyclone's position and direction of forward motion relative to each reef site of interest, as well as its speed and size (see chapter 3). Other studies (Woodley 1992, Treml et al 1997, chapter 2 of this thesis) used proximity to the cyclone path as a proxy for the potential for wave damage in the absence of more reliable data. However, proximity alone is insufficient to adequately model the spatial distribution of reef site damage (see chapter 3).

The incidence of a disturbance indicates the proportion of area affected by it. For cyclones on the GBR, this was measured by calculating the percentage of reef sites at which wave damage was predicted to occur during each cyclone. This was based on the decision rules derived in chapter 6.

I defined four parameters to describe the timing of cyclone disturbances in the GBR: 1) the number of disturbance-free intervals, 2) the mean number of years expected between successive disturbances (return interval) and 3) the maximum length of disturbance-free intervals, and 4) the number of years since the last cyclone event. These were measured for the GBR by constructing a spreadsheet of cyclone events from 1969 to 2003, noting predicted damage (value of 1) or not (value of 0) for each of the reef sites, and counting the number of disturbance-free intervals, as well as measuring the length (in years) of each one. A separate spreadsheet was created for each of the four damage types (breakage, dislodgement, exfoliation, severe damage of any type).

Examination of the resultant cyclone disturbance history reveals that very few sites were predicted to have been damaged during the first and last years of the study period (which, as previously mentioned, was chosen a priori based on the quality of the recorded cyclone database). Thus, for almost all the sites, both left and right censoring (D'Addio and Rosholm 2002, Singer and Willett 1991) is present in the data. That is, the first disturbance-free interval began before the start of the study period and thus its length as measured in this study represents a minimum estimate. Similarly, because the last disturbance-free interval remains open (no damage was predicted for any site in 2003 because no cyclones passed near the GBR during that season), its length also represents a minimum estimate of the last return interval. Further, for one type of damage (breakage), none was predicted to occur at any time during the study period for some or all of sites located north of 12^0S. All that can be said for the latter sites is that the most recent period of breakage occurred more than 35 years ago. For the remainder of the sites, discarding the disturbance intervals that are censored (nearly every first interval and every last interval in the dataset) is unacceptable due to the short length of the time series, the proportion of sites that are affected (nearly all), and the valuable information that would be lost. Statistical theory has recently been developed to deal with censored data (ie, survival analysis, hazard analysis) as it commonly occurs in time dependent datasets. However, using these methods to analyse data that is both left and right censored has rarely been attempted, as it is problematic and complex (D'Addio and Rosholm 2002). In the context of this study, it is the length of the typical return interval between predicted disturbance events that would be significantly affected by the censoring should it be calculated simply by taking the mean or median of all the intervals. Therefore, an alternate method was required to estimate the cyclone disturbance return interval for

this data. It is well recognised that the vulnerability of coral colonies to cyclone disturbance in a given year depends on whether those colonies have recently been damaged by cyclones or other disturbances and the nature and magnitude of that damage (see Chapter 5). Due to a lack of adequate data, the model used in this thesis to predict damage (as described in chapters 4, 5 and 6) did not incorporate these effects. As a consequence, the occurrence of damage at a given site in any given year as predicted in this study can be considered to be independent (the position, size or intensity of cyclones from year to year does not depend what happened in the previous year, as cyclones tend to be randomly distributed – Xue and Neumann 1984). For this reason, and because cyclone damage predictions are binary (0 versus 1), the prediction of cyclone damage or not over time at each site is an example of a Bernoulli process (Johnson and Kemp 1992). Given that the time between each predicted cyclone damage event was measured discretely (in years, rather than portions of years), the timing of the cyclone disturbance history can be modelled using a geometric distribution (the continuous analogue of which is the negative exponential distribution). This provides a method of estimating the probability of damage occurring at a site or group of sites over the entire study period that is less sensitive to the censoring in the data. From this probability, the expected typical number of years between disturbance events can be calculated as a measure of the return interval without having to discard the first and last disturbance interval for nearly every site in the dataset.

Although the frequency of disturbance events (number of cyclones) can be useful, it is the **number of undisturbed periods** during which recovery is possible that is more relevant to coral communities. For example, if five cyclones disturb a reef site over

twenty years, the effect on coral communities will be much different if those five cyclones occur five years in a row (resulting in two undisturbed periods) rather than intermittently throughout the time period (resulting in five or six undisturbed periods). If the number of cyclone events were counted instead of the number of disturbance-free periods, this distinction would be lost. Woodley (1992) counted the number of hurricane-free intervals at Discovery Bay, Jamaica from 1870-1989. For the GBR, I counted the number of contiguous intervals (measured in years) for which no damage was predicted (disturbance-free intervals) for each of the reef sites. The latest interval was included in the count except where no damage was predicted for the entire study period (sites located north of 12^0S for breakage only). Also important to the timing of disturbances is the number of years that typically pass between disturbances (return intervals). For example, Massel and Done (1993) estimated how the length of return intervals of cyclones of various intensities varied with latitude along the GBR. Woodley (1992) measured the length of each hurricane-free interval at Discovery Bay over 119 years, and calculated the return time as the median interval length (interval lengths, when measured continuously, formed a negative exponential distribution, for which the median better indicates central tendency). For the GBR, return times were estimated by the mean as calculated for a geometric distribution (Johnson and Kemp 1992). The mean of a geometric distribution is calculated by dividing 1 by the probability of damage occurring at any site within an area (in this case, a 1^0 latitude by longitude box) at any time during the time series (1969-2003). This probability was calculated for each box by dividing the total number of damage events predicted across the box over the time series by the number reef sites found in that box multiplied by the number of years in the study period (35). Thus, the return period was approximated as the **average number of years expected between successive**

disturbance events. The **maximum length of the disturbance-free intervals** was also measured, as this indicates the longest time period (albeit the least and most recent periods representing minimum estimates) during which coral communities could have grown undisturbed (holding other disturbances constant). When the **number of years since the last cyclone event** (measured from the present time – 2003 in this study) is compared to the mean number of years between subsequent events (return interval), it indicates the degree to which current conditions at a site reflect what was typical for that site over the entire study period (Woodley 1992).

Finally, synergism, the potential influence of cyclone disturbance on the effects of other disturbances in the GBR (i.e. outbreaks of predators or diseases, pollution, and bleaching caused by elevated sea surface temperature) was also considered.

7.3 Intensity

Cyclone wind speeds were used as a proxy for the potential for development of local wind-sea capable of damaging coral reef communities. Both the maximum wind speed and the duration of high winds are important in determining the strength of local wind-sea. These were hindcast for each of the 85 cyclones that passed near the GBR from 1969 to 2003 using the methods described in chapter 4. By combining the results from both of these over the time series, it was possible to crudely estimate the risk of cyclone wave damage across the GBR on susceptible sites within reefs.

7.3.1 Maximum winds

The minimum threshold maximum wind speed predicted to be capable of damaging reef sites was 24.7 $m.s^{-1}$. This was taken as the minimum wind speed predicted to cause damage of any of the types modelled (see Table 6.14, Chapter 6). The maximum wind speed grid for each cyclone from 1969 to 2003 was reclassified to assign a value of one to areas at or beyond this threshold and a value of zero to the remaining areas. The resultant 85 grids (one per cyclone) were summed to count the number of cyclone events during which each position across the GBR experienced maximum wind speeds capable of damaging reef sites (Figure 7.4).

Threshold wind speeds were exceeded during at least five cyclones over the past 35 years across the entire GBR. For coastal areas, near Gladstone and in the far north, the number of potentially damaging cyclones was less than ten. Areas that sustained more than 15 potentially damaging cyclones were patchily concentrated between Cooktown and just south of Townsville, as well as seaward from the Whitsunday Island region. Areas where the damage potential threshold was exceeded more than 20 times were all located seaward of the GBR.

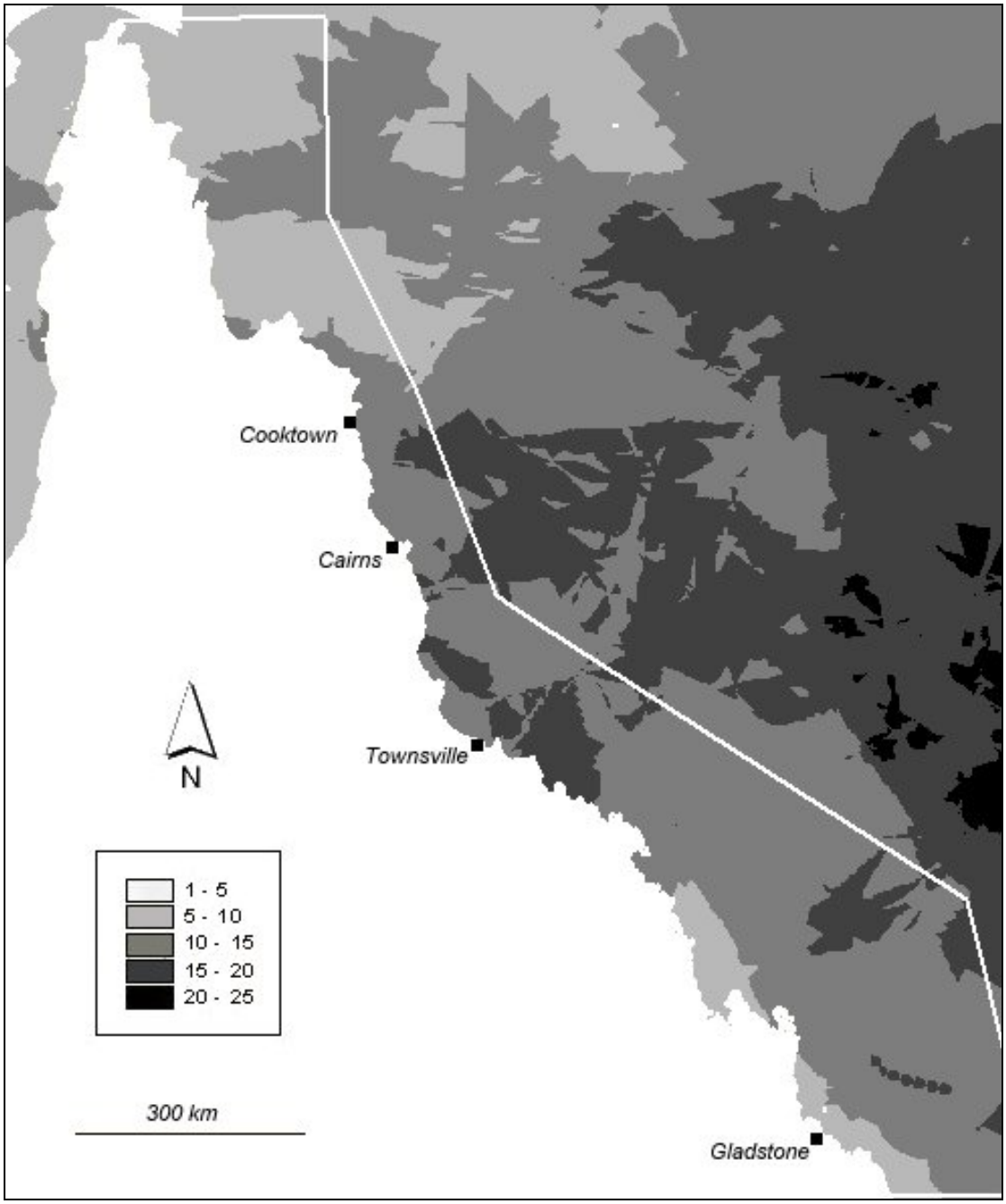

Figure 7.4. Number of cyclone events from 1969 to 2003 during which maximum wind speeds exceeded the minimum threshold speed predicted to cause damage (24.7 $m.s^{-1}$).

Only about 30% of the cyclones generated maximum winds that exceeded the predicted threshold for reef damage (25 of 85). Of these, only 19 (22%) generated these winds within the GBR. This supports the finding by Puotinen et al (1997) that the most common cyclones in the region over the last three decades were relatively weak.

7.3.2 Duration of gales

The minimum threshold duration of winds exceeding gale force predicted to be capable of damaging reef sites was 19.5 hours. This was taken as the minimum number of hours of gales predicted to cause damage (see dislodgement in Table 6.14, Chapter 6). The duration of gales grid for each cyclone from 1969 to 2003 was reclassified to assign a value of one to areas at or beyond this threshold and a zero to the rest, with the 85 grids summed as for maximum winds (section 7.3.1).

Gale force winds persisted long enough to damage reef sites during at least ten cyclones from 1969 to 2003 along all of the GBR except the far north, where only five to ten cyclones exceeded the threshold (Figure 7.5). Areas that sustained more than 15 potentially damaging cyclones were concentrated offshore from Cooktown and to the north; offshore from Cairns; and offshore from just south of Townsville to the far southern GBR, with the exception of an area just north of the Whitsunday Islands region and an area located near the coast just south of Gladstone. Areas where the damage potential threshold was exceeded more than 20 times were again all located seaward of the GBR. As with maximum wind speeds, only 19 (22%) of cyclones generated gales winds that endured long enough to damage reef sites.

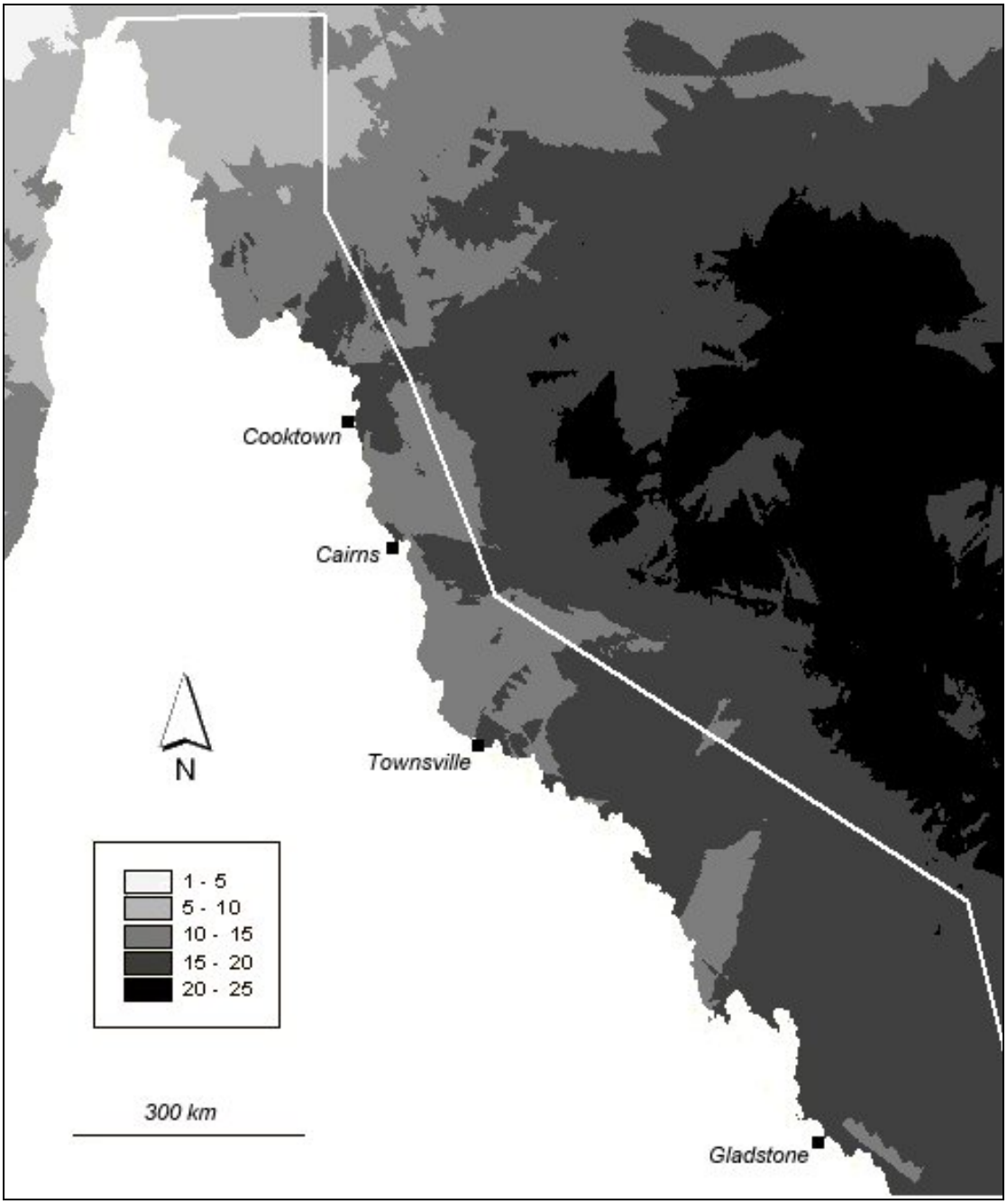

Figure 7.5. Number of cyclone events from 1969 to 2003 during which winds exceeding gale force persisted for longer than the minimum threshold predicted to cause damage (19.5 hours).

7.3.3 Cyclone damage risk

If we assume that there are coral communities within each reef site that are exposed to local wind-sea generated by a cyclone, and that those communities are susceptible to damage by waves (i.e. coral breakage, dislodgement, exfoliation or severe

[widespread] damage of any type), then it is possible to crudely estimate the relative risk of damage occurring somewhere along each reef across the GBR from 1969-2003 (Figure 7.6). This was done by adding the GIS maps shown in Figure 7.4 (number of times maximum winds exceeded the damage threshold) and Figure 7.5 (number of times gales persisted longer than the damage threshold), dividing by two, dividing the result by the number of years in the time series (35) and multiplying by 100. This gave the percentage of years from 1969-2003 during which local wind-sea generated by a cyclone was sufficient to damage reef sites across the GBR. More than two-thirds of the GBR sustained local wind-sea sufficient to damage susceptible reefs for 30-50% of the time series. The area at risk more than 50% of the time was very limited (two small patches on the outer reef in the far southern GBR). The bulk of these highest risk areas were concentrated seaward of the GBR, suggesting that isolated reef atolls in the southwest Pacific are generally at greater risk of cyclone damage than reefs within the GBR. The far northern GBR was at risk the least amount of time (< 20 to 30%), as cyclones rarely tracked that far north and those that did were weak.

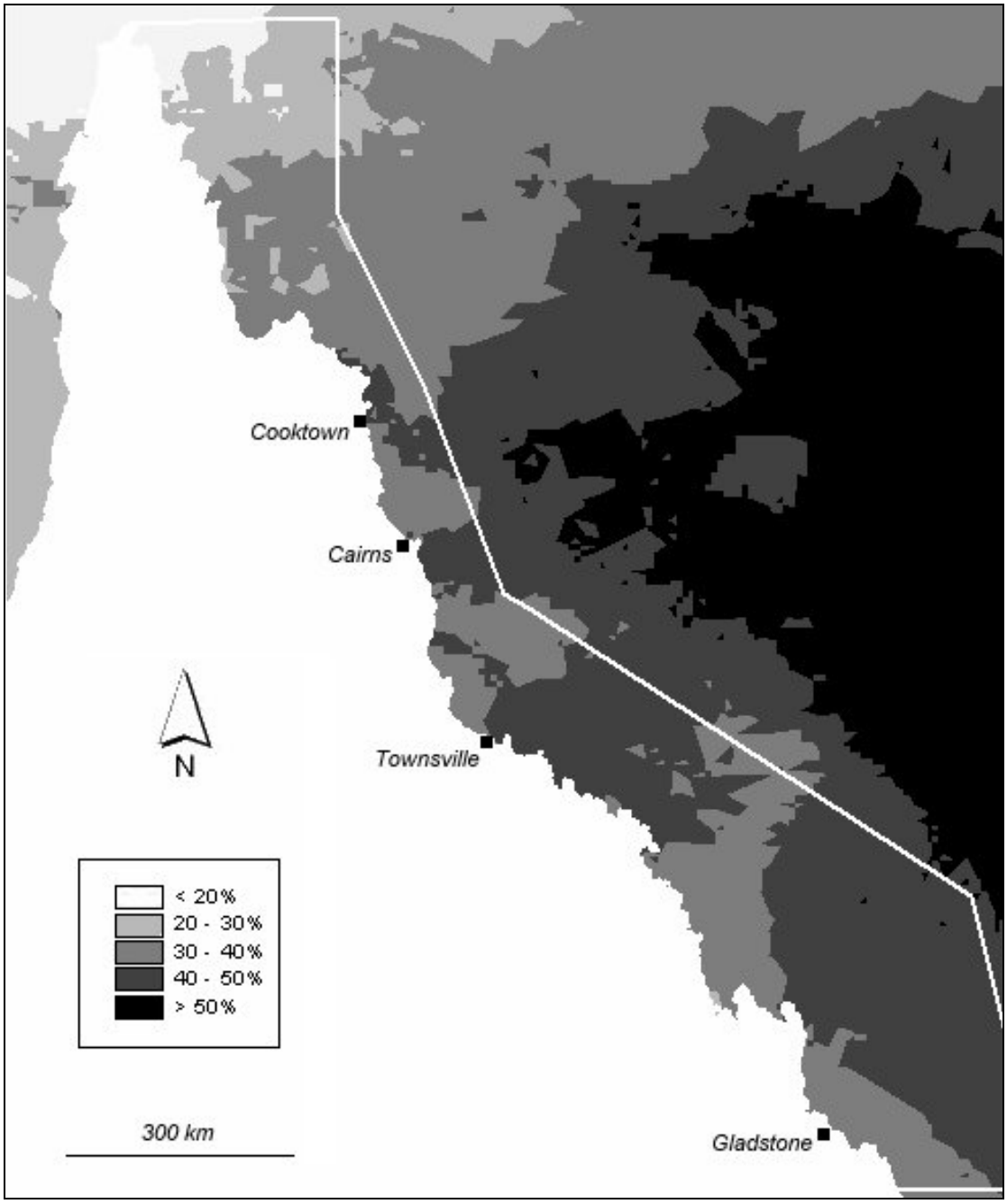

Figure 7.6. Percentage of years from 1969-2003 during which cyclone damage (coral breakage, dislodgement, exfoliation or severe damage of any type) could be possible at reef sites exposed to local wind-sea and susceptible to damage.

7.3.4 Summary

The magnitude and duration of local wind-sea during a cyclone can be approximated using cyclone-generated winds as a proxy for the waves that could develop (see Chapter 4), and by calculating the maximum wind intensity and duration of high

winds (gales or above) over an entire cyclone. Linking these measures to field data of recorded cyclone wave damage (see Chapter 6) suggested the existence of threshold values above which damage could be possible. Mapping the spatial distribution of the number of times these thresholds were exceeded over the past 35 years provides a crude estimate (not considering reef exposure and vulnerability as discussed in Chapter 5) of the long-term potential for cyclone damage across the GBR. From this, it is apparent that the potential for damage was much less in the far northern GBR than elsewhere over the past 35 years, and that mid-oceanic atolls were more frequently at risk from damage than reefs found within the GBR.

7.4 Incidence

The extent of the GBR disturbed by each cyclone is indicated by the percentage of reef sites for which damage was predicted during each event.

7.4.1 Breakage

Many (71%) cyclone events in the period 1969-2003 did not generate sufficient energy to break coral colonies at any of the reef sites (Figure 7.7).

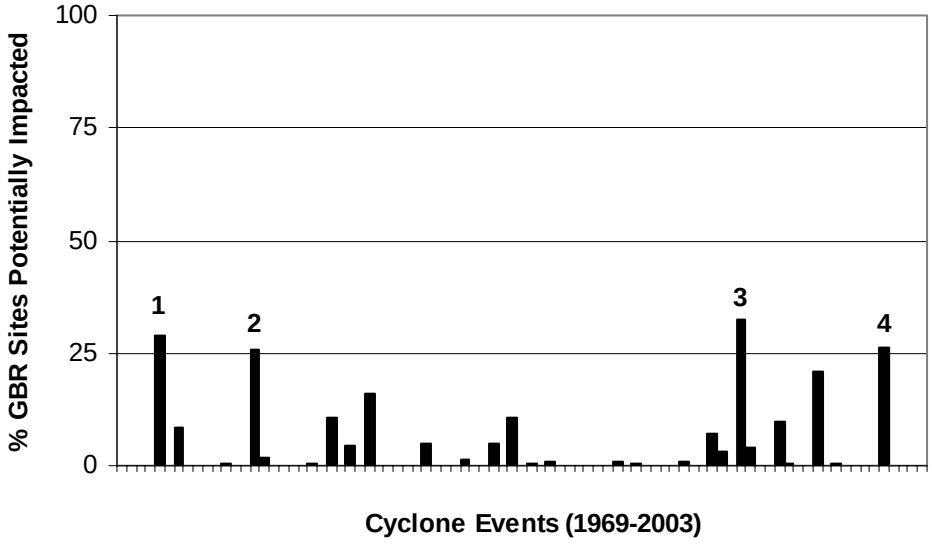

Figure 7.7. Percentage of GBR sites predicted to be potentially damaged by coral breakage for each cyclone event from 1969 to 2003 (no cyclone events occurred after 2000). In the absence of habitat data for most sites, half were assumed to be fronts and half to be backs. Cyclones predicted to have damaged more than 25% of GBR sites include: 1 – Althea 1971, 2 – Madge 1973, 3 – Ivor 1990, 4 – Justin 1997.

However, periodically widespread disturbance events did occur where waves could have broken corals at more than 25% of the reef sites across the region. These cyclones include Althea (1971), Madge (1973), Ivor (1990) and Justin (1997). This may be an over prediction for Madge because the cyclone hindcasting model performs poorly when cyclone translations speeds exceed ~30 km/hr (see chapter 4), as was common during this cyclone. Most of the cyclones that were predicted to break corals only affected about 10% of the sites.

7.4.2 Dislodgement

In contrast, most (80%) cyclone events in the period 1969-2003 were predicted to be capable of dislodging coral colonies somewhere within the GBR (Figure 7.8).

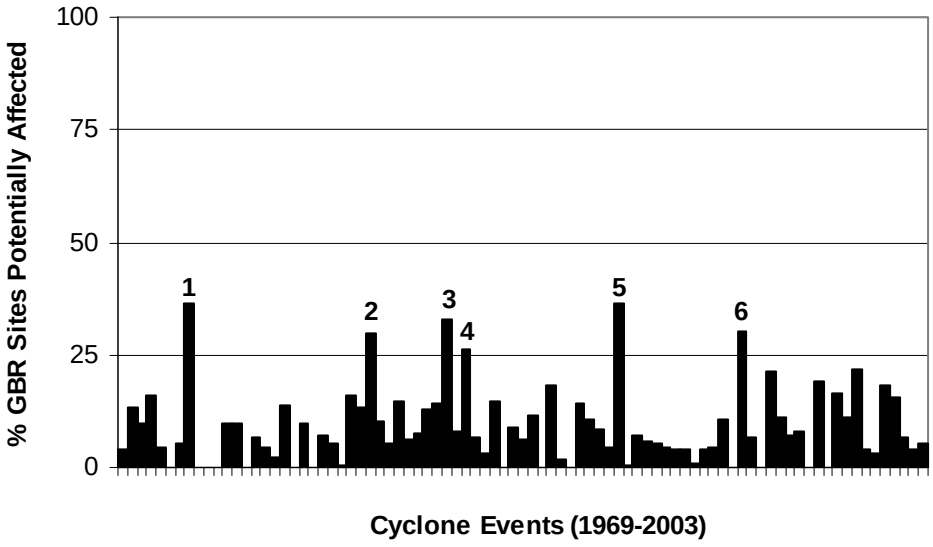

Figure 7.8. Percentage of GBR sites predicted to be potentially damaged by coral dislodgement for each cyclone event from 1969 to 2003 (no cyclone events occurred after 2000). Cyclones predicted to have damaged more than 25% of GBR sites include: 1 – Gertie 1971, 2 – Watorea 1976, 3 – Kerry 1979, 4 – Stan 1979, 5 – Pierre 1985, and 6 – Ivor 1990.

Six of these events (Gertie 1971, Watorea 1976, Kerry 1979, Stan 1979, Pierre 1985, and Ivor 1990) could have affected more than 25% of the reef sites, with most affecting less than 10%. This is largely due to the fact that distance was the sole predictor of damage potential for this type of damage (see Table 7.14, Chapter 6). Thus, nearly every cyclone passed reasonably close to at least a few GBR sites, but not many cyclones tracked extensively throughout the GBR (thus passing near many sites). It is important to note that massive corals may not actually be present on every reef (thus removing the possibility of their dislodgement). For this reason, these estimates represent a worst-case scenario of damage risk possible if they were present.

7.4.3 Exfoliation

Just over half (56%) of cyclone events from 1969 to 2003 were predicted to be capable of damaging reefs by exfoliation (Figure 7.9). Of these, eight could have

affected more than 25% of the reef sites, and one (Althea) could have damaged half of the sites. These include cyclones Althea (1971), Fiona (1971), Bronwyn (1972), Watorea (1976), Alan (1976), Paul (1980), Dominic (1982) and Ivor (1990). Some of these events may over predict cyclone energy due to high cyclone translation speeds.

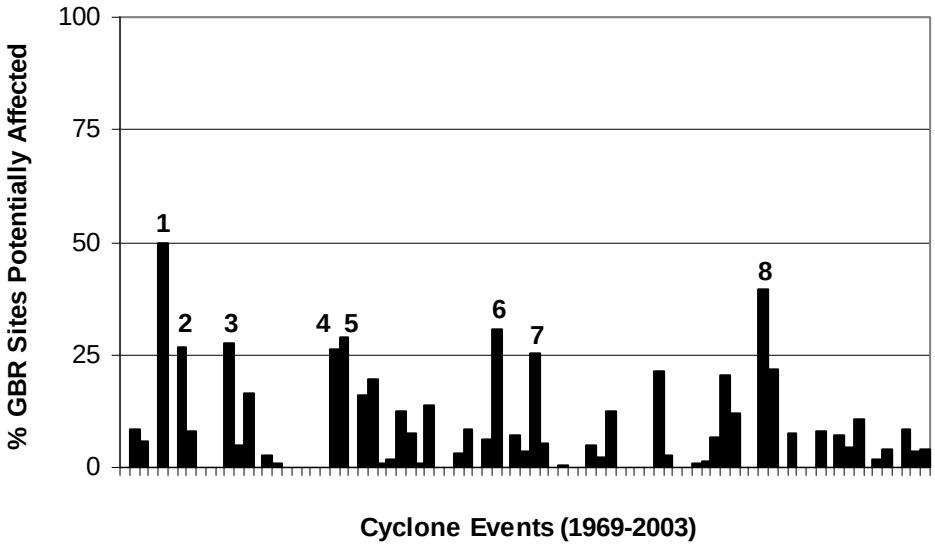

Figure 7.9. Percentage of GBR sites predicted to be potentially damaged by exfoliation for each cyclone event from 1969 to 2003 (no cyclone events occurred after 2000). In the absence of habitat data for most sites, half were assumed to be fronts and half to be backs. Cyclones predicted to have damaged more than 25% of GBR sites include: 1 – Althea 1971, 2 – Fiona 1971, 3 – Bronwyn – 1972, 4 – Watorea 1976, 5 – Alan 1976, 6 – Paul 1980, 7 – Dominic 1982, and 8 – Ivor 1990.

7.4.4 Severe (widespread) damage of any type

About 55% of cyclone events over the past 35 years were predicted to be capable of causing severe damage of any type (Figure 7.10). Of these, five could have affected more than 25% of GBR reef sites. These include cyclones Althea (1971), Fiona (1971), Alan (1976), Paul (1980) and Ivor (1990). As with the other damage types, some of these events may over predict cyclone energy due to high cyclone translation speeds. In addition, these results represent a worst-case scenario because they assume a susceptible slope at each site. The slope can vary considerably over small distances

and even within a single reef site. To take this into account, predictions could be made for a range of slope possibilities and the results stored as scenarios.

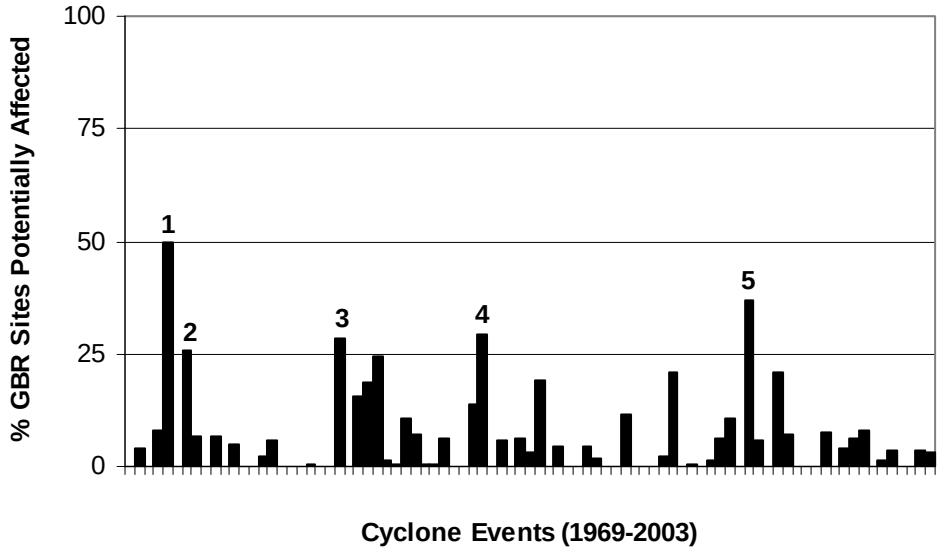

Figure 7.10. Percentage of GBR sites predicted to be potentially damaged by severe (widespread) damage of any type for each cyclone event from 1969 to 2003 (no cyclone events occurred after 2000). In the absence of habitat data for most sites, half were assumed to be fronts and half to be backs. These results assume that a susceptible slope exists at each site. Cyclones predicted to have damaged more than 25% of GBR sites include: 1 – Althea 1971, 2 – Fiona 1971, 3 – Alan 1976, 4 – Paul 1980, and 5 – Ivor 1990.

7.4.5 Summary

In summary, the potential for cyclone disturbance at the reef sites varied by the type of damage, but was generally intermittent. Cyclone events were rarely predicted to affect more than a quarter of the sites at once (<3 % in all cases). However, no unusually large and strong cyclones, which would have the potential to disturb a large proportion of the GBR at once (see chapter 3), passed nearby over the past three decades. Further, very strong cyclones located too distant from the GBR to be considered in this study could have damaged a large number of the outer reef sites with long-period ocean swell. For example, storm surge was recorded during cyclone

Pam in 1974 (Hopley and Harvey 1974) along the entire Queensland coast south of Cairns when the cyclone was located hundreds of km from the GBR.

The types of reef damage that are possible from cyclone waves vary along a continuum according to the extent of high-energy conditions, ranging from breakage (low-energy), to dislodgement, to exfoliation (high-energy). Thus, given that strong cyclones (categories 3 and above) have rarely crossed the GBR over the past three decades (Puotinen et al 1997), one would expect that the incidence of low-energy damage types would be greater than that of high-energy types. However, the opposite appears to be true for the GBR, with the highest incidence recorded for exfoliation and the lowest for breakage. This contrary result is largely due to bias in the conditions represented by the three test cyclones used to build the predictive model for individual damage types. In these cases (cyclones Ivor, Joy and Justin), cyclone-generated winds (and thus waves) predominantly approached reefs from a direction where the reefs are not normally sheltered (as discussed in Chapter 5 and evidenced by the predominance of damage on high-energy reef fronts). For these wave hardened sites, low-energy damage types are less likely to occur because the colonies present are likely to be small in size, and highly wave adapted (encrusting rather than branching forms, stream-lined in shape, orientated to the direction of flow). These colonies are likely to remain undamaged until a high-energy threshold is reached (ie a small, stream-lined colony will not break or dislodge, but with sufficient time and energy the entire reef matrix within which it sits may be peeled away). Detailed field surveys documenting damage following cyclones that approach reefs from an unusual direction, such that normally sheltered sites are exposed to high-energy conditions, are needed to overcome this. Also important is the fact that dislodgement of massives

would only be possible at those sites on reefs where massive corals are actually present – in the absence of data of their distribution across the GBR over the past 35 years, this analysis assumed they were present at every reef, which undoubtedly overestimates the potential for dislodgement during each cyclone.

7.5 Timing

The timing of cyclone disturbance from 1969-2003 is important for determining the influence of individual disturbances on coral communities and their structure. Useful measures of timing include the number of disturbance-free intervals, the expected mean length and maximum length of disturbance-free intervals, and the number of years since the last event (as of 2003, Table 7.1). These measures, with respect to each of the selected types of damage, were summarized across the GBR for one-degree latitude by one-degree longitude blocks (Figure 7.3).

7.5.1 Breakage

The number of breakage-free intervals (Figure 7.11-A) was predicted to generally increase for sites located more to the south. Acoordingly, both the mean (Figure 7.11-B) and maximum (Figure 7.11-C) length of undisturbed intervals became shorter with movement to the south. This trend is quite distinct, with expected mean intervals of 33 years at 10^0S, compared to 3 years at 24^0S. In general, breakage was predicted to have occurred least recently at sites situated in the far north (lower latitudes), where all (north of 11^0S) or many (11^0-12^0S) sites were not predicted to sustain any damage over the 35 year period (Figure 7.11-D). The number of years since the last

disturbance (Figure 7.11-D) was longer than the mean number of years between predicted breakage events (Figure 7.11-B), except for sites located between 12^0-15^0S, where it was noticeably shorter. This suggests that, for most of the sites (~81%), breakage may have been occurred less frequently in recent times than was typical from 1969-2003.

A

Latitude	Longitude 142	143	144	145	146	147	148	149	150	151	152	153	Mean
10	-	-	-										-
11	-	-	-										-
12		2											2
13		3	3										3
14		3	3	4									4
15				4									4
16				4	4								4
17					5								5
18					5	5	5						5
19					6	5	6	5	5				6
20							6	6	6	7	7		6
21								8	7	8	8		8
22								9	9	9	9		9
23									9	9	8		8
24										7	7	7	7
Mean	-	-	-	4	5	5	6	6	6	8	8	7	5

B

Latitude	Longitude 142	143	144	145	146	147	148	149	150	151	152	153	Mean
10	-	-	-										-
11	-	-	-										-
12		33											33
13		14	11										13
14		10	10	11									10
15				9									11
16				9	8								9
17					7								7
18					8	8	9						8
19					7	8	7	7	8				7
20							7	7	7	6	6		7
21								3	4	4	4		4
22								3	3	3	3		3
23									3	3	3		3
24										3	3	3	3
Mean	-	-	-	10	8	8	7	5	6	4	3	3	8

C

Latitude	Longitude 142	143	144	145	146	147	148	149	150	151	152	153	Mean
10	-	-	-										-
11	-	-	-										-
12		21											21
13		20	20										20
14		20	19	15									17
15				15									15
16				17	13								16
17					15								15
18					17	17	16						17
19					16	15	15	13	16				14
20							14	14	14	13	13		14
21								8	10	9	8		9
22								7	7	6	7		7
23									6	7	7		7
24										8	8	8	8
Mean	-	-	-	16	15	17	15	11	13	9	8	8	17

D

Latitude	Longitude 142	143	144	145	146	147	148	149	150	151	152	153	Mean
10	-	-	-										-
11	-	-	-										-
12		12											12
13		6	6										6
14		6	6	6									6
15				10									10
16				9	9								9
17					10								10
18					8	9	10						9
19					7	9	7	9	9				8
20							9	9	9	8	6		9
21								6	7	6	6		6
22								6	6	6	6		6
23									6	6	6		6
24										6	6	6	6
Mean		-	-	8	9	9	8	8	9	7	6	6	11

Figure 7.11. Breakage. Patterns in coral breakage across the GBR from 1969 to 2003: A – number of breakage-free periods, B – mean length of breakage-free periods, and C – maximum length of breakage-free periods, and D - number of years since the last breakage (as of 2003), averaged in each 1^0 latitude by 1^0 longitude box. The colour of each box indicates the relative number of years: white = <10, light grey = 10-20, dark grey = 20-30, black = >30. For some boxes an accurate determinations cannot be made because no cyclone damage was predicted during the 35 year period for all or some of the sites (dashes).

7.5.2 Dislodgement

As might be expected, dislodgement-free intervals were predicted to be least frequent (Figure 7.12-A) over the time series for reef sites situated within 10^0S - about 9% of the GBR sites. For the rest of the GBR, they were more than twice as frequent. Similarly, the length of both the mean (Figure 7.12-B) and maximum (Figure 7.12-C) dislodgement-free interval was greatest at 10^0S.

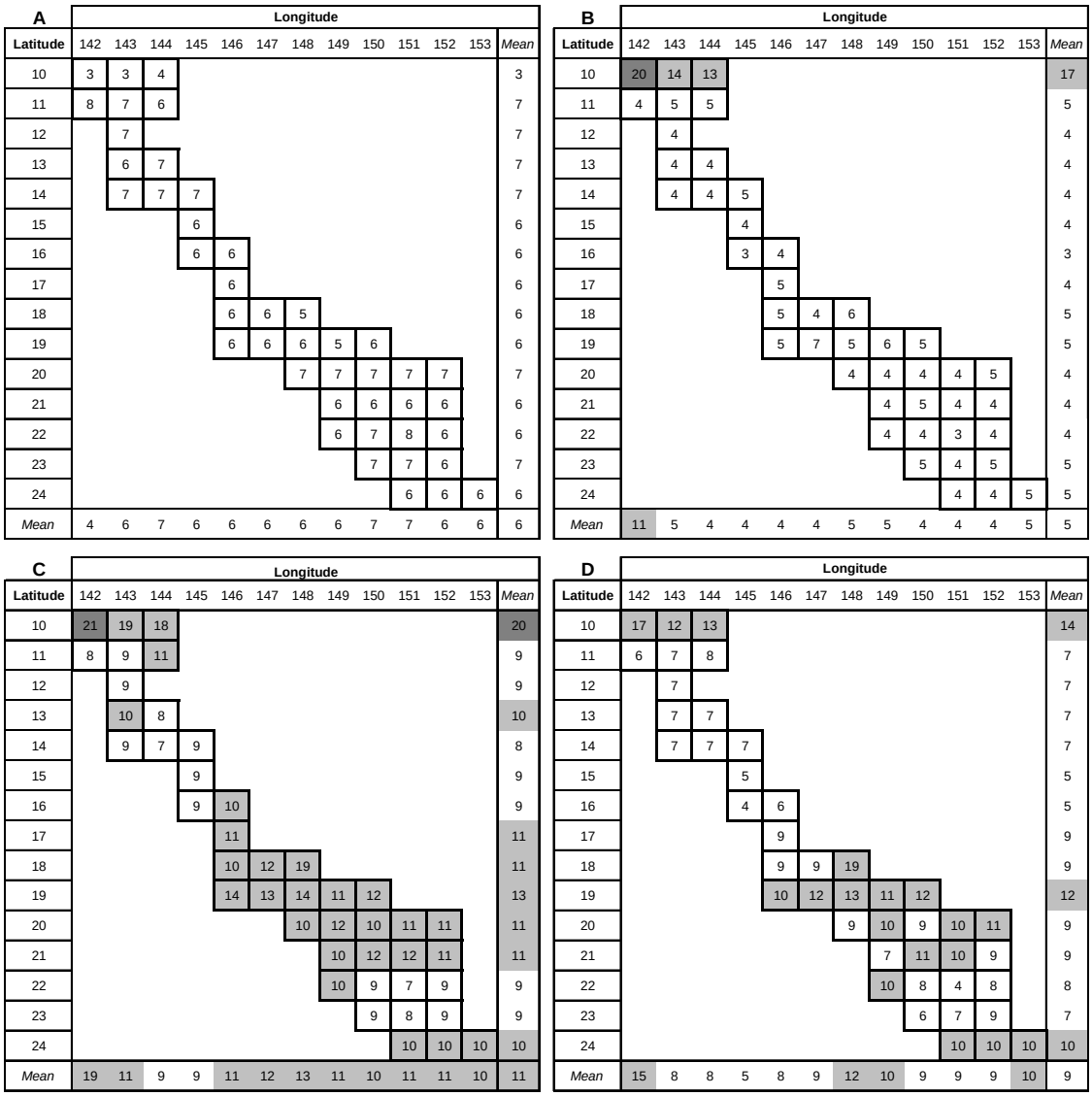

Figure 7.12. Dislodgement. Patterns in dislodgement across the GBR from 1969 to 2003: A – number of dislodgement-free periods, B – mean length of dislodgement -free periods, C – maximum length of dislodgement -free periods, and D - number of years since the last dislodgement (as of 2003), averaged in each 1^0 latitude by 1^0 longitude box. The colour of each box indicates the relative number of years: white = <10, light grey = 10-20, dark grey = 20-30, black = >30.

The maximum interval was about seven times longer than the mean interval (range = 1 to 17 times). In general, dislodgement was predicted to have occurred most recently at reef sites situated within 15^0-16^0S (Figure 7.12-D). For these sites, located between Cooktown and Cairns, the most recent event occurred between 4 and 6 years prior to 2003 when cyclones Nathan (1998), Rona (1999) and Steve (2000) passed nearby. In contrast, dislodgement was predicted to have occurred least recently (Figure 7.12-D) at reef sites situated within 10^0S (far northern GBR) and 19^0S (offshore from Townsville). For the far northern GBR, this time period, on average, extends to nearly two decades (17 years) close to shore. Although several cyclones have passed through 19^0S in recent times, such as cyclones Celeste (1996), Gillian, Ita and Justin (1997), and Tessi (2000), they were all relatively weak. The maximum length of time (Figure 7.12-C) since the last predicted dislodgement across the entire GBR was 21 years for sites located north of 11^0S and west of 143^0E. The longest maximum intervals were generally found in the far north, with the exception of sites situated in the box defined by 18^0S and 148^0E – about 230 km west of Hinchinbrook Island (19 years). In almost all cases (~95%), the time since the last predicted event (Figure 7.12-D) was longer than the mean length between events (Figure 7.12-B). This suggests that dislodgement has been less frequent in recent times than was the case in the past for most of the GBR. As previously noted, the distribution of massive corals across the reef sites of the GBR at the time of each cyclone could not be considered here but undoubtedly affected the potential for damage. Thus, these results represent a worst case scenario for the timing of dislodgement.

7.5.3 Exfoliation

For exfoliation, no clear trends are evident in any of the measures of disturbance timing (Figure 7.13).

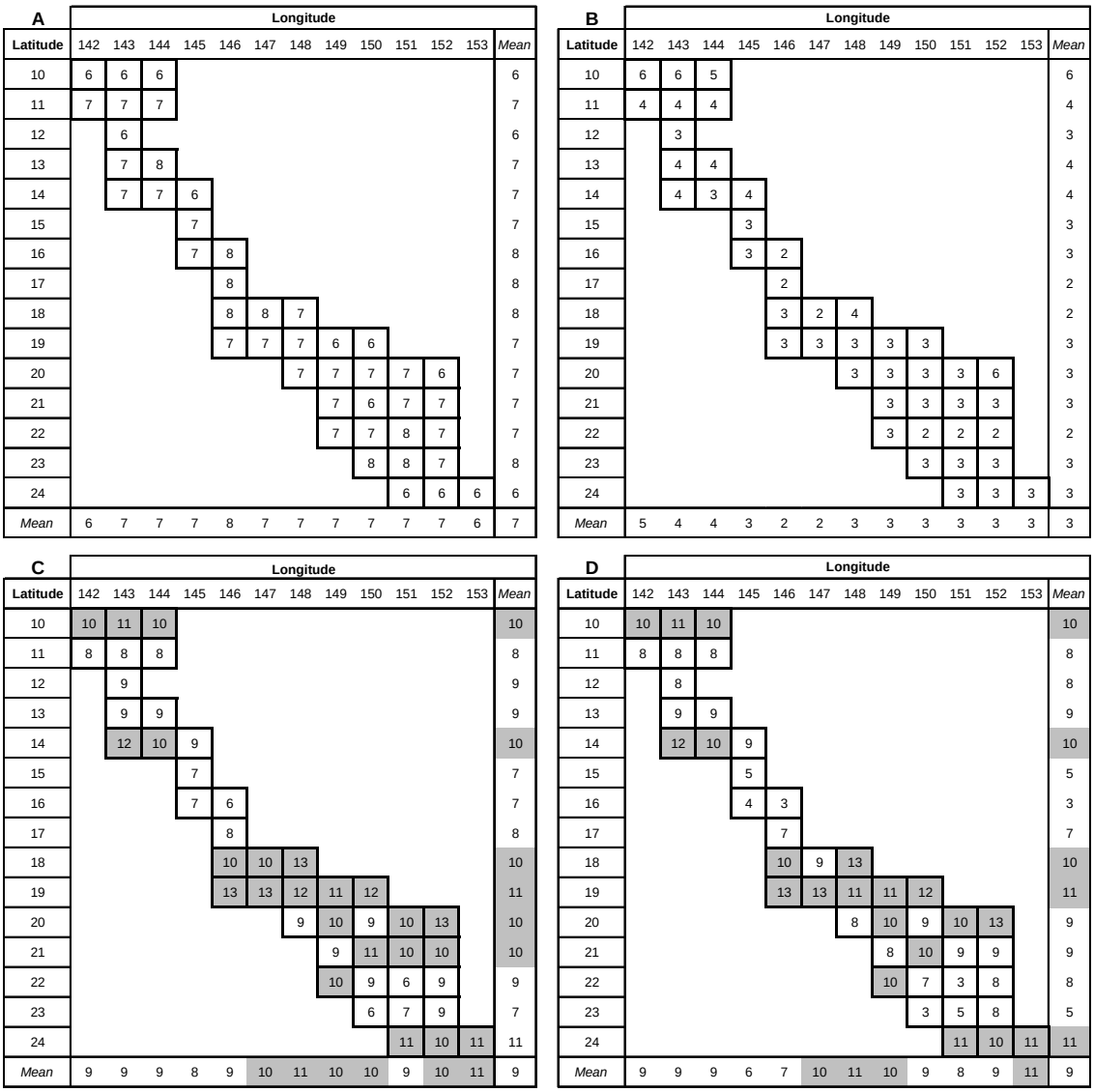

Figure 7.13. Exfoliation. Patterns in exfoliation across the GBR from 1969 to 2003: A – number of exfoliation-free periods, B – mean length of exfoliation-free periods, C – maximum length of exfoliation-free periods, and D - number of years since the last exfoliation (as of 2003), averaged within each 1^0 latitude by 1^0 longitude box. The colour of each box indicates the relative number of years: white = <10, light grey = 10-20, dark grey = 20-30, black = >30.

Exfoliation was predicted based on maximum wind speed (see Chapter 6, Table 6.14), which varies intermittently from north to south. Between six and eight exfoliation-

free intervals (Figure 7.13-A) were predicted to have occurred along the GBR, with no clear trends evident. The mean exfoliation-free interval (Figure 7.13-B) decreased gradually from north (6 years at 10^0S) to south (3 years at 24^0S). This was not the case for the maximum exfoliation-free interval (Figure 7.13-C), however. This interval was shortest for sites situated at 15^0-16^0S and 22^0S and 23^0S at 151^0E. As with dislodgement, exfoliation was predicted to have occurred least recently (Figure 7.13-D) at reef sites situated within 19^0S (offshore from Townsville). Although cyclones have passed through that area recently, they were relatively weak. Further, exfoliation was generally most recently predicted to have occurred at reef sites situated within 15^0-16^0S (between Cooktown and Cairns, affected by cyclones Ivor and Joy in 1990). The number of years since the last exfoliation event (Figure 7.13-D) was always longer (up to five times more) than the mean number of years (Figure 7.13-B) between predicted exfoliation events, suggesting that exfoliation was more frequent in the past than is the case at present across the GBR.

7.5.4 Severe (widespread) damage of any type

Between 6 and 8 intervals free of severe (widespread) damage (Figure 7.14-A) were predicted for the GBR, with no clear trend with change in latitude or longitude. The mean length of severe damage-free intervals (Figure 7.14-B) is generally similar across the region (range = 3-6 years), with the longest intervals found north of 10^0S. The maximum number of years between severe damage (Figure 7.14-C) was 13, with an average of 10 across all the sites. The distribution of the longest maximum intervals was patchy across the GBR. Severe damage of any type was generally predicted to occur most recently (in 1998) for sites situated from 15^0-16^0S (Figure

7.14-D), though sites located at 22^0S, 151^0E (offshore Rockhampton) and 23^0S, 150^0E (close to the coast north of Gladstone) were disturbed even more recently (2000).

A

Latitude	Longitude 142	143	144	145	146	147	148	149	150	151	152	153	Mean
10	6	6	6										6
11	8	7	7										7
12		6											6
13		7	8										7
14		6	7	6									7
15				7									7
16				7	8								7
17					7								7
18					7	8	7						8
19					7	7	7	6	6				7
20							7	6	7	6	6		7
21								7	6	7	7		7
22								6	7	9	7		7
23									8	8	6		7
24										6	6	6	6
Mean	6	7	7	7	7	8	7	6	7	7	7	6	7

B

Latitude	Longitude 142	143	144	145	146	147	148	149	150	151	152	153	Mean
10	6	6	6										6
11	4	4	5										4
12		4											4
13		4	4										4
14		5	4	5									4
15				4									4
16				3	3								3
17					3								3
18					3	3	3						3
19					3	3	3	3	3				3
20							3	3	3	4	4		3
21								3	4	3	3		3
22								3	3	3	3		3
23									3	3	3		3
24										3	4	4	4
Mean	6	4	4	4	3	3	3	3	3	3	3	4	4

C

Latitude	Longitude 142	143	144	145	146	147	148	149	150	151	152	153	Mean
10	11	11	10										11
11	8	8	9										8
12		10											10
13		9	9										9
14		12	10	10									10
15				8									8
16				10	8								10
17					11								11
18					12	11	13						12
19					13	13	12	11	12				12
20							10	11	10	11	13		10
21								10	11	10	11		10
22								11	9	6	9		9
23									6	8	10		8
24										11	11	11	11
Mean	10	9	9	9	11	11	11	11	10	10	10	11	10

D

Latitude	Longitude 142	143	144	145	146	147	148	149	150	151	152	153	Mean
10	11	11	10										11
11	8	8	9										8
12		10											10
13		9	9										9
14		12	10	10									10
15				6									6
16				8	6								8
17					11								11
18					12	11	13						11
19					13	13	12	11	12				12
20							9	10	9	10	13		10
21								8	11	9	10		9
22								11	8	3	9		8
23									3	5	9		6
24										11	11	11	11
Mean	10	9	9	8	10	11	11	10	10	9	9	11	10

Figure 7.14. Severe (widespread) damage of any type. Patterns in severe damage of any type across the GBR from 1969 to 2003: A – number of severe damage-free periods, B – mean length of severe damage-free periods, C – maximum length of severe damage-free periods, and D - number of years since the last severe damage (as of 2003), averaged in each 1^0 latitude by 1^0 longitude box. The colour of each box indicates the relative number of years: white = <10, light grey = 10-20, dark grey = 20-30, black = >30.

Sites situated between 18^0-19^0S were predicted to be severely damaged least recently, with the last event between 11 and 13 years ago. The number of years since the last severe damage (Figure 7.14-D) was never less than the mean predicted number of

years between successive events (Figure 7.14-B), though one instance it was equal (in the far southern GBR).

7.5.5 Summary

For all four damage types, the number of years since the most recent cyclone event (as measured from 2003) was usually greater than the median number of years between successive events over the time series. This suggests that reef sites have been less disturbed recently than what was typical over the past 35 years. The difference between the two measures (most recent versus mean interval) was most pronounced for breakage. This damage type was also the only one to show a clear trend from north to south in the frequency of disturbance-free intervals.

Massel and Done (1993), based on cyclone positions from 1910-1980, predicted that cyclones of all intensities return more frequently to latitudes from about 19^0-23^0S. That trend was not evident in this analysis for any of the four types of damage that were modelled. This suggests that the cyclone disturbance history over the past 35 years (1969-2003) may not be typical of what occurred further in the past (1910-1968). It also may reflect known uncertainties in the positioning of cyclone paths and their detection, known to be high in the time series prior to 1969 (Holland 1981).

Interestingly, sites located around 19^0S were typically disturbed the least recently, even though several cyclones have passed through that area in recent times (they were relatively weak). This highlights the inadequacy of considering the proximity to the cyclone path alone as well as the need to model intensity.

7.6 Synergism

Coral reef communities are at risk from a diverse mix of disturbances that are both natural and anthropogenic in origin (Table 7.2). The extent to which these disturbances interact to impact coral reefs (synergism) can greatly affect the severity of damage (McClanahan et al 2002).

Table 7.2: Major disturbances that affect coral reefs worldwide. Assembled from Wilkinson 1999.

Disturbances affecting coral reefs		
Type	*Natural*	Geological (sea level changes, meteor strikes, tectonic plate movement, etc)
		Tropical cyclones and storms
		Fresh water inundation
		Exposure during periodic low tides
		Outbreaks of predators and disease
	Direct Human Stresses	Increased sediment loads
		Pollution
		Overexploitation
		Oil spills
		Engineering / military damage
	Indirect Human Stresses	SST and bleaching
		Increasing CO2 / calcification
		Increasing UVB radiation
		Changes in sea level, weather and currents

At the broadest scales (the entire world over millennia), natural geological cycles, such as sea level change, glaciations and tectonic activity) determine the environmental gradients that make the development and growth of coral reefs possible (Wilkinson 1999). At these scales, tropical cyclone damage has little consequence. However, at the time scales of most relevance to humans (years to decades), cyclone disturbance plays a major role in determining the structure of coral reefs (Harmelin-

Vivien 1994). Consequently, patterns in the timing and distribution of cyclone damage can affect the vulnerability of reef communities to subsequent disturbances. The most obvious example is that a reef site very recently damaged by a severe cyclone will initially contain a lower than normal proportion of fragile corals, reducing vulnerability to damage from the next cyclone if it occurs before recovery is complete (Done 1992a).

Prior cyclone disturbance can also influence the impacts of other disturbances on reefs. For example, coral communities are vulnerable to exposure to fresh water, as they require an optimal range of salinity from 32-40 ppm (Veron 1986). After making landfall, cyclones can release considerable rainfall over a short period of time, leading to the propagation of plumes of fresh water over reefs, which can damage corals (King et al 2001). These plumes may affect corals that have already been damaged by the passage of the cyclone (though this depends on the cyclone's path before and after landfall). In this case, corals already damaged by cyclone waves may be more susceptible to stress from low salinity.

Further, periodic exposure to air at low tide can damage or kill corals (Fadlallah et al 1995). Wave damage from cyclones can alter the topography of the reef, resulting in subsequent exposure of corals to air during extreme low tides, such as occurred at Heron Island (Connell et al 1997). Cyclones can also contribute to the development, or destruction, of coral colonies growing in shallow areas along the reef flat that would normally be exposed to air at low tide. These corals, termed coral micro-atolls, survive because physical features (such as *Acropora* shingle, basset edges, or algal rims) block the outflow of water at low tide (Hopley and Isdale 1977). The

development of these features is associated with high-energy conditions, such as those generated by cyclones. For example, micro-atolls are common on the Holbourne Island reef flat, which is located offshore from Bowen in the central GBR. A 1918 cyclone disrupted the reef morphology, resulting in the development of three smaller moated areas from the prior single large one (Hopley and Isdale 1977).

Coral communities are also vulnerable to periodic outbreaks of disease or predators, such as the crown-of-thorns starfish (Moran 1986). Because severe cyclone damage can dramatically reduce the coverage of fragile corals across a reef (such as *Acropora spp*, which include the preferred food source of *Acanthaster planci*), recent severe cyclone disturbance may reduce food availability on a particular reef. The extent to which this is true will depend on the timing of the crown-of-thorns starfish infestation relative to the cyclone as well as the extent to which dislodged coral fragments survive. In contrast, some evidence suggests that the spread of white band disease through particular coral communities may be more rapid following cyclone damage (Bak and Criens 1981, Knowlton et al 1991). In addition, corals broken into surviving fragments by a cyclone may become more vulnerable to subsequent predation by the snail *Corallophila abbreviata* (Knowlton et al 1990).

Sustained unusually high sea surface temperatures (SST) can lead to coral death by bleaching, which has been increasingly documented world wide in recent times (Hoegh-Guldberg 1999). Cyclones are driven by heat they extract from the sea. The passage of a cyclone, therefore, can temporarily remove the conditions (high SST) that lead to coral bleaching. Temporary but significant drops in SSTs can also result

when turbulence from cyclone-generated wind waves results in the upwelling of cold water normally found at much greater depths (Wang and Wu 2003).

Finally, repeated cyclone damage combined with chronic human disturbance can limit the ability of the community to recover to its former state. For example, Hughes (1994) documented a shift in Jamaican coral reefs from hard coral to algal domination due to a mixture of hurricane impacts, grazing echinoid mortality and overfishing over time. Thus, an understanding of the nature of the cyclone disturbance regime is necessary to understand how ecological processes (disturbance and recovery) interact across scales to produce patterns of coral community structure at any given time.

7.7 Implications for coral reef communities

The frequency, timing and severity of cyclone damage on reef sites can play a major role in determining their structure. Thus, the cyclone history has implications for coral community structure, such as the level of coral coverage (Figure 7.15). For example, reef sites that are frequently damaged (at intervals of less than 10 years) are likely to be characterised by low coral coverage and dominated by smaller sized colonies for much of the time. In contrast, reef sites that are damaged at intermediate intervals (one to several decades) are at times left undisturbed long enough for high coral coverage and large sized colonies to dominate. The extent to which this is true at a given time period will depend on the length of time since the last severe cyclone disturbance relative to the typical interval.

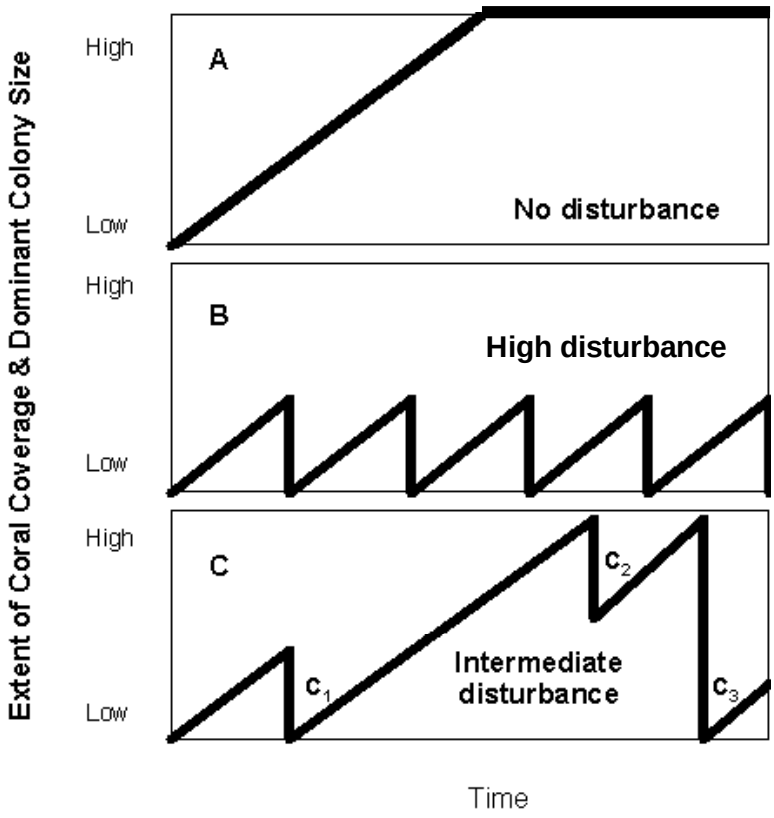

Figure 7.15: Effects of cyclone disturbance regimes on the extent of coral coverage and dominant colony size (thick black line) over decades (adapted from Done 1992a and Dollar and Tribble 1993). As the time since the last disturbance increases, coral coverage and the dominant colony size increase until crowding results in biological interactions that reduce species diversity. In A, the maximum coverage that can be supported in the available space is reached. In B, periodic major disturbance reduces coral coverage and colony size before the maximum can be reached. In C, the timing of intermittent minor (C_2) and severe (C_1 and C_3) disturbances determine whether and for how long the maximum is reached. Note that the colony size – disturbance relationship is more complex for massive corals and in general has a more gradual slope than shown here.

For the GBR, the nature of the cyclone disturbance history predicted from 1969-2003 for each of the four damage types can be classified as high or intermediate based on the timing of cyclone damage and the number of years estimated to be required for recovery of coral communities to their prior state (Table 7.3).

Table 7.3: Summary of the predicted timing of cyclone disturbance in the GBR from 1969 to 2003 for four measures of damage: breakage, dislodgement, exfoliation and severe damage of any type.

Type of damage	**Estimated time to recover**	**Typical return times**		**Years since last event**
		Mean	*Maximum*	
Breakage	Years	Short (3 years) in the southern GBR, to long (33 years) in the far north. Undisturbed at 10^0S. Mean = 8.	All but the southern GBR more than a decade. Two decades or more north of 14^0S. Mean = 17.	All of the GBR $\geq$ 6 years. More than a decade north of 15^0S. Undisturbed at 10^0S. Mean = 11.
Dislodgement	Years to decades	Short (< 10 years) for entire GBR except 10^0S. Mean = 5.	Most of the GBR close to a decade. Around two decades at 10^0S. Mean = 11.	Least recent (more than a decade ago) at 18-19^0S and 10^0S. Mean = 9.
Exfoliation	Decades	Short ($\leq$ 6 years) for entire GBR. Mean = 3	Medium (6-13 years), with no clear pattern across the GBR. Mean = 9.	Close to a decade for much of the GBR. Mean = 9.
Severe damage of any type	Decades to centuries	Short ($\leq$ 6 years) for entire GBR. Mean = 4.	Medium (6-13 years), with no clear pattern across the GBR. Mean = 10.	More than a decade for much of the GBR. Mean = 10.

The mean cyclone-free interval (return interval) for the period 1969-2003 indicates the average number of years that coral communities had to recover following cyclone events in that period. If the time needed for recovery was shorter than this interval, sites generally had time to recover from one disturbance before the next one hit (intermediate disturbance). If the time needed for recovery was longer than the return interval, sites did not always have enough time to recover. In the latter case, disturbance would still be intermediate as long as the maximum interval between

disturbances was sufficient for sites to recover at least once during the study period. If not, disturbance would be high as sites would never have time to fully recover.

Based on this rationale, coral breakage and dislodgement by cyclone waves can be classified as intermediate disturbances for most of the GBR. In contrast, exfoliation and severe damage of any type appear to be high (frequent) disturbances. It is important to note, though, that all the damage types represent worst-case scenarios because vulnerability factors (habitat: front versus back, slope; the actual distribution of massives at the time of each cyclone) have not been mapped for most of the GBR and could not be used in predictions. Including these factors would likely decrease the frequency of disturbance-free intervals and increase their lengths for the GBR overall, though it is unclear how this would vary across the region. Further, the first period in the time series for most of the sites is a minimum estimate because the earliest cyclone damage event occurred before the start of the study period. Give this, as well as indications that fewer cyclones tracked near the GBR prior to 1969 (albeit based on data of dubious quality, see chapter 2), it is possible that the maximum intervals could be longer than reported for some sites. It is also possible that recovery times could be shorter than those predicted. Given this, exfoliation and severe damage of any type may actually be intermediate disturbances.

Another important point to consider is that cyclone winds (and thus waves) primarily approached reefs at aspects that are not normally sheltered from waves during the three primary test cyclones (Ivor, Joy and Justin) upon which the predictive modelling was based. Because of this, high-energy types of damage (dislodgement, exfoliation) were more likely within the field data set than lower energy types (breakage). For

dislodgement, this was exacerbated by the fact that this type of damage cannot occur in the absence of massive corals which were assumed to exist at every site which is unlikely to be true. For example, estimates of the probability of damage occurring at any site within each box any time during the 35 year period (calculated as described in section 7.2.3) suggest that, of the four types of damage modelled, breakage was least likely to occur across much of the GBR (Figure 7.16).

A

Latitude	Longitude													Mean
	142	143	144	145	146	147	148	149	150	151	152	153		
10	-	-	-											-
11	-	-	-											-
12		3%												3%
13		7%	9%											8%
14		10%	10%	9%										10%
15				9%										9%
16				11%	13%									11%
17					14%									14%
18					12%	12%	11%							12%
19					14%	13%	14%	14%	13%					14%
20							14%	15%	14%	16%	17%			15%
21								29%	24%	26%	28%			27%
22								34%	35%	31%	34%			34%
23									32%	33%	34%			33%
24										39%	39%	40%		40%
Mean	-	-	-	10%	12%	12%	14%	19%	18%	25%	30%	40%		13%

B

Latitude	Longitude													Mean
	142	143	144	145	146	147	148	149	150	151	152	153		
10	5%	7%	8%											6%
11	27%	22%	19%											22%
12		25%												25%
13		24%	28%											25%
14		27%	27%	20%										24%
15				24%										24%
16				32%	28%									31%
17					22%									25%
18					20%	25%	16%							22%
19					20%	15%	19%	18%	21%					19%
20							24%	23%	24%	23%	22%			23%
21								24%	22%	23%	23%			23%
22								22%	26%	32%	24%			25%
23									22%	23%	21%			22%
24										23%	23%	21%		22%
Mean	9%	21%	24%	25%	23%	24%	20%	21%	23%	23%	23%	21%		22%

C

Latitude	Longitude													Mean
	142	143	144	145	146	147	148	149	150	151	152	153		
10	17%	18%	20%											18%
11	26%	25%	24%											25%
12		30%												30%
13		26%	27%											26%
14		26%	29%	25%										27%
15				32%										32%
16				40%	41%									40%
17					42%									42%
18					44%	42%	37%							43%
19					37%	38%	39%	40%	37%					39%
20							40%	37%	38%	35%	36%			38%
21								40%	34%	36%	38%			37%
22								40%	43%	46%	41%			42%
23									39%	40%	38%			39%
24										37%	37%	36%		36%
Mean	19%	25%	26%	32%	43%	42%	39%	39%	38%	37%	39%	36%		33%

D

Latitude	Longitude													Mean
	142	143	144	145	146	147	148	149	150	151	152	153		
10	16%	17%	18%											16%
11	25%	23%	22%											23%
12		25%												25%
13		24%	26%											24%
14		20%	25%	22%										23%
15				28%										28%
16				33%	34%									33%
17					34%									34%
18					34%	33%	30%							34%
19					30%	31%	31%	32%	30%					31%
20							31%	29%	29%	26%	28%			29%
21								32%	27%	29%	31%			30%
22								31%	35%	39%	33%			34%
23									32%	32%	31%			32%
24										29%	27%	27%		27%
Mean	17%	23%	24%	27%	34%	33%	31%	31%	38%	29%	31%	27%		27%

Figure 7.16. Estimated probability of cyclone damage across the GBR at any time during the period 1969-2003. The probability was calculated over the time series (total number of damage events / [total number of sites * number of years], as per the geometric distribution) across each 1^0 latitude by 1^0 longitude box for: A –coral breakage, B – dislodgement, C – exfoliation, and D – severe (widespread) damage of any type. Gray boxes indicate that the probability of damage within the box over the study period was 25% or greater. For some boxes an accurate determinations cannot be made because no cyclone damage was predicted during the 35 year period for all or some of the sites (dashes).

Logic dictates that this is unlikely to be the case – instead, one would expect low-energy damage to be more probable than high-energy damage over time. More field surveys, primarily conducted after cyclones generating waves that propagate in directions that affect normally sheltered sites on reefs, are needed to eliminate this effect.

Across most of the GBR, with the exception of areas north of 15^0S for coral breakage and north of 11^0S for dislodgement, the latest event occurred much longer ago (as measured from 2003) than was typical over the time period 1969-2003 (Figure 7.17). When a much longer time period (90 years) was considered for many fewer sites (211 versus 24,224), and using a much simpler analysis (see chapter 2), only reef sites located between 19-21^0S were predicted to be disturbed less frequently than normal in recent times, due to a hotspot of cyclone tracks in the central GBR near Townsville (18-19^0S at 147^0E, see Figure 2.5, Chapter 2). This occurred despite the generally increased number of cyclones detected (due to improved observation techniques) tracking near the GBR from 1970 to the present compared to the rest of the time series (see chapter 2, Figure 2.6) and the fact that the first disturbance-free interval for many of the sites may represent a minimum estimate. However, the degree to which cyclones were undetected earlier in the time series due to limitations of observation techniques is unknown. Because cyclones rarely form (due to the lessening of the Coriolis Effect) close to the equator, the potential for missing observations early in the time series may be less of an issue for the far northern GBR. Regardless, these results suggest that these reef sites, as currently observed, have had more time to recover from the last cyclone disturbance than normal and thus could be expected to have fully recovered and perhaps reached a ‘mature’ state.

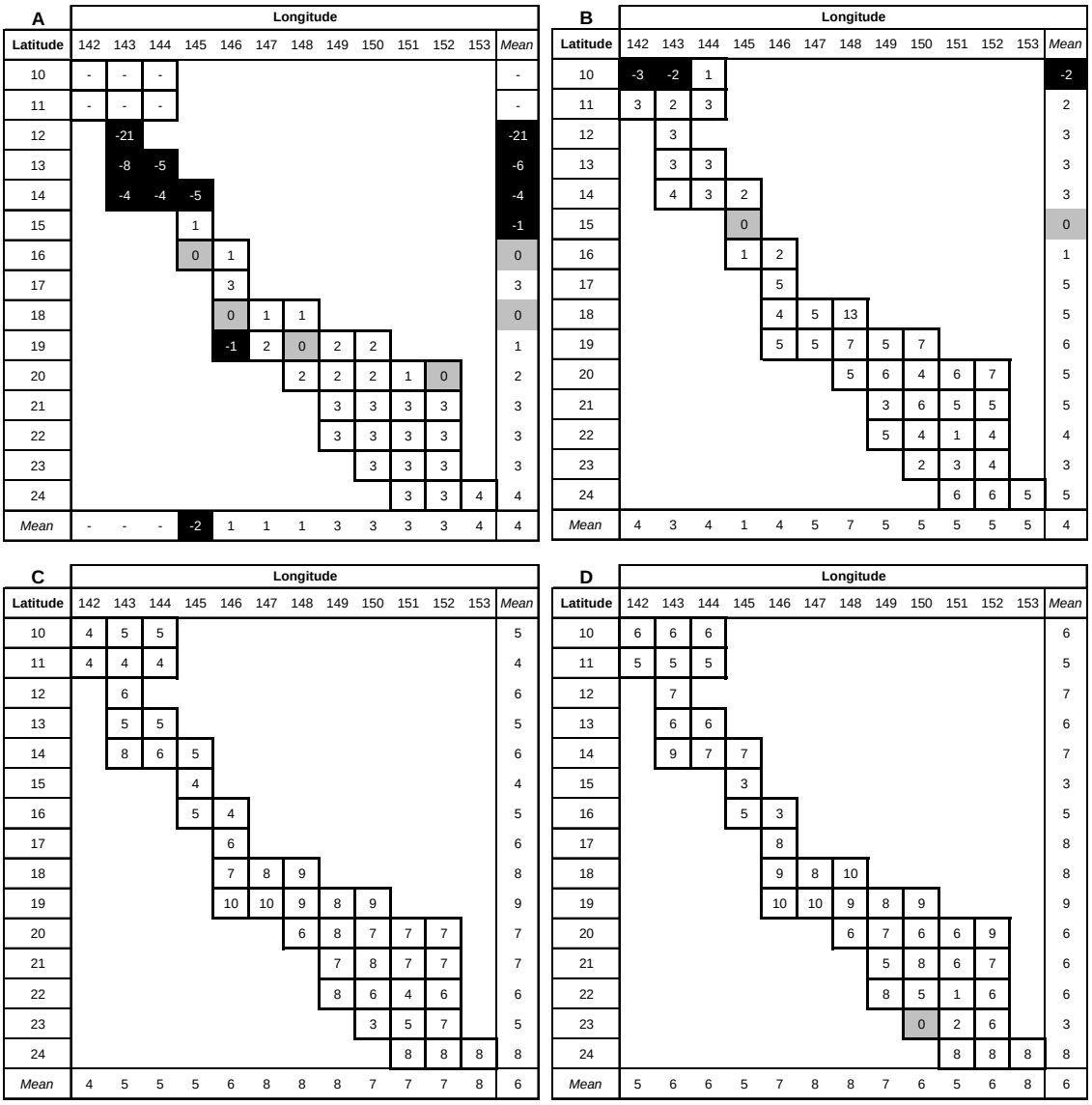

A

Latitude	Longitude 142	143	144	145	146	147	148	149	150	151	152	153	Mean
10	-	-	-										-
11	-	-	-										-
12		-21											-21
13		-8	-5										-6
14		-4	-4	-5									-4
15				1									-1
16				0	1								0
17					3								3
18					0	1	1						0
19					-1	2	0	2	2				1
20							2	2	2	1	0		2
21								3	3	3	3		3
22								3	3	3	3		3
23									3	3	3		3
24										3	3	4	4
Mean	-	-	-	-2	1	1	1	3	3	3	3	4	4

B

Latitude	Longitude 142	143	144	145	146	147	148	149	150	151	152	153	Mean
10	-3	-2	1										-2
11	3	2	3										2
12		3											3
13		3	3										3
14		4	3	2									3
15				0									0
16				1	2								1
17					5								5
18					4	5	13						5
19					5	5	7	5	7				6
20							5	6	4	6	7		5
21								3	6	5	5		5
22								5	4	1	4		4
23									2	3	4		3
24										6	6	5	5
Mean	4	3	4	1	4	5	7	5	5	5	5	5	4

C

Latitude	Longitude 142	143	144	145	146	147	148	149	150	151	152	153	Mean
10	4	5	5										5
11	4	4	4										4
12		6											6
13		5	5										5
14		8	6	5									6
15				4									4
16				5	4								5
17					6								6
18					7	8	9						8
19					10	10	9	8	9				9
20							6	8	7	7	7		7
21								7	8	7	7		7
22								8	6	4	6		6
23									3	5	7		5
24										8	8	8	8
Mean	4	5	5	5	6	8	8	8	7	7	7	8	6

D

Latitude	Longitude 142	143	144	145	146	147	148	149	150	151	152	153	Mean
10	6	6	6										6
11	5	5	5										5
12		7											7
13		6	6										6
14		9	7	7									7
15				3									3
16				5	3								5
17					8								8
18					9	8	10						8
19					10	10	9	8	9				9
20							6	7	6	6	9		6
21								5	8	6	7		6
22								8	5	1	6		6
23									0	2	6		3
24										8	8	8	8
Mean	5	6	6	5	7	8	8	7	6	5	6	8	6

Figure 7.17. Patterns in the timing of the most recent disturbance-free interval across the GBR from 1969 to 2003. The mean disturbance interval was subtracted from the number of years since the last disturbance for: A –coral breakage, B – dislodgement, C – exfoliation, and D – severe damage of any type, averaged in each 1^0 latitude by 1^0 longitude box. The colour of each box indicates whether the result was positive (white): disturbed less recently than normal, negative (black): disturbed more recently than normal or zero (grey): disturbed at the median interval. For some boxes an accurate determinations cannot be made because no cyclone damage was predicted during the 35 year period for all or some of the sites (dashes).

The degree to which the latter actually occurred depended on the effects of other disturbances and routine ecological processes (i.e. competition, growth rates) at each site since the last cyclone disturbance.

For some reef sites that have been surveyed in relative detail (such as those sites monitored periodically by AIMS), coral coverage has been measured yearly since the mid 1990s. Comparing this data (whether coral coverage in 2003 was higher than normal over the past ~decade) to a priori predictions based on the results described above would provide a useful test of the degree to which the predicted cyclone history alone can explain broad measures of coral community structure. The quality of this test would improve as the time series of monitoring data (and the cyclone disturbance history) is extended. This would estimate the relative contribution of the cyclone history versus other disturbances and routine ecological processes in shaping coral community structure. This is important because coral reef communities, like any ecosystem, are affected by a range of disturbances that operate across a continuum of spatial and temporal scales. The interactions of these disturbances combine to create the patterns of ecological structure that exist at any given time, and their level of connectedness influences the ability of the system to remain in its current state: its ecological resilience (Gunderson et al 2002). To assess the threat of any given disturbance (such as global climate change or pollution) to coral reef communities thus requires an understanding of the importance and dynamics of other relevant disturbances, most notably cyclones. To that end, this thesis provides the first broad-scale synthesis of the cyclone disturbance regime across the GBR, or indeed any marine ecosystem of a comparable size.

7.8 Conclusion

The primary aim of this research was to characterise the tropical cyclone disturbance regime for the GBR region from 1969 to 2003. To achieve this aim, I reconstructed

the history of predicted cyclone wave damage at each of 24,224 sites across the 2,728 reefs of the GBR using a model based on field data from five test cyclones (Ivor, Joy, Justin, Althea and Celeste). Four types of damage (coral breakage, dislodgement of massive corals, exfoliation and severe damage of any type) were successfully modeled using a mix of cyclone energy (maximum and duration of high winds) and reef vulnerability (geomorphologic type, slope, normal wave exposure) parameters. Using this hindcast cyclone history, I examined patterns in the intensity, incidence and timing of damage of any type across the region. On average, the most recent predicted cyclone damage event (measured from 2003) occurred less recently than what was typical over the entire time series. This suggests that coral communities have had more time to recover since the last cyclone disturbance than would normally be the case, which could mean that present measures of broad community structure are not indicative of past conditions. Overall, the timing of predicted damage indicates that cyclone disturbance of the GBR is most likely intermediate in nature, and that the likelihood of cyclone disturbance was consistently lowest in the far northern GBR.

The state of a coral reef community at any given time is shaped by the complex interplay between a range of disturbances (coral bleaching, crown-of-thorns starfish predation, tropical cyclone waves) and routine ecological processes (competition, recruitment, recovery) that act across a range of spatial and temporal scales. From a management perspective, understanding the extent of human disturbances (fishing pressure, pollution) that a coral community can sustain before 'phase shifting' to a non-coral dominated state (ecological resilience) is necessary to devise long-term conservation strategies. An examination of the dynamics of each disturbance that

affects a given community, as well as how they interact across time and space scales, is necessary to estimate these thresholds. This thesis provides a first step towards this goal by characterizing the dynamics of the tropical cyclone disturbance regime in the GBR. The cyclone disturbance history it presents can be used in conjunction with long term monitoring data from AIMS to test the relative contribution of cyclone wave damage to broad measures of coral community structure. Subsequently, other disturbance regimes of importance in the GBR (coral bleaching, crown-of-thorns starfish predation, fresh water flood plumes) could be characterized, and the time-space interactions between them examined. In the shorter term, this thesis provides a valuable resource for researchers who need to assess the likelihood that cyclone disturbance has affected coral reef community structure at study sites of interest. The development of an interactive atlas of the tropical cyclone disturbance regime in the GBR using GIS-based visualization would greatly facilitate this. The development of such a tool is currently underway, as well as an assessment of the extent to which the proposed new zoning scheme for the GBR recently released by GBRMPA is threatened by spatial and temporal patterns in cyclone disturbance across the region.